Michigan Technological University

Michigan Technological University
Digital Commons @ Michigan Tech

Dissertations, Master's Theses and Master's Reports

2017

Computational Studies on Biomechanics of Concussion and on Efficacy of Football Helmets

David Labyak
Michigan Technological University, dmlabyak@mtu.edu

Copyright 2017 David Labyak

Recommended Citation

Labyak, David, "Computational Studies on Biomechanics of Concussion and on Efficacy of Football Helmets", Open Access Dissertation, Michigan Technological University, 2017.
https://doi.org/10.37099/mtu.dc.etdr/345

Follow this and additional works at: https://digitalcommons.mtu.edu/etdr


Part of the Applied Mechanics Commons, Biomechanics and Biotransport Commons, and the Other Mechanical Engineering Commons

www.manaraa.com

COMPUTATIONAL STUDIES ON BIOMECHANICS OF CONCUSSION AND ON EFFICACY OF FOOTBALL HELMETS

By

David M. Labyak

A DISSERTATION

Submitted in partial fulfillment of the requirements for the degree of

DOCTOR OF PHILOSOPHY

In Mechanical Engineering-Engineering Mechanics

MICHIGAN TECHNOLOGICAL UNIVERSITY

2017

© 2017 David M. Labyak

www.manaraa.com

This dissertation has been approved in partial fulfillment of the requirements for the Degree of DOCTOR OF PHILOSOPHY in Mechanical Engineering-Engineering Mechanics.

Department of Mechanical Engineering-Engineering Mechanics

Dissertation Advisor: *Dr Gopal Jayaraman*

Committee Member: *Dr. Allan Struthers*

Committee Member: *Dr. Ibrahim Miskioglu*

Committee Member: *Dr. Mahesh Gupta*

Department Chair: *Dr. William Predebon*

www.manaraa.com

Table of Contents

www.manaraa.com

www.manaraa.com

www.manaraa.com

www.manaraa.com

www.manaraa.com

www.manaraa.com

www.manaraa.com

Table of Figures

www.manaraa.com

www.manaraa.com

www.manaraa.com

www.manaraa.com

www.manaraa.com

www.manaraa.com

www.manaraa.com

www.manaraa.com

www.manaraa.com

www.manaraa.com

Tables

www.manaraa.com

Acknowledgements

First and foremost I would like to thank my wife, Elissa, for her unwavering support of me throughout this entire doctoral process. You are my best friend. Thank you for taking care of all the aspects of our lives that I had to pass off. You have encouraged me when I needed it and pushed me when I needed pushing. My only wish is that I can fully express my appreciation.

To our children, Madison, Marissa, and Evan: You three have been the most patient with me throughout my studies. It took longer than I hoped, but the time we've spent together is priceless.

I would like to thank my mother, Nancy Labyak. Thank you for understanding the time commitment I needed to devote to this work over the years.

I would like to thank my late father, John Labyak. His frankness and demeanor have influenced who I am today. I only wish he was still around to see me complete my work.

I would like to thank my father in-law and mother in-law, Bob and Bonnie Johnson, for the encouragement and support they have given to me and my family during the past years. Your help has been invaluable.

I am so grateful to my advisor Dr. Gopal Jayaraman. Dr. Jay has been incredibly supportive of my work. You have been understanding beyond belief. Without your encouragement and guidance, I don't think I could have completed this work.

Thanks to the rest of my defense committee, Dr. Allan Struthers, Dr, Ibrahim Miskioglu, and Dr. Mahesh Gupta for being so patient with the completion of my work. I have great respect for all of you. The classes you've taught, the feedback you've given, and support you've shown me has been an inspiration for me.

www.manaraa.com

Abstract

Football helmets have been used for many years to prevent head injuries to players. Over the years, the helmet design has evolved from a crude leather head covering to the more recent form fitting helmets that are seen today. The one design feature that has been common in the majority of all helmets is a hard polycarbonate shell with a foam cushion padding. The main goal of the padding layer was to reduce the amount of linear acceleration during an impact event. The one feature that has been overlooked is how stiff the padding is in rotation.

The purpose of this work is to evaluate how well the Enhanced Bio-Morphic (EBM) football helmet performs as compared to a commercially available football helmet. The EBM helmet is designed to capture the existing features of the current football helmet, but to also include a shear layer between the polycarbonate shell and foam padding. The shear layer is included to help reduce the severity of angular acceleration that is imposed on the human head that is responsible for concussions.

This dissertation presents the makeup of the EBM helmet, the rational for selecting the components of the EBM IEA system, and a comparison of the predicted performance of the EBM as compared to a commercially available VSR4 helmet by Riddell. The results will show the EBM helmet has the ability to reduce the angular acceleration for an oblique impact, thereby reducing the amount of stress in the human brain. This stress reduction has the ability to help reduce the possibility of concussion more commonly

www.manaraa.com

seen in sports related injuries. This finding is an important discovery in helmet technology. Although the technology studied here is focuses on football helmets, it is not by any means limited to football helmets. This can be used throughout different sports as well as throughout other applications where helmets are used.

www.manaraa.com

1 Introduction

1.1 Introduction

Over the past decade, from 2001 to 2010, the amount of Traumatic Brain Injury (TBI) related emergency department visits have increased by 70%. It is estimated that approximately 2.8 million Americans sustained a Traumatic Brain Injury in 2013. Traumatic Brain Injury (TBI) can range from a mild injury that involves a brief change in consciousness or mental status, to a severe injury that can result in an extended period of unconsciousness or possibly memory loss [1].

As a result of these injuries, approximately 282,000 people are hospitalized and survive, 80,000 people experience the onset of long-term disability, and 50,000 people die. Studies indicate that males are about three times as likely to incur TBI as compared to females, and persons 15 to 24 years of age are at highest risk of TBI. In 2012 alone, approximately 329,290 children (ages 19 and younger) were diagnosed with a concussion or TBI for sports and recreation-related related injuries [2]. Consequences of TBI are problems with memory, judgment, mood, strength, coordination, balance, and vision. TBI can also cause seizures such as epilepsy. Repeated mild brain impacts occurring within hours, days, or even weeks, can be fatal [1].

www.manaraa.com

1.2 Problem Statement

For closed head trauma there are two theories that are used to describe the cause of brain injuries: injuries caused by the translational motion of the head and injuries caused by rotational motion of the head. A head injury caused by translational motion of the head has been postulated to be the sole cause of injuries at the site of impact, or coup injuries, and opposite the site of impact, or countercoup injuries. Head injuries caused by rotational motion of the head, on the other hand, have been postulated to be the sole cause of injuries on a global scale, or diffuse axonal injuries. Although there has been a great deal of research done in the area of brain injuries and the mechanisms that cause brain injuries, these two theories have been studied most often exclusively.

Concussion is a type of traumatic brain injury (TBI) [1]. It is a brain injury due to linear and angular acceleration/deceleration of the head due to impacts forcing interactions between the inner surface of the skull and the floating brain. Most impacts on the helmet cause both linear and angular accelerations. Linear acceleration causes pressure gradient while angular acceleration causes shear strain gradient. Frontal and posterior impacts cause both pressure and shear stress distributions in the brain. While comparable compressive pressures developed in the countercoup regions, shear stress distributions remained identical regardless of the impact direction, correlating with clinically observed patterns for contusion. Therefore, shear strain theory appears to account better for the clinical findings in cerebral contusion [7]. Angular acceleration is therefore the primary causation factor for concussion.

www.manaraa.com

A football helmet, is a safety headgear to protect players from head injuries due to impacts on the field. Head injuries include skull fractures and brain concussion. Current football helmets are designed with a stiff plastic outer shell to distribute impact forces combined with an elastic foam inner layer to absorb the impact shock and to reduce the impact forces in order to minimize the risk of skull fractures. Current helmet technology does provide adequate design provisions to attenuate normal impact forces, but it lacks design provisions to attenuate tangential impact forces.

The goal of this research is to propose a new football helmet, the Enhance Bio-Morphic Helmet (EBM), that provides adequate attenuation for normal impact forces and adds provisions to attenuate angular acceleration. The purpose of the EBM helmet is not only to minimize linear acceleration of the head to prevent catastrophic brain injury like hemorrhages, but also to minimize angular accelerations of the head to prevent concussion.

www.manaraa.com

1.3 Objective

In order to present the EBM helmet as a viable helmet for football players, a full assessment of the design features against the current football helmet technology is required. The methods and materials used evaluate the EBM helmet are as follows:

- Study of head impacts on the football field.
- Brain injury dynamics due to head impacts on the football field.
- Development of Impact Energy Attenuators (IEAs).
- Impact study of the helmet fitted on the human head model by FEM.
- Impact study of the EBM helmet fitted onto human head model by FEM.
- Comparative study of the overall effectiveness of the EBM helmet.

www.manaraa.com

2 Head Impacts on the Football Field

2.1 Introduction

Traumatic Brain Injury (TBI) is defined by the Centers for Disease Control (CDC) as “a disruption in the normal function of the brain that can be caused by a bump, blow, or jolt to the head, or penetrating head injury." "The severity of a TBI may range from mild (i.e., a brief change in mental status or consciousness) to severe (i.e., an extended period of unconsciousness or memory loss after the injury)." In the United States alone, it is estimated that 2.8 million Americans sustain a TBI each year [1].

Of the estimated 2.8 million TBI's each year, over 300,000 of these injuries are related to sports or other physical activities. From 2001 to 2012, studies show that the rate of emergency room visits have more than doubled for sports and recreation related injuries for children 19 years of age and younger. The main diagnosis for these injuries was concussion or TBI. Although the amount of deaths have decreased by approximately 7% between the years of 2007 and 2013, the hospitalization rates have increased by approximately 11% [2]. With the increase in TBI related injuries that is seen in a clinical setting, the need for better sports equipment is very important.

www.manaraa.com

2.2 Objective

The main objective of this study is to investigate the effect an oblique impact has on the pressure and shear stress distribution in the human brain. Specifically, this study will address the following questions:

- Is there a critical angle of oblique impact at the given site on the head which will cause the shear stress in the brain to reach a concussion tolerance?
- Is there any relationship between the peak pressure and peak shear stress distribution at each site of oblique impact on the head to identify a critical angle for a given site?

2.3 Relevance of Research

For closed head trauma there are two theories that are used to describe the cause of brain injuries: injuries caused by the translational motion of the head and injuries caused by rotational motion of the head. A head injury caused by translational motion of the head has been postulated to be the sole cause of injuries at the site of impact, or coup injuries, and opposite the site of impact, or countercoup injuries. Head injuries caused by rotational motion of the head, on the other hand, have been postulated to be the sole cause of injuries on a global scale, or diffuse axonal injuries. Although there has been a great deal of research done in the area of brain injuries and the mechanisms that cause brain injuries, these two theories have been studied most often exclusively.

www.manaraa.com

2.4 Methods and Materials Used to Achieve Results

To address these questions, the following goals are established:

- Develop and validate a biomechanical 3-D finite element model of the human head.
- Subject the validated FE human head model to oblique impacts on the frontal, lateral, posterior, and superior aspects of the head.
- Identify the peak pressure, the peak shear stress, and the corresponding regions in the brain with respect to angle of oblique impact.
- Correlate the stress criteria to the type of injury.

2.5 Development of 3D FE model

The development of the 3D FE model of the human head was achieved through the use of CT image files of the 50th percentile male human from the National Library of Medicine (NLM) Visible Human Project [3]. The Visible Human Project (VHP) provides complete anatomically detailed 3-D representation of the male and female human body. CT scans and image files of the head and neck were used to construct a head surface model. The CT scans and image files consist of axial scans taken at 1 mm intervals of the head and neck. With permission from NLM, the CT scans and image files were downloaded from the VHP web site to generate the transverse surfaces of the geometric model.

www.manaraa.com

The model was developed by taking axial scans of the head and neck and then convert them to points, lines, and surfaces. The first step in this process was to extract point data from CT scans and image files. A solid model of the skull was then generated by from the surface data that was ultimately imported and meshed using HyperMesh, by Altair Engineering Inc. The skull, dura, brain, and scalp were all generated in HyperMesh [4]. The model consists of 40,018 first order tetrahedral elements and 7,819 first order penta elements. Figure 2-1 shows the finite element mesh of the skull.

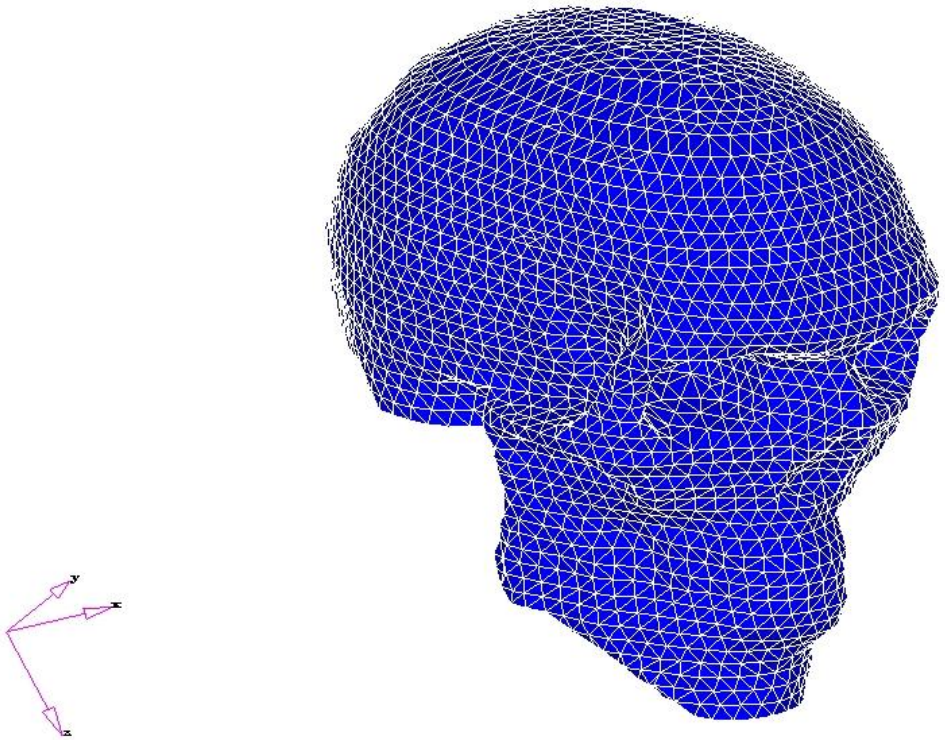

Figure 2-1 Finite Element Mesh of the Skull (isometric view)

www.manaraa.com

2.6 Validation of the 3D FE Model

The 3-D FE model, was then validated using Nahum et al's [5] frontal head impact experiments for impact force, intracranial pressures, and linear head acceleration. The linear frontal head impact experiment # 37 by Nahum et al [5] was chosen to validate the FE model. Towards this goal, the same general setup, as in the experiment had to be employed when modeling the 3-D FE model. The impactor in this FE model is a steel, cylindrical impactor with padding, traveling at an initial constant velocity. Impactor mass was fixed at 5.6 kg. The impactor travels in an anterior-posterior motion in the mid-sagittal plane directed at the frontal bone. The head, shown in Figure 2-2 is rotated such that the transverse plane of the skull is inclined 45º relative to horizontal. The impact is essentially normal to the surface of the skull and directly in line with the head's center of mass.

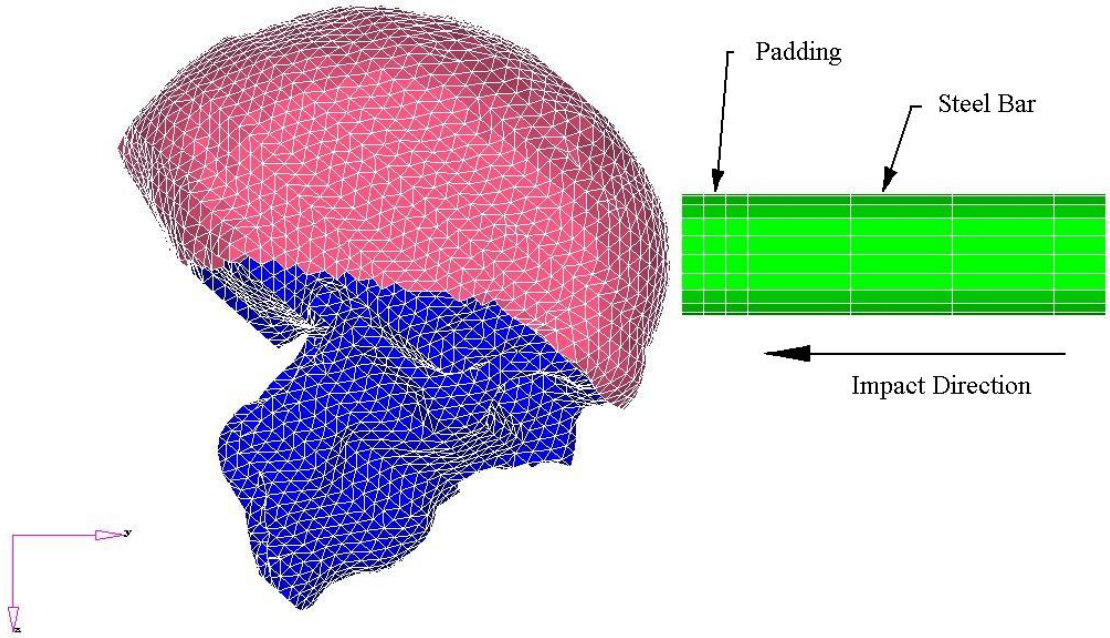

Figure 2-2 Head Impact - Validation Setup

www.manaraa.com

Validation of the model was done by comparing impact force, coup pressure, contrecoup pressure, left parietal pressure, occipital #1 pressure, and occipital #2 pressure. The impact force is measured at the site of impact, for the contact pairs: scalp and padding. Coup pressure is measured below the site of impact, on the surface of the brain. Contrecoup pressure is measured on the surface of the brain at the posterior fossa. Parietal pressure is measured on the surface of the brain immediately posterior and superior to the coronal and squamosal sutures respectively in the parietal bone. Finally, occipital pressures #1 and #2 are both measured on the surface of the brain inferior to the lambdoidal suture in the occipital bone; one on the left and one on the right. Although the finite element model lacks the exact anatomical features of a real human head, a great deal of effort was spent making sure the locations of measurements closely matched the anatomical location described by Nahum et al [5].

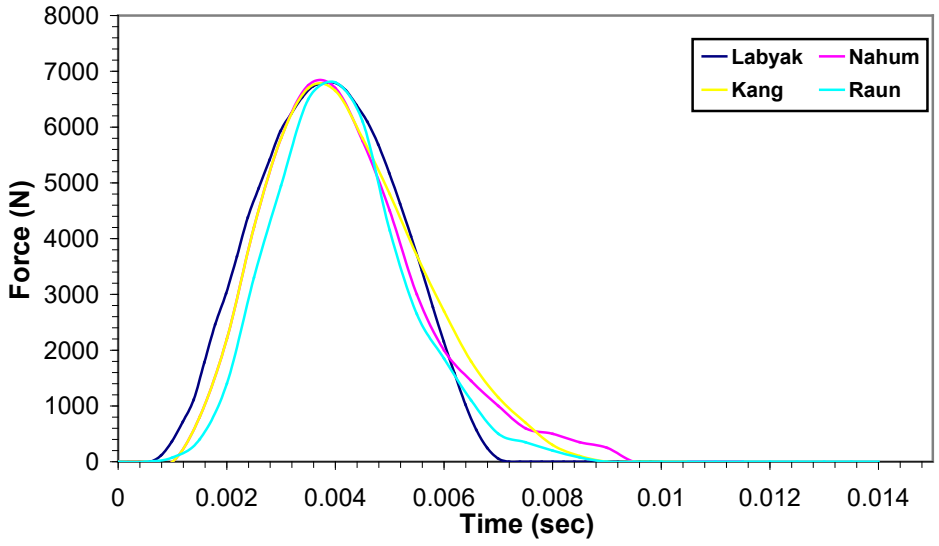

Figure 2-3 Impact Force Time History – Validation Model

www.manaraa.com

The coup pressure time history curve, Figure 2-4, of the validation model also validate with the coup pressure histories by Nahum's experiments [5] and 3-D FE models by Kang [6] and Raun [7]. Coup pressure is measured below the site of impact, on the surface of the brain. The pressure time histories for six adjacent elements on the surface of the brain were used to obtain an average pressure for the impact event. The positive value of pressure indicates compression. Error bars are included to show the pressure variation for the six elements due to the profile of the brain surface. The pressure results from the finite element model qualitatively agree with the published results.

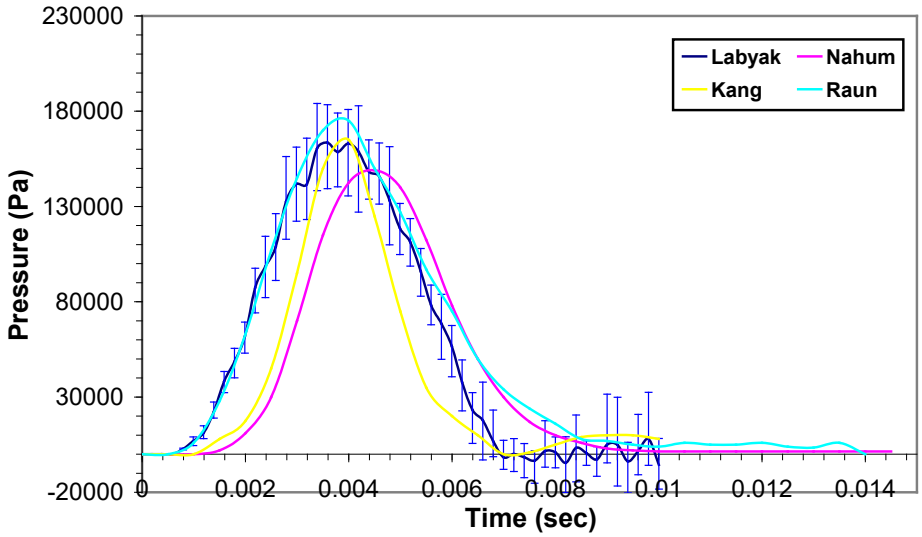

Figure 2-4 Coup Pressure Time History

Contrecoup pressure results shown in Figure 2-5, also validate with the contrecoup pressure histories by Nahum's experiments [5] and 3-D FE models by Kang [6] and Raun [7]. Contrecoup pressures are measured opposite the site of impact.

www.manaraa.com

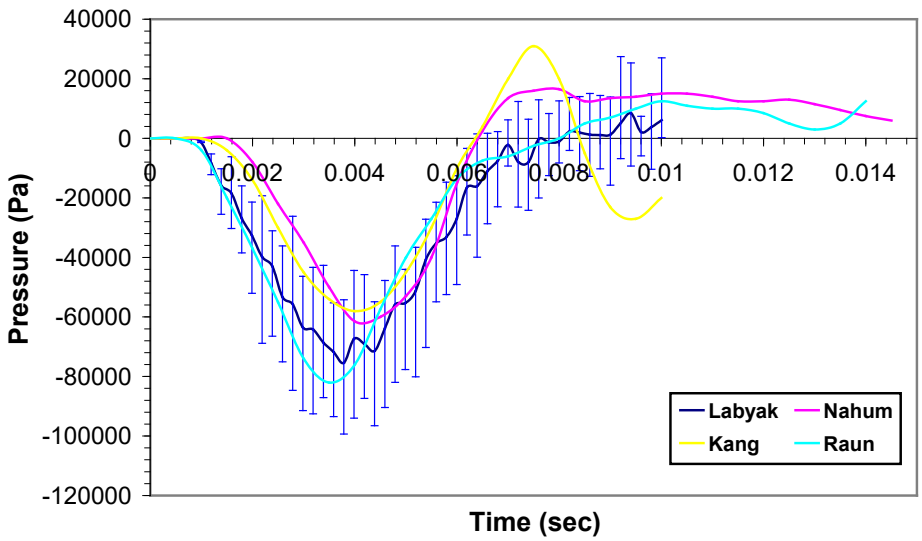

Figure 2-5 Contrecoup Time History

The left parietal pressure time history curve, seen in Figure 2-6, of the validation model also validate with the contrecoup pressure histories by Nahum's experiments [5] and 3-D FE models by Kang [6] and Raun [7]. Left parietal pressure is measured on the surface of the brain immediately posterior and superior to the coronal and squamosal sutures respectively in the parietal bone. The pressure time histories for five adjacent elements on the surface of the brain were used to obtain an average pressure for the impact event. The positive value of pressure indicates compression. Error bars are included to show the pressure variation for the five elements due to the surface profile of the lateral side of the brain. The pressure results from the finite element model qualitatively agree with the published results.

www.manaraa.com

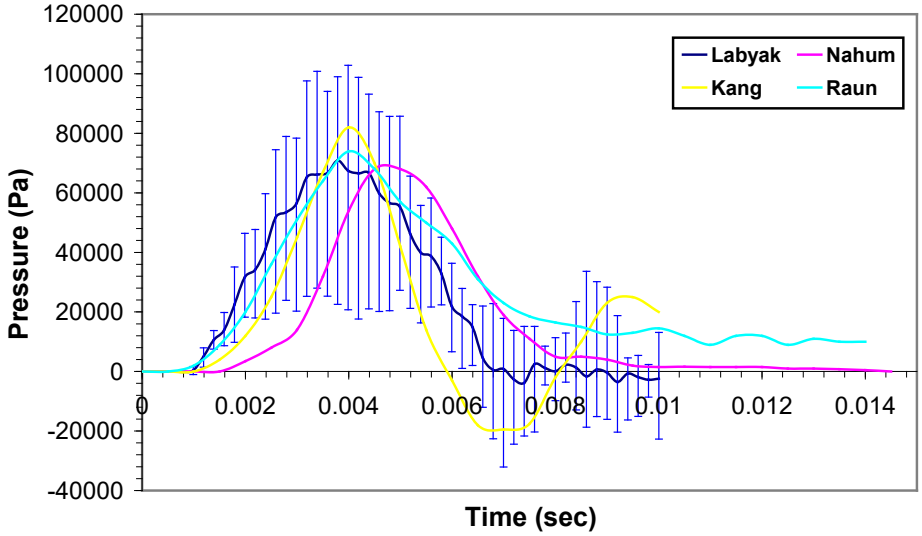

Figure 2-6 Left Parietal Pressure Time History

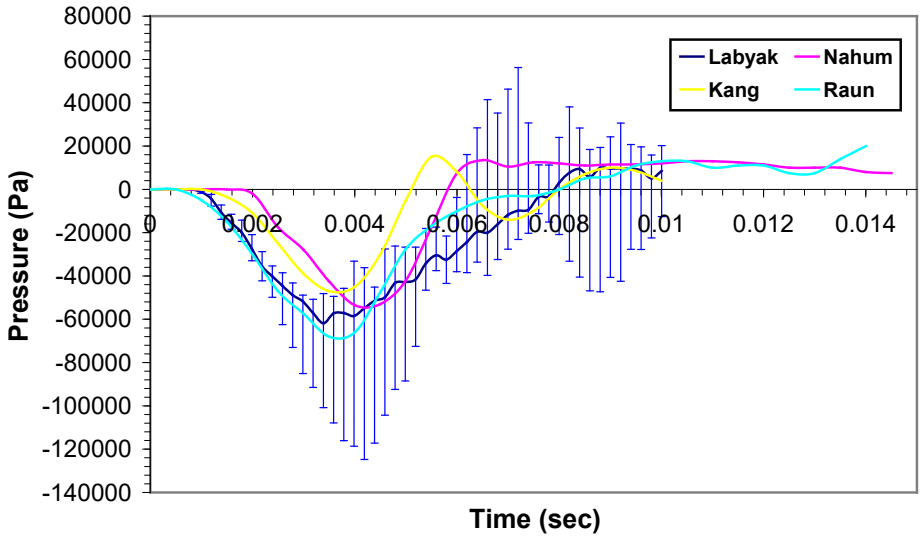

Figure 2-7 Occipital #1 Pressure Time History

www.manaraa.com

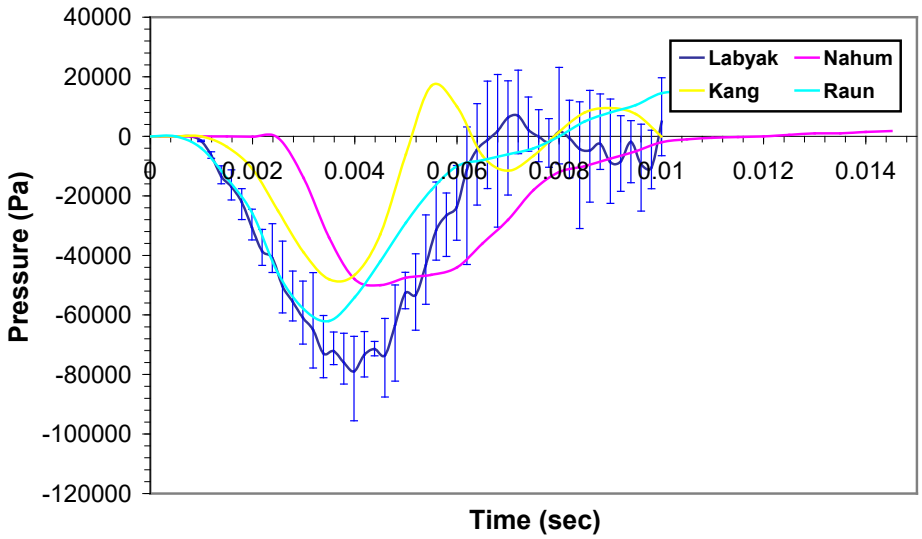

Figure 2-8 Occipital #2 Pressure Time History

The linear head acceleration history curve, shown in Figure 2-9 of the validation model also validate with the linear head acceleration histories by Nahum's experiments [5] and 3D FE model by Kang [6]. Linear head acceleration is measured on the outer surface of the skull on the occipital bone. Although the acceleration curve in Figure 2-9 is averaged and not filtered beyond the sampling frequency, additional filtering would eliminate the unwanted noise.

www.manaraa.com

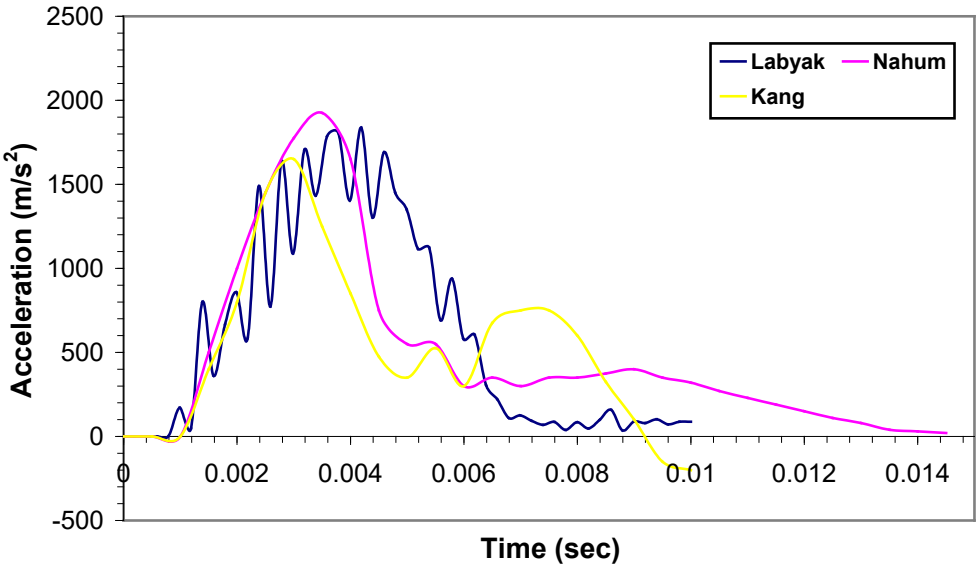

Figure 2-9 Linear Head Acceleration Time History

Final material properties for the FE model was determined from validating the model to the pressures and accelerations in the reviewed literature. Table 2-1 lists the final material properties used in the validated FE model.

Table 2-1 Material Properties – FEM Head Model

	Density (kg/m^3)	Bulk Modulus (GPa)	Young's Modulus (MPa)	Shear Modulus (MPa)	Poisson's Ratio
Skull	2700	3.87E+03	6.50E+03	2.66E+03	0.22
Scalp	1412	17	8.05	2.83	0.42
Dura-matter	1040	2	0.148	0.05	0.49
Brain tissue	1040	89	0.533	0.18	0.499

www.manaraa.com

2.7 Head Impact Simulations

Since it is postulated that some combination of translation and rotational motion of the head is involved with the majority of head impacts, this objective is to investigate the effect an oblique impact has on the pressure and shear stress distribution in the human brain. The 3D FE model developed earlier was used to simulate four different types of impact: frontal, lateral, posterior, and superior. At each impact location, oblique impacts are simulated by an increasing angle of impact incidence. Impact angles start at a direct inline impact of 0º and increase to 15º, 30º, and 45º. The angles simulate the increasing tangential component of an oblique impact relative to the impact site. These impact simulations are used as a tool in determining the critical impact angle at which the shear stress in the brain becomes more critical than pressure. For frontal, lateral, and posterior impact locations the angles are increased relative to the transverse plane. The superior impacts, on the other hand, are increased in the coronal plane. Figure 2-10 is an illustration of the impact locations and angles. The output results of the finite element analysis are impact force, pressure stress (or octahedral normal stress), and shear stress (or von-Mises stress). Impact pressure and shear stress distributions are displayed in different shades in the color distribution plots.

www.manaraa.com

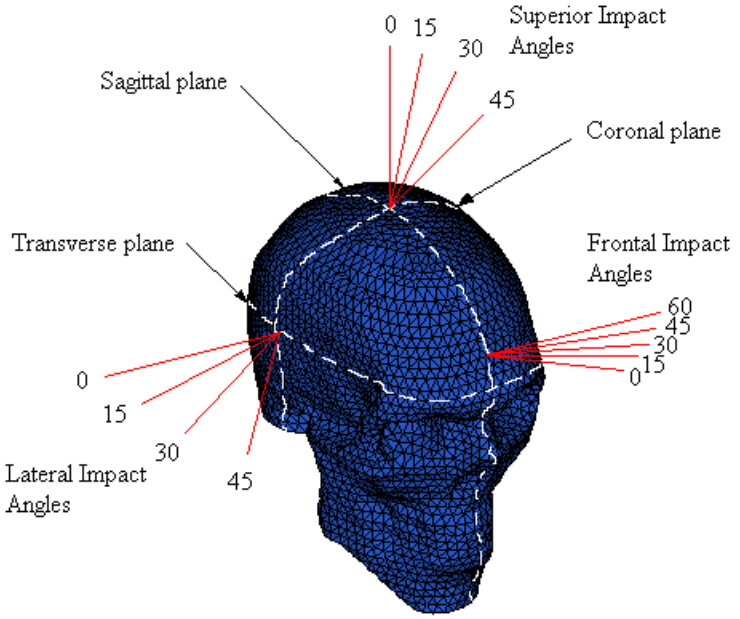

Figure 2-10 Frontal, Lateral, and Superior Impact Angles

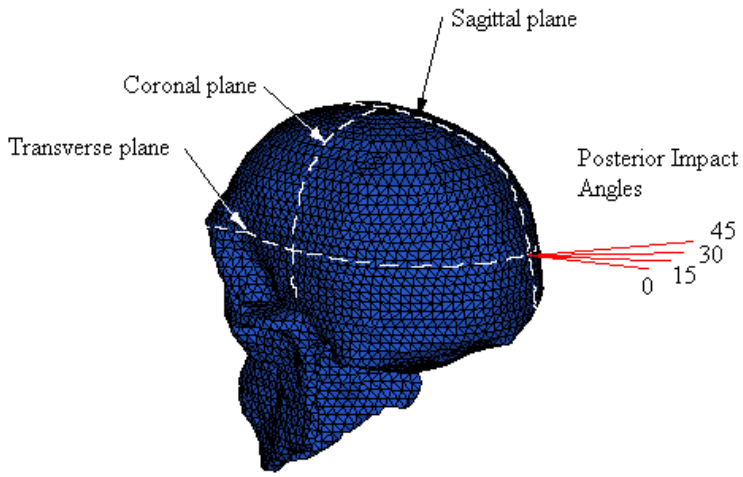

Figure 2-11 Posterior Impact Angles

www.manaraa.com

2.7.1 Injury Severity Scale

The individual results of FE simulations were coded using an injury severity scale for pressure and shear stress. The injury severity scale code relative to intracranial pressure results (absolute pressure, or |pressure|), are described as follows:

0 – No injury, or no hemorrhage (pressure less than 0.18 MPa)

1 – Minor injury, or petechial hemorrhaging in high-pressure regions (pressure range 0.08 MPa to 0.24 MPa)

2 – Moderate injury, or possible contusion or subdural hemorrhage in high-pressure regions (pressure range 0.18 MPa to 0.32 MPa)

3 – Severe or fatal injury, or contusion in high-pressure regions (pressure greater than 0.24 MPa)

Note: The pressure range described above is used according to Ward et al [8].

For shear stress, a risk factor is used to describe the potential of injuries related to shear stress. The ratio is calculated using Kang et al's [6] finding for an upper tolerance of the human brain in shear of 16.5 kPa, causing a contusion or subdural hematoma. The ratio is defined in the present equation:

$$Shear\ Stress\ Risk\ Factor = \frac{Shear\ Stress\ from\ FE\ Simulation}{16.5\ kPa} \qquad (2.1)$$

$Risk\ Factor < 1 \rightarrow$ injury related to shear stress is not likely to occur.

$Risk\ Factor \geq 1 \rightarrow$ injury related to shear stress is likely to occur.

www.manaraa.com

2.8 Interpretation of Results from Head Impact Simulations

The FE results of the head impact simulations were used to relate a specific brain injury to the brain's pressure and shear stress response when the head is subjected to a defined impact. By identifying the areas of the brain that have a greater pressure severity index and a shear stress risk factor, it is possible to indicate areas of the brain that are particularly at risk to injury. The key factor in assigning a specific brain injury is being able to identify the angle of impact at which pressure and shear stress are or are not critical.

2.9 Frontal Impact

From the FE results of a 0º frontal impact, it is shown that the severity index for pressure is severe at the site of impact (severity index of 3) and moderate on the opposite site of impact (severity index of 2). Another inherent feature is the shear stress risk factor around the cerebral hemispheres is < 1, indicating no injury from shear, but is > 1 in the brain stem region indicating an injury from shear. Since the head mainly experiences linear acceleration, there is no surprise with these initial results. As the impact takes place, the cerebral hemispheres deform little from compression, while the brain stem has the tendency to be pulled into the cranial cavity. In other words, linear acceleration does not cause distortion of the brain.

www.manaraa.com

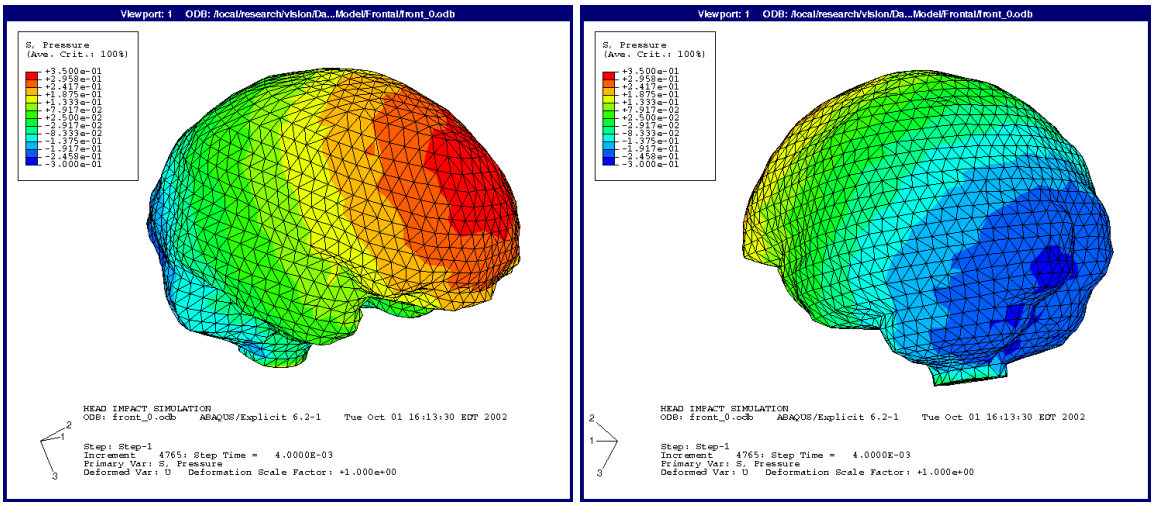

Figure 2-12 Frontal Impact 0º - Pressure Distribution

For all of the pressure distribution images, peak positive pressure, or compression, is indicated in (red). Negative pressure, or tension, is indicated in (blue).

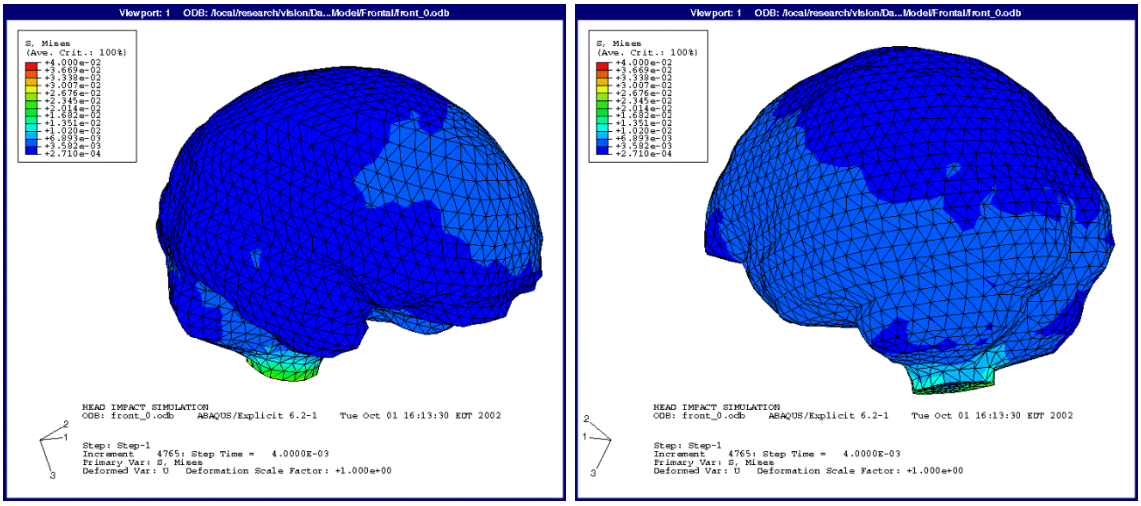

Figure 2-13 Frontal Impact 0º - von Mises Stress Distribution

As the impact angle increases to 15º, the severity index for coup and contrecoup pressure remains unchanged at 3 and 2 respectively. Also unchanged from the 0º impact, the shear stress risk factors. In the cerebral hemispheres the shear stress risk factor is < 1,

www.manaraa.com

indicating no injury from shear, and is > 1 in the brain stem region indicating an injury caused by shear. See Figure 2-14 and Figure 2-15.

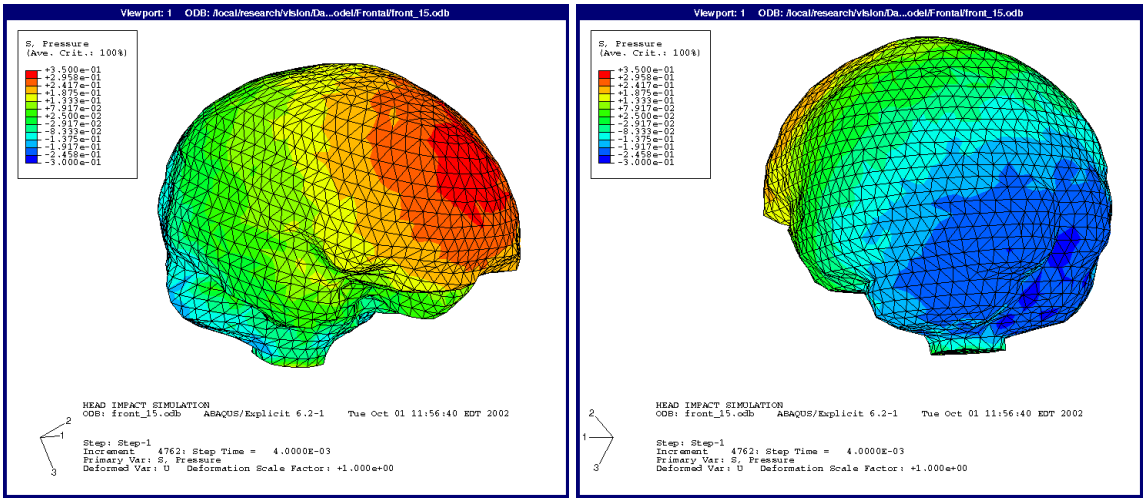

Figure 2-14 Frontal Impact 15º - Pressure Distribution

Therefore, for an impact angle of 0º and 15º, an injury to the frontal lobe, in the form of a contusion, is most likely to occur due to the severity of pressure in the frontal lobe and a subdural injury in the brain stem due to the high shear stress. The contusion in the frontal lobe would more than likely be fatal. The subdural injury to the brain stem, if not fatal, could cause problems with heart rate, blood pressure, breathing, reflexes to hearing, and vision just to name a few.

www.manaraa.com

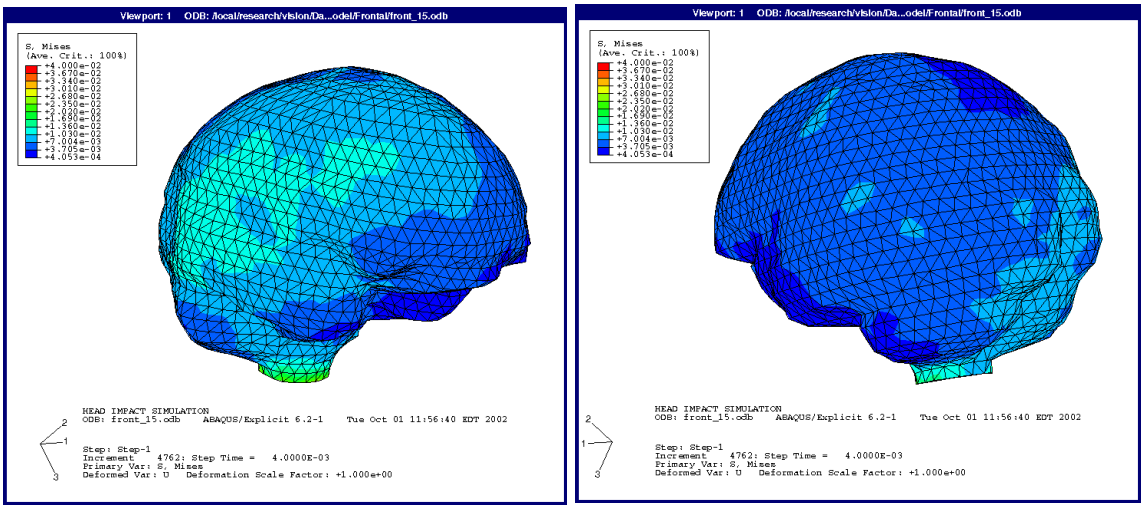

Figure 2-15 Frontal Impact 15º - von Mises Stress Distribution

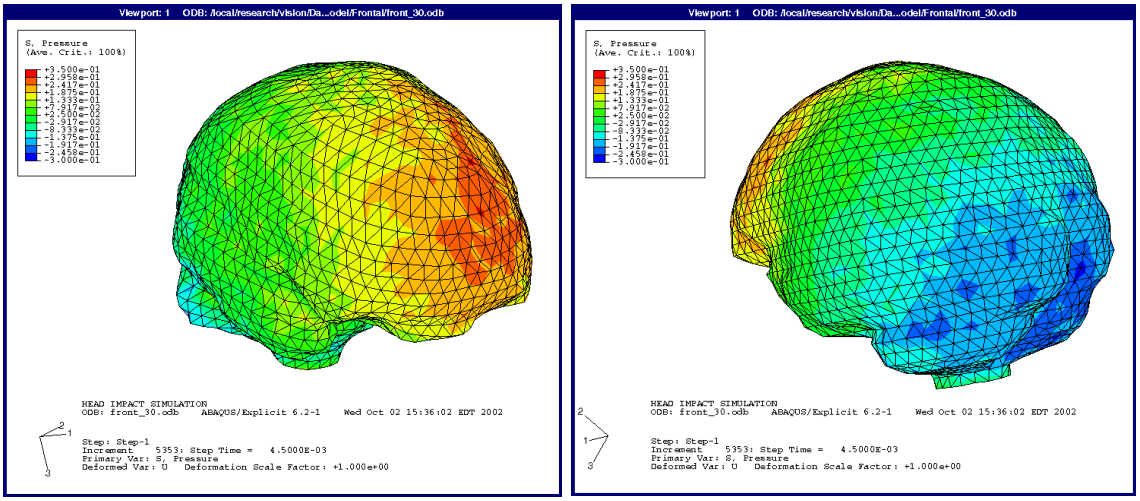

Figure 2-16 Frontal Impact 30º - Pressure Distribution

www.manaraa.com

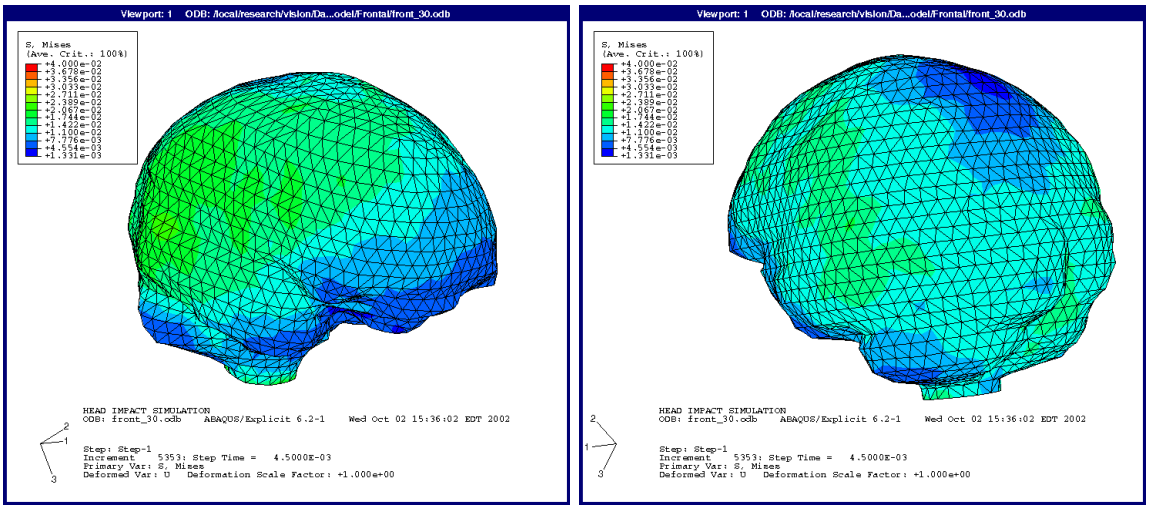

Figure 2-17 Frontal Impact 30º - von Mises Stress Distribution

At a 30º impact angle, the severity index for pressure remains at 3 on the coup side and 2 on the contrecoup side. The severity index almost reduces one level for coup and contrecoup pressure, however, the pressures do not change significantly enough to rate them as lower indices. The shear stress risk factor for 30º, is still > 1 in the brain stem region and now at 1.4 in the posterior temporal lobe indicating a temporal lobe injury due to shear. See Figure 2-16 and Figure 2-17.

Once the impact angle reaches 45º, the pressure severity index on the coup side reduces to a moderate injury index of 2, and a minor injury index of 1 on the contrecoup side. See Figure 2-18. Although pressure is no longer severe at 45º, the shear stress continues to increase around the entire surface of the brain, as seen in Figure 2-19. Along the posterior border of the right temporal lobe, the shear stress risk factor increases to 1.65.

www.manaraa.com

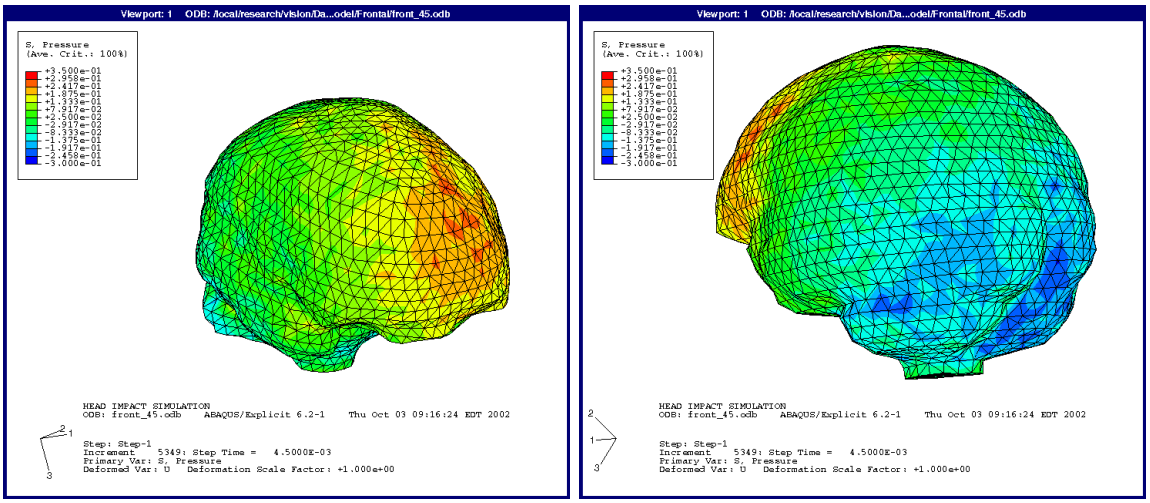

Figure 2-18 Frontal Impact 45º - Pressure Distribution

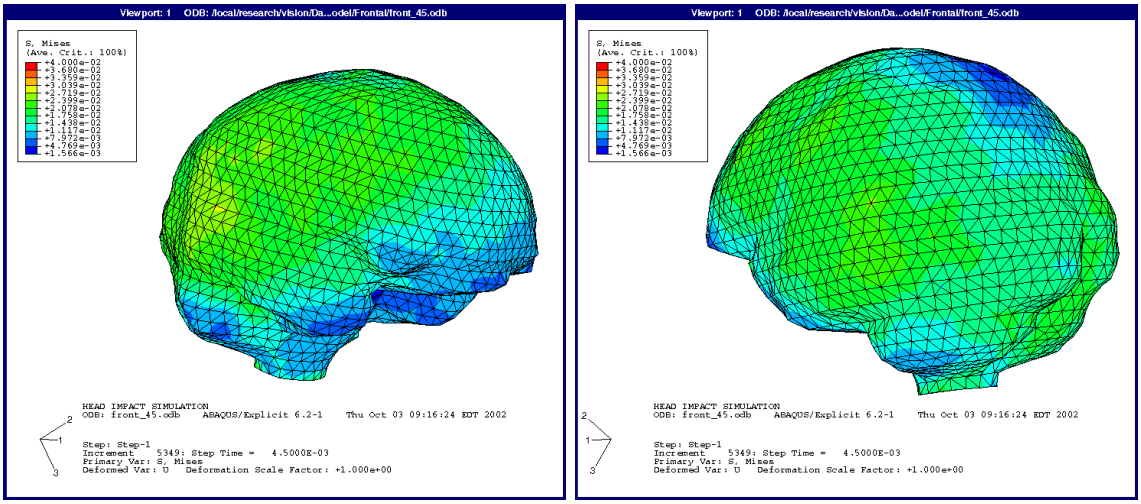

Figure 2-19 Frontal Impact 45º - von Mises Stress Distribution

What is very interesting about this area of peak shear is it is located approximately opposite the site of impact. Since brain movement with respect to the skull has been postulated as an injury mechanism for surface contusions in the frontal and temporal lobes [45], this may be the development of a contrecoup injury. In other words, the peak pressure at the site of impact being responsible for causing a cerebral contusion and the

www.manaraa.com

shearing action in the posterior location of the temporal lobe causing a surface contusion or subdural hematoma. Figure 2-20 is a cross-sectional slice through the peak area of shear stress for a frontal impact at 45º to give an indication of the depth of high risk factor shear stress. A contusion in the frontal lobe is likely to affect memory, emotions (irritability), and expressive language (word association). A surface contusion or subdural injury in the temporal lobe, given the high risk factor, could be fatal.

As seen in Figure 2-20, there is very little shear stress in the central portion of the brain, with the increased shear stress on the outer surface of the brain. This also indicates that the injury location would be near the surface of the brain or in the subdural space.

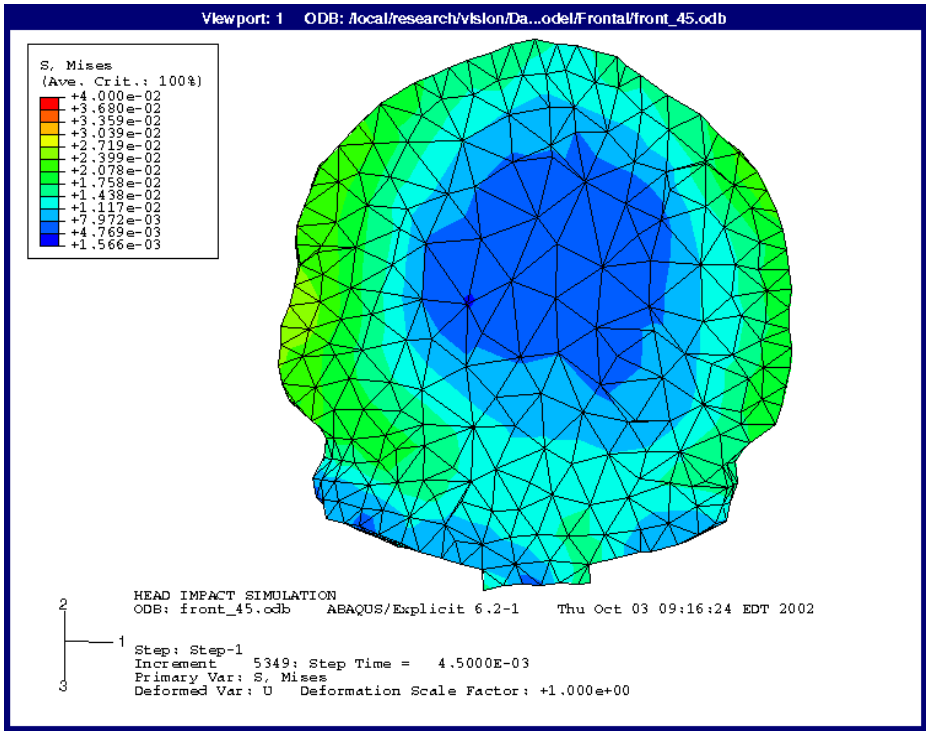

Figure 2-20 Frontal Impact 45º, Cross-Section View

www.manaraa.com

2.10 Lateral Impact

From the lateral impact FE results, as similarly seen with frontal, posterior, and superior impacts, a 0º impact in Figure 2-21 produces peak positive pressure at the site of impact with a reduced pressure distribution to the area opposite the site of impact. The pressure distribution is not as uniform as with frontal impacts, but a severity index of 3 on the coup side and of 2 on the contrecoup side coincide with frontal, posterior, and superior impact locations. Once the impact angle reaches 45º, the coup pressure on the right lateral side changes to a moderate severity index of 2 and a minor severity index of 1 on the contrecoup, or left lateral, side.

How lateral impacts differ from frontal, posterior, and superior impacts is the high shear stress risk factor at an impact angle of 0º. See Figure 2-22. At 0º, the shear stress risk factor throughout the temporal lobe, occipital lobe, and the inferior side of the parietal lobe is already at a risk factor of 1.05, which predicts an injury related to shear. When the angle of impact increases to 45º, the risk factor increases in the frontal lobe and posterior fossa to 1.65, which was previously < 1, and peaks in localized areas on the coup and contrecoup locations to > 2.

www.manaraa.com

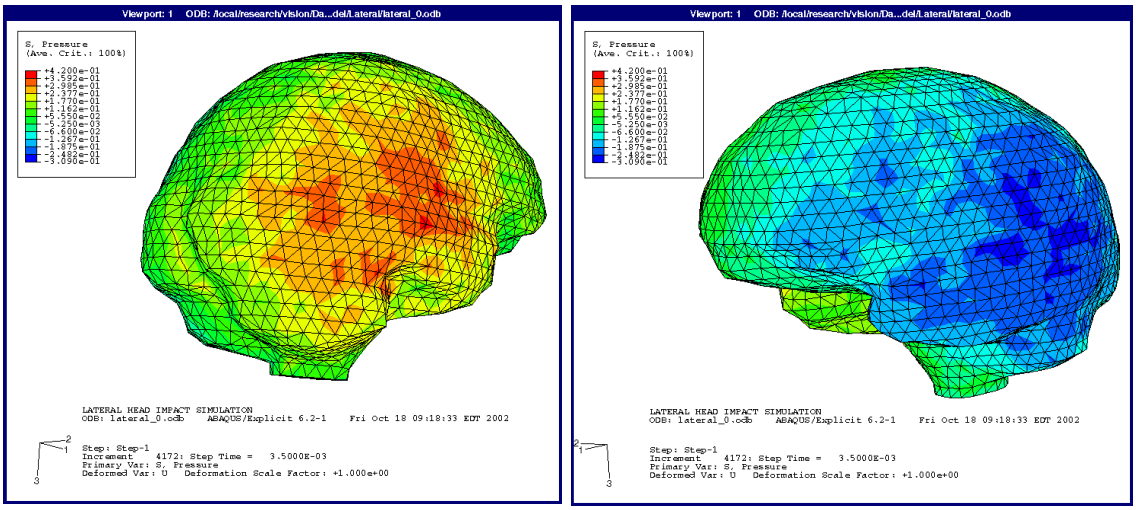

Figure 2-21 Lateral Impact 0º - Pressure Distribution

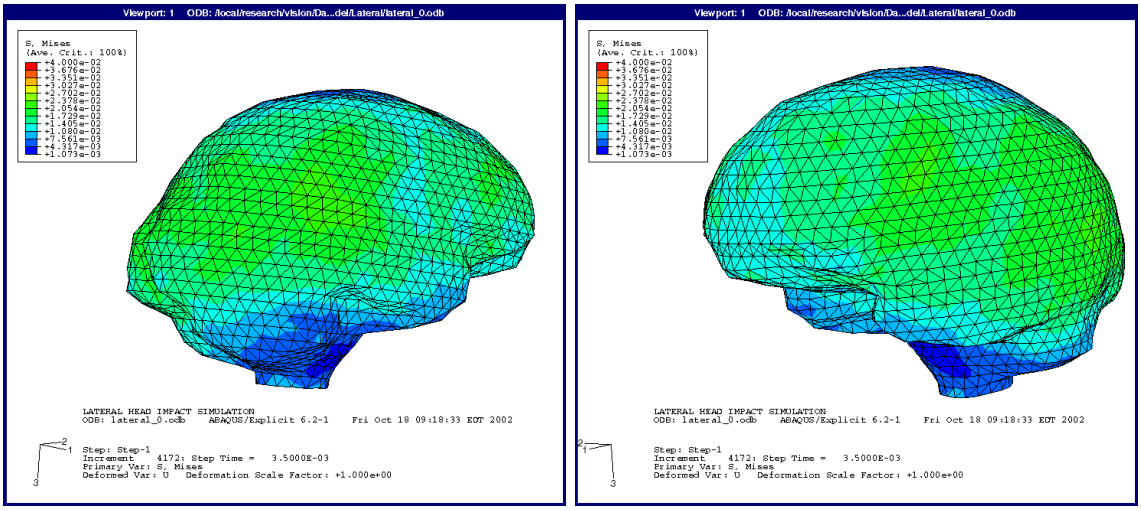

Figure 2-22 Lateral Impact 0º - von Mises Stress Distribution

The severe shear stress risk factor in localized areas on the coup and contrecoup sides can be attributed to the direction of impact relative to the head's center of mass. A unique phenomenon with this type of impact is that at 0º, the impact force vector is eccentric with respect to the center of mass of the head. With 0º frontal, posterior, and superior impact arrangements, the force vector passes closely to the head's center of mass. The

www.manaraa.com

impact becomes oblique when the angle of impact increases. Regardless of the impact angle simulated in this study, the force vector for lateral impact is always eccentric to the head's center of mass. Therefore, even a 0º impact on the lateral side of the head has the capability of producing high shear stress throughout the surface of the brain.

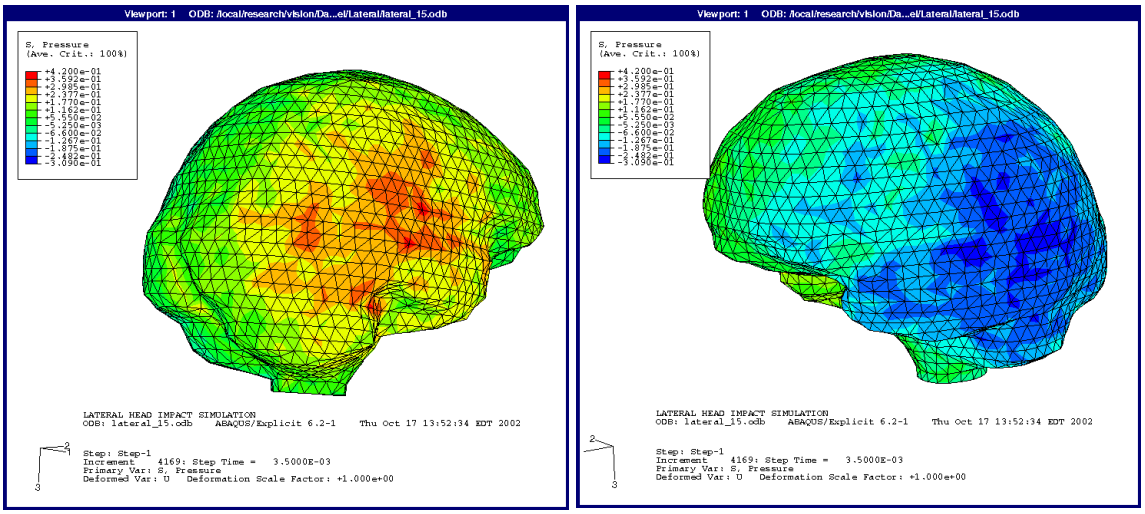

Figure 2-23 Lateral Impact 15º - Pressure Distribution

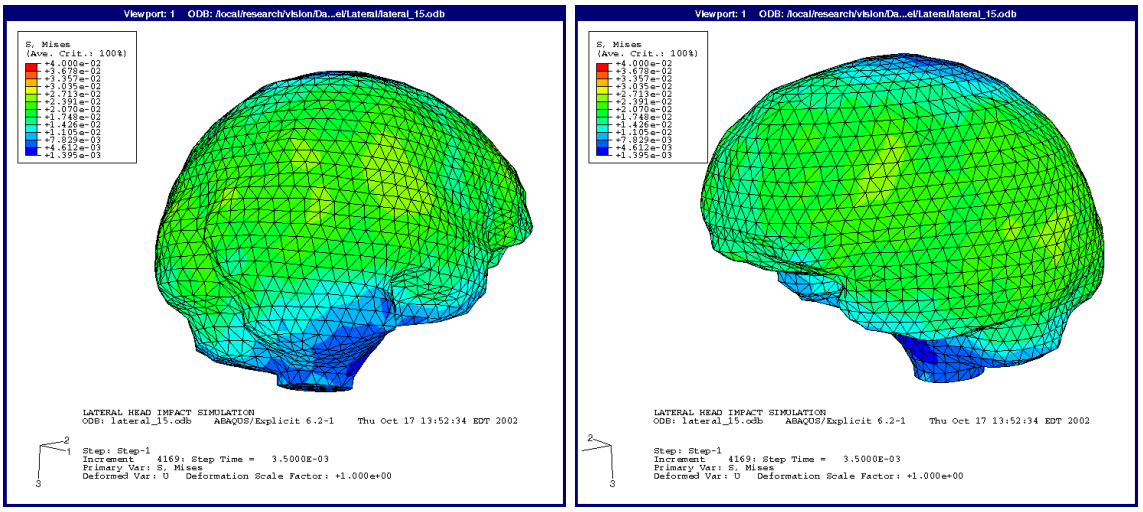

Figure 2-24 Lateral Impact 15º - von Mises Stress Distribution

www.manaraa.com

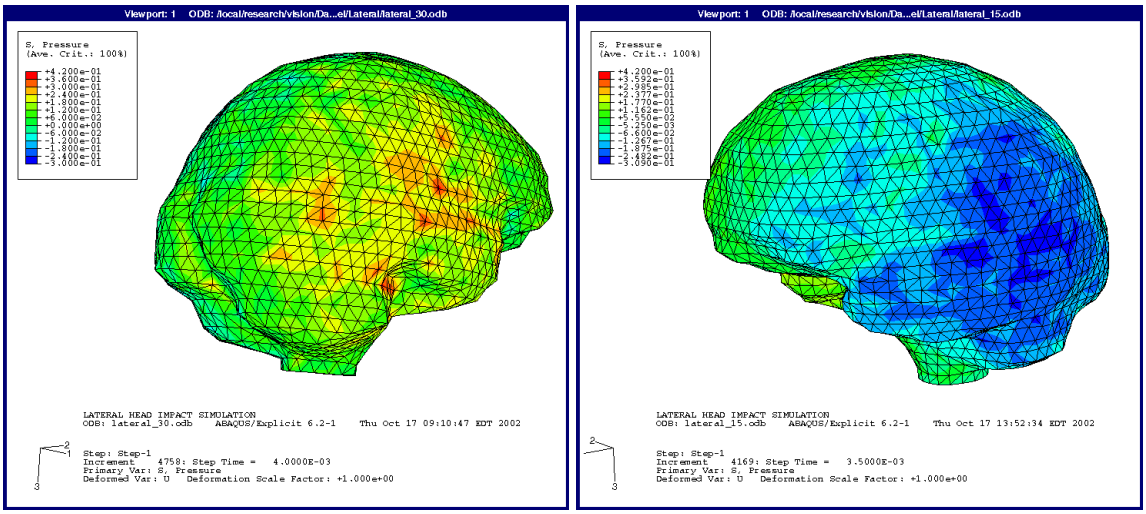

Figure 2-25 Lateral Impact 30º - Pressure Distribution

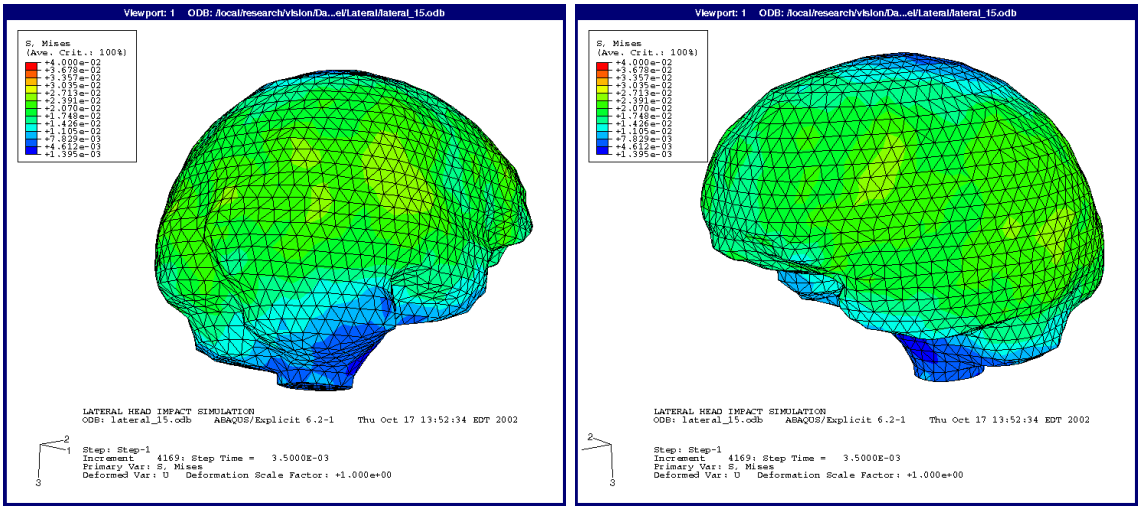

Figure 2-26 Lateral Impact 30º - von Mises Stress Distribution

www.manaraa.com

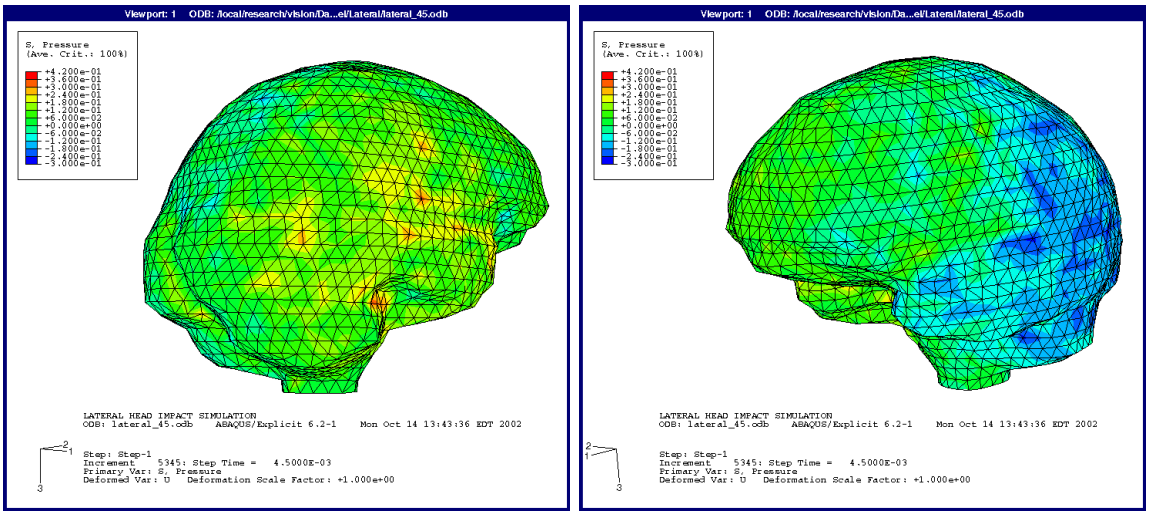

Figure 2-27 Lateral Impact 45º - Pressure Distribution

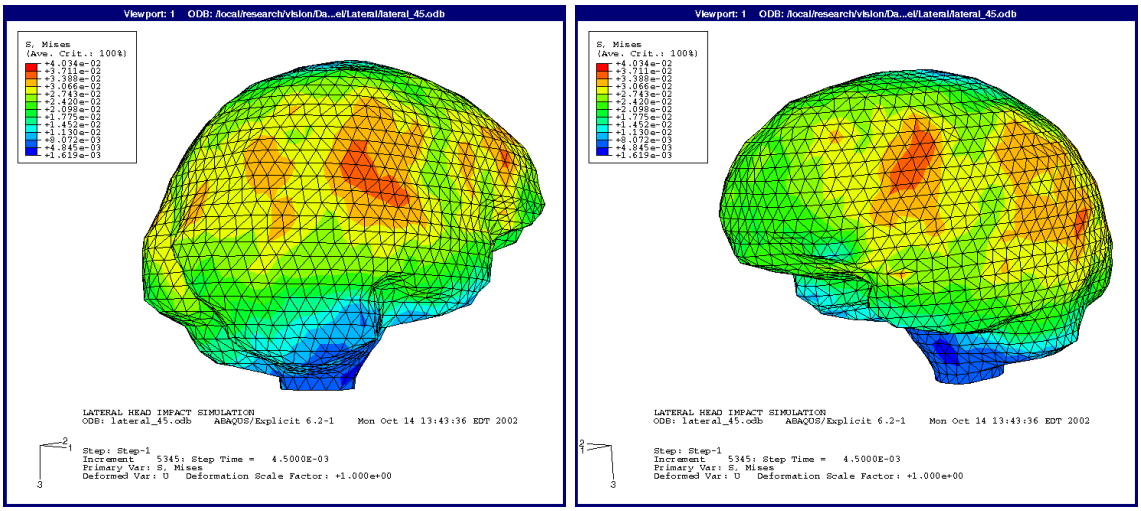

Figure 2-28 Lateral Impact 45º - von Mises Stress Distribution

Given the significantly high shear stress risk factor (i.e. > 2) for 30º and 45º lateral impacts, a diffuse axonal injury appears to be the most probable form of injury. See Figure 2-23 through Figure 2-28. While a contusion or subdural hematoma may be caused by pressure at the site of impact for 0º or 15º, this does not appear to be an injury mechanism for 30º or 45º. At 30º and 45º, there is far more rotation of the brain relative

www.manaraa.com

to the skull as compared with frontal, posterior, and superior impacts at the same angles. Given the overall magnitude of shear stress around the brain, a global injury to the brain appears to be the only basis for injury. Therefore, the diffuse axonal injury appears to be the most realistic type of injury for all of the lateral impacts. A diffuse axonal injury, in the form of a severe concussion, for 0º and 15º impacts would probably cause immediate loss of consciousness. A diffuse axonal injury, in the form of severe global bleeding, for 30º and 45º impacts could cause immediate loss of consciousness, rapid neurological dysfunction, and death. Figure 2-29 is a cross-sectional view of the shear stress distribution that indicates how a lateral impact at 45º produces a great deal of displacement of the brain relative to the skull. Also, with the exception of a small area in the center of the brain, the majority of the cerebral hemispheres are at a shear stress risk factor > 1.

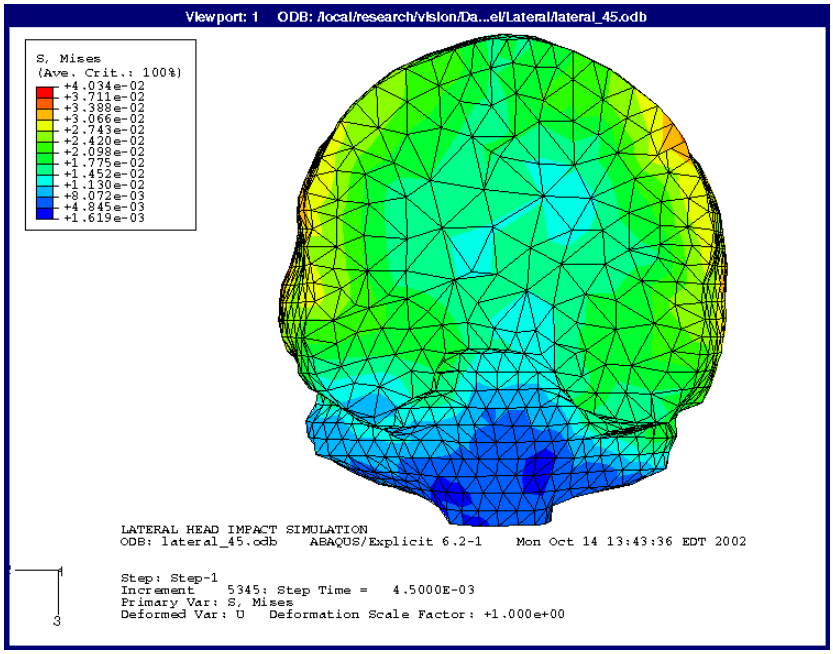

Figure 2-29 Lateral Impact 45º, Cross-Section View

www.manaraa.com

2.11 Posterior Impact

From the posterior impact FE results, there is also no surprise for intracranial pressure results at an angle of 0º. Raun et al [7] also modeled a posterior impact in the anterior-posterior direction, and show similar pressure distributions [7]. The pressure distribution for a 0º impact is similar in nature to frontal and superior impacts in that the pressure is uniformly distributed. The pressure severity index of 3 on the coup side and 2 on the contrecoup side coincides with 0º frontal, lateral, and superior impacts. Since the shear stress risk factor is < 1 for 0º and 15º impacts, this indicates that these impacts produce mostly translation acceleration and very little angular acceleration. At 30º, the shear stress risk factor for the left posterior border of the frontal lobe and superior border of the temporal lobe is 1.23, indicating a shear related injury. Once the impact angle reaches 45º, the pressure severity index for the occipital lobe reduces from 3 to 2 and in the frontal lobe from 2 to 1. Shear stress at 45º continues to rise globally with the highest risk factor around the left posterior border of the frontal lobe and superior border of the temporal lobe at 1.65.

www.manaraa.com

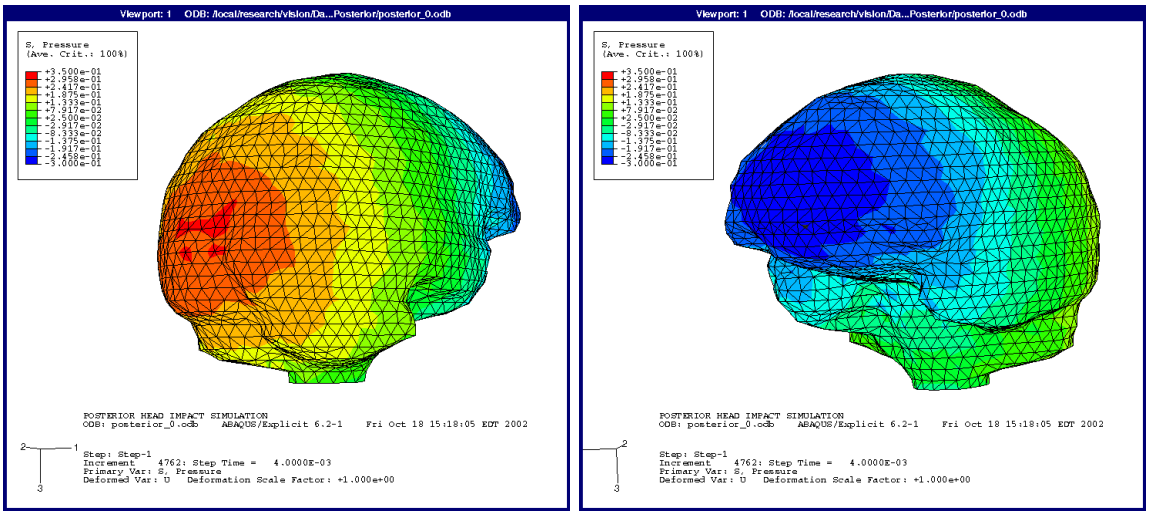

Figure 2-30 Posterior Impact 0º - Pressure Distribution

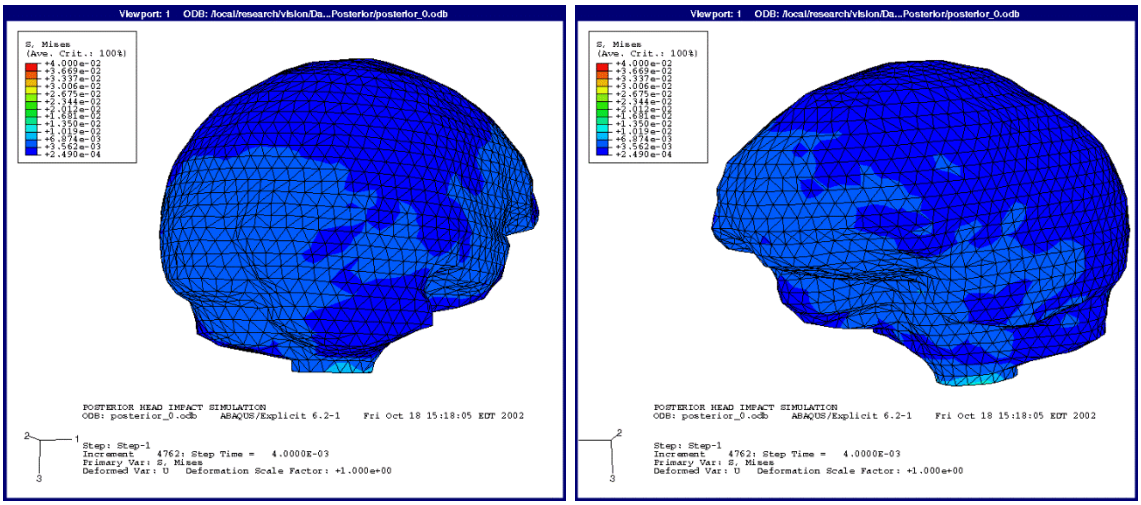

Figure 2-31 Posterior Impact 0º - von Mises Stress Distribution

An interesting point to note is the location of the maximum shear stress. For the posterior impacts, the head is traveling in the posterior direction from left to right. Therefore, the impact force vector on the head is directed in the posterior to anterior direction from right to left. The peak positive pressure indicates the impact site, but the peak shear stress is located approximately opposite the site of impact. As previously seen with frontal

www.manaraa.com

impacts, peak pressure is located on the coup side and maximum shear around the contrecoup side. Therefore, from the results in Figure 2-34 and Figure 2-35, it appears an oblique posterior impact of 30º has the potential of producing coup injury in the occipital lobe in the form of a contusion and a contrecoup injury in the frontal lobe in the form of a surface contusion or subdural hematoma. A contusion at 0º, and a surface contusion or subdural hematoma at 30º would probably be fatal given the high severity index and shear stress risk factor respectively. Figure 2-38 is a cross-sectional view through the high shear stress risk factor area of the left posterior border of the frontal lobe showing the shear stress distribution through the depth of the brain. Note the high risk factor shear stress is along the outer surface of the brain near the subdural space.

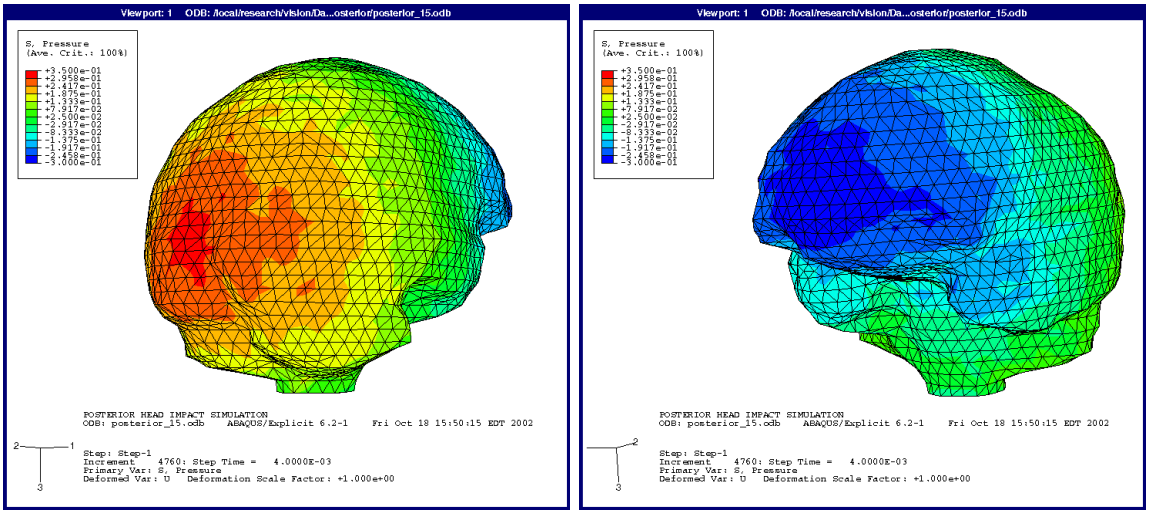

Figure 2-32 Posterior Impact 15º - Pressure Distribution

www.manaraa.com

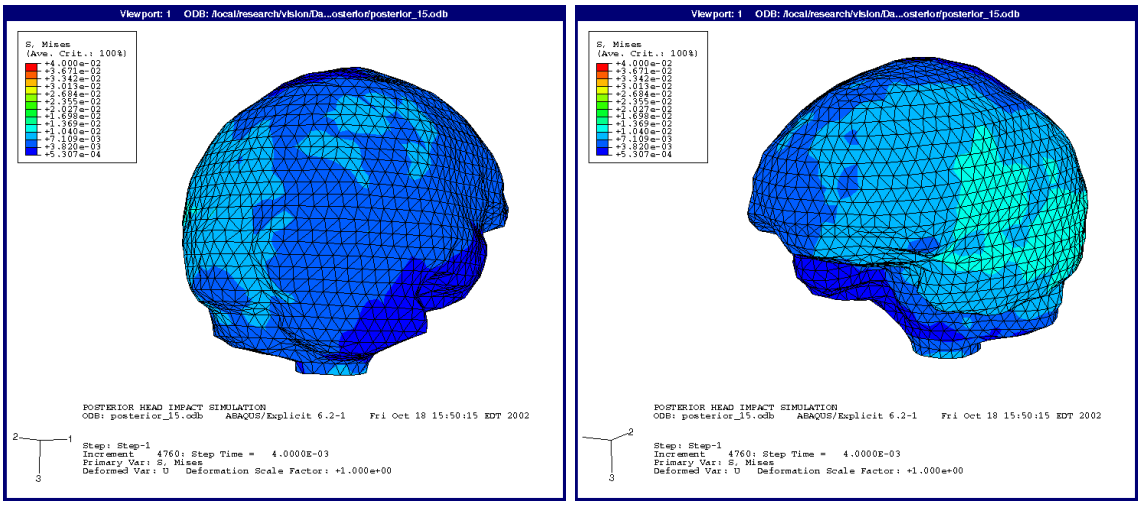

Figure 2-33 Posterior Impact 15º - von Mises Stress Distribution

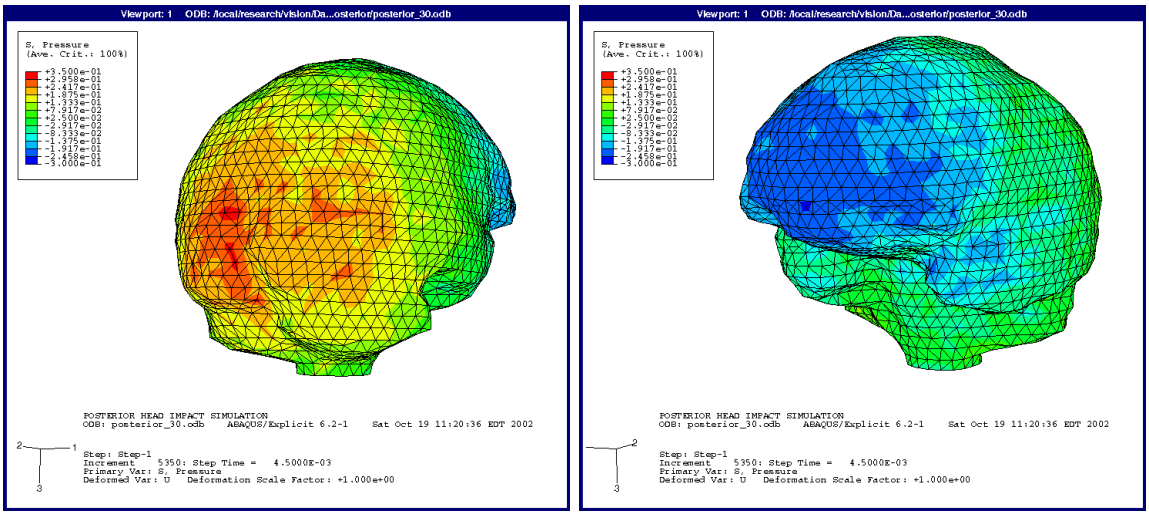

Figure 2-34 Posterior Impact 30º - Pressure Distribution

www.manaraa.com

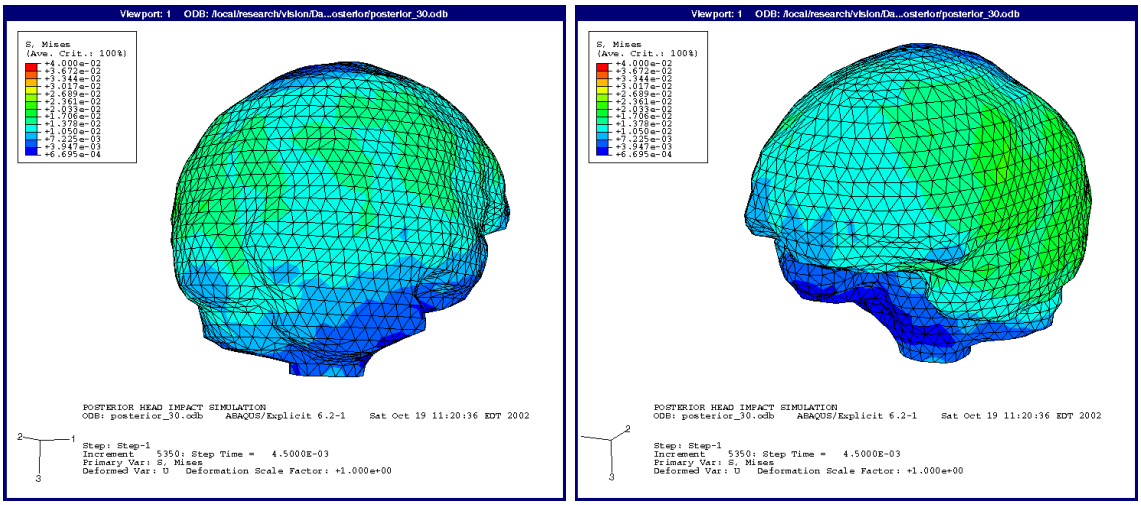

Figure 2-35 Posterior Impact 30º - von Mises Stress Distribution

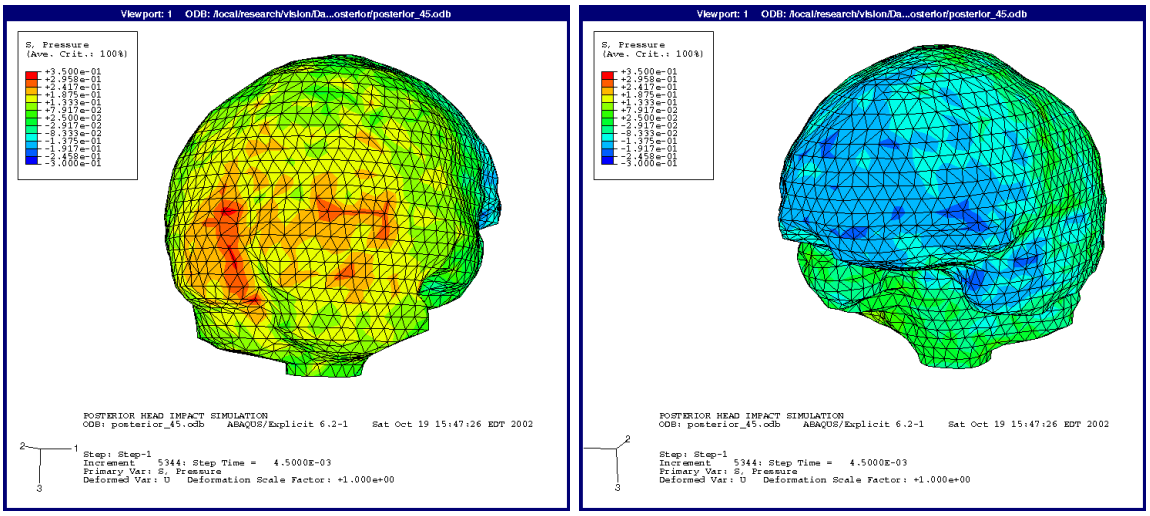

Figure 2-36 Posterior Impact 45º - Pressure Distribution

www.manaraa.com

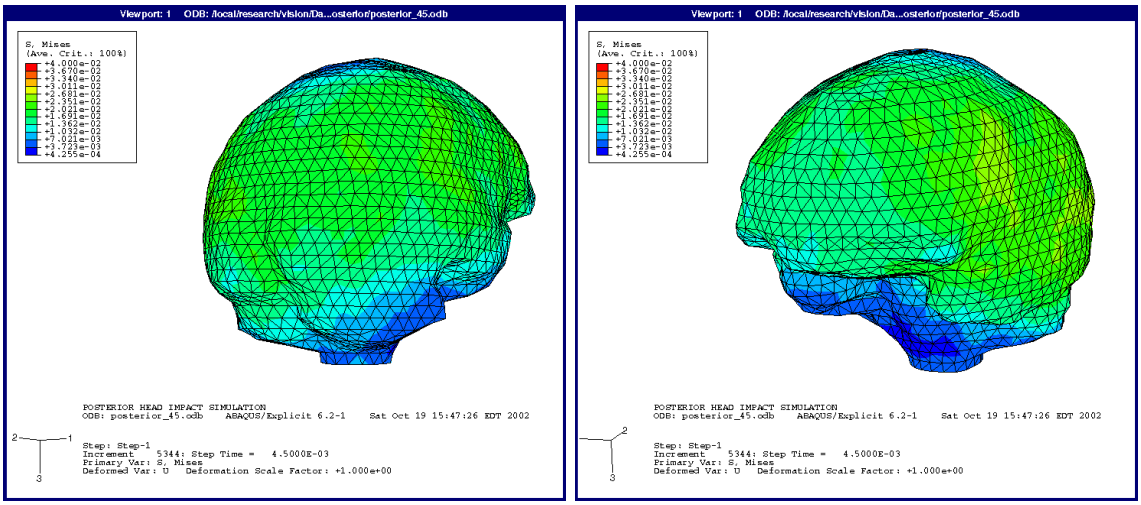

Figure 2-37 Posterior Impact 45º - von Mises Stress Distribution

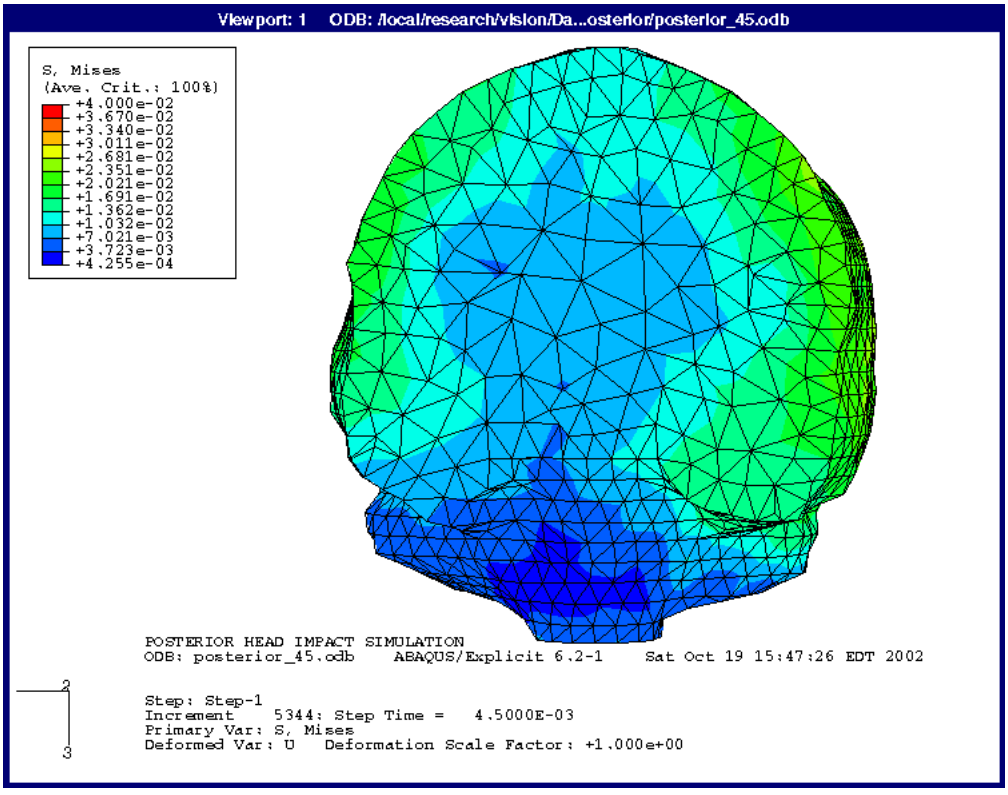

Figure 2-38 Posterior Impact 45º, Cross-Section View

www.manaraa.com

2.12 Superior Impact

From the FE results of a 0º superior impact, intracranial pressures coincide with frontal, lateral, and posterior impacts for a severity index of 3 for coup pressure and 2 for contrecoup pressure. The pressure distribution is also uniformly distributed as seen in Figure 2-39 with frontal and posterior 0º impacts. Since the pressure severity index does not change for impacts of 0º and 15º, this indicates these impacts produce mostly translation acceleration and very little angular acceleration, as seen with frontal and posterior of 0º and 15º. As the angle of impact increases, in the sagittal plane, the pressure decreases and moves towards the frontal lobe. This is due to the impact force spinning the head in a backwards direction. At an impact angle of 45º, the severity index for coup pressure is rated at 2, or a moderate injury, and is no longer severe.

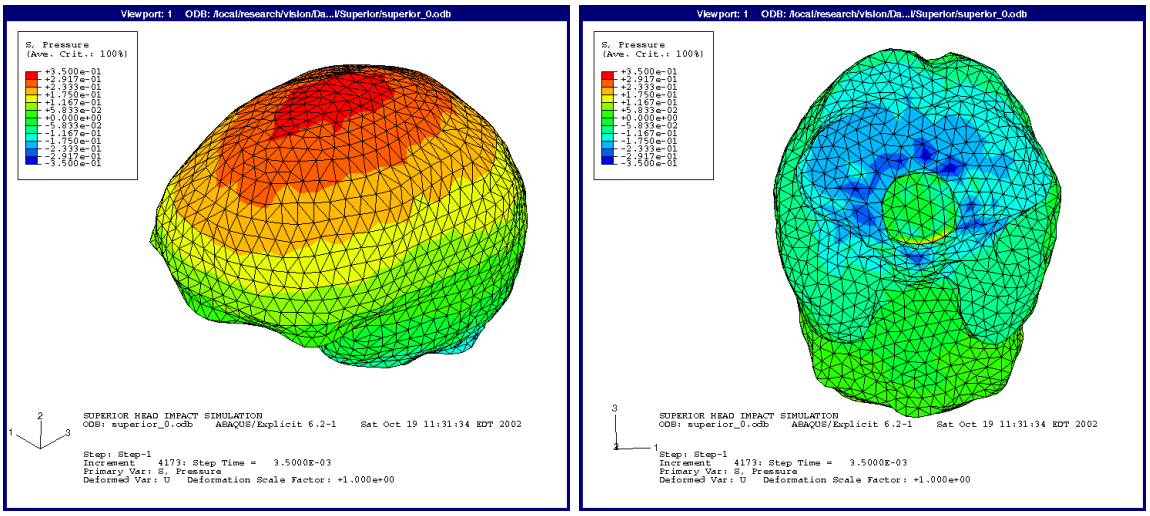

Figure 2-39 Superior Impact 0º - Pressure Distribution

www.manaraa.com

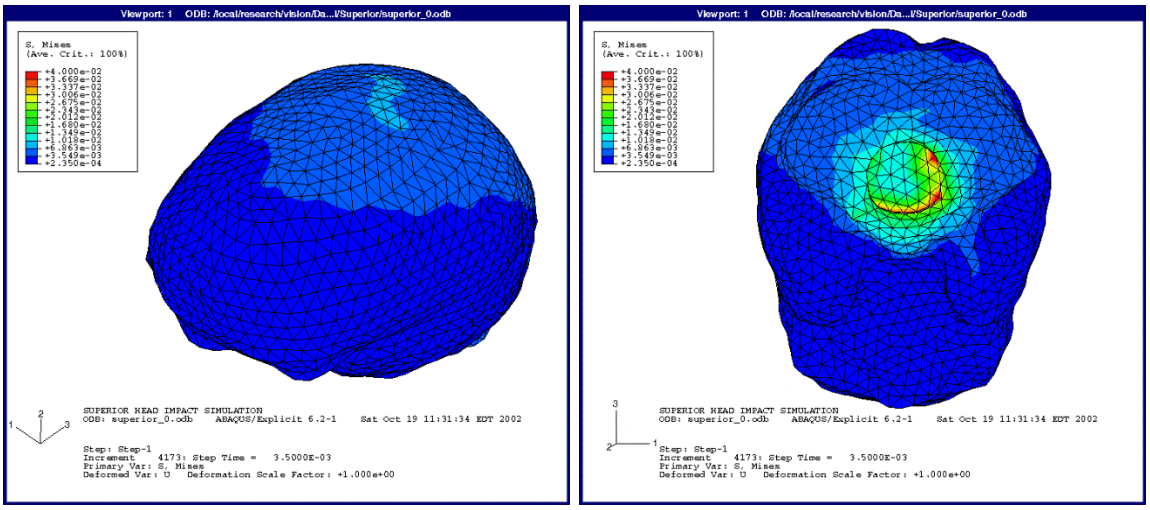

Figure 2-40 Superior Impact 0º - von Mises Stress Distribution

Shear stress in Figure 2-40, on the other hand, is quite different from frontal and posterior impact simulations. The shear stress risk factor in the brain stem region is > 2, and remains at this level for all superior impact angles. High shear stress in the brain stem is caused by the spinal cord being pulled through the foramen magnum of the skull into the cranial vault. For 0º and 15º impacts, the shear stress risk factor is < 1 in the frontal, temporal, parietal, and occipital lobes. At 30º, the shear stress risk factor in the superior parietal lobe is 1.03, which is just at the injury tolerance and predicts an injury due to shear. Once the angle of impact reaches 45º, the shear stress risk factor in the superior parietal lobe is 1.23, while the frontal, temporal and occipital lobes are < 1.

www.manaraa.com

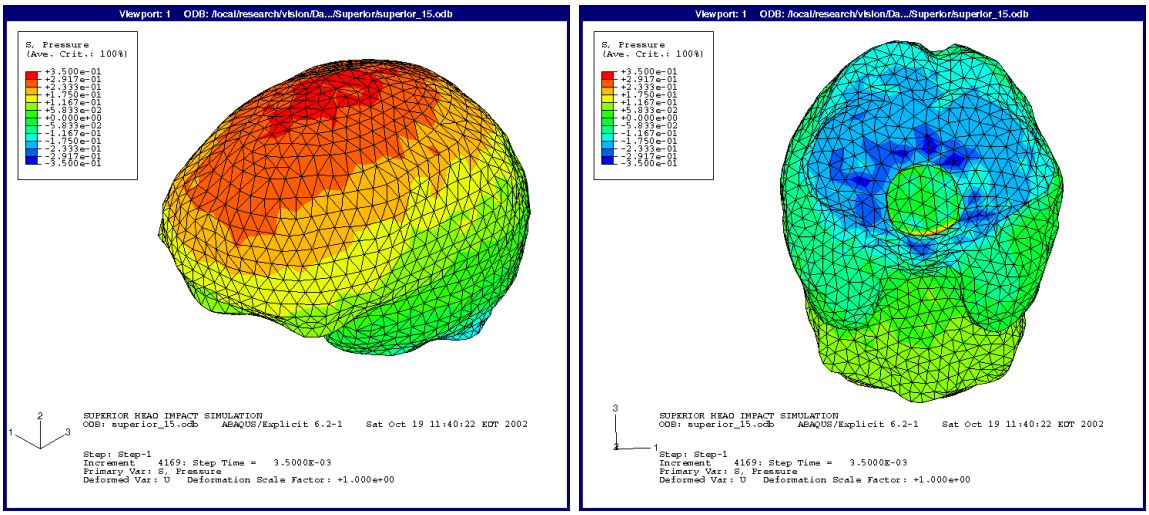

Figure 2-41 Superior Impact 15º - Pressure Distribution

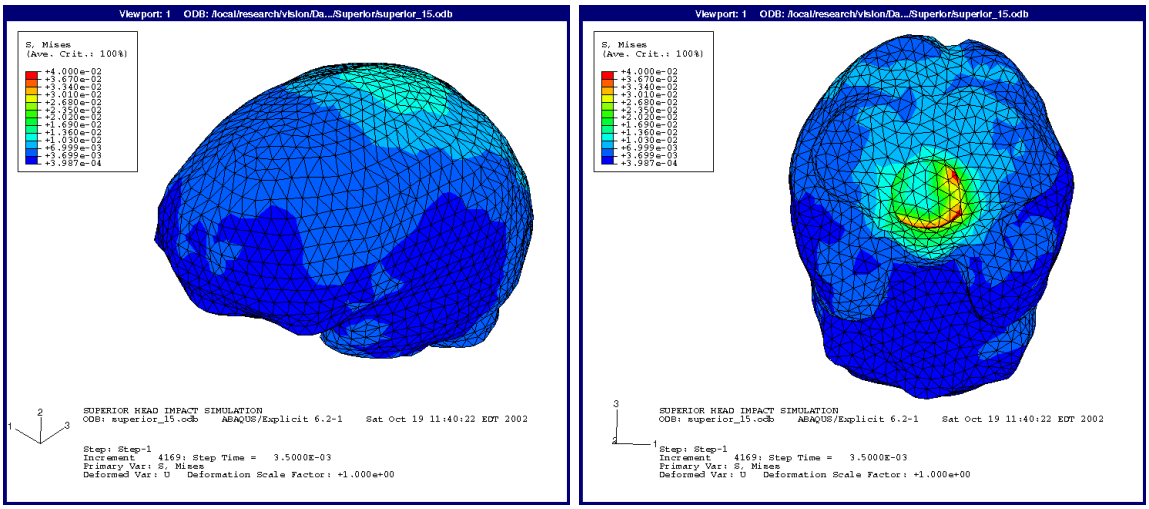

Figure 2-42 Superior Impact 15º - von Mises Stress Distribution

www.manaraa.com

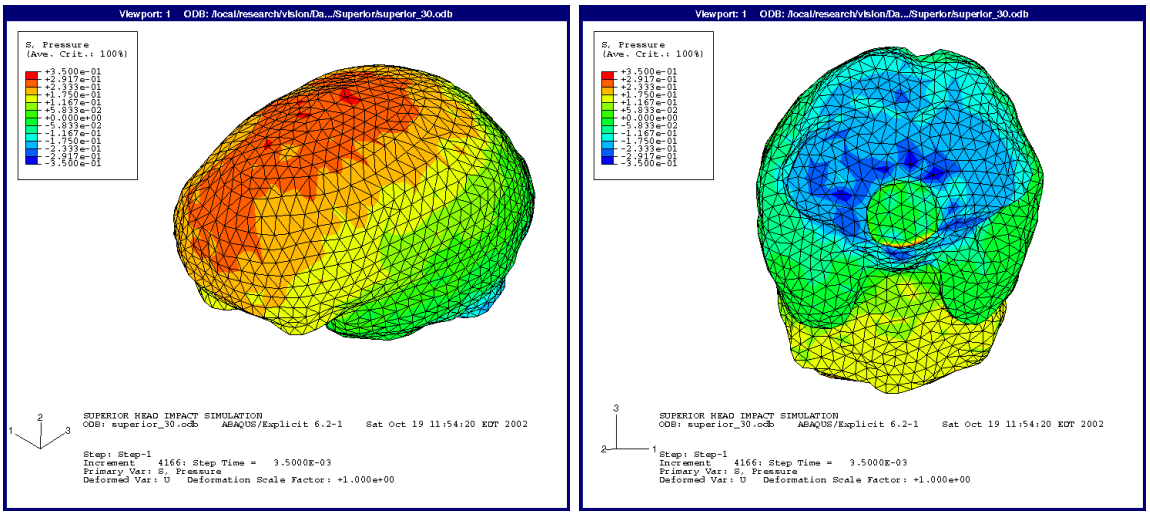

Figure 2-43 Superior Impact 30º - Pressure Distribution

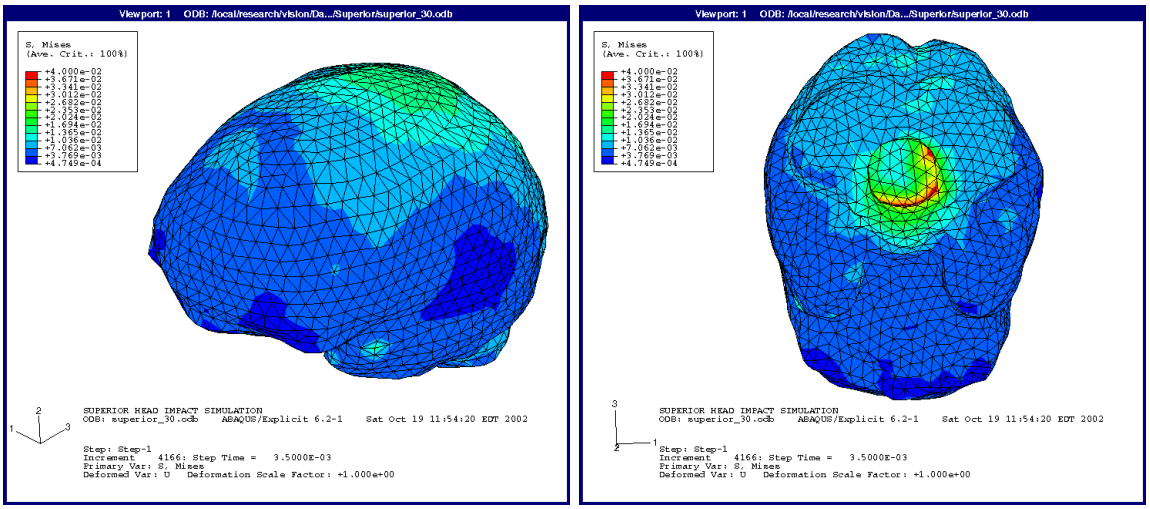

Figure 2-44 Superior Impact 30º - von Mises Stress Distribution

From the FE results, it can be concluded that all the superior impacts simulated could produce an injury to the brain stem due to a risk factor > 2. A brain stem injury with this high of a risk factor, if not fatal, would definitely cause problems with heart rate, blood pressure, breathing, vision, and reflexes to hearing just to name a few. In the frontal, temporal, and occipital lobes, however, no injury relative to shear would be predicted for

www.manaraa.com

all the impact angles simulated. At 30º and 45º impact angles, the shear stress risk factors in the superior parietal lobe are slightly > 1, indicating a possible injury related to shear, most likely in the form of a subdural hematoma. See Figure 2-44 and Figure 2-46. The subdural hematoma, given the location in the parietal lobe, could cause problems with visual attention, touch perception, or manipulation of objects to name a few. Contusions on the coup side, or superior frontal lobe, would be possible with impact angles of 0º and 15º and have the potential of being fatal.

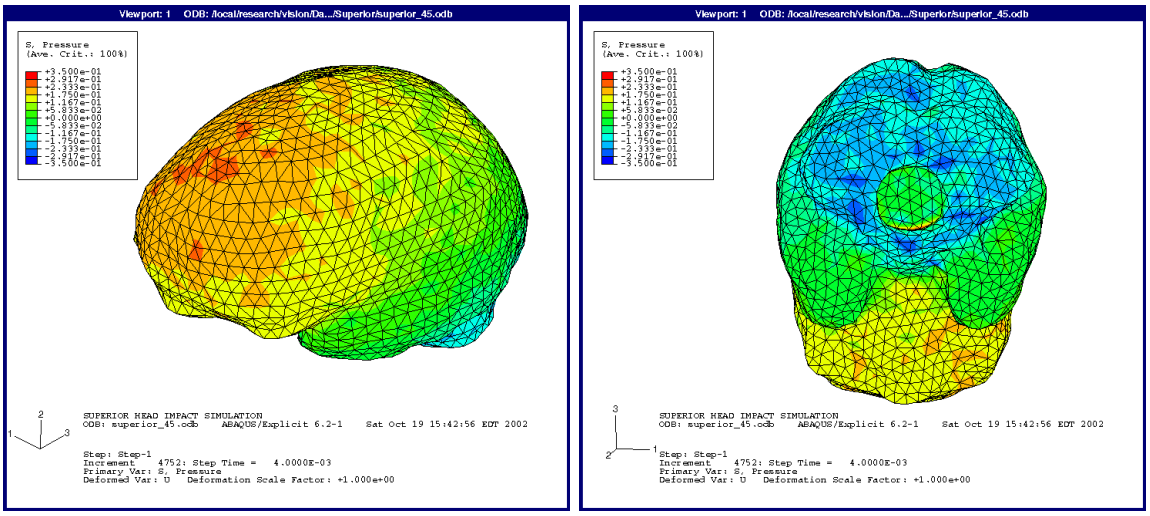

Figure 2-45 Superior Impact 45º - Pressure Distribution

www.manaraa.com

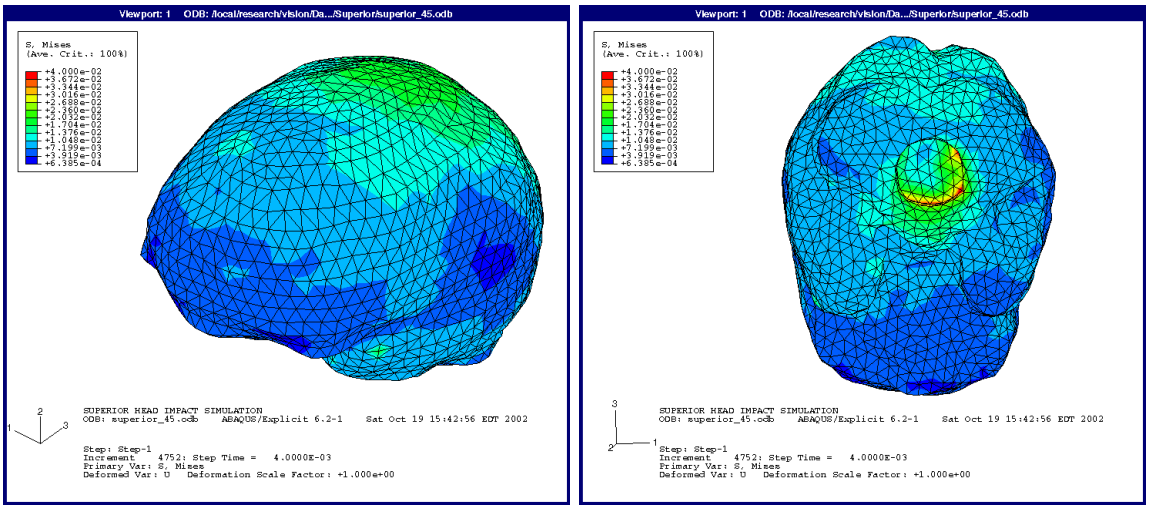

Figure 2-46 Superior Impact 45º - von Mises Stress Distribution

2.13 Conclusion For Head Impacts

For the first question listed at the beginning of this chapter, the following responses are discussed:

- Is there a critical angle of oblique impact at the given site on the head which will cause the shear stress in the brain to reach a concussion tolerance?

2.13.1 Frontal Impact – Shear Stress Risk Factor

For frontal impacts, the shear stress risk factor doesn't reach a concussion tolerance level greater than 1 until 30°, in the right temporal lobe at a value of 1.4 Once the angle is increased to 45°, globally the shear stress risk factor is 1.26 and locally at 1.65 in right temporal lobe.

2.13.2 Side Impact – Shear Stress Risk Factor

For side impacts the shear stress risk factor reaches a concussion tolerance level at 0°. At 0°, the shear stress risk factor is 1.05 in temporal lobe, occipital lobe, and parietal lobe.

www.manaraa.com

At a 15° impact angle, the shear stress risk factor increases to 1.65. At 30°, shear stress risk factor is 1.84. Once the angle of impact increases to 45°, the shear stress risk factor increases to a level greater than 2. From the results, the side impact is clearly produces the highest stress levels around the brain.

2.13.3 Posterior Impact – Shear Stress Risk Factor

For posterior impacts the shear stress risk factor doesn't reach a concussion tolerance level that is greater than 1 until 30° in the left temporal lobe at a value of 1.05. For an impact of 45° the shear stress risk factor in the left temporal lobe increases to a value of 1.23.

2.13.4 Superior Impact – Shear Stress Risk Factor

For superior impacts, the shear stress risk factor in the brain stem, for all impacts 0° to 45°, is greater than 2.0. Globally, specifically in the parietal lobe of the brain, the shear stress risk factor reaches a value of 1.23 once the angle of impact increases to 45°..

For the second question listed at the beginning of this chapter, the following responses are discussed:

- Is there any relationship between the peak pressure and peak shear stress distribution at each site of oblique impact on the head to identify a critical angle for a given site?

www.manaraa.com

2.13.5 Frontal Impacts – Peak Pressure and Peak Shear Stress

For all frontal impacts, the peak positive pressure, or compression, is located at the site of impact and peak negative pressure, or tension, is located opposite the site of impact. This is true for all angles of impact. For the location where the shear stress risk factors increase greater than 1, however, they are located on the temporal lobe, or the lateral side of the head.

2.13.6 Side Impacts – Peak Pressure and Peak Shear Stress

For all side impacts, the peak positive pressure, or compression, is located at the site of impact and peak negative pressure, or tension, is located opposite the site of impact. This is true for all angles of impact. Although the pressure distributions are not as well defined for the side impacts as they are for the frontal, posterior, and superior impacts. For the location where the shear stress risk factors increase greater than 1, however, they are located around the entire perimeter of the brain, regardless of the angle of impact.

2.13.7 Posterior Impacts – Peak Pressure and Peak Shear Stress

Posterior impacts follow the same trend as frontal impacts where, the peak positive pressure, or compression, is located at the site of impact and peak negative pressure, or tension, is located opposite the site of impact. For the location where the shear stress risk factors increase greater than 1, however, they are located on the temporal lobe, or the lateral side of the head.

www.manaraa.com

2.13.8 Superior Impacts – Peak Pressure and Peak Shear Stress

Superior impacts follow the same trend as frontal and posterior impacts where, the peak positive pressure, or compression, is located at the site of impact and peak negative pressure, or tension, is located opposite the site of impact. A unique result with superior impacts shear stress risk factors locations is that the risk factor is always greater than 2 in the brain stem region. The parietal lobe sees a shear stress risk factor, near the site of impact, at 1.23 only until the angle of impact is increased 45°.

www.manaraa.com

3 TBI Dynamics due to Head Impacts on the Football Field

3.1 Objective

The main objective of this study is to contribute to the field of youth TBIs. Specifically, this study will address the following questions:

- Do angular accelerations of the head play a prominent role in causing TBI along with linear accelerations of the head?
- Can a TBI criterion be derived through their relation?
- Do TBIs causing high stress concentrations also cause detectable structural damage (i.e.: coup, countercoup, diffuse axonal injuries) in the brain tissue?
- Do impact tolerances change with respect to impact regions of the human head?

3.2 Relevance of Research

Earlier studies of head impacts have related head kinematics (linear and angular accelerations) to TBIs, however, fewer studies have dealt with brain kinetics (impact pressures and shear stresses) occurring during head impacts. In order to study the effect of angular acceleration on the brain a series of experimental tests were performed [11].

www.manaraa.com

The National Operating Committee on Standards for Athletic Equipment (NOCSAE) drop tests [9] were conducted for linear head accelerations and the Head Impact Contact Pressures (HICP) calculated from them are applied to a validated FE head model.

3.3 Methods and Materials Used to Achieve Results

To address these questions, following milestones were established:

- Propose to conduct NOCSAE drop tests to acquire linear accelerations of the head and head contact impact pressures.
- Carry out analytical procedures to determine impact contact pressures and angular accelerations of the head from available linear accelerations and headform dimensions.
- For various impact regions, determine the relationship between linear and angular accelerations (at specific drop heights) of the head.

3.4 NOCSAE Drop Tests

The experimental method used to acquire linear accelerations of the head and head contact impact pressures was to use the NOCSAE drop tester at MTU. The NOCSAE drop tester is equipped with a tri-axial accelerometer to measure the impact event. The standard NOCSAE drop tester comes with a Severity Index Computer to report the peak acceleration and calculate the corresponding severity index from the impact event [9]. A

www.manaraa.com

Siglab data acquisition system was used to record the impact time history event, that could be used for input for the FE head model. Impact locations for the frontal, lateral, posterior, and front boss (or 45° to the frontal region) were measured.

Figure 3-1 NOCSAE Standard Drop Tester at MTU based upon NOCSAE Standard Drop Test Equipment [9]

www.manaraa.com

In addition to the measured accelerometer impact time histories, impact pressure measurements were also recorded through the use of Fuji Prescale pressure film (provided by Sensor Products, Inc.) [10]. The pressure film is a Mylar based film that contains a layer of microcapsules that rupture upon contact. See Figure 3-2. The resulting outcome is a pressure image across the contact area where the color contrast directly correlates to the pressure gradient. The color contrast can be determined by scanning the exposed film in a Topaq analyzer scanner to determine the resulting pressure gradient.

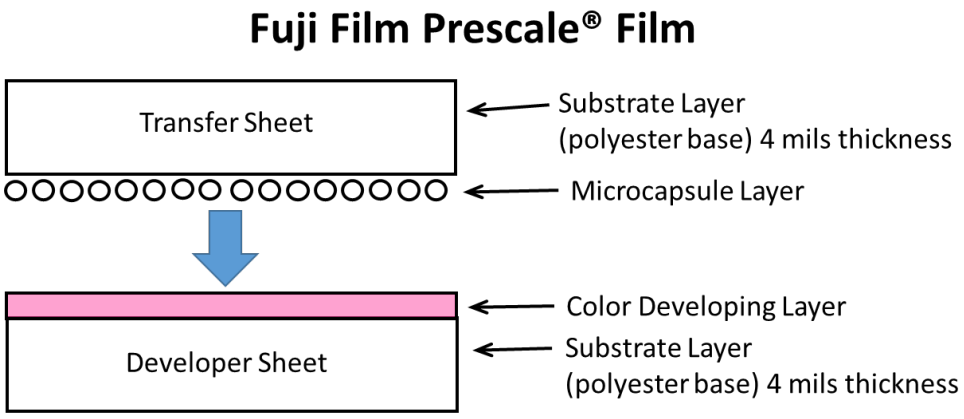

Figure 3-2 Representation of Fujifilm Prescale that is available from Sensor Products Inc. [10]

www.manaraa.com

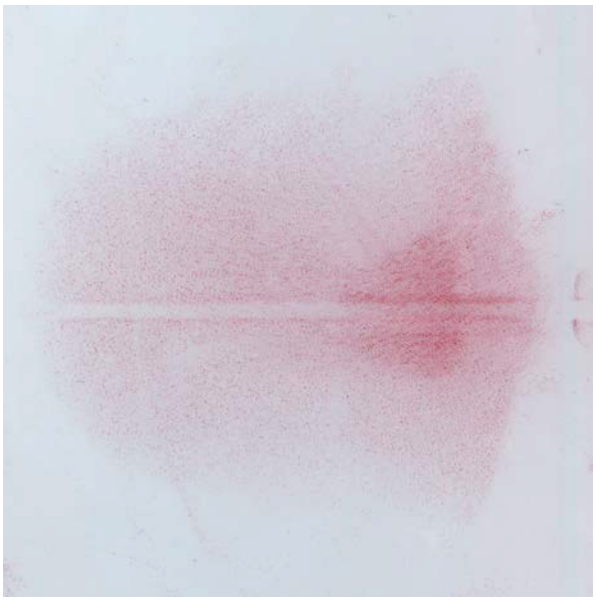

Figure 3-3 Exposed Fujifilm from 2 Foot Drop - Experimental Results [11]

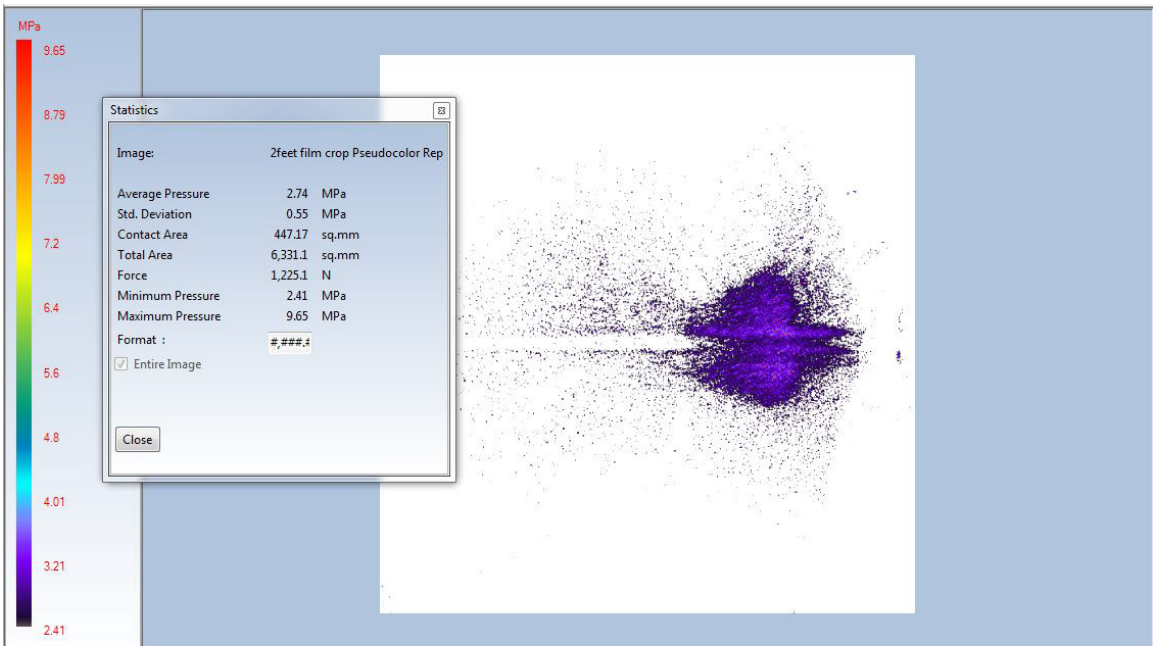

Figure 3-4 Digitized Pressure Results of Exposed Fujifilm [11]

Although this method has some validity for obtaining maximum impact pressure, the pressure contour was not well enough defined to obtain an average value for use as an

www.manaraa.com

input for the FE head model. In addition, another issue with using the pressure film was the film is only good for a single impact. With the drop tester there are additional rebound impacts that occur after the initial impact that potentially introduce additional reading errors. The impact pressure images were, however, useful in determining impact areas and served useful in correlating the analytical method.

3.5 Analytical Procedures to Determine Impact Pressure

An alternative approach to obtain the average pressure input for the FE head model was employed by using the experimental results of the drop test where the impact area and acceleration time history were used to calculate an average pressure measurement [11]. This average pressure measurement was used for the input for the FE model. Using the equation:

$$P = \frac{m_{headform} \cdot \vec{a}_{droptest}}{A} \qquad (3.1)$$

Where:

P = Head Impact Contact Pressure (HICP)

$m_{headform}$ = mass of the head form

$\vec{a}_{droptest}$ = linear acceleration time history from drop test experiment.

A = area of impact measured from the pressure film.

www.manaraa.com

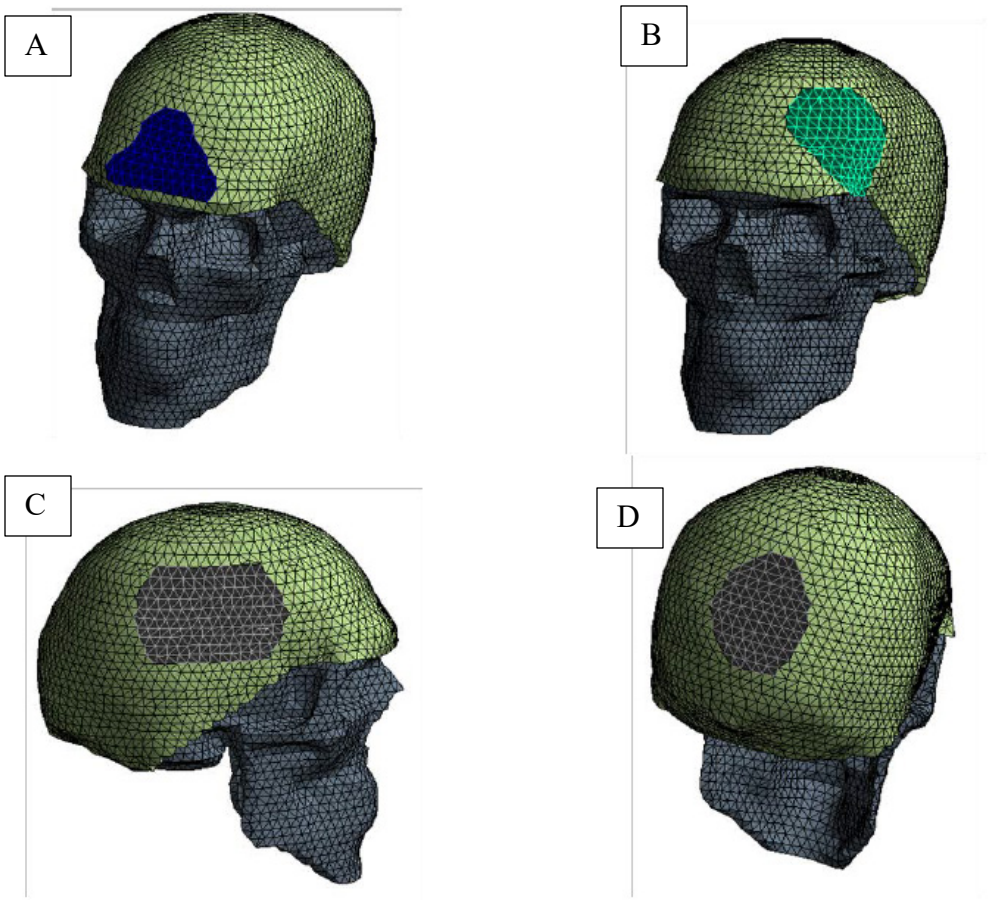

Figure 3-5 Impact Pressure Areas on the Frontal (A), Front Boss (B), Lateral (C), and Posterior (D) Regions of the FE Model [11]

The impact regions that were obtained from the NOCSAE drop test experiments were then applied to the validated FE model of the 50th percentile human male. The areas shown in Figure 3-5 were manually applied to the FE head model. [11]

www.manaraa.com

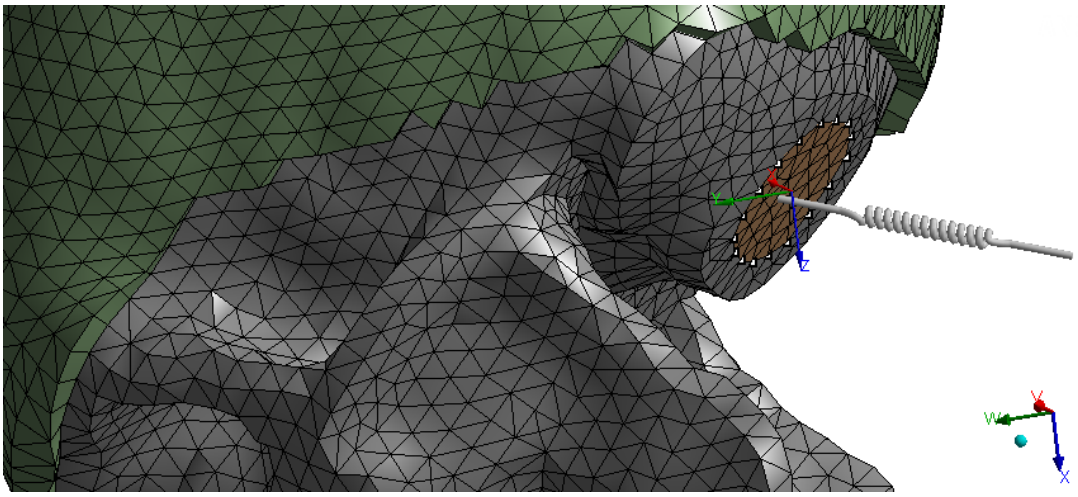

Figure 3-6 Spring Element Added to Base of Skull [11]

To simulate the connection of the neck, a spring element was added to the base of the skull around the brain stem as seen in Figure 3-6. The addition of this spring element not only adds a boundary condition to the model, but helps to simulate the stiffness offered by the presence of the neck. Chandrika Abhang also added a remote measurement point to the base of the skull, at the brain stem opening seen in Figure 3-7. The remote point was used to obtain acceleration measurements of the FE head model. [11]

www.manaraa.com

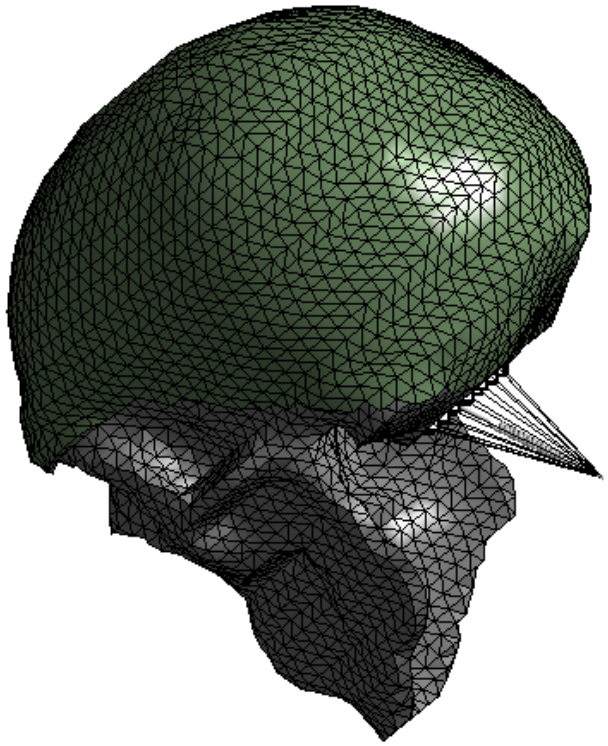

Figure 3-7 Remote Measurement Point Relative to the Base of the Skull [11]

3.6 Simplified Analytical Procedure to Determine Rotational Acceleration

Because the NOCSAE drop tester measures linear acceleration, a method for obtaining the calculated rotational acceleration is determined by using the following equation [11]:

$$\vec{F} = m_{headform} \cdot \vec{a}_{droptest} \qquad (3.2)$$

Where: $\vec{F}$ = Impact force

$m_{headform}$ = mass of headform

$\vec{a}_{droptest}$ = measured linear acceleration of drop test

www.manaraa.com

$$\vec{T} = I \cdot \vec{\alpha} \qquad (3.3)$$

Where: $\vec{T}$ = torque or moment

I = mass moment of inertia

$\vec{\alpha}$ = angular acceleration

The torque or moment is also expressed as the cross product of the position and force vector, by the equation [11]:

$$\vec{T} = \vec{r} \cdot \vec{F} \qquad (3.4)$$

Where: $\vec{r}$ = position vector from the axis of rotation to the point of impact

$\vec{F}$ = impact force

By substituting the values of r_x, r_y, and r_z and values of F_x, F_y, and F_z the torque values T_x, T_y, and T_z can be calculated.

By substituting the calculated values of torque into equation (3.3) the resulting angular acceleration can be calculated by the equation [11]:

$$\vec{\alpha} = \frac{\vec{T}}{I} \qquad (3.5)$$

www.manaraa.com

Which results in the angular acceleration about the X, Y, and Z axis by:

$$\alpha_{xx} = \frac{T_x}{I_{xx}} \qquad (3.6)$$

$$\alpha_{yy} = \frac{T_y}{I_{yy}} \qquad (3.7)$$

$$\vec{\alpha}_{zz} = \frac{T_z}{I_{zz}} \qquad (3.8)$$

Where: α_{xx}, α_{yy}, and α_{zz} are the angular accelerations components with respect to the X, Y, and Z axes.

The resulting angular acceleration, α_R, is calculated by the following equation [11]:

$$\alpha_R = \sqrt{\alpha_{xx}^2 + \alpha_{yy}^2 + \alpha_{zz}^2} \qquad (3.9)$$

3.7 Relationship between Linear and Rotational Acceleration

Figure 3-8 through Figure 3-11 show the experimental and analytical results taken by Chandrika Abhang [11]. Plotted in these figures are the linear acceleration results calculated from the pressure area measurements, linear acceleration experimental results from the NOCSAE drop tester and Siglab data acquisition system, and the calculated angular acceleration results.

www.manaraa.com

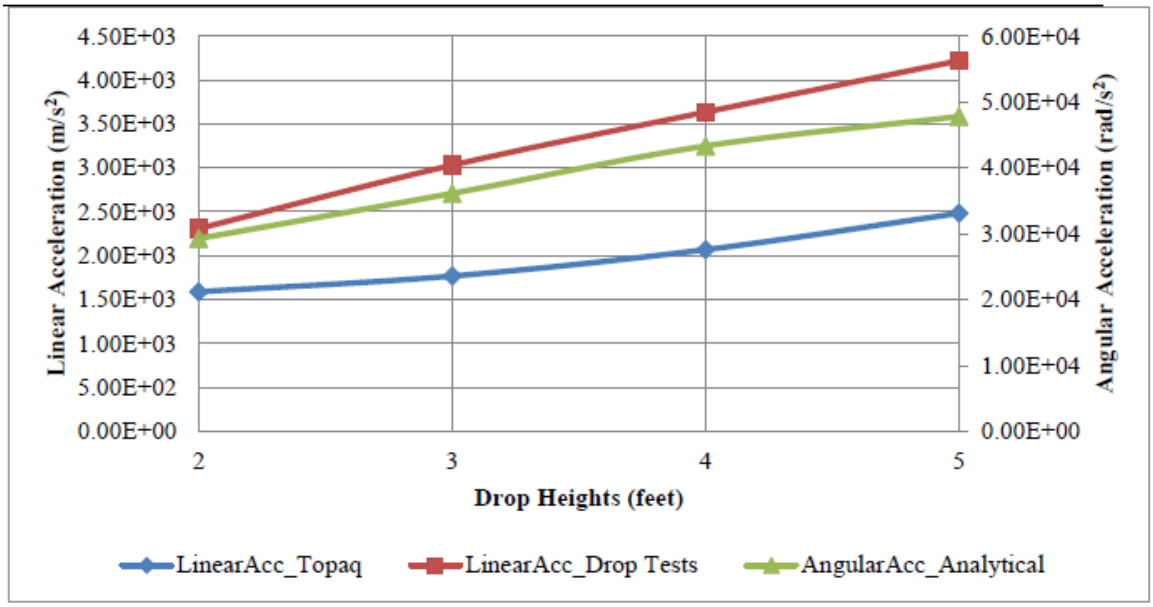

Figure 3-8 Frontal Impact Acceleration Results [11]

The linear acceleration calculated from the pressure measurements underestimates the linear acceleration of the linear acceleration from the experimental tests. This is due to the discrepancy between the calculated area of impact for pressure measurement.

www.manaraa.com

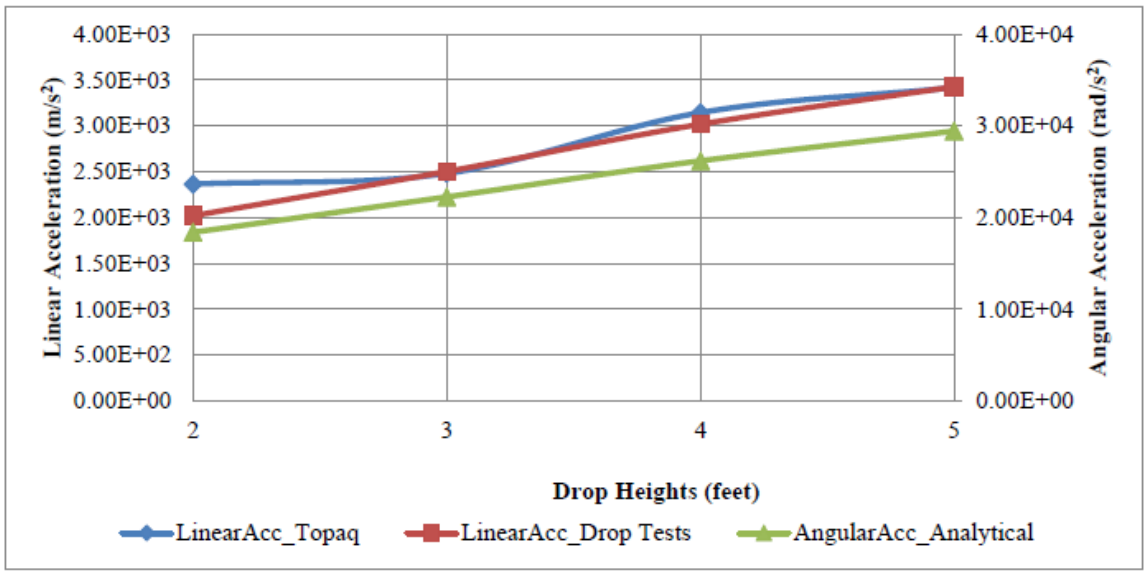

Figure 3-9 Front Boss (45° to frontal) Impact Acceleration Results [11]

With the front boss acceleration results seen in Figure 3-9, the calculated linear acceleration closely agrees with the drop test linear acceleration.

In Figure 3-10 and Figure 3-11, the calculated linear acceleration over estimates the linear acceleration obtained from the drop test linear acceleration. The discrepancy between calculated linear acceleration and experimental linear acceleration is due to the measurement error in pressure calculation in both cases.

www.manaraa.com

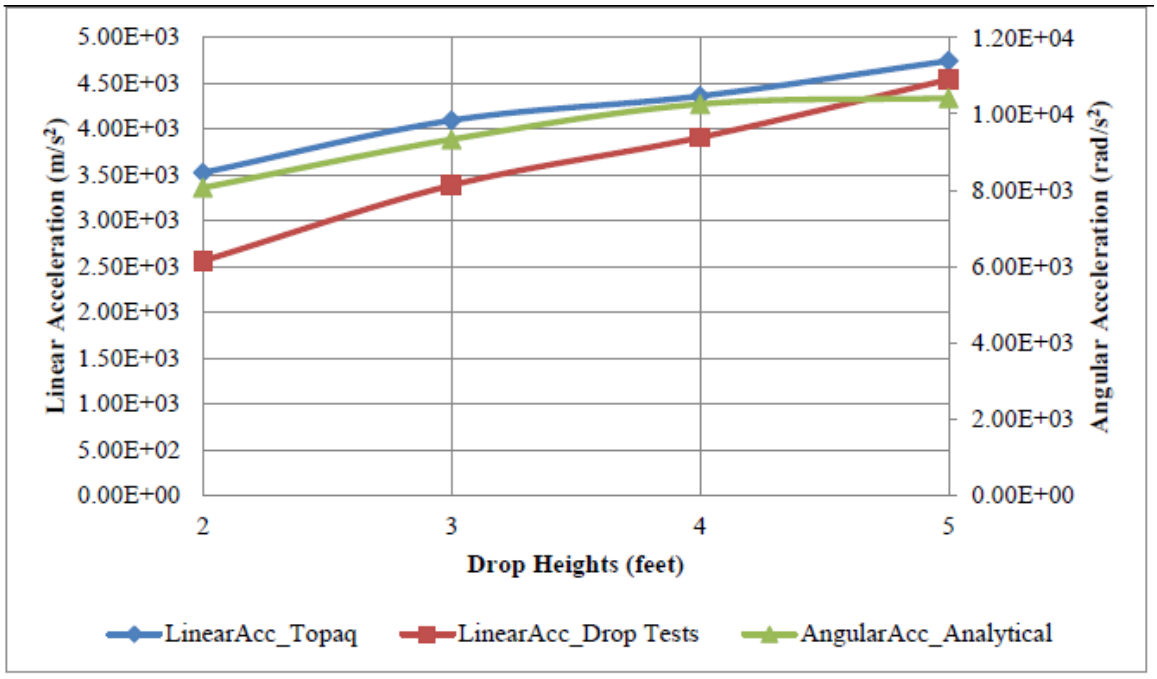

Figure 3-10 Lateral Impact Acceleration Results [11]

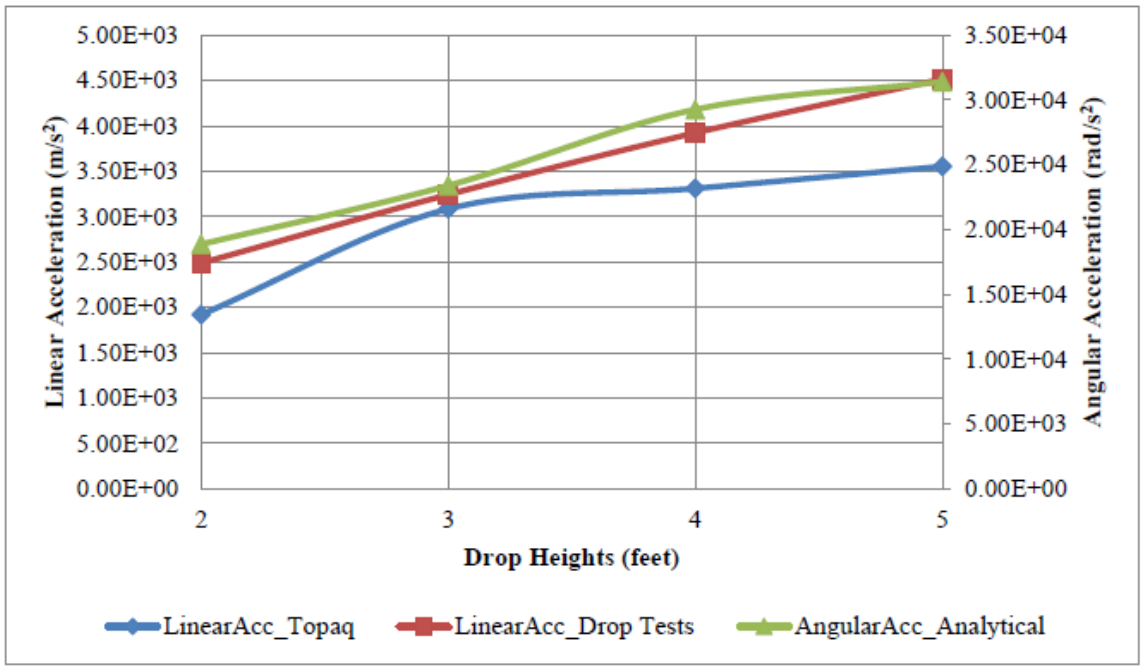

Figure 3-11 Posterior Impact Acceleration Results [11]

www.manaraa.com

It is proposed in this work to define a new concussion criteria which combines the effects of linear and angular acceleration. Concussion criteria is defined as:

$$\frac{a_{regional}}{a_{TBI\,(\max)}} + \frac{\alpha_{regional}}{\alpha_{TBI(\max)}} \leq 1\ then\ no\ TBI \qquad (3.10)$$

Where:

$a_{regional}$ = linear impact acceleration for a specific impact region and drop height.

$a_{TBI(\max)}$ = TBI tolerant linear impact acceleration (318 G's) [12]

$\alpha_{TBI(\max)}$ = angular impact acceleration for a specific impact region and drop height.

$\alpha_{TBI(\max)}$ = TBI tolerant angular impact acceleration (23 krad/s^2) [12]

In order to use the equation above to determine the tolerance level for TBI likelihood, the results from the linear acceleration and angular acceleration are used. Since impacts on the head are a combination of linear and angular acceleration, the equation above is used to determine what contribution is due to each. The reported TBI tolerance level due to linear acceleration has been proposed by [12] at 318 G's and angular acceleration TBI tolerance level due to angular acceleration at 23 krad/s^2 [12]. By using the equation above, along with the analytical results of the FE model, a determination can be drawn from the impact results.

www.manaraa.com

Table 3-1 TBI Tolerance Results [11]

Frontal Impact					
Drop Height (ft)	**Linear Acceleration (G's)**	**Linear TBI Tolerance**	**Angular Acceleration (rad/s^2)**	**Angular TBI Tolerance**	**TBI Tolerance Level**
2	235	0.74	29273	1.27	2.01
3	309	0.97	36129	1.57	2.54
4	370	1.16	43319	1.88	3.05
5	430	1.35	47785	2.08	3.43
Lateral Impact					
Drop Height (ft)	**Linear Acceleration (G's)**	**Linear TBI Tolerance**	**Angular Acceleration (rad/s^2)**	**Angular TBI Tolerance**	**TBI Tolerance Level**
2	261	0.82	8066	0.35	1.17
3	345	1.08	9331	0.41	1.49
4	399	1.25	10254	0.45	1.70
5	463	1.46	10410	0.45	1.91
Front Boss (45° to frontal)					
Drop Height (ft)	**Linear Acceleration (G's)**	**Linear TBI Tolerance**	**Angular Acceleration (rad/s^2)**	**Angular TBI Tolerance**	**TBI Tolerance Level**
2	206	0.65	20888	0.91	1.56
3	255	0.80	25118	1.09	1.89
4	308	0.97	29575	1.29	2.25
5	349	1.10	33220	1.44	2.54
Posterior Impact					
Drop Height (ft)	**Linear Acceleration (G's)**	**Linear TBI Tolerance**	**Angular Acceleration (rad/s^2)**	**Angular TBI Tolerance**	**TBI Tolerance Level**
2	254	0.80	18875	0.82	1.62
3	331	1.04	23401	1.02	2.06
4	400	1.26	29268	1.27	2.53
5	460	1.45	31407	1.37	2.81

Shown in Table 3-1 are the resulting TBI tolerance levels for the analytical results. The results show the lateral region of the head as the most vulnerable region to damage from any from height or impact distance followed by the posterior region. What is interesting

www.manaraa.com

in all the measured results is that all of the resulting impacts have a total TBI tolerance value that is greater than 1, indicating the possibility of a TBI. If the measured values are measured separately, a false conclusion can be drawn showing a TBI tolerance less than 1, as in the case for all of the drop heights. This information is extremely important when evaluating the possibility of TBI and also in designing a football helmet that can minimize both linear and angular acceleration of the head.

www.manaraa.com

4 EBM Helmet Impact Energy Attenuator

The principal function of the EBM helmet is to minimize the risk of concussion injury to football players by absorbing head impact energy and reducing head translational and rotational accelerations. The Impact Energy attenuating (IEA) System of the EBM helmet is modelled to help protect the brain against impacts to the head. The IEA system of the EBM helmet, consists of four layers of four materials bonded together to diffuse, distribute, dissipate, and absorb impact force and shock energy. This effort is based on a finite element (FE) study of the impact response of FE model IEA systems of the EBM helmet and the currently available commercial helmet due to direct impacts.

4.1 Objective

- The development of a head Impact Energy Attenuator (IEA) for the EBM helmet.
- The head impact energy attenuating system of the EBM helmet is modelled to help protect the brain against impacts to the head.
- The IEA system of the EBM helmet, consists of four layers of four materials bonded together to diffuse, distribute, dissipate, and absorb impact force and shock energy.

www.manaraa.com

4.2 Relevance of Research

The current football helmet design involves a stiff plastic outer shell to distribute impact forces combined with an elastic foam inner shell to absorb the impact shock and to reduce the impact forces in order to minimize the risk of skull fractures. The National Operating Committee on Standards for Athletic Equipment (NOCSAE) provides a set of voluntary standards based on the Wayne State Tolerance Curve (WSTC) to assess a helmet's ability to prevent skull fracture. NOCSAE standards have helped to successfully eliminate skull fractures due to impacts in football games while wearing helmets designed with an impact distributor in the form of a stiff plastic outer shell and an impact attenuator in the form of an elastic foam inner shell [9].

Impacts on a helmet cause linear and angular accelerations of the head which bring forth pressure and shearing interactions between the skull and the brain resulting in concussion. The purpose of the EBM helmet is not only to minimize linear acceleration of the head to prevent catastrophic brain injury like hemorrhages, but also to minimize angular accelerations of the head to prevent concussion. Current helmet technology does provide adequate design provisions to attenuate normal impact forces, but it lacks design provisions to attenuate tangential impact forces.

www.manaraa.com

4.3 Methods and Material Used to Achieve Results

- Create a IEA finite element model of the commercial IEA system to determine the impact characteristics.
- Create a IEA finite element model of the proposed EBM IEA system to determine the impact characteristics.
- Compare the two IEA systems.

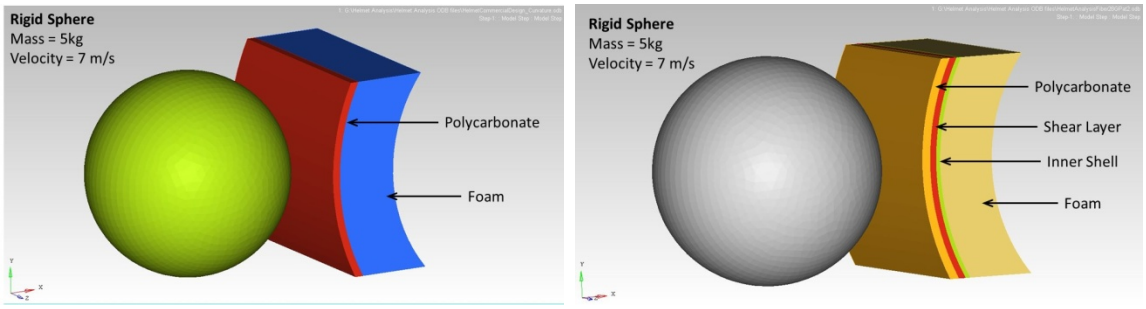

Figure 4-1 Impact Models – Commercial Helmet IEA Model (left) and EBM Helmet IEA Model (right)

The two finite element models are used to evaluate the IEA systems are shown in Figure 4-1. The first IEA model, is a model simulating the makeup of a commercially available football helmet. The second IEA model, represents the makeup of the EBM helmet. Both IEA models are setup using linear elastic material properties. The mass of the rigid sphere was set to 5 kg with an initial velocity of 7 m/s. The commercial helmet IEA model uses a layer of polycarbonate for the outer surface and an inner layer of foam

www.manaraa.com

padding. The total thickness of the cross-section is 35mm, which represents a cross-section of a typical helmet. Table 4-1 lists the materials used for each layer and their corresponding material properties and thicknesses.

The EBM IEA model uses four layers: a layer of polycarbonate for the outer surface, a shear layer, an inner shell layer, and an inner layer of foam padding. The outer polycarbonate layer replicates the same shape and thickness as the commercially available polycarbonate shell. The shear layer, below the polycarbonate layer, provides a compliant shear layer for the EBM IEA system. The inner shell, separating the shear layer from the foam padding layers, encapsulates the shear layer to help it perform in shear only. The inner layer of foam, which is thinner than the commercially available helmet, conforms to the same inner shape as the commercially available helmet. The total thickness of the EBM IEA system is 35mm. Table 4-2 lists the materials used for each layer and their corresponding material properties and thicknesses.

www.manaraa.com

4.4 Commercial Helmet IEA System

4.4.1 Components of the Commercial Football Helmet

Standard commercially available football helmets consist of the following components:

1. Outer Polycarbonate Shell
2. Impact Padding and Comfort Foam

4.4.1.1 Outer Polycarbonate Shell

The outer polycarbonate shell of the helmet is primarily designed to provide protection against penetrating injuries to the head. It is also designed to distribute impact forces over a larger area. Since the outer shell is a critical part of the helmet, it needs to function in a variety of conditions. The most common material used for football helmets are Rubber-reinforced thermoplastics like Polycarbonate or Acrylonitrile Butadiene Styrene polymer and Fiber reinforced thermoset resin composites.

4.4.1.2 Impact Padding and Comfort Foam

The impact padding and comfort foam components of the helmet provide the impact energy attenuation system of the standard helmet. Impact padding for different helmet brands vary, however, the typical material is expanded polystyrene foam. Some other padding used are semi rigid polyurethane foams, vinyl nitrile, or inflatable rubber bladders filled with air. Since the Impact padding layer is used as an energy attenuation system for the helmet, the padding is typically placed in a compressive nature.

www.manaraa.com

Table 4-1 Elastic Material Properties of a Commercial Helmet

Commercial Helmet IEA Model					
Layer Number	**Material**	**Young's Modulus (MPa)**	**Poisson's ratio**	**Density (g/cc)**	**Layer Thickness (mm)**
1	Polycarbonate	2750	0.32	1.3	4
2	Foam	2.7	0.01	0.32	31

4.4.2 Impact Results

The impact results shown in Figure 4-2 through Figure 4-3 plot the Strain Energy of the polycarbonate and foam layers respectively. Since the energy of the impact event is dissipated as strain energy, the corresponding plots shown here are used to evaluate the individual layers of the system.

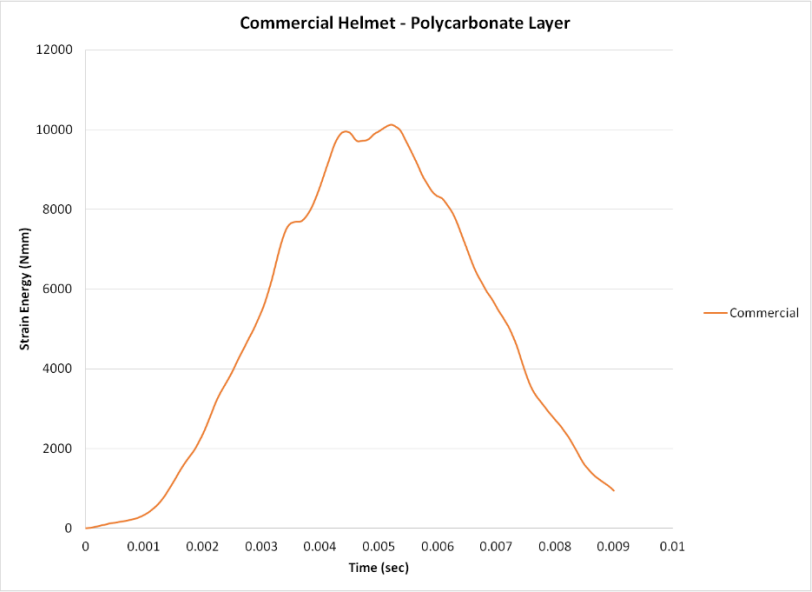

Figure 4-2 Strain Energy Absorption of the Commercial Helmet IEA Polycarbonate Shell

www.manaraa.com

Shown in Figure 4-2 is the strain energy of the polycarbonate layer during the impact event.

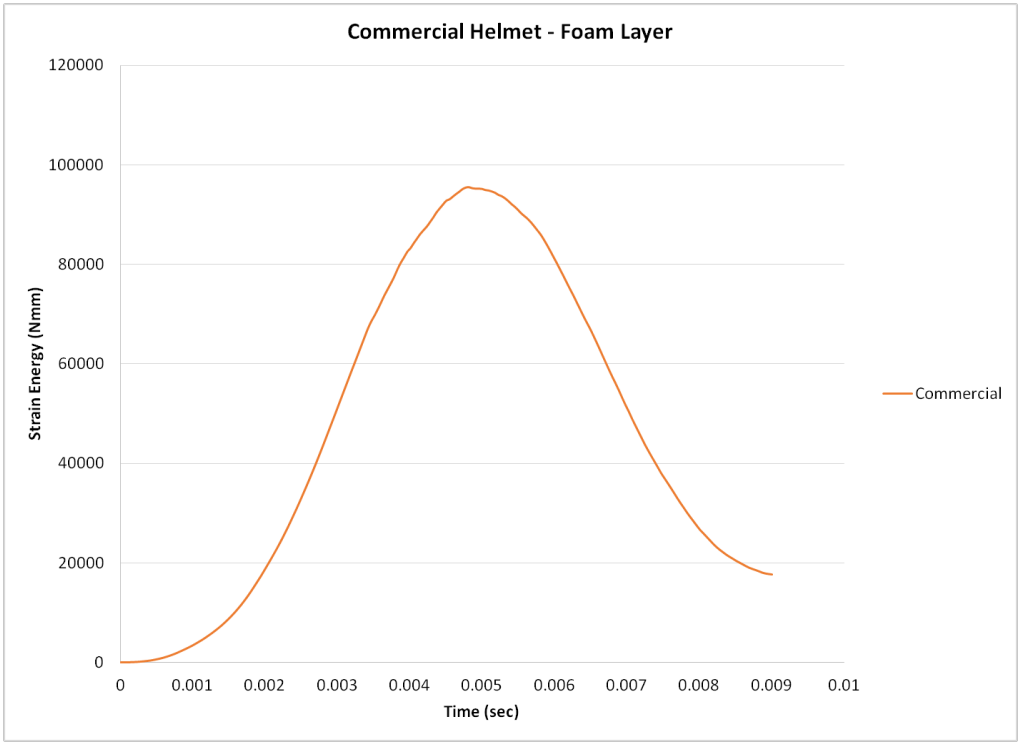

Figure 4-3 Strain Energy Absorption of the Commercial Helmet IEA Foam Padding

Shown in Figure 4-3 is the strain energy of the foam layer for the commercial helmet IEA. Although the foam layer for the commercial helmet is thicker, by 6mm, than the EBM helmets, the strain energy for the three types of helmets are very comparable.

www.manaraa.com

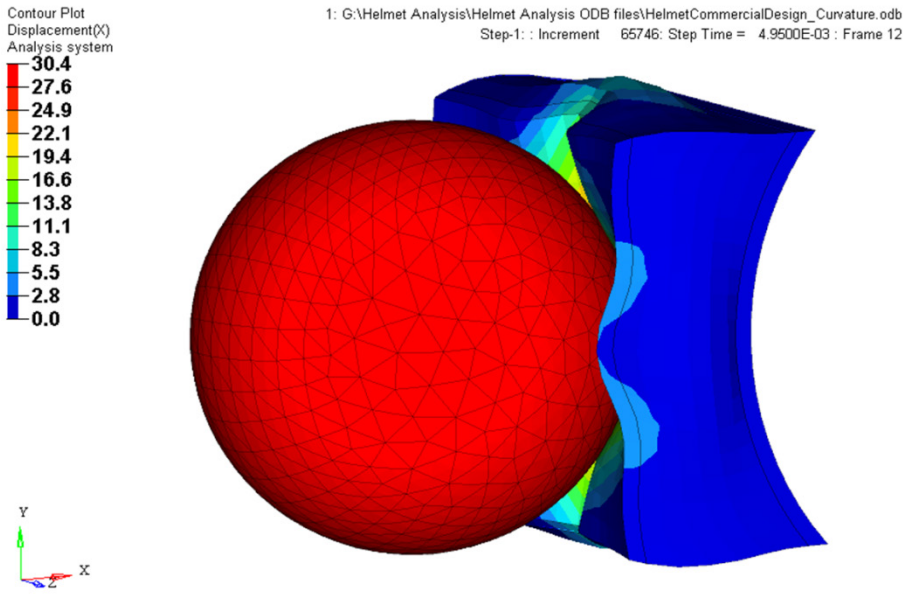

Figure 4-4 Deflection Results of Commercial Helmet IEA FE Model

Figure 4-4 shows the deformation configuration for the maximum deflection of the commercial helmet IEA system. The full comparison of deflections results can be seen in Figure 4-14.

www.manaraa.com

4.5 EBM Helmet IEA Model

4.5.1 Components

The proposed EBM helmet consists of the following components:

1. Outer Polycarbonate Shell
2. Inner Shear Layer (Sorbothane®) [13]
3. Inner Shell (Fiberglass)
4. Impact Padding and Comfort Foam

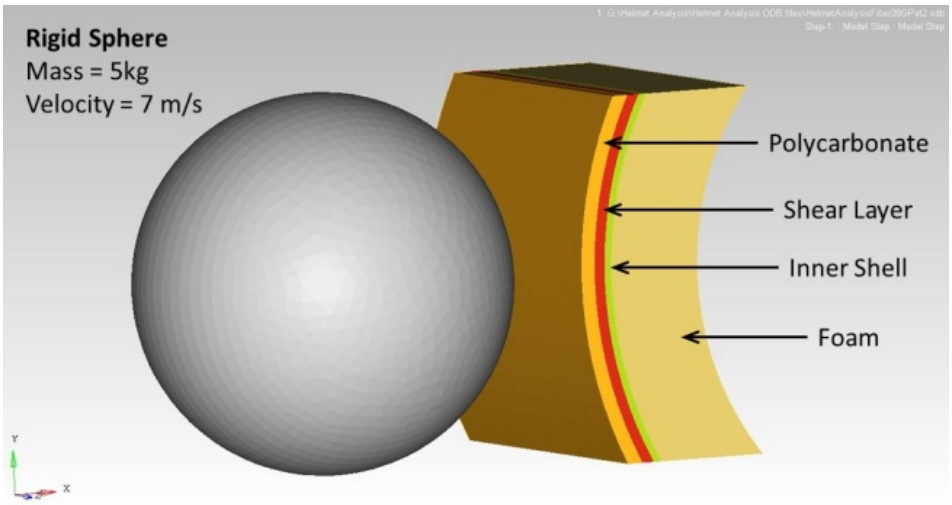

Figure 4-5 EBM Helmet IEA Cross-Section

4.5.1.1 Outer Polycarbonate Shell

The outer polycarbonate layer replicates the same shape and thickness as the commercially available polycarbonate shell. The outer polycarbonate shell of the EBM helmet functions in the same manner as the commercially available helmet, where it

www.manaraa.com

provides protection against penetrating injuries to the head and distributes impact forces over a larger area.

4.5.1.2 Shear Layer

The shear layer, below the polycarbonate layer, provides a compliant shearing layer for the EBM IEA system. The material used for the shear layer is Sorbothane®. Sorbothane® is a thermoset, polyether-based, polyurethane material that is a visco-elastic polymer. For the purposes of this evaluation, linear elastic material properties are used to define the material characteristics [13].

4.5.1.3 Inner Shell Layer

The inner shell, separating the shear layer from the foam padding layers, encapsulates the shear layer to help it perform in shear only. Since the inner shell of the EBM IEA system has to be thin and light, a fiberglass composite layer is chosen. For this study, the material properties and thicknesses are changed in order to maximized the thickness and material strength characteristics. Thickness of 2mm and 3mm are chosen for evaluation. Since this is an additional component to be added to the helmet IEA system, the thickness is a critical value. Since this layer is critical, there are three criteria that need to be considered in designing the inner shell.

1. The inner shell has to be light (i.e.: it cannot add a significant amount of mass to the helmet).
2. The inner shell has to be strong, yet flexible (i.e.: it has to be provide backing stiffness for the shear layer, yet flexible enough to move with the polycarbonate

www.manaraa.com

shell of the helmet when it deforms during impact or when the helmet is fitted onto the players head).

3. The inner shell has to be able to be manufactured.

Comparison graphs, shown in the following sections, indicate the bounding thicknesses and material properties results.

4.5.1.4 Impact Padding and Comfort Foam

The impact padding and comfort foam components of the helmet provide the impact energy attenuation system of the standard helmet. Impact padding for different helmet brands vary, however, the typical material is expanded polystyrene foam.

4.5.2 Material Properties

Table 4-2 lists the materials used in the EBM IEA helmet model. As noted below, the elastic modulus and thickness values were varied to achieve the best possible combinations. The following impact results will show the analysis results.

Table 4-2 Elastic Material Properties of EBM Helmet IEA

EBM Helmet IEA Model					
Layer Number	**Material**	**Young's Modulus (GPa)**	**Poisson's ratio**	**Density (g/cc)**	**Layer Thickness (mm)**
1	Polycarbonate	2.75	0.32	1.3	4
2	Sorbothane	1.69 MPa	0.499	1.412	3
3	Fiberglass	4 to 28	0.13	1.9	2 to 3
4	Foam	2.7 MPa	0.01	0.32	25

www.manaraa.com

4.5.3 Impact Results

The impact results shown in Figure 4-6 through Figure 4-15 plot the Strain Energy of the IEA polycarbonate, shear, inner shell, and foam layers respectively. Also included are comparison charts showing the peak strain energy for the different layers. Since the goal of this study was to determine the bounding material properties for the inner shell layer, different models were analyzed using the corresponding material properties and thicknesses. Shown in the following figures are the shear strain results for the different layers.

It should be noted the results for the 4 GPa models were not successful analysis runs. The elastic modulus for the inner shell was too low to obtain good results. This was evident in both the 2mm thickness and 3mm thickness models. In addition, this low elastic modulus is below the range for physically producing an effective fiberglass layup. Since the possibility for achieving a layup of resin and glass layers is above the 4 GPa elastic modulus range, this serves as a lower bounds for the material.

www.manaraa.com

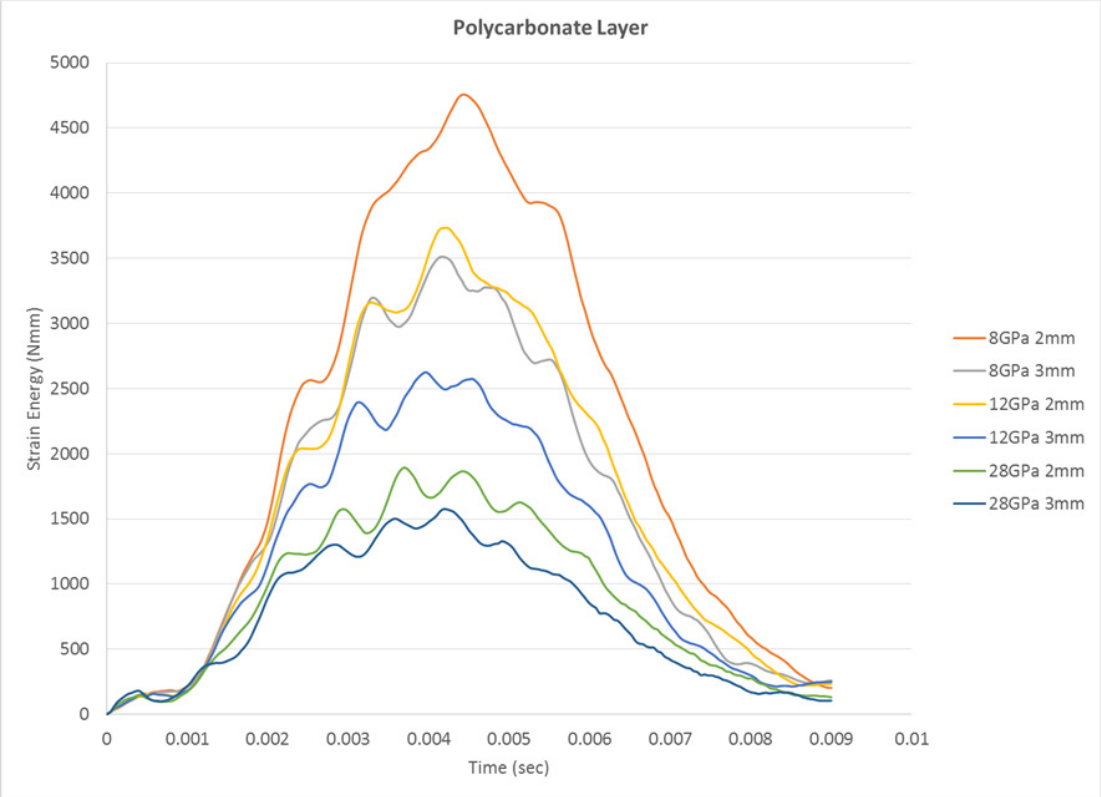

Figure 4-6 Strain Energy Absorption of Polycarbonate Shell with Various Inner Shell Layers

Shown in Figure 4-6 are the strain energy results for the EBM IEA helmet polycarbonate layer with different inner shell material properties. From the results shown above it can be observed that as the elastic modulus for the inner shell is increased the strain energy for the polycarbonate layer decreases. As well, as the thickness of the shell increases the strain energy for the polycarbonate layer decreases. These results indicate the presence of the inner shell provides more structure to the outer shell of the helmet preventing the outer polycarbonate shell of the EBM IEA helmet from deforming as significantly compared to the commercial helmet.

www.manaraa.com

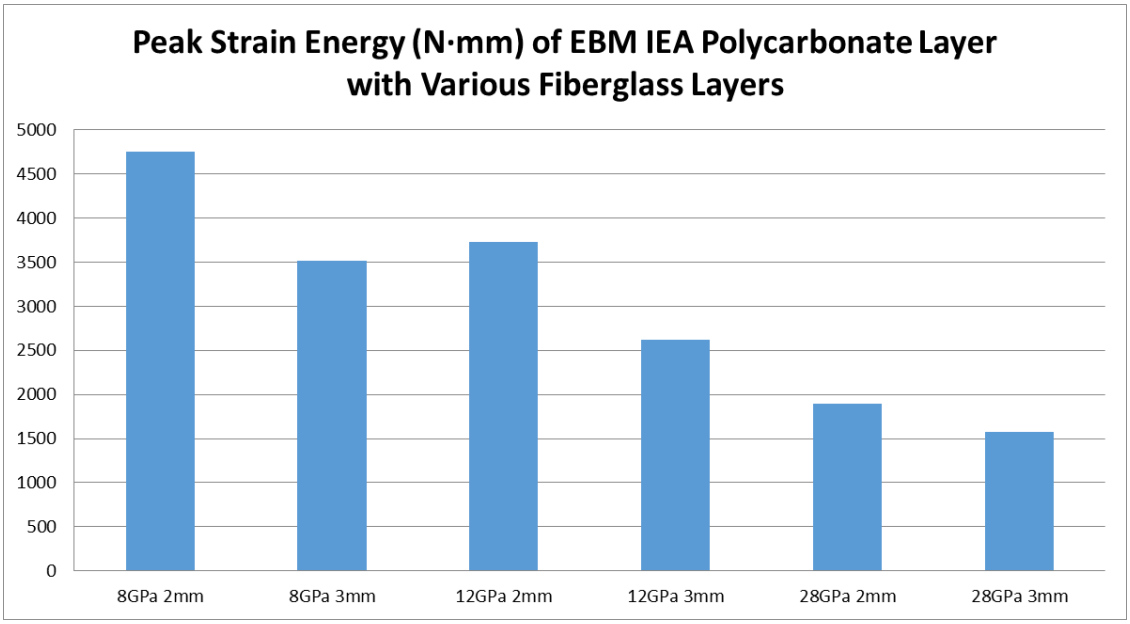

Figure 4-7 Peak Strain Energy of Polycarbonate Shell with Various Inner Shell Layers

www.manaraa.com

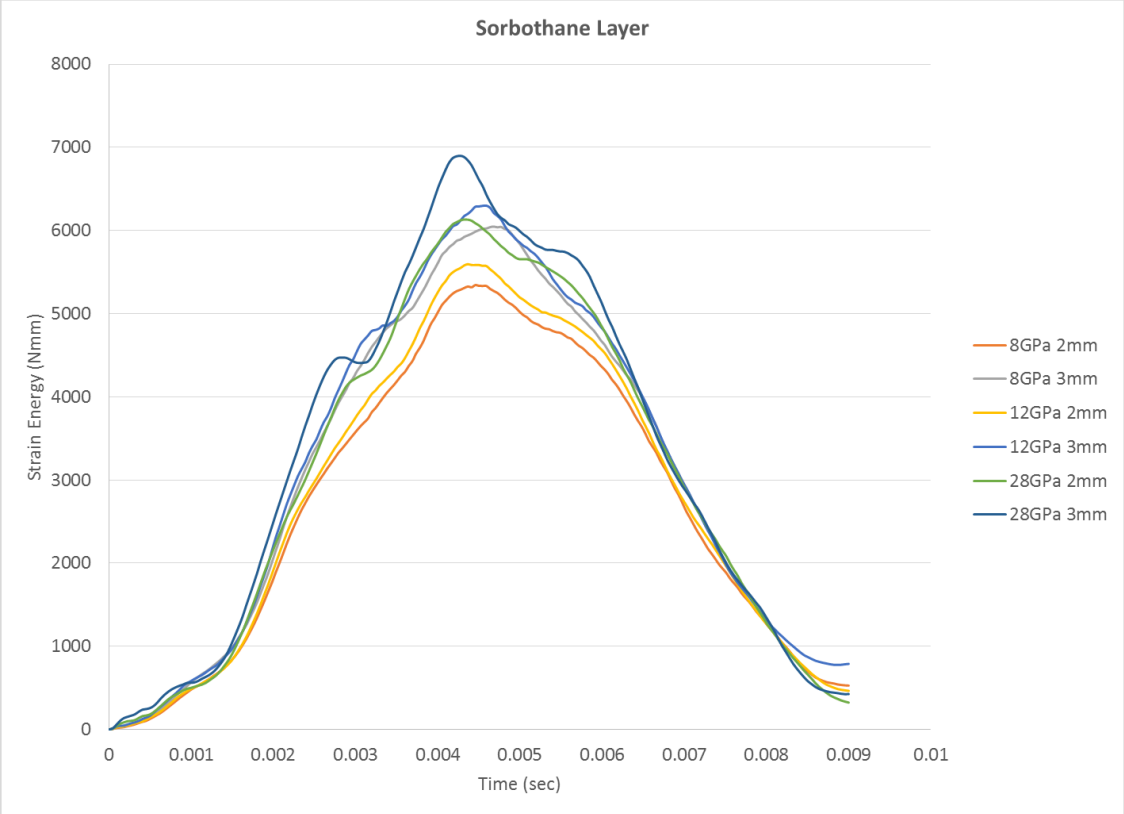

Figure 4-8 Strain Energy Absorption of Sorbothane® Layer

Shown in Figure 4-8 are the strain energy results for the EBM IEA helmet shear layer with different inner shell material properties. From the results shown above it can be observed that as the elastic modulus for the inner shell is increased the strain energy for the shear layer increases. As well, as the thickness of the shell increases the strain energy for the polycarbonate layer increases. These results indicate the addition of the inner shell reduces the deformation of the outer polycarbonate shell and transfers some of that strain energy to the shear layer.

www.manaraa.com

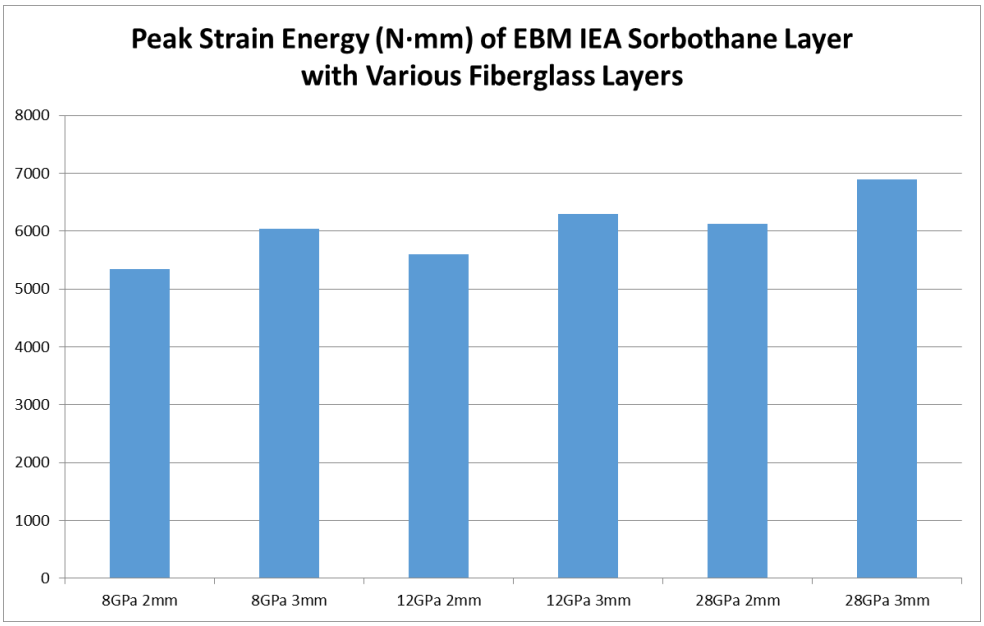

Figure 4-9 Peak Strain Energy for Sorbothane® Layer with Various Inner Shell Layers

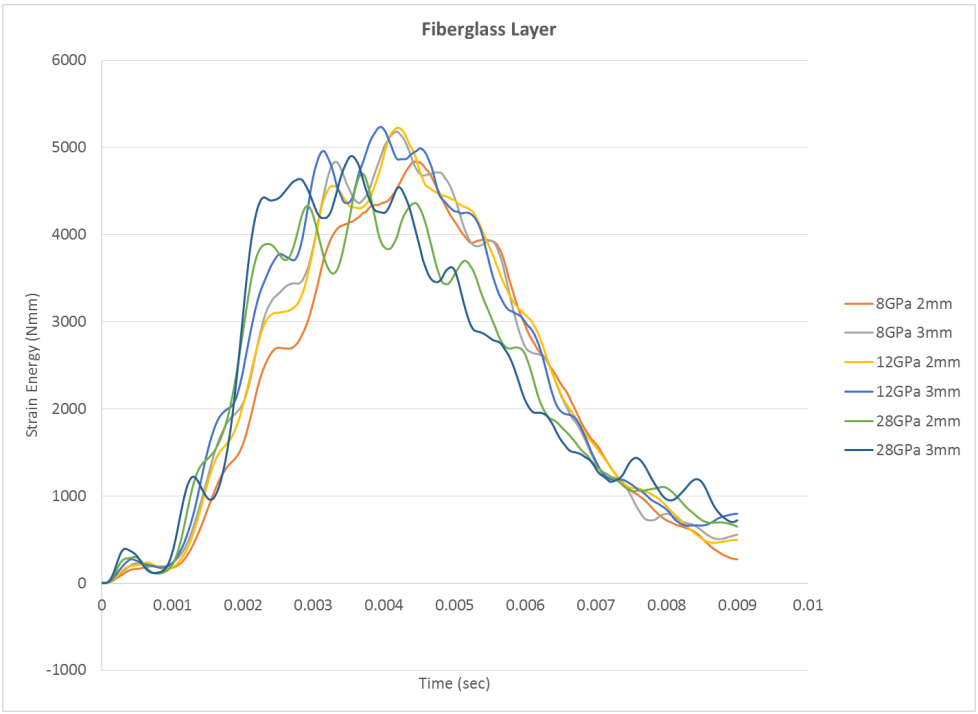

Figure 4-10 Strain Energy Absorption of Various Inner Shell Layers

www.manaraa.com

Shown in Figure 4-10 are the strain energy results for the EBM IEA helmet inner shell layer. From the results shown above it can be observed that as the elastic modulus for the inner shell is increased the strain energy within this layer remains consistent between 8GPa and 28GPa. There is some variation, with slightly lower peak strain energy at 28GPa, however the strain energy is relatively consistent.

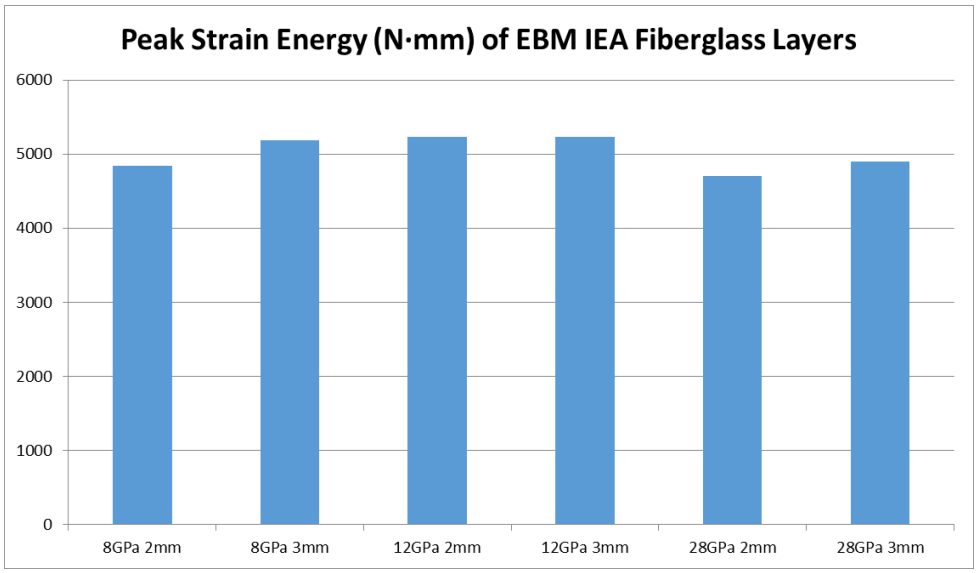

Figure 4-11 Peak Strain Energy for Various Inner Shell Layers

www.manaraa.com

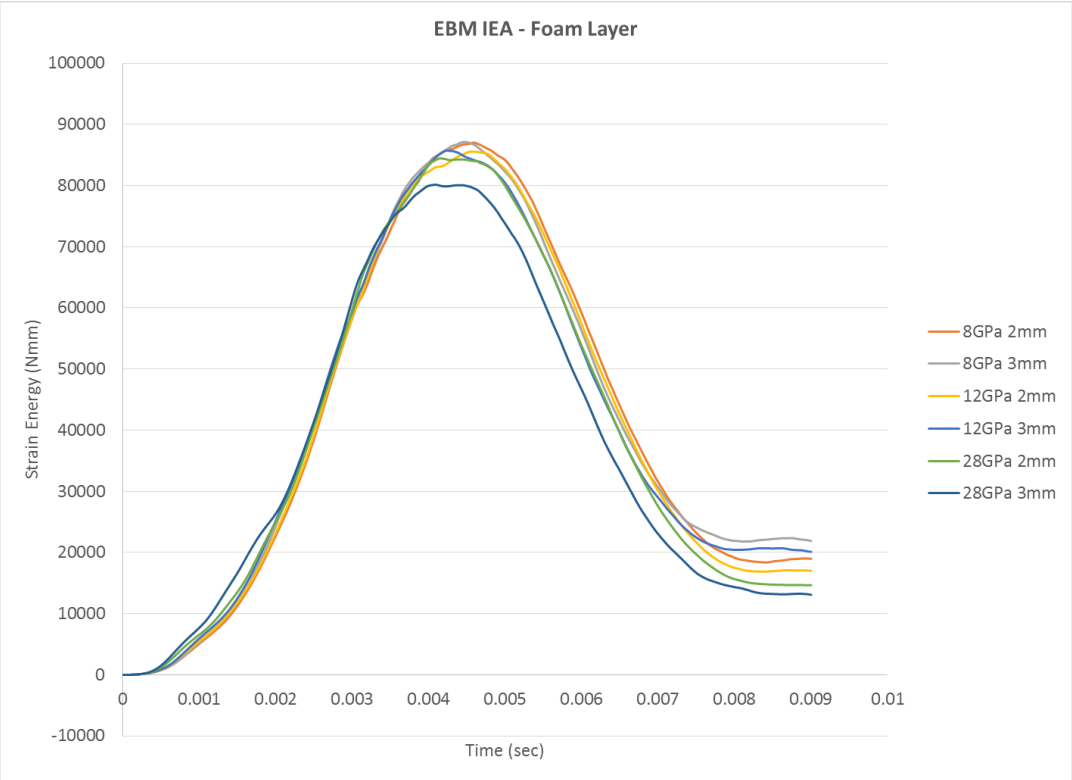

Figure 4-12 Strain Energy Absorption for Foam Padding with Various Inner Shell Layers

Shown in Figure 4-12 are the strain energy results for the EBM IEA helmet foam layer. From the results shown above it can be observed that as the elastic modulus for the inner shell is increased the strain energy within this layer remains consistent for all the inner shell elastic modulus and thickness combinations. There is some slight variation, with the higher thickness and higher elastic modulus properties resulting in lower strain energies in the foam layer, however the strain energy is relatively consistent.

www.manaraa.com

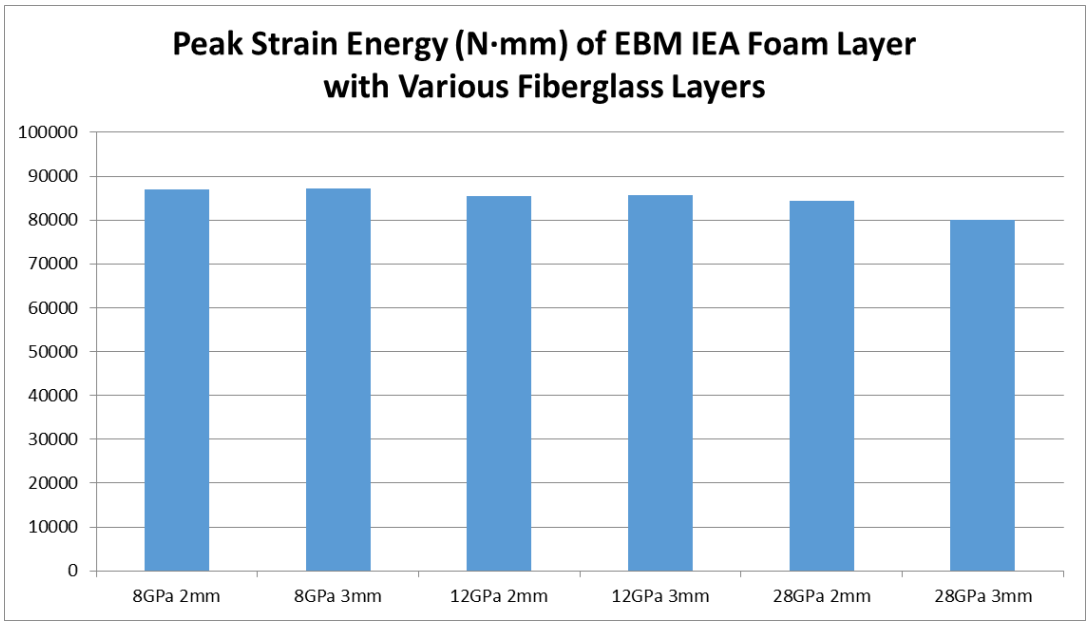

Figure 4-13 Peak Strain Energy for Foam Padding with Various Inner Shell Layers

Also included are the maximum displacement results for all the material models. From the results in Figure 4-14, the peak displacement for all combinations of inner shell materials remain consistent around 21mm to 22mm. The peak displacement for the commercially available football helmet material model is approximately 30mm. The reason for the difference in displacement is the commercial helmet material model has 6mm more foam padding than compared to the EBM helmet.

www.manaraa.com

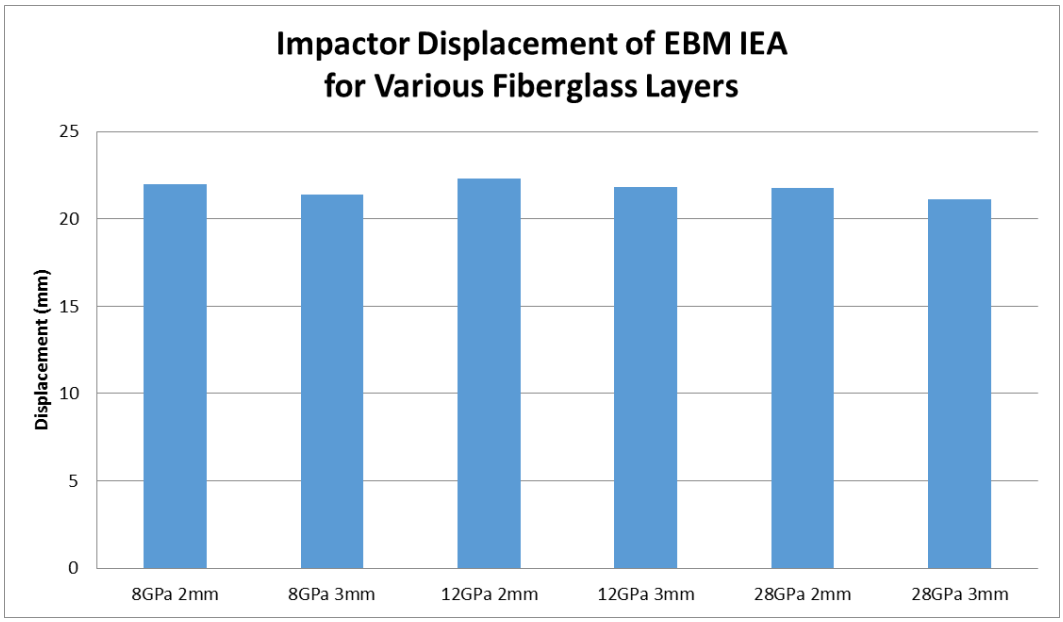

Figure 4-14 Peak Impactor Displacement of EBM IEA with Various Inner Shell Layers

In order to evaluate the strength requirements of the inner shell layer, the peak von Mises stress results are displayed in Figure 4-15. These results indicate that the higher elastic modulus materials experience a higher stress during impact. They also indicate the thinner the inner layer experiences a higher stress. These results indicate a lower overall elastic modulus should be used for the inner shell that is on the thicker side of the spectrum.

www.manaraa.com

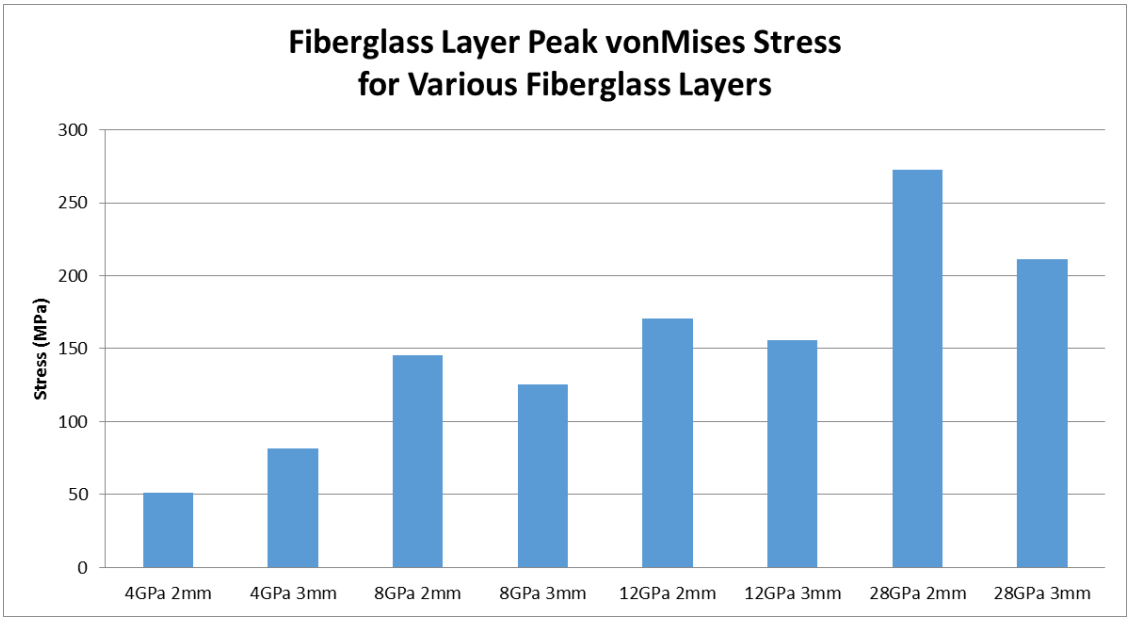

Figure 4-15 Peak Stress Values of Various Inner Shell Layers

4.6 Maximized EBM Helmet IEA System

For the final material makeup of the EBM helmet IEA system, the following materials were chosen:

- Polycarbonate thickness = 4mm
- Sorbothane thickness = 3mm
- Fiberglass (12GPa) thickness = 3mm
- Foam Padding thickness = 25mm

The final thickness and material strength for the fiberglass layer was chosen because it provided good energy absorption characteristics, good strength characteristics, and did not have too high of an elastic modulus to cause brittle failure concerns. When

www.manaraa.com

comparing at the peak von Mises stress for the different layer strengths, the 28 GPa material had an approximately 100 MPa high peak stress compared to the 12 GPa layer. This would be a concern for possible fatigue failure.

When comparing results for the thicknesses of the 12 GPa IEA models, there is no significant difference between the peak strain energy absorption, deflection, or peak von Mises stress. The deciding factor came down to ability to manufacture the two layers. Since the 2mm thickness is more difficult to manufacture, the 3mm thickness was chosen. The 3mm thickness provides a better opportunity to make a strong composite, without having the possibility of having the percent matrix to fiber being difficult to achieve.

www.manaraa.com

4.7 Final EBM IEA System

Once the maximized IEA makeup was chosen for the EBM helmet IEA system, a finite element model of the helmet and human head was developed. From the initial impact analysis, it was observed that the four layer IEA system was too stiff in rotation as compared to the standard VSR4 helmet. The EBM helmet performed as expected for the 0° impact angles, but as the angle of impact increased to 30°, the stress levels on the surface of the brain increased over those of the VSR4 helmet.

A re-evaluation was then done to eliminate the fiberglass layer from the EBM IEA system. The reason behind removing the fiberglass layer are listed below:

- There is no significant change in strain energy absorption between the various IEA models for the Sorbothane layer.
- There is no significant change in strain energy absorption between the various IEA models for the foam layer.
- The fiberglass layer does provide strain energy absorption for the EBM IEA system, which also reduces the strain energy absorbed by the polycarbonate layer. By eliminate the fiberglass layer, the amount of strain energy absorption for the polycarbonate layer will increase, but it will not be greater than the commercial helmet IEA system.

www.manaraa.com

For these reasons the fiberglass layer was removed and the final EBM IEA system was defined using three layers as listed:

- Polycarbonate thickness = 4mm
- Sorbothane thickness = 3mm
- Foam Padding thickness = 28mm

The final thickness for the EBM IEA will obviously vary for different areas of the helmet, where the padding thickness changes, however, the final three layers are listed.

www.manaraa.com

5 Concept and Configuration of VSR4 Football Helmet by Riddell

The principal function of the VSR4 football helmet by Riddell is to minimize the risk of concussion injury to football players by absorbing head impact energy thereby reducing head translational acceleration. The main goal of a helmet is to prevent skull fractures and reduce the acceleration to the player by absorbing some of the impact energy. Helmets have been designed with the intent to reduce the linear acceleration due to normal impacts. Normal impacts, or translational motion impacts, on football helmets have been well studied through the use of the NOCSAE drop tester and FE head modeling. However, in actual real life scenarios, very few impacts actually result in just normal impacts. In reality, the majority of impacts on the football field are in some form or another oblique type impacts. Furthermore, there are very few studies that evaluate the response of the human head and helmet as they are subjected to oblique impacts. This makes it difficult to accurately study the effect of the helmet in reducing the peak pressure stress and peak shear stress on the brain. A fully integrated helmeted head FE model system is needed to truly assess the underlying head response due to impact on the helmet.

www.manaraa.com

5.1 Objective

The goal of the research is to study the efficacy of the football helmet against normal and oblique impacts at the frontal, lateral, superior, and posterior location on the helmet. This study will evaluate the performance of a current football helmet fitted onto a human head model by FEM.

The specific objectives of the study are to:

- Develop an integrated FE model of a current football helmet and head.
- Evaluate the helmet performance and study the effect of the helmet in reducing the shear stress and pressure on the brain.

5.2 Relevance of Research

This study is an attempt to fill the gap in the computational analysis of an integrated 3D head and football helmet. The goal of the research is to study the efficacy of the current football helmet against normal and oblique impacts at the frontal, lateral, superior, and posterior location on the helmet.

5.3 Methods and Materials Used to Achieve Results

- Develop a FE model of the VSR4 football helmet made by Riddell.
- Validate the FE model of the helmet with respect to ASTM impact test results.

www.manaraa.com

5.4 Finite Element Modeling of the Riddell VSR4 Football Helmet

The Riddell VSR4 football helmet was used for the purpose of this study to represent the commercial football helmet. The helmet geometry was digitized, to obtain a point cloud of the outer profile of the helmet shell. The helmet was digitized where a white light scanner was used [14] to measure the outer surface of the helmet shell. A solid model was then built off the point cloud by generating spline curves. Corresponding surfaces were then generated by connecting the spline curves from the obtained data points [14].

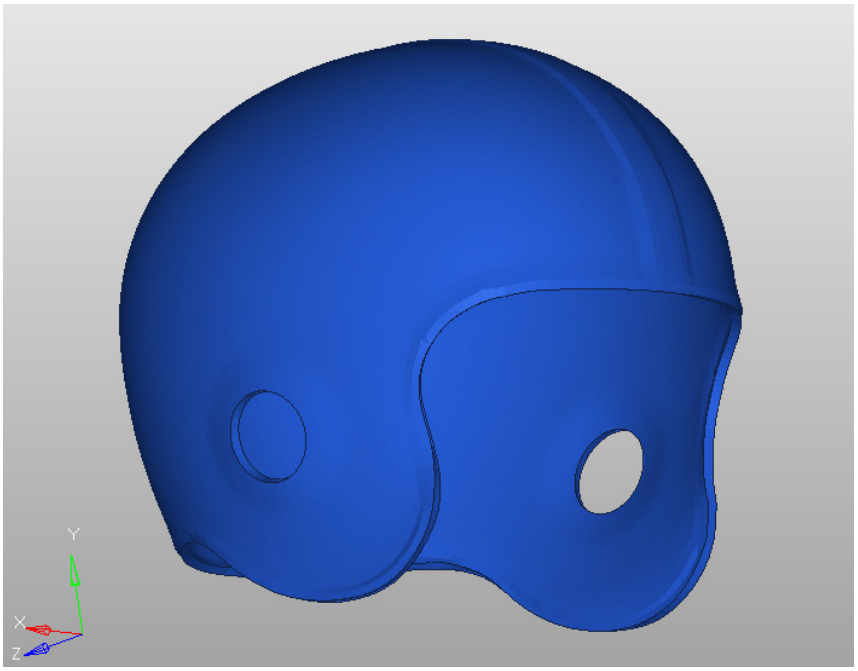

Figure 5-1 Geometry of VSR-4 Helmet Shell

Since the model developed by Kangana was not available, a new FE model was generated by importing the original geometry file, used by Bhushan [13], as a *.stp file, to HyperMesh 14.0 [4]. The outer surface geometry, in Figure 5-1, was then used to

www.manaraa.com

develop the entire FE model used by Bhushan [14]. The model generated consists of 90,486 nodes and 81,039 elements. Elements used in the helmet model are HEXA8 and PENTA6 solid elements. Total mass of the FE model matches the actual mass of the existing helmet at 1.5kg and the mass of the FE model developed by Bhushan [14]. This recreated model uses the same geometry file.

Table 5-1 VSR-4 Football Helmet FE Model Breakdown

Details of VSR 4 Football Helmet FE Model				
	Location	**Number of Elements**	**Element Type**	**Layer Thickness (mm)**
Shell	Outer Surface	25,770	hexa8 & penta6	4
Padding	Forehead	4,410	hexa8 & penta6	24
	Side/Posterior	21,590	hexa8 & penta6	20
	Crown	7,590	hexa8 & penta6	27.5
	Jaw	2,440	hexa8 & penta6	20

The internal padding of the helmet was meshed separately to incorporate the different thicknesses of the pads on the interior of the helmet. The forehead pad, crown pad, side and rear pads were modeled according to the measured thickness of the existing helmet. The corresponding thickness of the internal padding is as follows:

- Forehead pad = 24mm
- Crown pad = 27.5mm
- Side pad = 20mm
- Rear pad = 20mm

www.manaraa.com

Figure 5-2 through Figure 5-4 shows FE model of the complete football helmet. For this study, the facemask is not included in the analysis. Since the facemask is removed from the helmet during standard NOCSAE testing, it was excluded from this analysis [9].

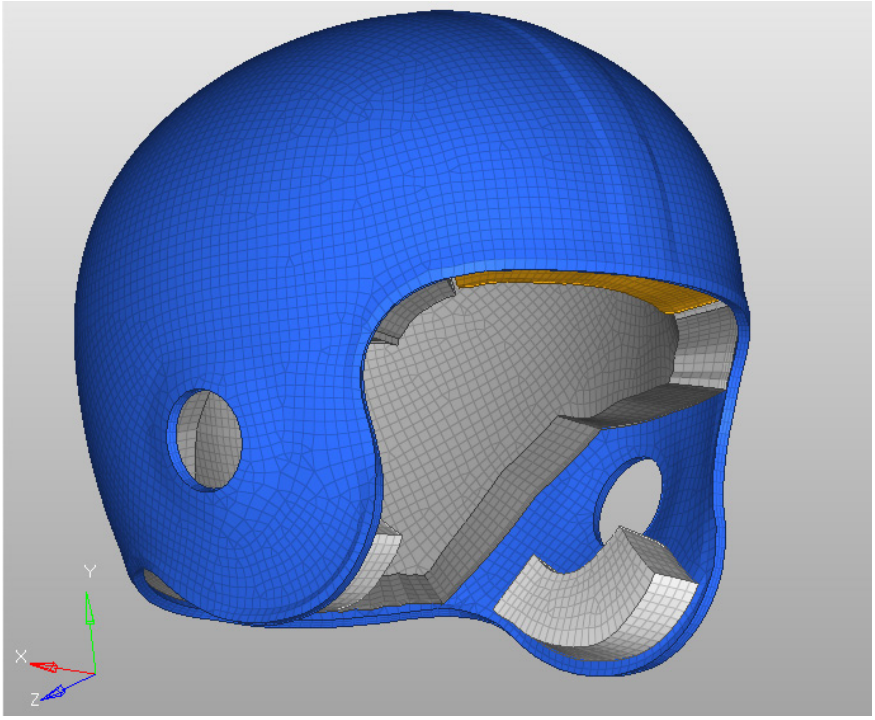

Figure 5-2 VSR-4 Football Helmet by Riddell without Facemask

www.manaraa.com

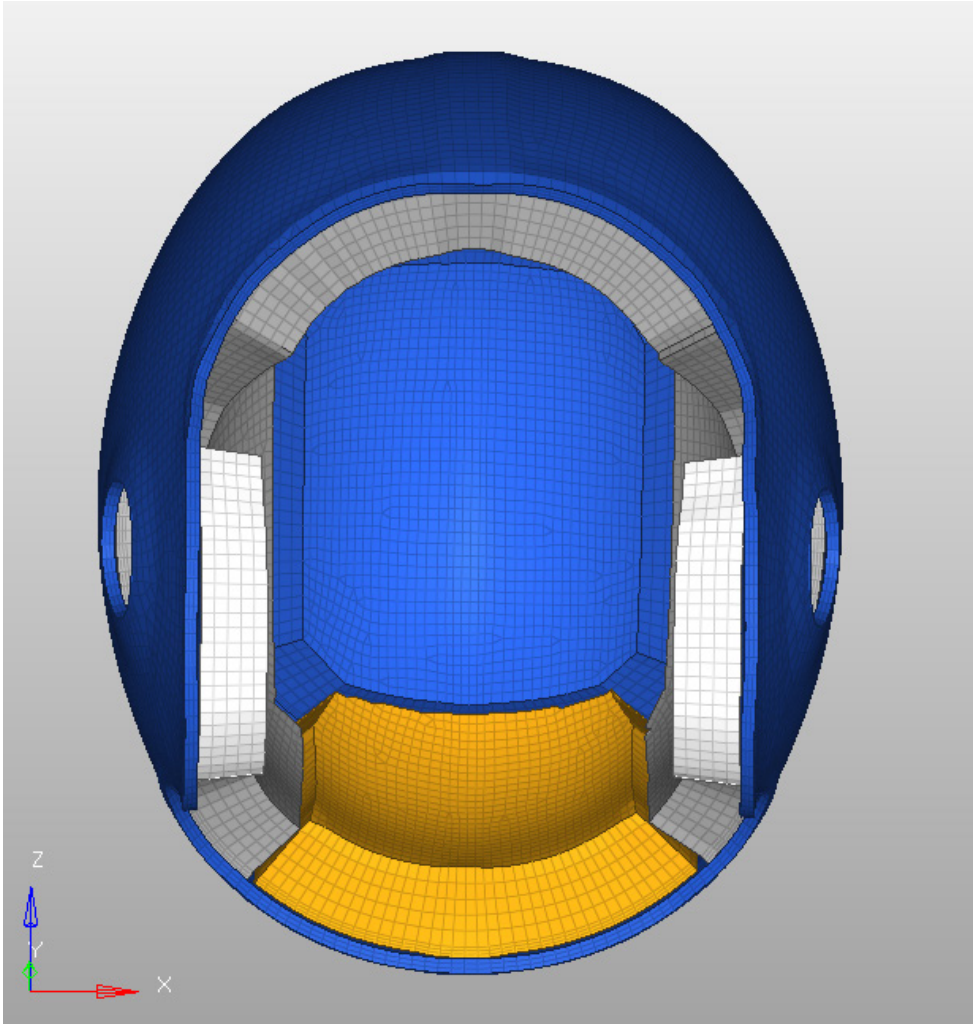

Figure 5-3 VSR-4 Football Helmet by Riddell Bottom View

www.manaraa.com

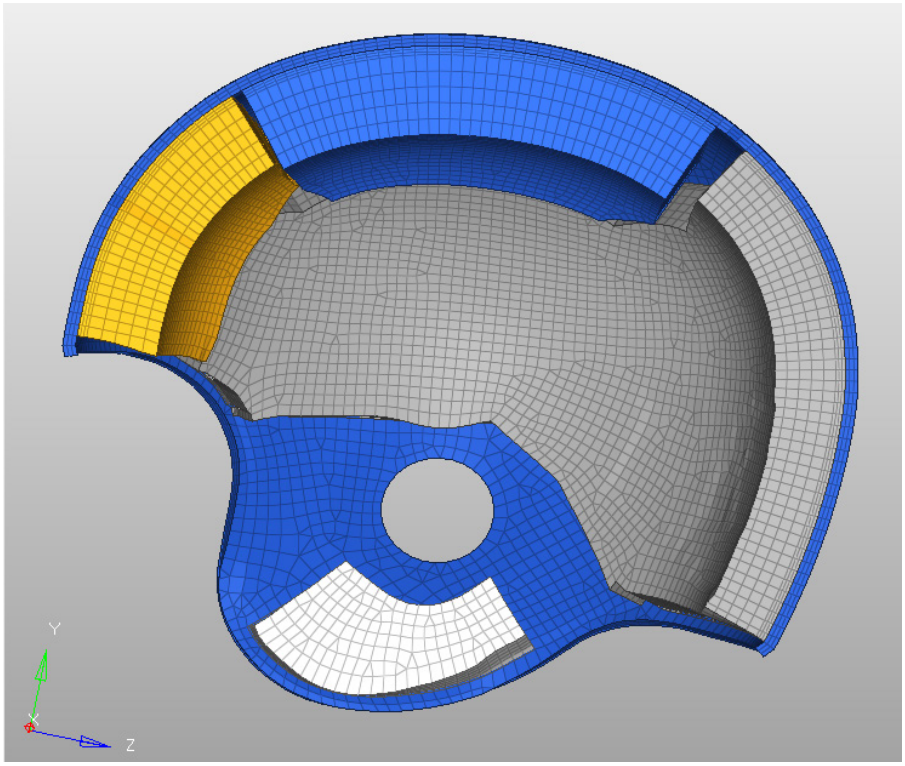

Figure 5-4 VSR-4 Football Helmet by Riddell Cross-Sectional View

5.5 Validation of the Helmet Model

The material properties used in the FE model were validated by Bhushan [14]. Kangana's FE model was validated with respect to the ASTM test results published by Zhang [15] that was performed on the VSR-4 large helmet by Riddell. ASTM test results for the Frontal, Lateral, Posterior, and Superior locations were available and were subsequently used to validate the model.

The headform used by Bhushan [14], to simulate the ASTM drop tests, was the NOCSAE headform. The headform was digitized using a coordinate measuring machine (CMM)

www.manaraa.com

available in the ME-EM Department at MTU. This method used is a similar method in which the FE model of the helmet was developed.

The coordinate points obtained from the CMM were used to create a point cloud of the headform. The point cloud was then used to generate a surface model that could be later used to generate a FE headform model. The exterior surface of the headform was then generated using shell elements, where the material density was modified to match the total mass of the headform. The center of mass (COM) and COM location was defined in accordance with the physical location of the NOCSAE headform.

To simulate the impact test, the helmet and NOCSAE headform were assembled in accordance with the guidelines and instructions provided by Riddell, Inc. [14]. The assembled model was given an initial velocity of 5.47 m/s, to simulate the headform and helmet assembly being dropped from a 60 inch vertical height. The corresponding velocity was used to validate the impact acceleration for the ASTM experimental event by Zhang [15].

ASTM F429, F717, and F1446 [16], [17], [18] define the testing method for evaluating the shock attenuating characteristics of a commercially available football helmet. The test apparatus can be setup in six different headform positions and dropped from a vertical height of 60 inches to an impact velocity of 5.47 ± 0.04 m/s. The six different headform positions are: Front, Front Boss, Side, Posterior, Posterior Boss, and Crown. A

www.manaraa.com

triaxial accelerometer, mounted at the center of mass, is used to measure the impact event. The NOCSAE drop tester is based upon these standards and shown below.

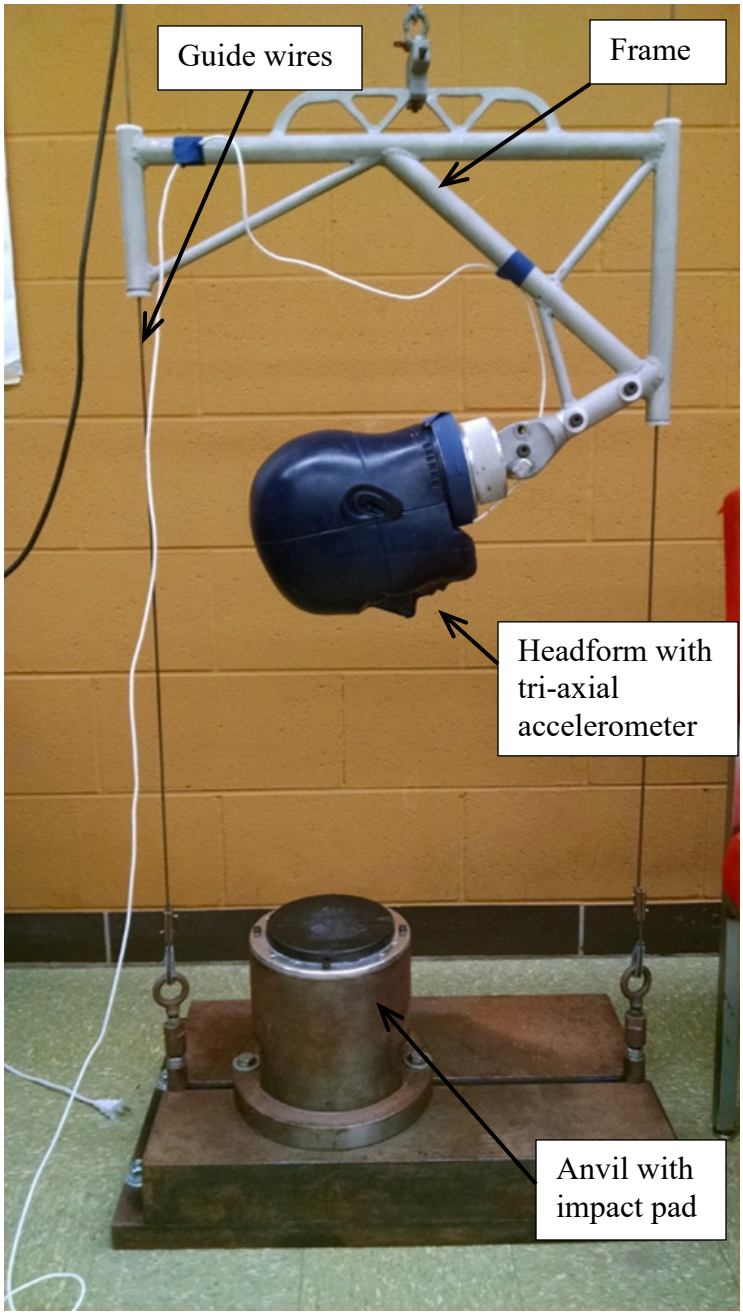

Figure 5-5 NOCSAE Standard Drop Tester at MTU for Football Helmet Testing based upon NOCSAE Standard Drop Test Equipment [9]

www.manaraa.com

Since the exact material properties of the helmet were not available during Kangana's study, a reverse engineering approach was used to estimate the material characteristics of each padding region [14]. A list of material properties used for the validation of the helmet is listed in Table 5-2. The approach taken to finalize these material properties is described below.

Table 5-2 VSR-4 Football Helmet Material Properties

Material Properties of VSR 4 Football Helmet FE Model				
	Location	**Material Model**	**Density (kg/mm^3)**	**Poission's Ratio**
Shell	Outer Surface	Elastic	1.30E-06	0.32
Padding	Forehead	Foam	3.20E-07	0.01
	Side/Posterior	Foam	2.00E-07	0.01
	Crown	Foam	2.80E-07	0.01
	Jaw	Foam	2.00E-07	0.01

The helmet padding of the VSR-4 Riddell helmet is made of vinyl nitrile and polyurethane foam [14]. This foam material is a highly compressible elastic material. The pads within the helmet are separated into different regions, corresponding to their physical location and measured thicknesses. The Forehead pad, Crown pad, Side/Posterior pad, and the Jaw pad designations are used to identify the padding regions. The material model used in the analysis model in Radioss by Altair [4] is the Visco-elastic Plastic Foam Material. In Radioss, this material model is typically used to model

www.manaraa.com

low density, closed cell polyurethane foams used for impact. The calculated densities of each region were based upon measured volume and mass of each pad region by using the equation [14]:

$$\rho = \frac{m}{V} \qquad (5.1)$$

Where: ρ is the objects density in kg/mm^3

m is the objects mass in kg

V is the objects volume in mm^3

Uniaxial compression data was used to define the material of the helmet pads. The compressive stress and strain data of the pad regions was tuned to get the required acceleration response of the headform [14]. Kangana Bhushan first used material properties derived by Zhang [15] for the padding material and then modified the properties once subsequent iterations were performed. It was determined that the maximum compression had little effect on the peak acceleration of the headform due to helmet impact. Changing the initial elastic region of the stress strain curve, however, had a strong influence of the peak acceleration. The stress-strain data that best matched the ASTM test results used by Kangana Bhushan [14] are presented and re-plotted in Figure 5-6.

www.manaraa.com

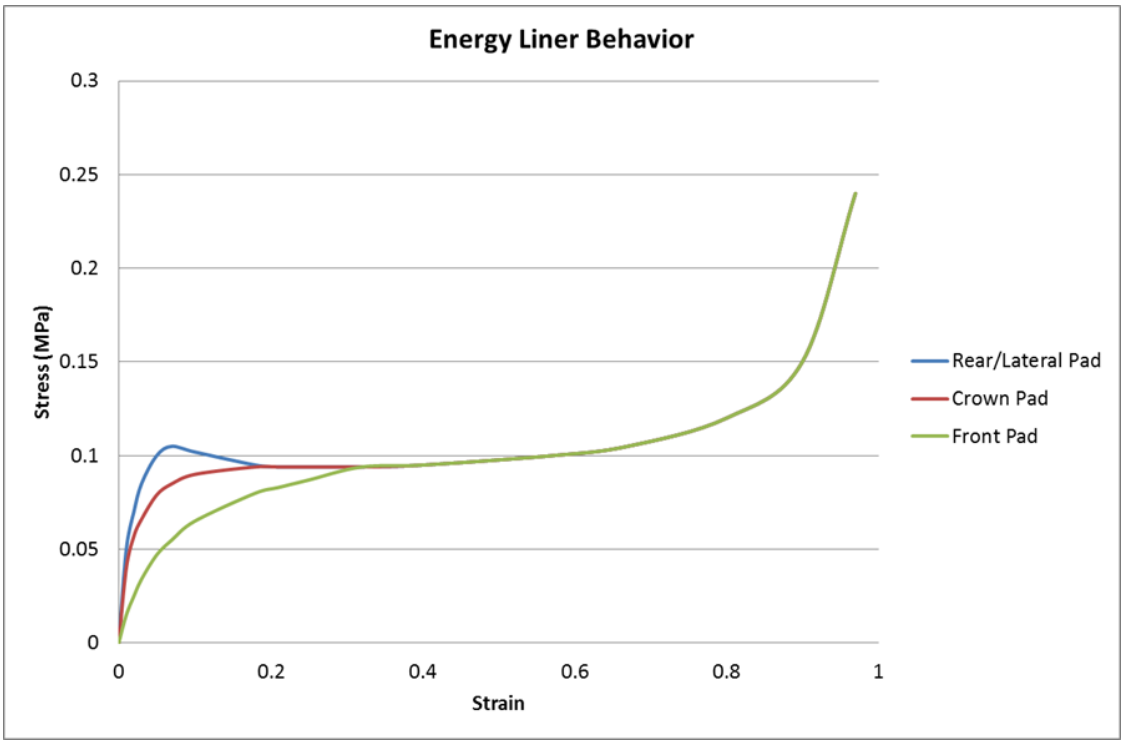

Figure 5-6 Stress-Strain Energy Liner Behavior

5.6 Impact Validation

Validation of the VSR-4 and the drop test headform finite element model was performed for the Frontal, Side, Posterior, and Superior impact regions. Kangana Bhushan performed a series of simulations, as a tuning process, for estimating the material properties of the football helmet padding. The resulting acceleration responses from the simulations were compared to the published ASTM test results by Zhang [14]. From the results the impact results closely matched the published results.

www.manaraa.com

6 VSR4 by Riddell Football Helmet Fitted onto a Human Head Model by Finite Element Modeling

Since the model developed by Kangana Bhushan was not available, a new FE VSR4 Riddell helmet model was generated by importing the original geometry file, used by Bhushan [14], as a *.stp file, to HyperMesh 14.0. The outer surface geometry was then used to develop the entire FE model used by Kangana Bhushan [14]. The model generated consists of 90,486 nodes and 81,039 elements. Elements used in the helmet model are HEXA8 and PENTA6 solid elements. Total mass of the FE model matches the actual mass of the existing helmet at 1.5kg and the mass of the FE model developed by Bhushan [14]. This recreated model uses the same geometry file.

Table 6-1 VSR-4 Football Helmet FE Model Breakdown

Details of VSR-4 Football Helmet FE Model				
	Location	**Number of Elements**	**Element Type**	**Layer Thickness (mm)**
Shell	Outer Surface	25,770	hexa8 & penta6	4
Padding	Forehead	4,410	hexa8 & penta6	24
	Side/Posterior	21,590	hexa8 & penta6	20
	Crown	7,590	hexa8 & penta6	27.5
	Jaw	2,440	hexa8 & penta6	20

www.manaraa.com

The internal padding of the helmet was meshed separately to incorporate the different thicknesses of the pads on the interior of the helmet. The forehead pad, crown pad, side and rear pads were modeled according to the measured thickness of the existing helmet. The corresponding thickness of the internal padding is as follows:

- Forehead pad = 24mm
- Crown pad = 27.5mm
- Side pad = 20mm
- Rear pad = 20mm

Figure 6-1 through Figure 6-2 shows FE model of the complete football helmet. For this study, the facemask is not included in the analysis. Since the facemask is removed from the helmet during standard NOCSAE testing, it was excluded from this analysis.

www.manaraa.com

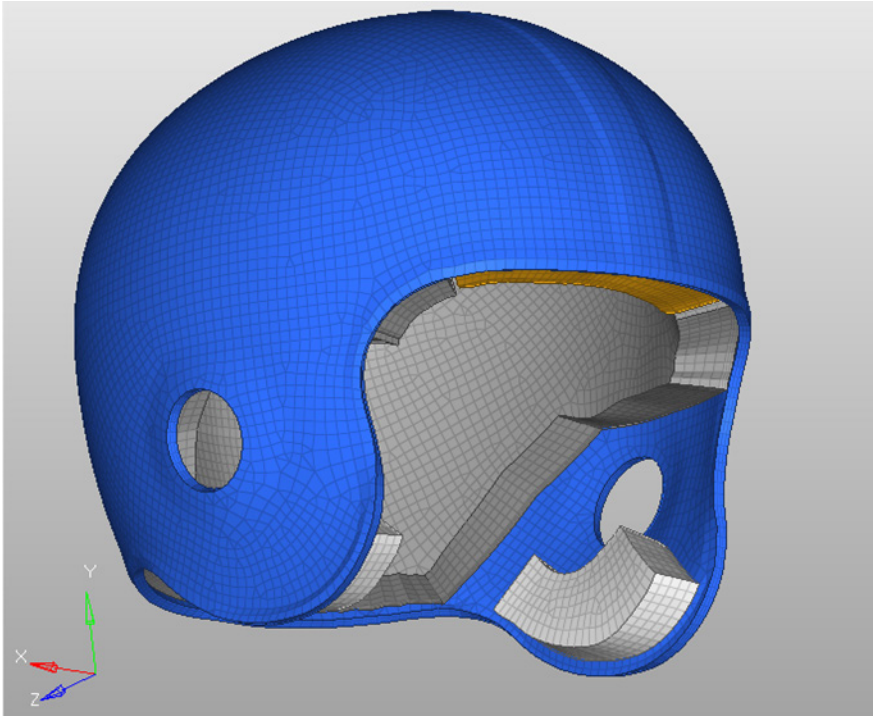

Figure 6-1 VSR-4 Football Helmet by Riddell without facemask

6.1 Helmet and Human Head Model

The validated VSR4 Riddell helmet model described in Section 4.4 and the validated FE model of the human head described in Section 2.5 were assembled for Frontal, Lateral, Posterior, and Superior impacts. Each impact location simulates the impact location that is performed on the NOCSAE drop tester. The impact locations are standard impact locations used with the NOCSAE drop tester to determine the effectiveness of a football helmet with respect to linear impact acceleration. Within this study, the overall effectiveness of the football helmet is evaluated with respect to linear impact acceleration along with pressure distribution, von Mises stress distribution in the brain, and angular acceleration of the human head model.

www.manaraa.com

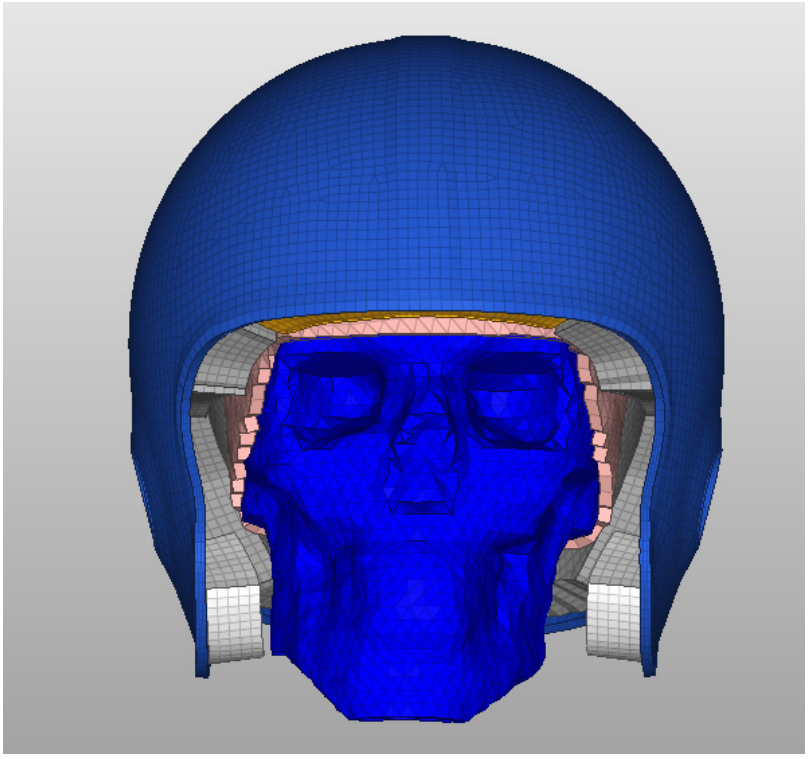

Figure 6-2 VSR-4 Football Helmet and Human Head Model Assembly

6.2 Impact Simulation and Boundary Conditions

Impact simulations for the frontal, lateral, posterior, and superior locations are shown in Figure 6-3 through Figure 6-10. To be consistent with the NOCSAE drop test setup, the head model was positioned using the same impact angles the NOCSAE drop test frame. The impactor used in these simulations is a flat steel plate with an elastic padding surface. The impactor is the same impactor that was used in the human head impact simulations done previously. The material properties of the impactor are listed in Table 6-2.

www.manaraa.com

Table 6-2 Impactor Material Properties

Material Properties of Impactor				
	Material Model	**Young's Modulus (Mpa)**	**Density (kg/m^3)**	**Poission's Ratio**
Padding	Elastic	10	1200	0.3
Steel	Elastic	209000	7800	0.29

For the impact simulations, the impactor is stationary, whereas, the helmet and head model are given an initial velocity to simulate the impact event. For all impact simulations an initial velocity of 5.47 m/s is prescribed for the helmet and human head assembly. All simulations were performed using Radioss, by Altair Engineering Inc. [4]. To define an oblique impact, the vector quantity of the 5.47 m/s velocity is divided to result in an angle of impact. The helmet and head assembly have a free-free boundary condition associated to them to simulate the impact.

Contact conditions between the helmet and impactor, and the head and helmet were defined in the finite element model using a multi-usage impact interface, type 7, in Radioss [4]. Contact between contact pairs was defined using a master surface and group of slave nodes. This type of contact definition has the advantage of increasing the contact stiffness to limit penetration, which lends itself well to simulating high speed impact for contact between parts.

www.manaraa.com

6.2.1 Frontal Impact Simulation

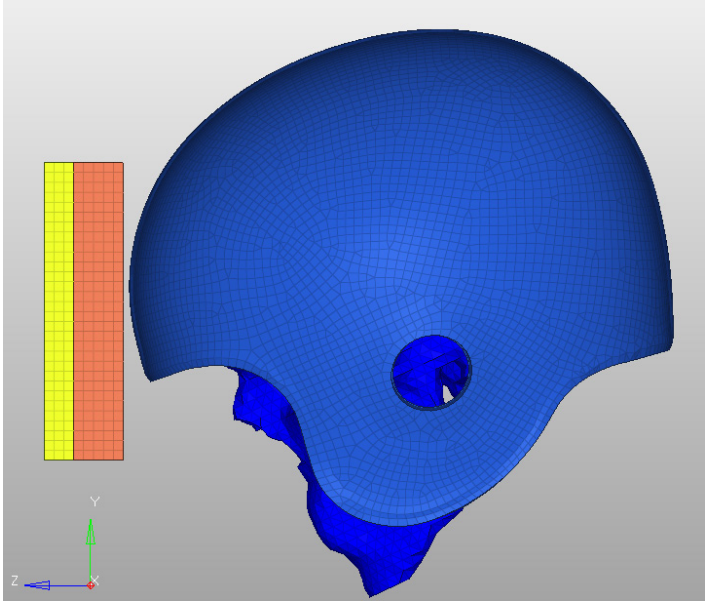

Figure 6-3 Frontal Impact 0° Simulation Model

The frontal impact simulation model is shown in Figure 6-3. The linear head impact acceleration time history for the simulation is show in Figure 6-4.

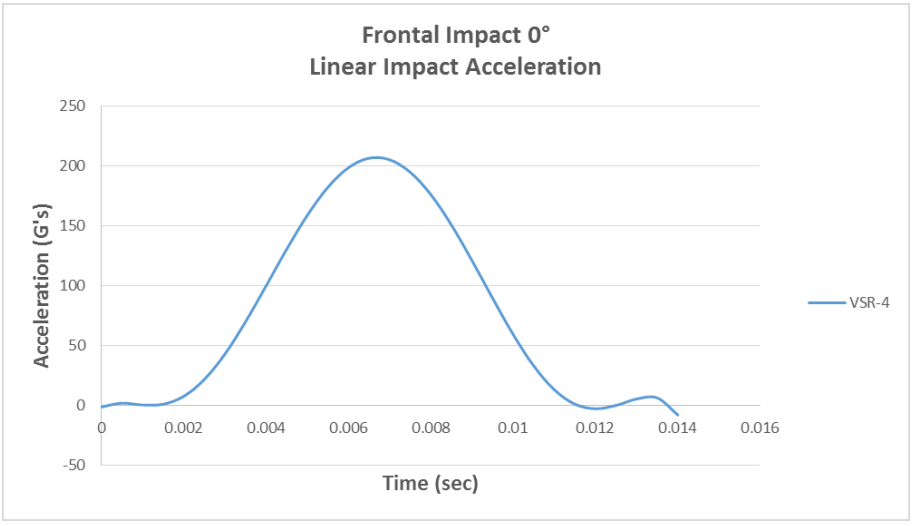

Figure 6-4 Frontal Impact 0° Linear Head Acceleration

www.manaraa.com

6.2.2 Lateral Impact Simulation

The lateral impact simulation model is shown in Figure 6-5. The linear head impact acceleration time history for the simulation is shown in Figure 6-6.

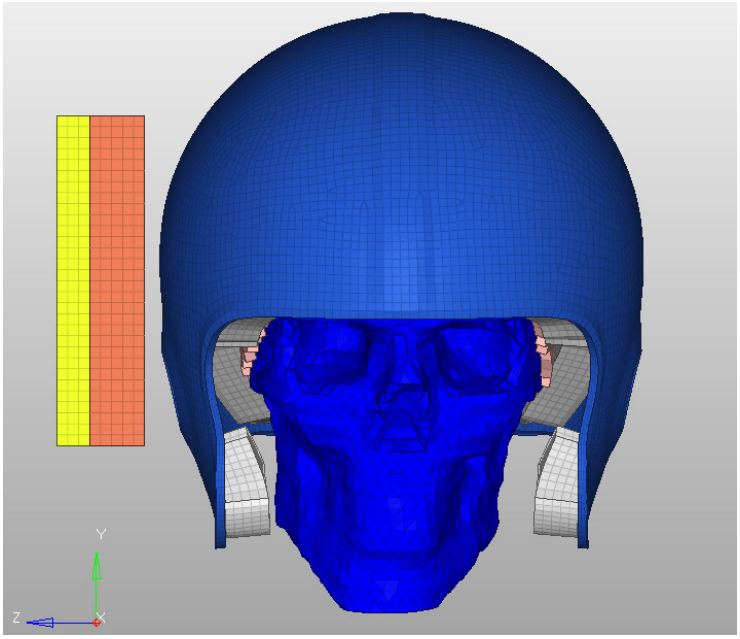

Figure 6-5 Lateral Impact 0° Simulation Model

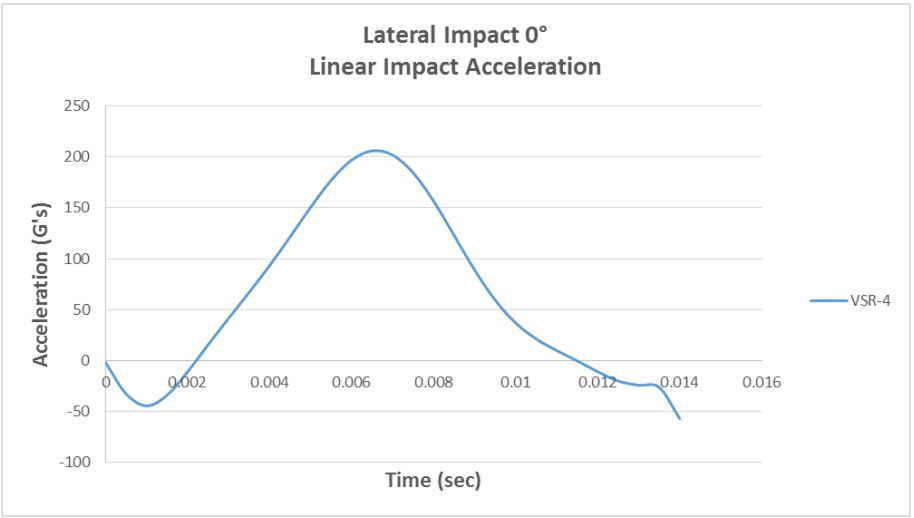

Figure 6-6 Lateral Impact 0° Linear Head Acceleration

www.manaraa.com

6.2.3 Posterior Impact Simulation

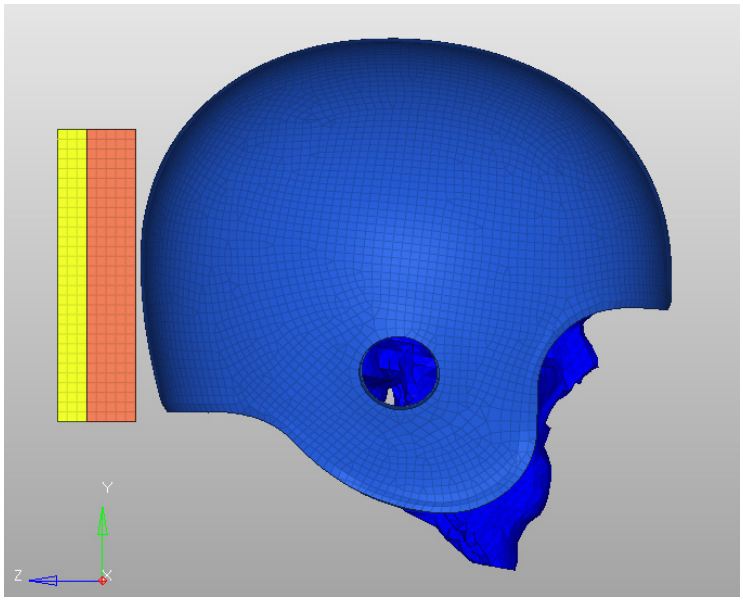

Figure 6-7 Posterior Impact 0° Simulation Model

The posterior impact simulation model is shown in Figure 6-7. The linear head impact acceleration time history for the simulation is shown in Figure 6-8.

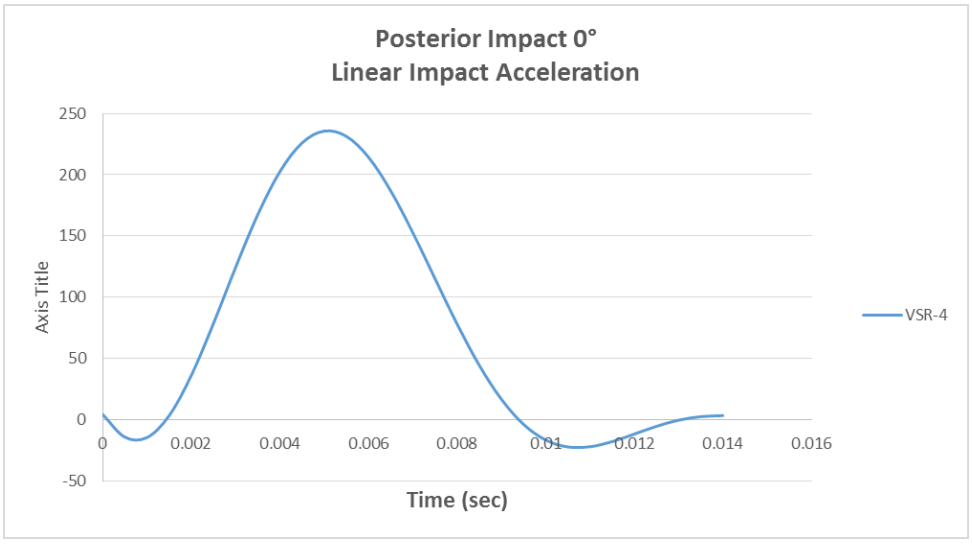

Figure 6-8 Posterior Impact 0° Linear Head Acceleration

www.manaraa.com

6.2.4 Superior Impact Simulation

The superior impact simulation model is shown in Figure 6-9. The linear head impact acceleration time history for the simulation is shown in Figure 6-10.

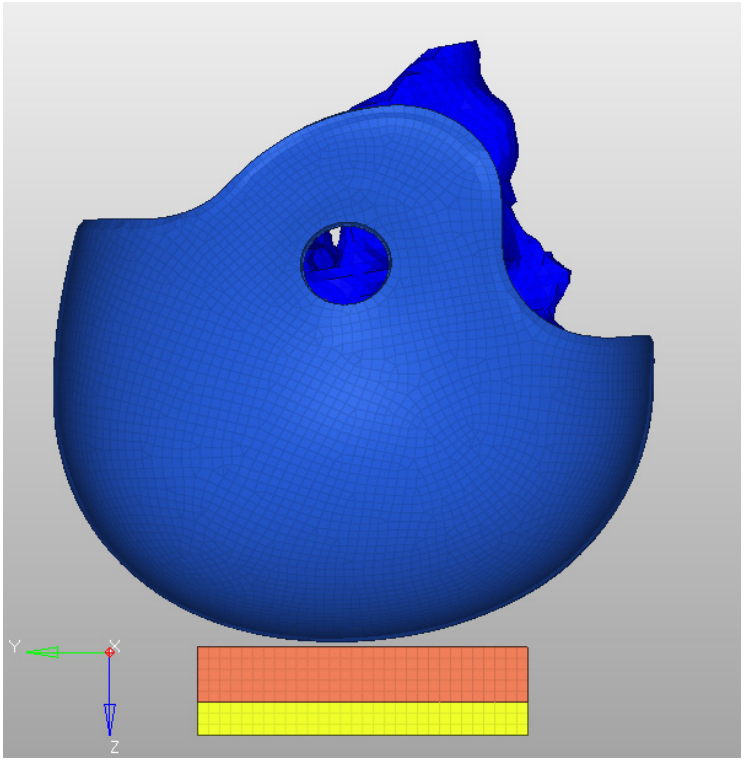

Figure 6-9 Superior Impact 0° Simulation Model

www.manaraa.com

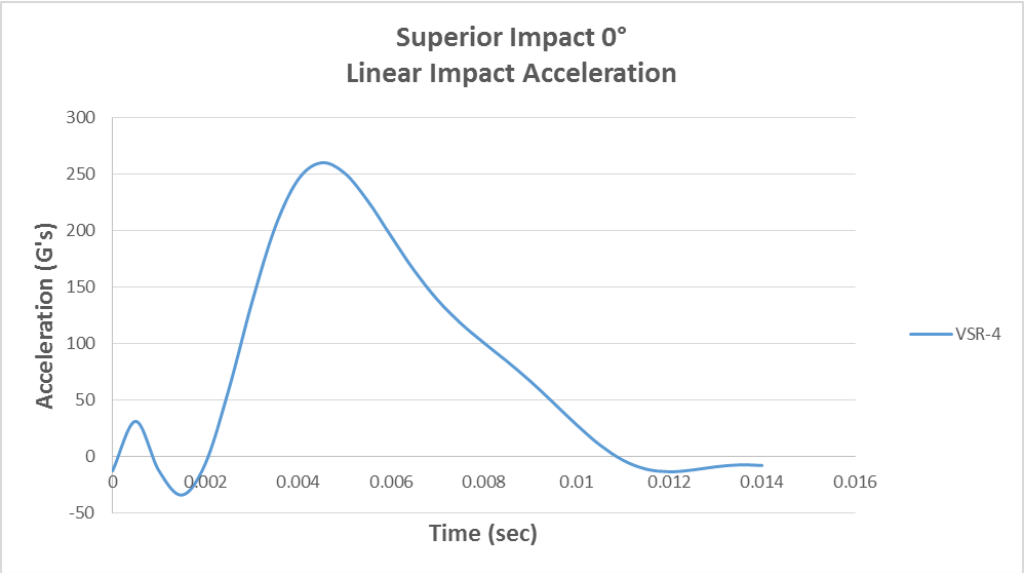

Figure 6-10 Superior Impact 0° Linear Head Acceleration

For all of the impact simulations, the stress results and rotational acceleration results are shown in Chapter 8. The results in Chapter 8 are used to evaluate the performance of the VSR-4 helmet against the EBM helmet. A complete list of helmet performance evaluation is given in Chapter 8.

www.manaraa.com

7 Concept and Configuration of the EBM Helmet Fitted onto a Human Head Model by Finite Element Modeling

The principal function of the EBM helmet is to minimize the risk of concussion injury to football players by absorbing head impact energy and reducing head translational and rotational accelerations. Since the majority of impacts on a helmet cause both linear and angular accelerations, the design of the EBM helmet is to utilize the existing padding for linear accelerations and provide an additional shear layer to address rotational accelerations. Linear acceleration causes pressure gradient while angular acceleration causes shear strain gradient. Frontal and occipital impacts cause both pressure and shear stress distributions in the brain [30].

7.1 Design Methodology of the Enhanced Bio-Morphic Football Helmet

As stated previously, concussion is a type of traumatic brain injury (TBI). It is a brain injury due to linear/angular acceleration/deceleration of the head due to impacts forcing interactions between the inner surface of the skull and the floating brain. Most impacts on the helmet cause both linear and angular accelerations. Linear acceleration of the head has been postulated to be the sole cause of injuries at the site of impact, or coup injuries, and opposite the site of impact, or countercoup injuries. Angular acceleration of the head, on the other hand, have been postulated to be the sole cause of injuries on a global scale, or diffuse axonal injuries. "While comparable negative pressure developed

www.manaraa.com

in the countercoup regions, shear stress distributions remained identical regardless of the impact direction, consistent with the clinically observed pattern for contusion. Therefore, shear strain theory appears to account better for the clinical findings in cerebral contusion [21]." Angular acceleration is therefore the primary causation factor for concussion.

A football helmet is a safety head gear used to protect players from head injuries due to impacts on the field. Head injuries include skull fractures and brain concussion. A given impact force at any location on the helmet can be resolved into normal and tangential impact forces. The tangential impact force at any location can be replaced by a tangential impact force (*TIF*) at the center of mass and torque (*TTIF*) about the center of mass due to *TIF*. Similarly, the normal impact force at any location can be replaced by a normal impact force (*NIF*) at the center of mass and a torque (*TNIF*) about the center of mass due to *NIF*. Resultant impact force (*RIF*) at the center of mass can be shown as:

$$RIF = (TIF) + (NIF) \qquad (7.1)$$

Resultant impact moment (*RIM*) about the center of mass is equal to:

$$RIT = (TTIF) + (TNIF) \qquad (7.2)$$

Kinetics:

$$RIF = m\,\bar{a}_G \qquad (7.3)$$

$$RIT = I_G\,\vec{\alpha} \qquad (7.4)$$

www.manaraa.com

Where:

m = mass of the helmet

$\bar{a}_G$ = linear acceleration of the center of mass

I_G - Mass moment of inertia of the helmet

$\vec{\alpha}$ = angular acceleration about the center of mass

$\bar{a}_G$ directly proportional to *RIF*, is a measure of skull fractures while m is a measure of resistance to linear acceleration. On the other hand, both I_G and α, directly proportional to *RIT,* are a measure of concussion, while I_G is a measure of resistance to angular acceleration.

The current football helmet design involves a stiff plastic outer shell to distribute *RIF* combined with an elastic foam inner shell to absorb the impact shock and to reduce the *RIF* in order to minimize the risk of skull fractures. The National Operating Committee on Standards for Athletic Equipment (NOCSAE) provides a set of voluntary standards, based on the Wayne State Tolerance Curve (WSTC), to evaluate a helmet's ability to prevent skull fracture. NOCSAE standards have helped to successfully eliminate skull fractures due to impacts in football games while wearing helmets designed with an *RIF* distributor; a stiff plastic outer shell and a RIF attenuator in the form of an elastic foam inner shell [22].

www.manaraa.com

As per Equations (7.3) and (7.4), the impacts on the helmet cause linear and angular accelerations of the head which bring forth pressure and shearing stress due to interactions between the skull and the brain resulting in concussion. To minimize linear acceleration, as seen from Equation (7.1), one can either minimize *RIF* or maximize the mass of the helmet. But "I can't have the helmet weigh too much because then I am putting stress loads on the neck and I am creating a whole set of different problems. I can't put in too much padding, then I am creating a heat-related issue. I can't make it too thin, I can't make it too thick," said Schutt Sports President and CEO, Robert Erb.[22] Similarly, to minimize angular acceleration, one can maximize the mass moment of inertia. But, "fashion cues are a factor. Older helmets such as the VSR-4 have smooth styling that players find cool: concussion resistant helmets bulge outward like the heads of cartoon space aliens" [23]. Besides, it maximizes *TTIF*.

During the 2012 and 2013 high school football season, U.W. Madison researchers [26], collected data from thirty-four public and private high schools in Wisconsin. Players in the study wore helmets from one of three helmet manufacturers: Riddell, Schutt, and Xenith. The researchers found no differences in the rate of sports-related concussions among helmet brands, the age of helmets, or reconditioned helmets. Of the 2081 high school athletes followed during the two year period, approximately 10% sustained a concussion. "Helmets of present day technology are supposed to prevent catastrophic brain injury like hemorrhages," said Kevin Guskiewicz, Chair of the NFL Subcommittee

www.manaraa.com

on Safety Equipment and Playing Rules. "They do a good job of that, but we want a helmet that does that as well as prevent concussion" [27].

The purpose of the EBM helmet is not only to minimize linear acceleration of the head to prevent catastrophic brain injury like hemorrhages, but also to minimize angular accelerations of the head to prevent concussion. In order to minimize linear acceleration, the helmet must have design provisions to attenuate *RIF* (See Equation (7.1)). Similarly, to minimize angular acceleration, the helmet must have design provisions to attenuate *RIT* (See Equation (7.2)). Current helmet technology does provide adequate design provisions to attenuate *NIF*, but it lacks design provisions to attenuate *TIF*.

The goal of EBM helmet technology is to introduce both impact force distributors and impact shock energy absorbers, not only to address *NIF,* but also to address *TIF*. Towards this goal, the EBM helmet is modeled to incorporate the addition of a shear layer, between the outer polycarbonate shell and the internal impact padding, to minimize the *TIF* that is imposed on the human head. All three materials bonded together to diffuse, distribute, dissipate, and absorb impact force and shock energy.

From the NFL, the injury tolerance for angular acceleration for a football player is 5757 to 5900 rad/sec^2 [27]. Zhang determined that the maximum resulting angular accelerations for a 50% probability of sustaining a Mild Traumatic Brain Injury (MTBI) is approximately 5900 rad/sec^2 for impact duration lasting between 10 and 30

www.manaraa.com

milliseconds [19]. For this reason, the EBM helmet was designed to help reduce the amount of angular acceleration that is transferred to the human brain.

www.manaraa.com

8 EBM Helmet Fitted onto a Human Head Model by Finite Element Method

The generation of the finite element model of the EBM helmet was performed in a same manner as how the VSR-4 helmet model was developed. The model was constructed from the same geometry model used to generate the VSR-4 finite element model. Using the same shell geometry and padding assured that a good and accurate comparison between the two types of helmets could be presented.

As stated previously the goal of the EBM helmet is to introduce both impact force distributors and impact shock energy absorbers, not only to address the normal impact force, but also to address the oblique impact force. This is accomplished by adding a shear layer between the polycarbonate shell and internal impact padding. This additional material is a key factor in addressing the oblique impact force reduction. The following sections describes the EBM finite element model in detail.

www.manaraa.com

8.1 EBM Finite Element Model

The EBM helmet model generated consists of 91254 nodes and 83,175 elements. Elements used in the model are HEXA8 and PENTA6 solid elements. Total mass of the FE model is 1.76kg, which is approximately 0.26kg heavier than the VSR-4 helmet of the same size. The additional mass associated with the EBM helmet is due to the additional shear layer.

Table 8-1 EBM Football Helmet FE Model Breakdown

Details of EBM Football Helmet FE Model				
	Location	**Number of Elements**	**Element Type**	**Layer Thickness (mm)**
Shell	Outer Surface	25,770	hexa8 & penta6	4
Sorbothane	Between Shell and Padding	21,375	hexa8 & penta6	3
Padding	Forehead	4,410	hexa8 & penta6	21
	Side/Posterior	21,590	hexa8 & penta6	17
	Crown	7,590	hexa8 & penta6	24.5
	Jaw	2,440	hexa8 & penta6	17

The internal padding of the helmet was meshed, in the same manner as the standard football helmet, to incorporate the different thicknesses of the pads on the interior of the helmet. The difference between the EBM helmet and the standard football helmet is the addition of the shear layer between the outer shell and padding material. The overall thickness of each region of padding is reduced to take into account of the additional thickness introduced by the shear layer. Therefore, the large EBM helmet will fit the

www.manaraa.com

same as a large VSR-4 football helmet. The forehead pad, crown pad, side and rear pads were modeled according to the measured thickness of the existing helmet, minus the thickness of the shear layer. The corresponding thickness of the internal padding is as follows:

- Forehead pad = 21mm
- Crown pad = 24.5mm
- Side and Posterior pad = 17mm
- Jaw pad = 17mm

Figure 8-1 through Figure 8-3 shows FE model of the complete EBM football helmet. For this study, the facemask is not included in the analysis.

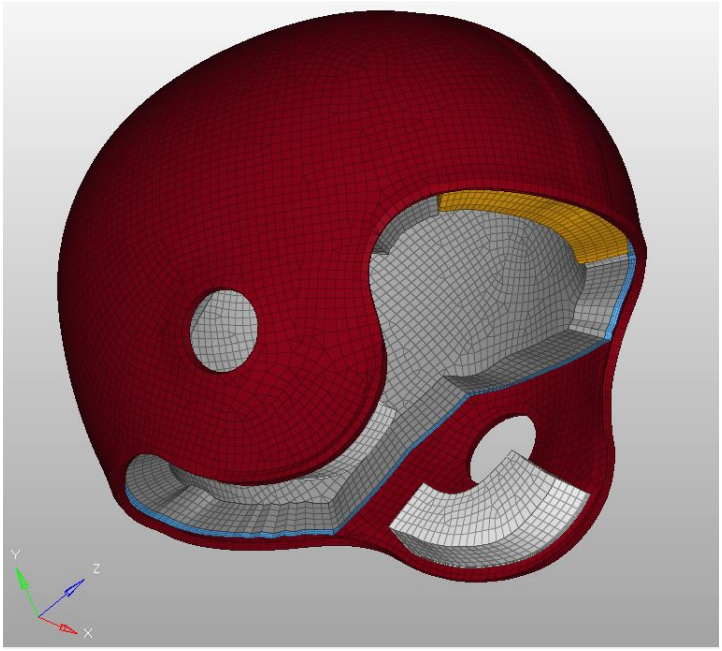

Figure 8-1 EBM Football Helmet without Facemask

www.manaraa.com

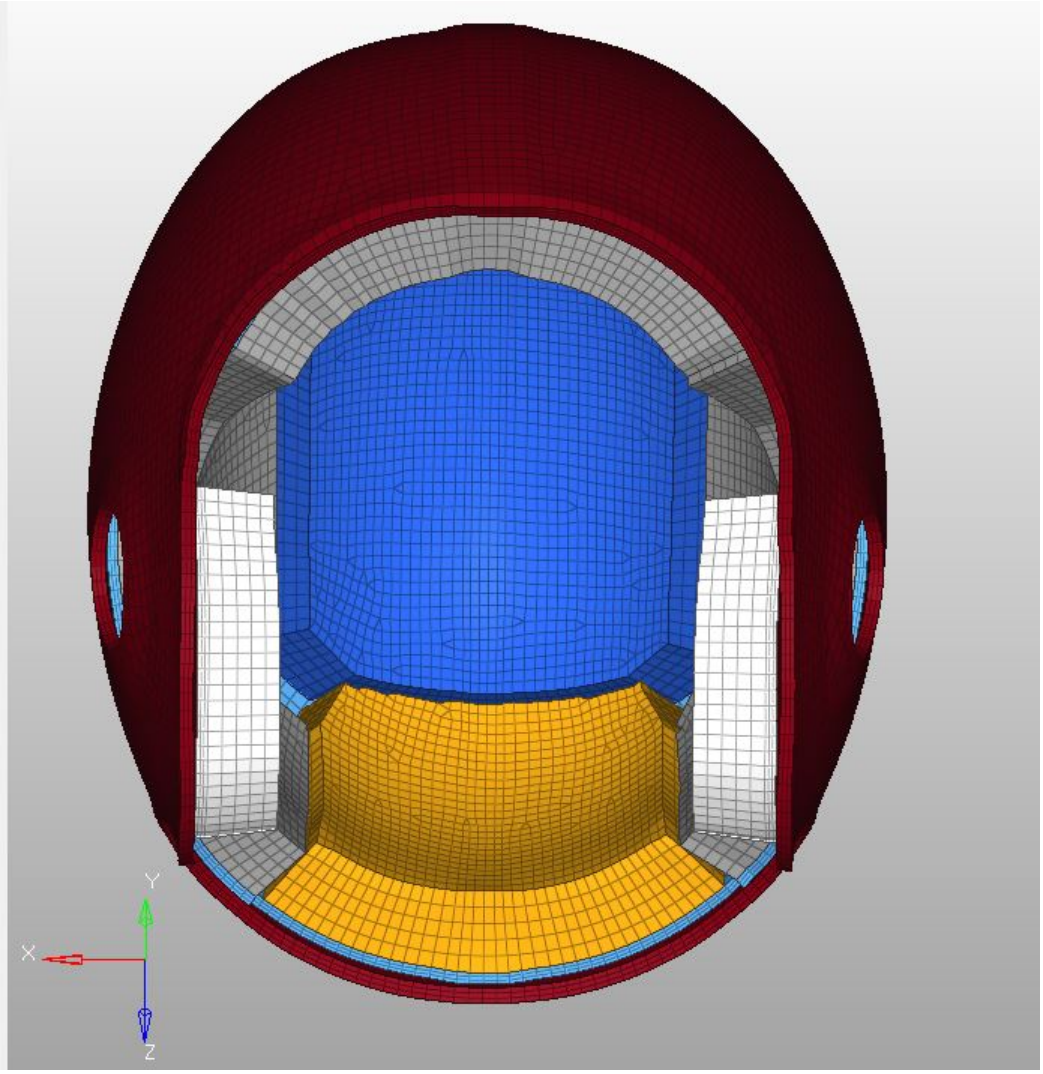

Figure 8-2 EBM Football Helmet Bottom View

www.manaraa.com

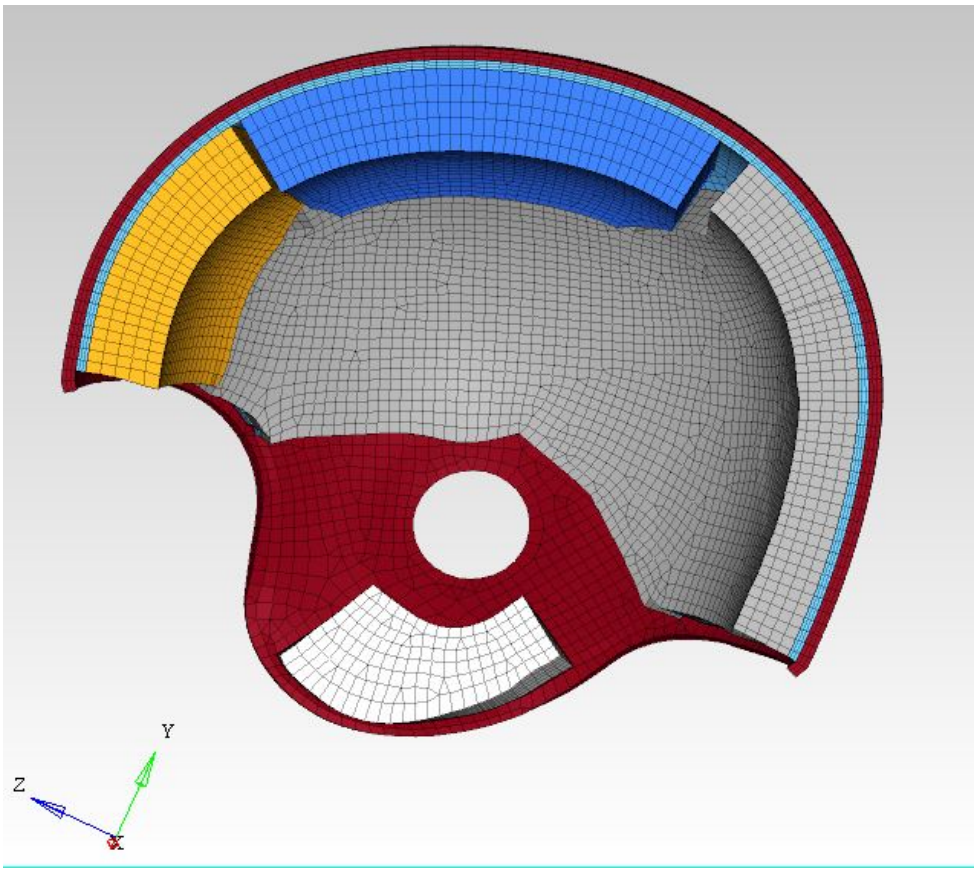

Figure 8-3 EBM Football Helmet Cross-Sectional View

8.2 Shear Layer – Sorbothane Material

The material used to represent the shear layer in the EBM helmet is Sorbothane®. Sorbothane® is the brand name of a polyether-based synthetic viscoelastic urethane polymer [13]. It is a thermoset with a very high damping coefficient. It is regarded as an excellent material for attenuating shock, isolating vibration, and damping. Sorbothane® is a solid that behaves like a liquid by absorbing shock in all directions. It is a stable material over a wide range of temperatures with a long fatigue life.

www.manaraa.com

The method used to define the material model in the finite element model is a material complex shear modulus, shear storage modulus, and loss factor is defined using the following equation [29]:

$$G(\omega) = G'(\omega) \cdot [1 + j\eta(\omega)] \qquad (8.1)$$

Where: $G(\omega)$ = complex shear modulus

$G'(\omega)$ = shear storage modulus

$\eta(\omega)$ = loss factor

For Sorbothane® DURO 50, the storage modulus used was 194 kPa and a loss factor used was 0.570 [29].

8.3 Material Properties of the EBM Helmet Model

The material properties used in the EBM helmet model are the same materials that were used to validate the VSR-4 football helmet by Kangana Bhushan [14], with the exception of the Sorbothane® layer. The material properties displayed in Table 8-2 is a list of the material used in the FE model and the corresponding material model used for the finite element analysis.

www.manaraa.com

Table 8-2 EBM Football Helmet Material Properties

Material Properties of EBM Football Helmet FE Model				
	Location	**Material Model**	**Density (kg/mm^3)**	**Poission's Ratio**
Shell	Outer Shell	Elastic	1.30E-06	0.32
Sorbothane	Between Shell and Padding	Hyperelastic	1.41E-06	0.499
Padding	Forehead	Foam	3.20E-07	0.01
	Side/Posterior	Foam	2.00E-07	0.01
	Crown	Foam	2.80E-07	0.01
	Jaw	Foam	2.00E-07	0.01

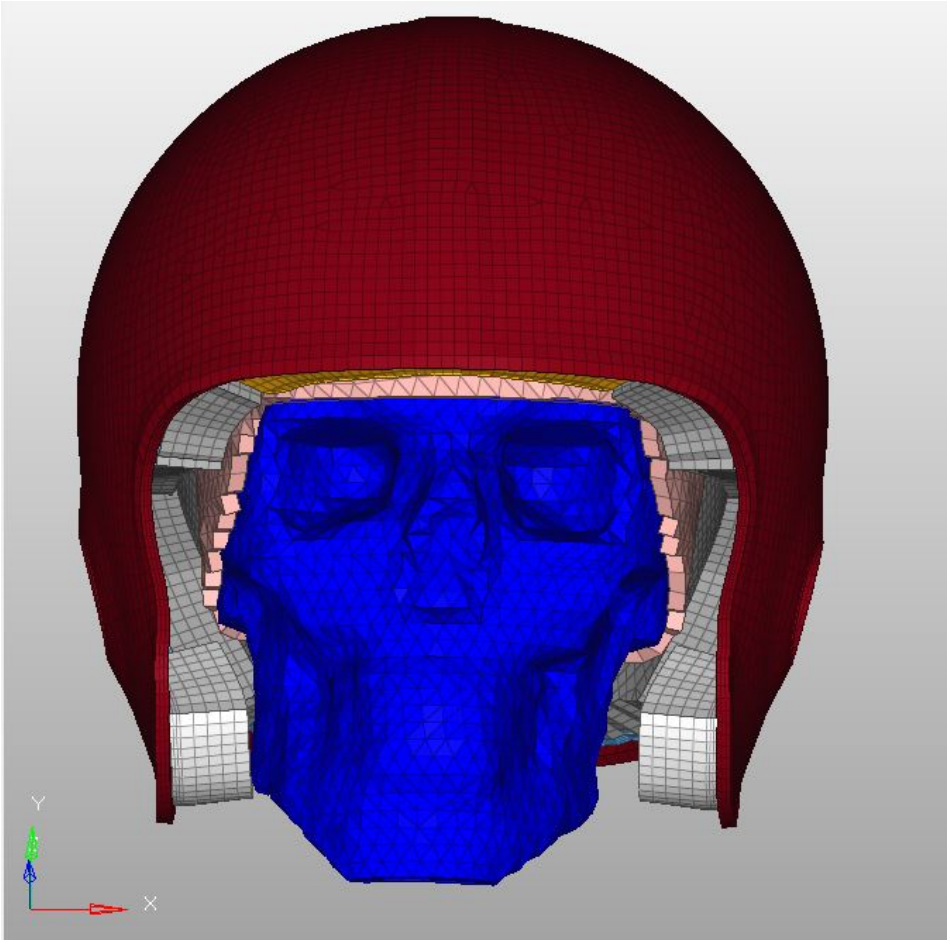

Figure 8-4 EBM Football Helmet and Human Head Model Assembly

www.manaraa.com

8.4 Impact Simulation and Boundary Conditions

Impact simulations for the frontal, lateral, posterior, and superior locations are shown in Figure 8-5. To be consistent with the NOCSAE drop test setup, the head model was positioned using the same impact angles the drop test frame uses. The impactor used in these simulations is the same impactor that was used in the VSR-4 helmet evaluation by Kangana [14] and human head impact evaluation by myself [30]. The material properties of the impactor are listed in Table 8-3.

Table 8-3 Impactor Material Properties

Material Properties of Impactor				
	Material Model	**Young's Modulus (Mpa)**	**Density (kg/m^3)**	**Poission's Ratio**
Padding	Elastic	10	1200	0.3
Steel	Elastic	209000	7800	0.29

The impactor in this set of analyses is actually fixed to ground and the helmet and head model are given an initial velocity to simulate the impact event. For all impact simulations an initial velocity of 5.47 m/s is prescribed for the helmet and human head assembly. To define an oblique impact, the vector quantity of 5.47 m/s velocity is resolved to an angle of impact. The helmet and head assembly do not have any other boundary conditions associated to them other than the initial velocity.

www.manaraa.com

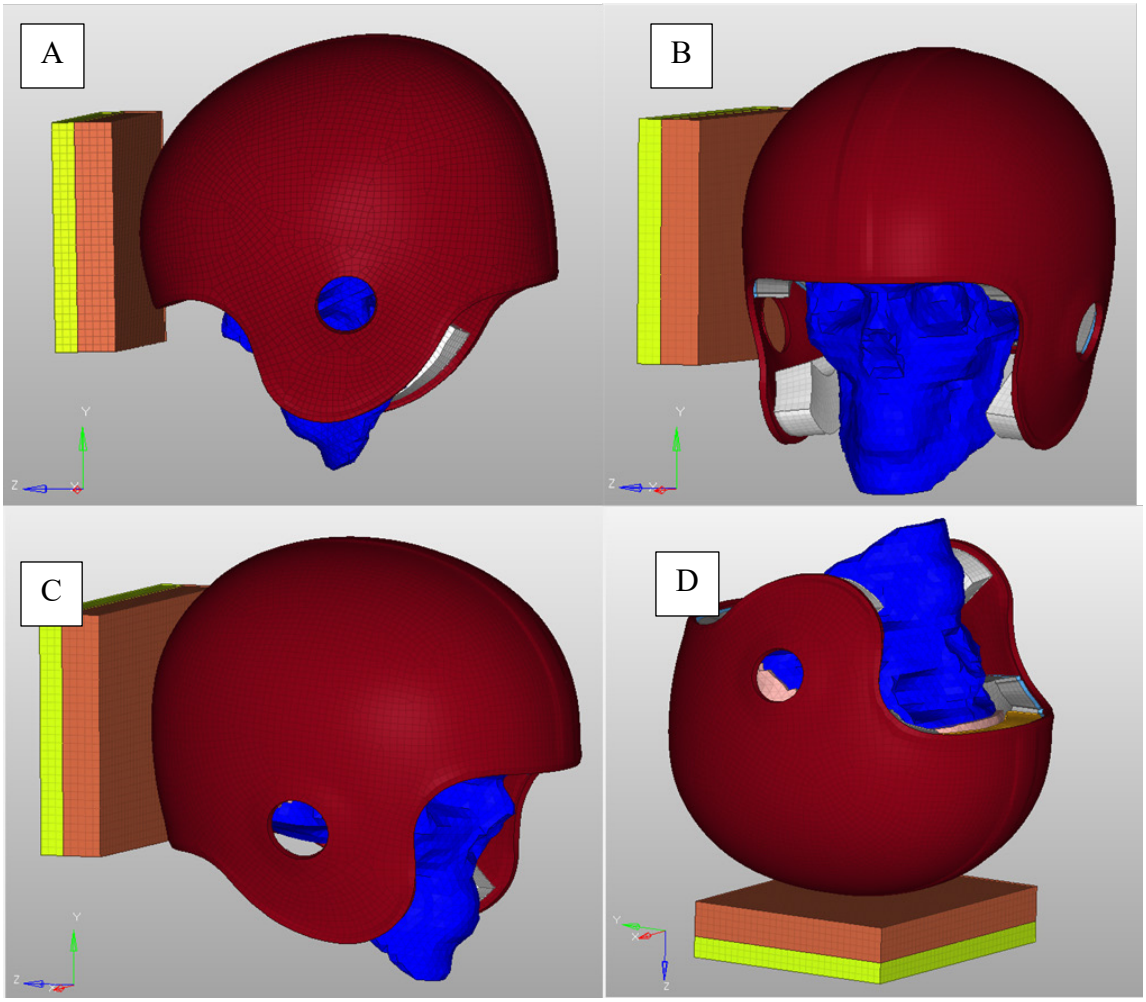

Figure 8-5 Frontal (A), Lateral (B), Posterior (C), and Superior (D) Impact Models

Contact conditions between contact pairs was defined using the same multi-usage impact interface, as described in Chapter 5.2 for the simulation of the VSR-4 helmet impacts. The use of the same contact definitions applied with the EBM helmet model assured the two models would be using the same model descriptions.

www.manaraa.com

9 VSR4 and EBM Helmet Comparison

In order to quantify the benefit of the EBM helmet over the commercially available VSR4 football helmet, a full helmet to helmet comparison is required. In this chapter, the impact results of the EBM helmet are shown adjacent to the results of the VSR4 helmet. The ultimate evaluation of a helmet is to show how well it performs in reducing the transfer of energy from the impacting surface to the human brain. The primary design consideration in every helmet is to reduce the impact energy. That energy transfer, results in stress distribution to the brain is the proving factor in determining how well a helmet performs.

9.1 Angular Acceleration Calculation

The method used to calculate angular acceleration is described using the coordinate system triad in Figure 9-1. Linear accelerations for nodes within the brain are recorded for the center of mass, frontal region, lateral region, superior region, and posterior region. The nodes used coincide with the global coordinate system. Distances of each node is measured relative to the center of mass node. The X, Y, and Z component of acceleration is then calculated using the difference in acceleration between that corresponding node and the center of mass. The angular acceleration about each direction is then calculated from the linear acceleration. As an example, the angular acceleration about the X-axis is calculated using the amount of linear Z-axis acceleration and Y-axis acceleration that

www.manaraa.com

cause the angular acceleration about the X-axis. The same methodology is used to calculate the angular acceleration about the Y-axis and Z-axis.

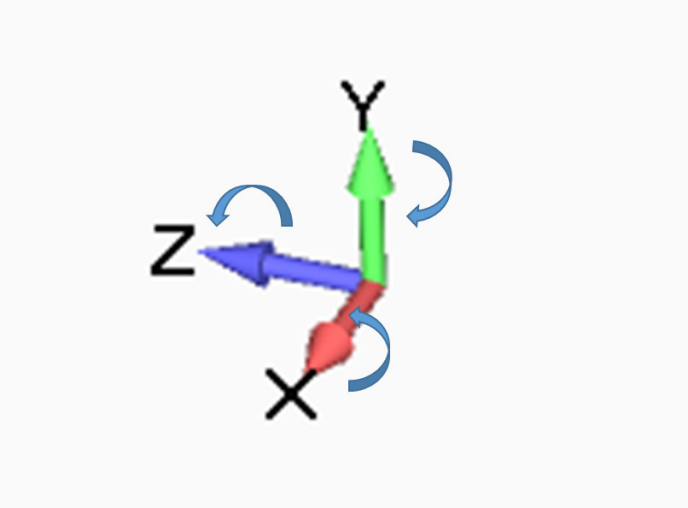

Figure 9-1 Angular Acceleration Calculation Methodology

Nodal results for the different regions of the brain are then used to calculate angular acceleration for the Frontal, Side, Posterior, and Superior impact simulations. This methodology is used to calculate angular acceleration to account for the off axis rotation that is expected with an impact event.

www.manaraa.com

9.2 Frontal Impact

The setup for the frontal impact simulation is shown in Figure 9-2. The head is inclined at a 5° angle relative to the transverse plane similar to the NOCSAE drop test configuration for frontal impacts. As previously stated in Chapter 7, the impactor used is a stationary impactor with the velocity of the head given an initial velocity boundary condition. The initial velocity of the head and helmet assembly is 5.47 m/s. For all of the impact simulations, the 15° impact angle is eliminated. This is due to the relative small difference from a normal impact angle. Although the final outcome of the analysis can be determined for 15°, the simulation results were not performed.

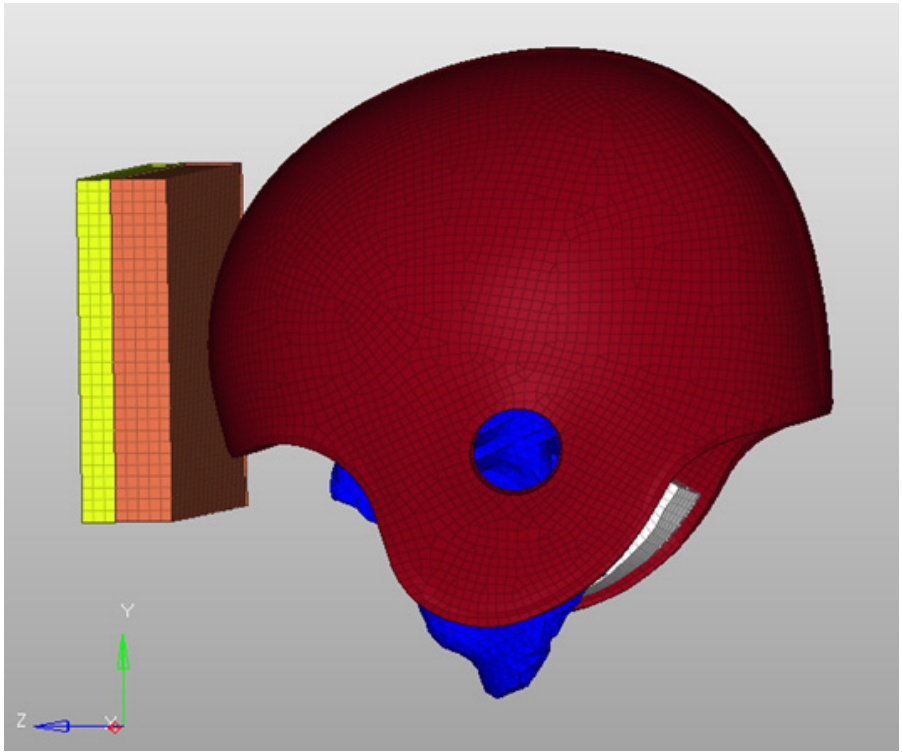

Figure 9-2 Frontal Impact Arrangement

www.manaraa.com

A comparison of the impact results of the EBM helmet and VSR4 helmet are shown in Figure 9-3 through Figure 9-6. The impact force, in Figure 9-3, and linear impact acceleration, in Figure 9-6, for both helmets are very close to each other for the 0° impact simulation, with the VSR4 impact force and acceleration being slightly higher. Upon reviewing the results, this is the outcome for all the impact simulations. The difference can be most likely explained by the fitting of the head model into the padding of the helmet once impact is initiated. Although this happens with both helmet types, the EBM helmet's shear layer helps provide a cushioning effect for the inconsistencies between the contour of the helmet padding and the contour of the forehead. Thereby, allowing a better fit transition during the impact event. This can also be seen in the time duration of the impact curve comparison where the impact event of the EBM helmet is slightly longer than that of the VSR4. Although there is only a small difference between the two, there is still a difference.

What becomes apparent between the two helmet types, however, is the reduction in angular acceleration with the EBM helmet once the angle of impact increases from 0° to 30°. The additional shear layer provides a attenuation mechanism to reduce the amount of rotational acceleration transferred to the brain. The largest percent reduction of 46% is seen with the 30° impact angle. This reduction in angular acceleration is very important when reviewing the stress results for the various impacts.

www.manaraa.com

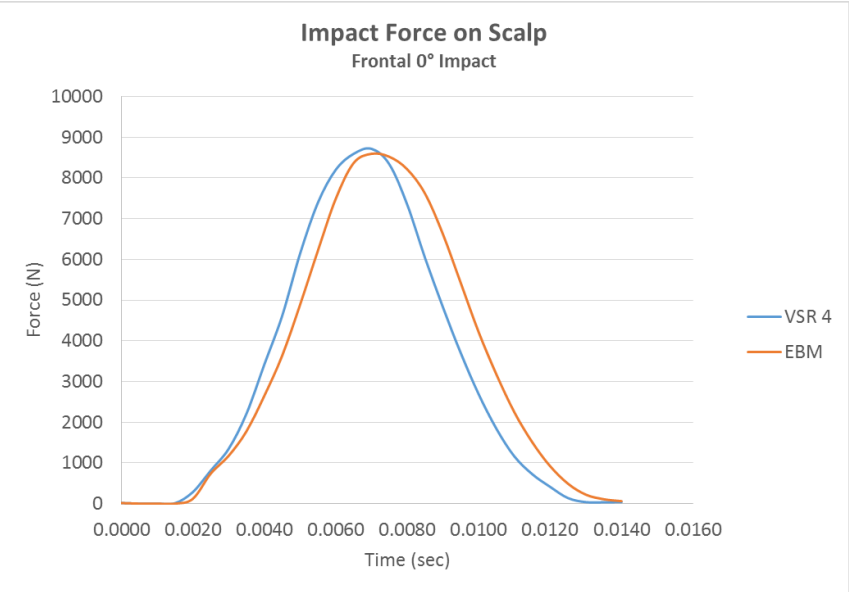

Figure 9-3 VSR4 and EBM Helmet – Frontal Impact – Impact Force on the Scalp at the Site of Impact

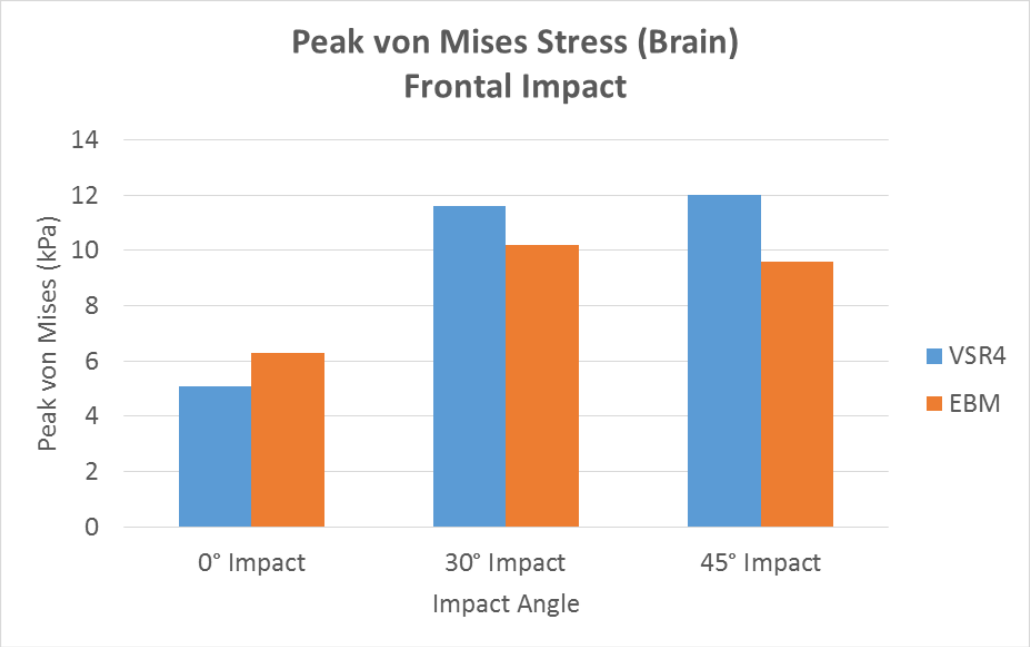

Figure 9-4 VSR4 and EBM Helmet - Frontal Impact – Brain Peak von Mises Stress

www.manaraa.com

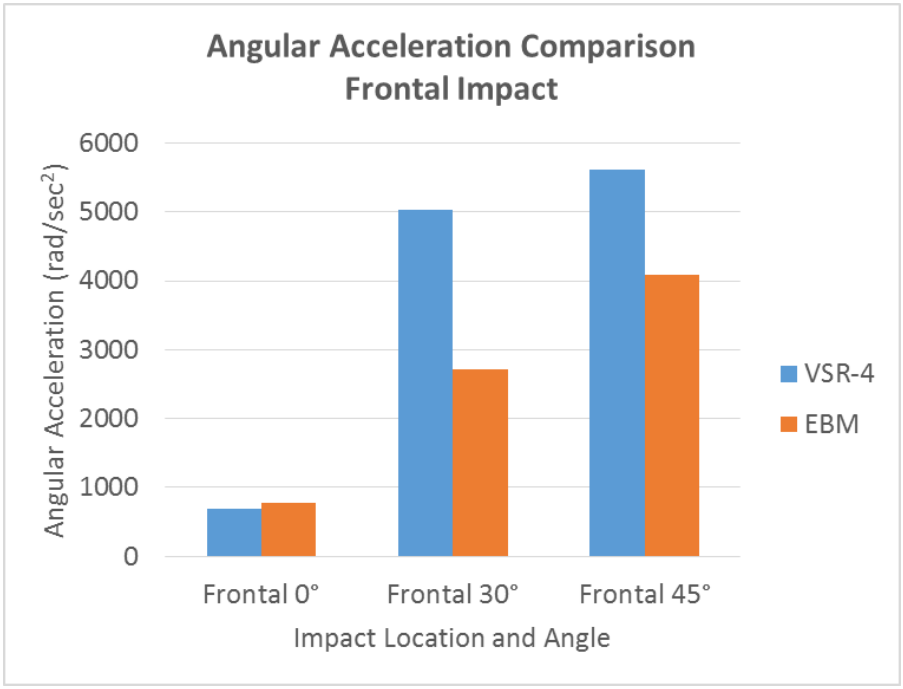

Figure 9-5 VSR4 and EBM Helmet – Frontal Impact - Angular Acceleration Comparison

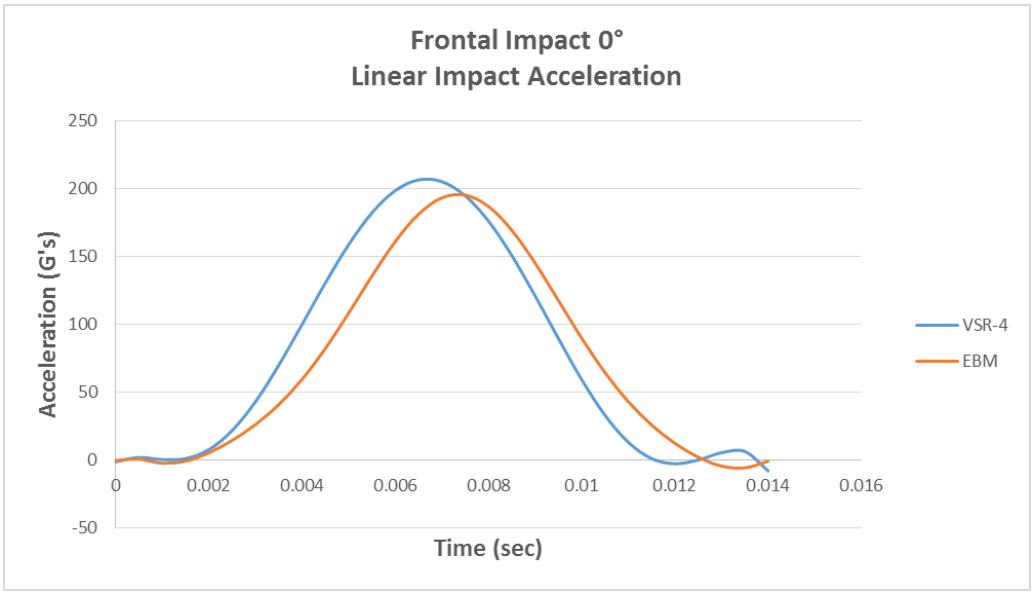

Figure 9-6 VSR4 and EBM Helmet – Frontal Impact - Linear Acceleration

www.manaraa.com

9.2.1 Frontal Impact 0° - von Mises Stresses

Stress comparison on the brain of VSR4 and EBM helmet impacts follows the predicted results of the calculated angular acceleration. The EBM helmet shows a 12% increase in angular acceleration over the VSR4 helmet. The results from the EBM helmet show a peak stress range of 5.1 kPa to 6.3 kPa as compared to the VSR4 helmet of 3.9 kPa to 5.1 kPa, which is a slight increase in stresses over the superior area of the brain. The stress area of 3.9 kPa to 5.1 kPa for the EBM helmet also covers a larger area over the superior region of the brain. Both stress results are scaled the same for a direct comparison.

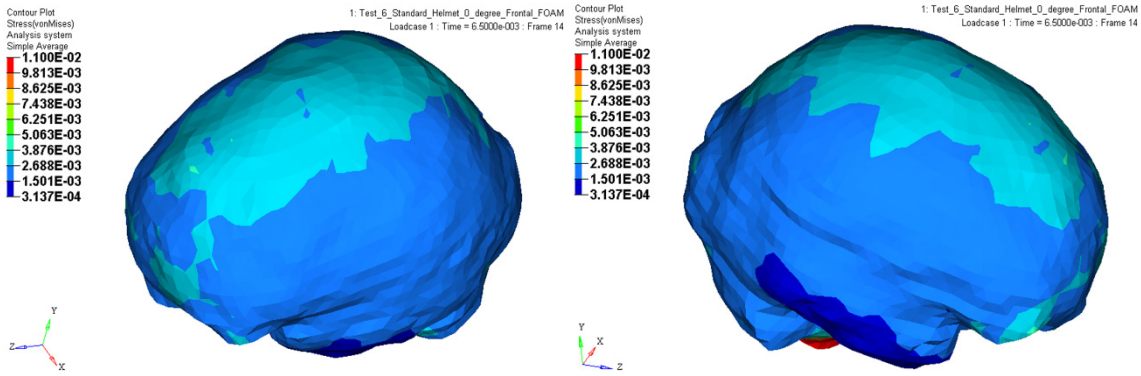

Figure 9-7 VSR4 Helmet - Frontal Impact 0° - von Mises Stress

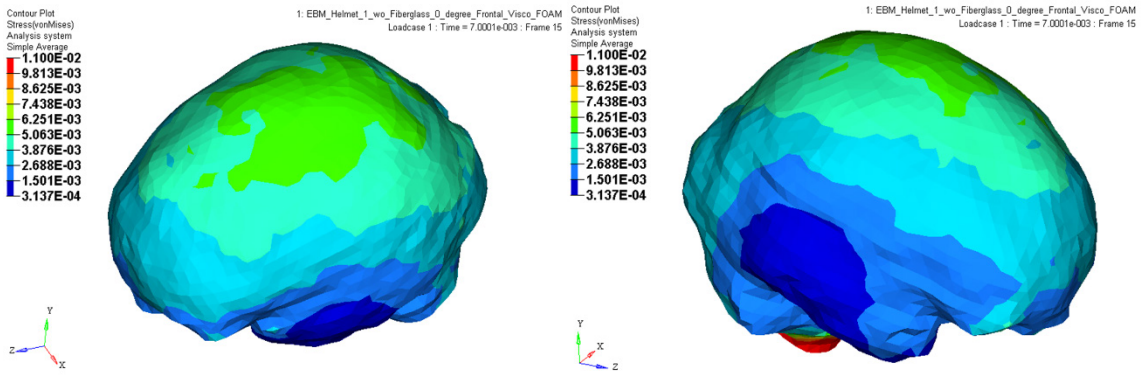

Figure 9-8 EBM Helmet - Frontal Impact 0° - von Mises Stress

www.manaraa.com

9.2.2 Frontal Impact 30° - von Mises Stresses

As seen in Figure 9-5, the EBM helmet provides an added feature in reducing angular acceleration transferred to the brain. As seen below, the additional shear layer provides means for reducing the stresses caused by the helmet and head rotating from the impact event. The stress peak stress level for the EBM helmet is between 8.9 kPa to 10.2 kPa over a small region of the left lateral side of the brain. Whereas, the VSR4 helmet model shows a peak stress level between 10.2 kPa and 11.6 kPa. The peak stress area for the VSR4 helmet is small, but a greater increase overall. In addition, the stress level between 8.9 kPa to 10.2 kPa covers a much larger area for the VSR4 helmet.

Stress levels on the right side of the brain are also higher for the VSR4 helmet. Stress levels for this helmet are between 6.2 kPa and 7.3 kPa as compared to 4.9 kPa to 6.3 kPa for the EBM helmet. Another significant point to note is the area of stress between 0.93 kPa to 2.2 kPa for the EBM helmet being much larger than the VSR4 helmet.

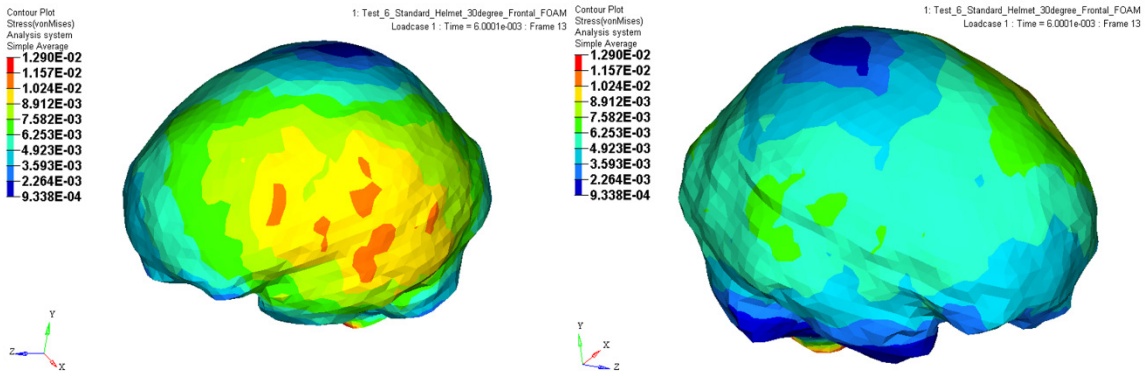

Figure 9-9 VSR4 Helmet - Frontal Impact 30° - von Mises Stress

www.manaraa.com

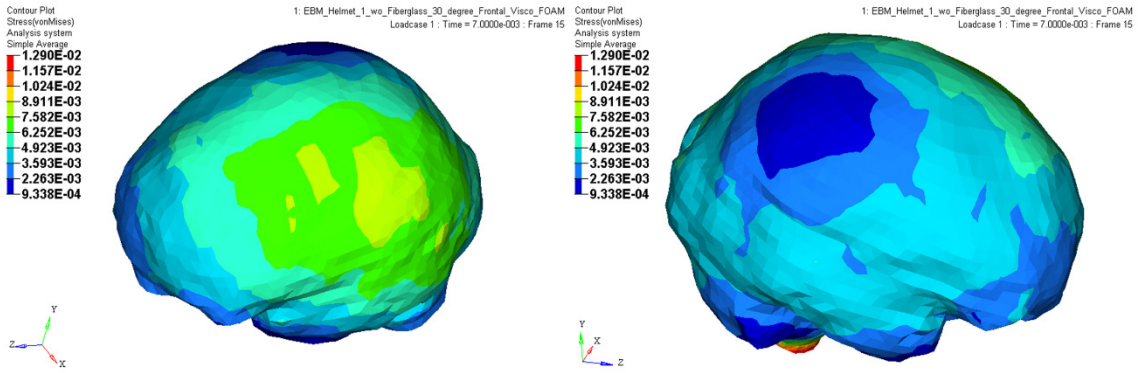

Figure 9-10 EBM Helmet - Frontal Impact 30° - von Mises Stress

www.manaraa.com

9.2.3 Frontal Impact 45° - von Mises Stresses

Although, the amount of angular acceleration reduction for the 45° impact is not as significant as compared to the 30° impact (27% reduction compared to 46%), the added benefit is still present. As seen below, the stress reduction for the EBM helmet is significantly better than the VSR4 helmet. The peak stress level on the left lateral side for the VSR4 helmet is between 10.8 kPa to 12.0 kPa as compared to a peak stress between 8.4 kPa to 9.6 kPa for the EBM helmet. This reduction in peak stress is significant for the EBM helmet. In addition, the area of peak stress for the VSR4 helmet covers a larger area as compared to the peak stress area for the EBM helmet.

Stress levels on the right side of the brain are also higher for the VSR4 helmet. Stress levels for this helmet are between 8.4 kPa to 9.6 kPa as compared to 5.9 kPa to 7.1 kPa for the EBM helmet. Another significant point to note is the larger area of low stress for the EBM helmet being between 0.93 kPa to 2.2 kPa as compared to the area of low stress for the VSR4 helmet.

www.manaraa.com

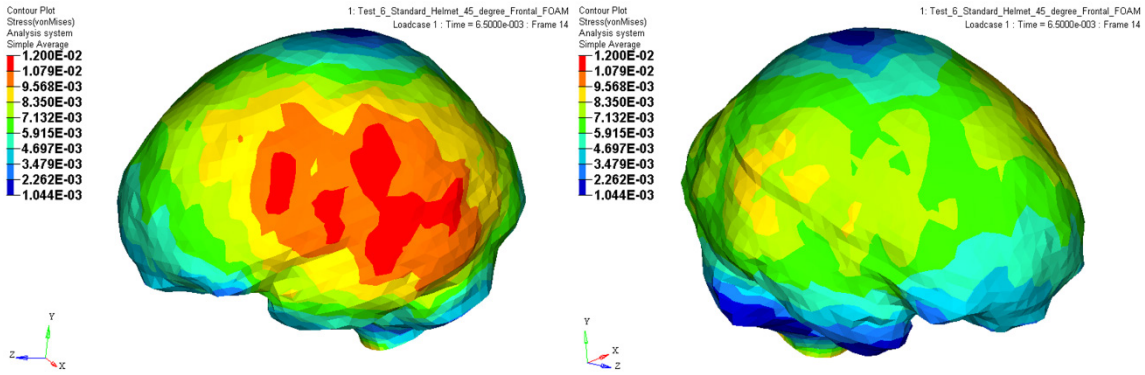

Figure 9-11 VSR4 Helmet - Frontal Impact 45° - von Mises Stress

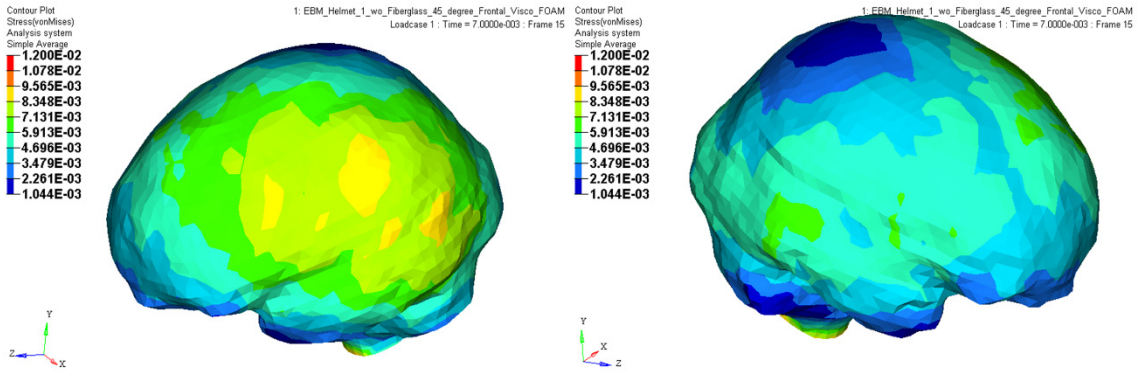

Figure 9-12 EBM Helmet - Frontal Impact 45° - von Mises Stress

For the 45° impact results, a cross-section of the transverse plane and sagittal plane is shown. See Figure 9-13 and Figure 9-14. As seen in these stress contours, the highest stress is located around the perimeter surface of the brain, were as, the central portion of the brain is lower. The area of stress, in the interior of the brain for the EBM helmet are between 2.6 kPa to 3.5 kPa are lower compared to a higher level for the VSR4 helmet between 3.5 kPa to 4.7 kPa. The sagittal plate cross-section also indicates an axis of

www.manaraa.com

rotation for the head. With these results, the injury mechanism points toward a global shearing type of injury around the outer region of the brain, commonly found with concussions.

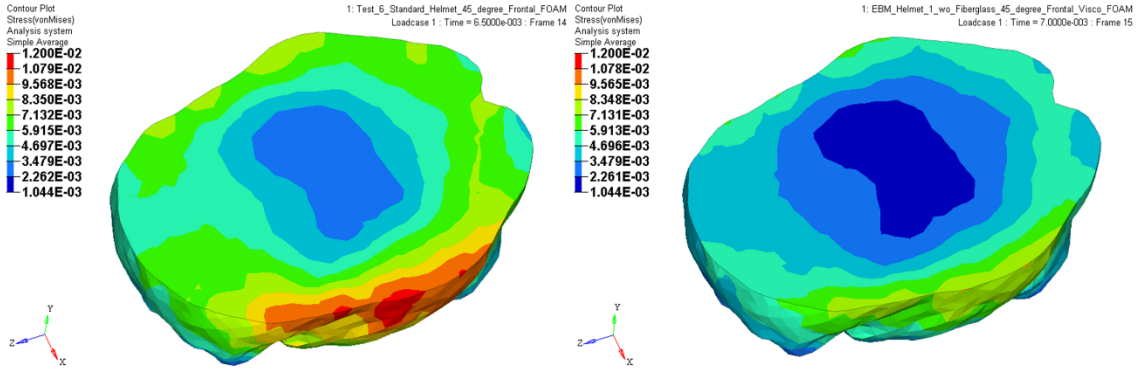

Figure 9-13 VSR4 (left) and EBM (right) Helmet - Frontal Impact 45° - von Mises Stress Traverse Plane Cross-Section

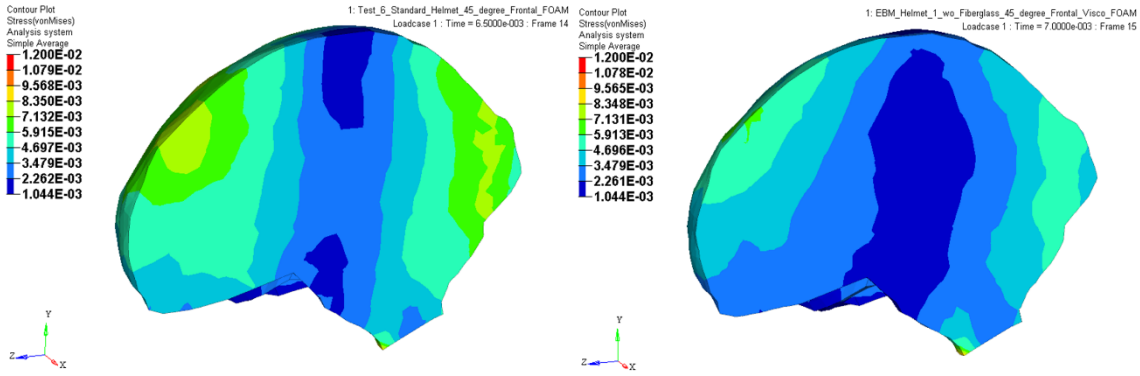

Figure 9-14 VSR4 (left) and EBM (right) Helmet - Frontal Impact 45° - von Mises Stress Sagittal Cross-Section

www.manaraa.com

9.2.4 Frontal Impact 0° - Principal Stresses

Principal stress comparison of the VSR4 and EBM helmets are shown in Figure 9-15 and Figure 9-16. For the principal stresses, the peak stress shown in (red) indicates the region in tension (opposite the site of impact), whereas, the peak stress shown in (blue) is compression (site of impact). Both the VSR4 and EBM helmet yield similar results, however the area of peak compression for the EBM helmet is smaller as compared to the area of the VSR4 helmet.

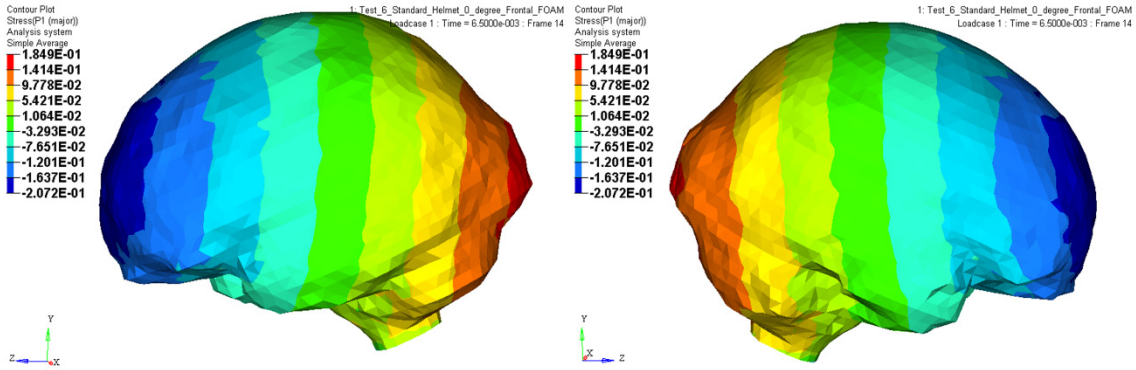

Figure 9-15 VSR4 Helmet - Frontal Impact 0° - Principal Stress

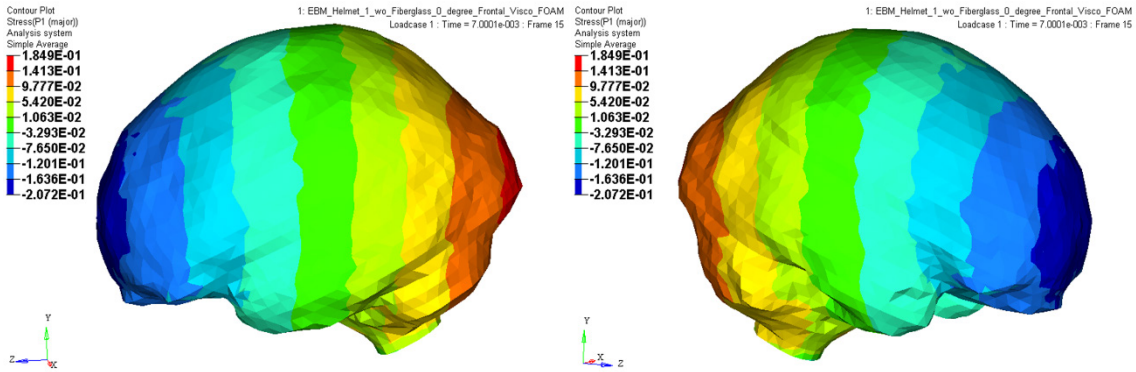

Figure 9-16 EBM Helmet - Frontal Impact 0° - Principal Stress

www.manaraa.com

9.2.5 Frontal Impact 30° - Principal Stresses

Principal stresses for the 30° Frontal impact yield similar results for both helmets. Differences between the peak compressive and tensile stresses for either helmet is insignificant.

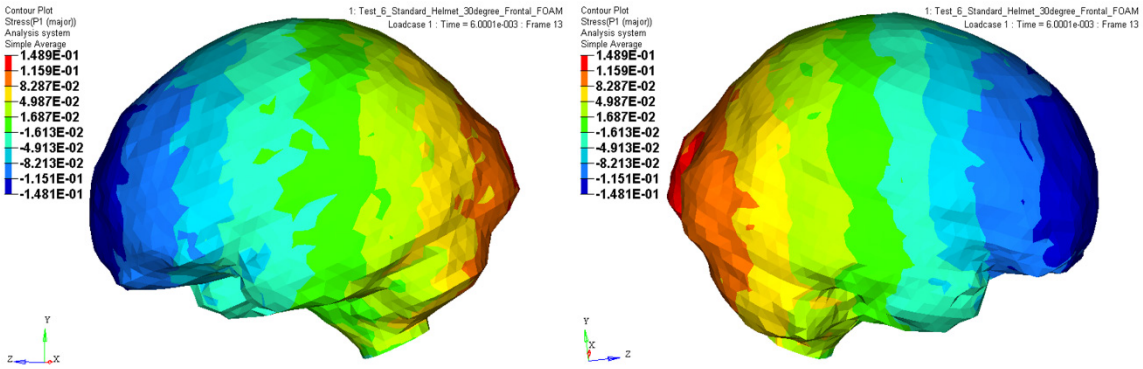

Figure 9-17 VSR4 Helmet - Frontal Impact 30° - Principal Stress

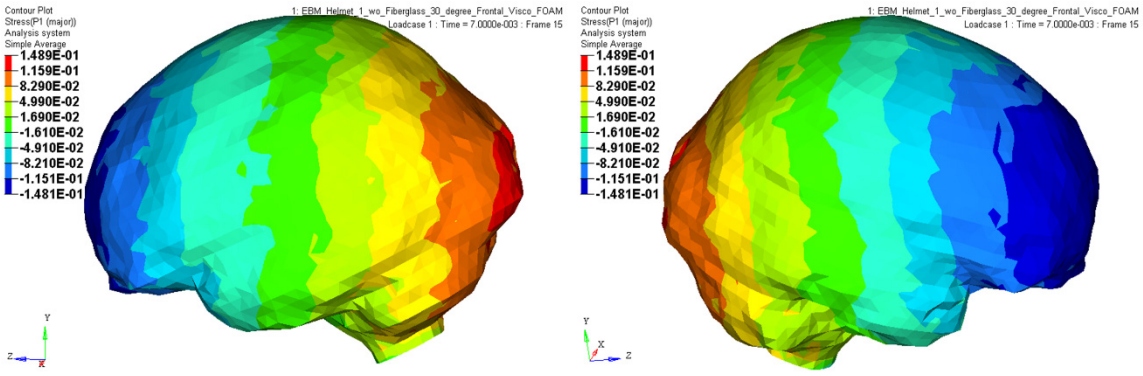

Figure 9-18 EBM Helmet - Frontal Impact 30° - Principal Stress

www.manaraa.com

9.2.6 Frontal Impact 45° - Principal Stresses

Principal stresses for the 45° frontal impact yield similar results for both helmets as well. Differences between the peak compressive and tensile stresses for either helmet is insignificant.

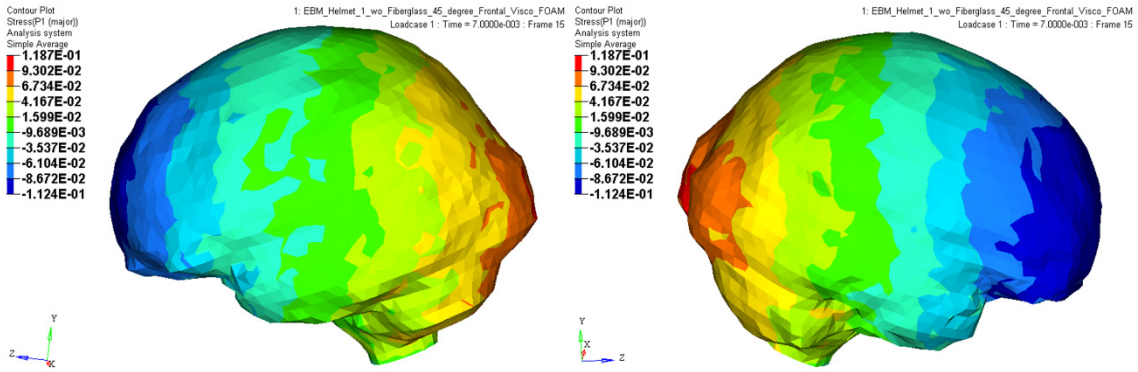

Figure 9-19 VSR4 Helmet - Frontal Impact 45° - Principal Stress

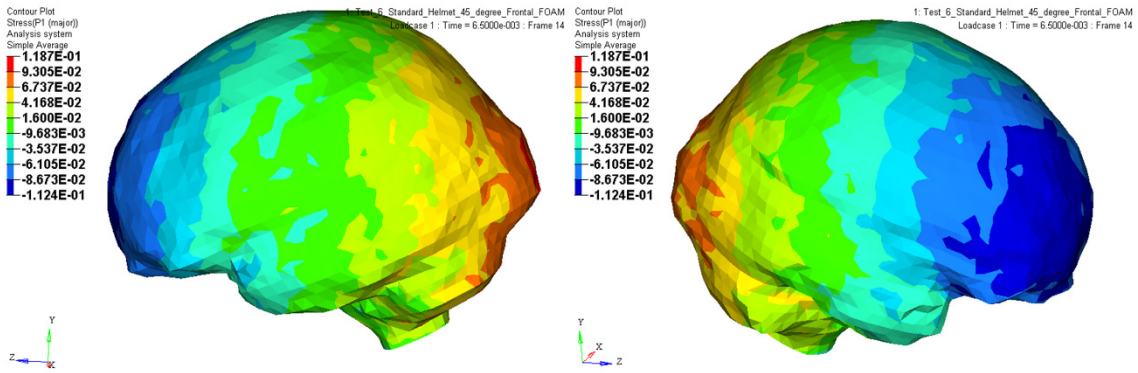

Figure 9-20 EBM Helmet - Frontal Impact 45° - Principal Stress

www.manaraa.com

9.3 Lateral Impact

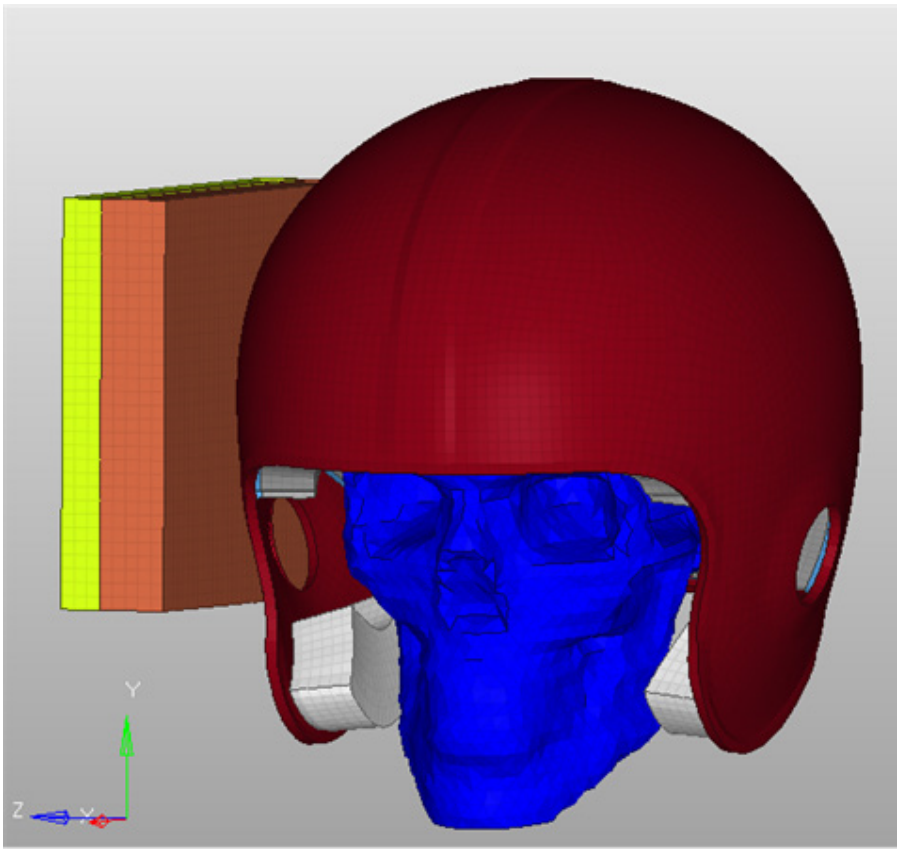

Figure 9-21 Lateral Impact Arrangement

The setup for the lateral impact simulation is shown in Figure 9-21. The head is oriented in line with the global coordinate system and perpendicular to the impacting surface. With the lateral impact, there is no angle of incline associated with the helmet relative to the impactor. This impact configuration coincides with the NOCSAE drop test configuration for lateral impacts. The initial velocity of the head and helmet assembly is 5.47 m/s traveling in the +Z axis, into the impactor plate.

www.manaraa.com

A comparison of the lateral impact results of the EBM and VSR4 helmets are shown in Figure 9-22 through Figure 9-25. The linear impact acceleration for both helmets are very close to each other for the 0° impact simulation, with the VSR4 helmet being slightly higher than the EBM helmet. This difference follows the same logic for the fit between the head and helmet explained in the frontal impacts. Since the side, or lateral, area of the head is flatter than the frontal region of the head, the impact duration is similar in both cases.

The impact force, at the surface of the scalp, for the VSR4 and EBM helmet are nearly the same without any significant differences. See Figure 9-22. Both time duration and peak impact force are very similar. Since the area of impact on the surface of the scalp is large for lateral impacts, a good measurement for impact force was achieved. This is a common result with all lateral impacts.

An interesting result of the lateral impact, as compared to the frontal impact, is the amount of reduction of angular acceleration at 0° and then the similar results at 45°. For the lateral impact, the amount of angular acceleration for a 0° impact is large, due to the impact vector not being in line with the center of mass of the head. This is an inherent problem with lateral impacts in general. With the normal impact not being in line with the center of mass of the head, the resulting shearing stresses on the brain are higher than all the other impact arrangements. From the impact simulations, the center of mass of the head is slightly forward of the impact location on the helmet. Once the impact angle

www.manaraa.com

increases, however, the impact vector is directed more in line with the center of mass of the head. This is apparent from the reduction in angular acceleration once the impact angle increases.

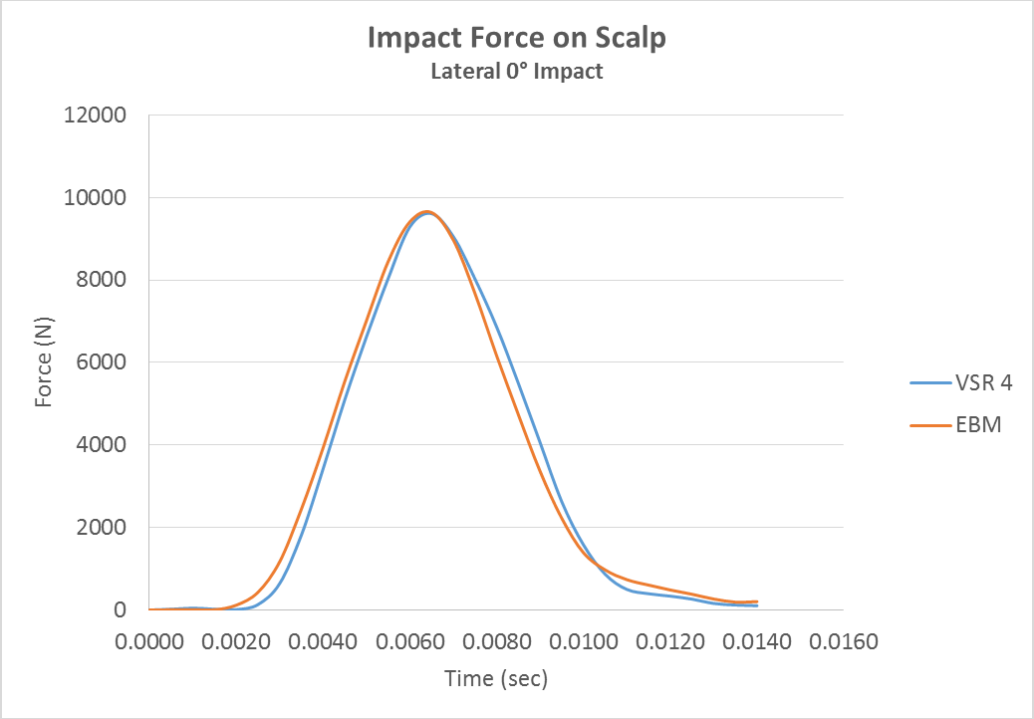

Figure 9-22 VSR4 and EBM Helmet – Lateral Impact – Impact Force on the Scalp at the Site of Impact

www.manaraa.com

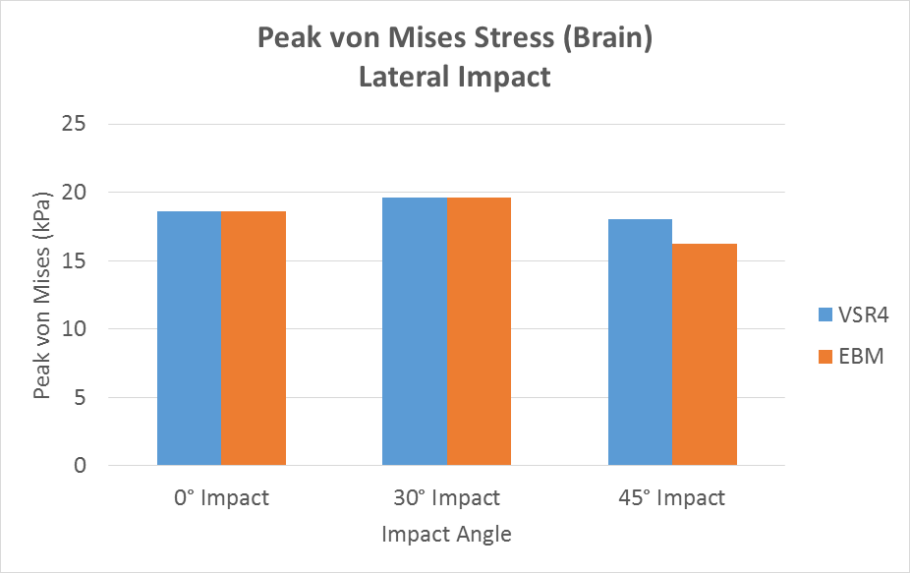

Figure 9-23 VSR4 and EBM Helmet - Lateral Impact – Brain Peak von Mises Stress

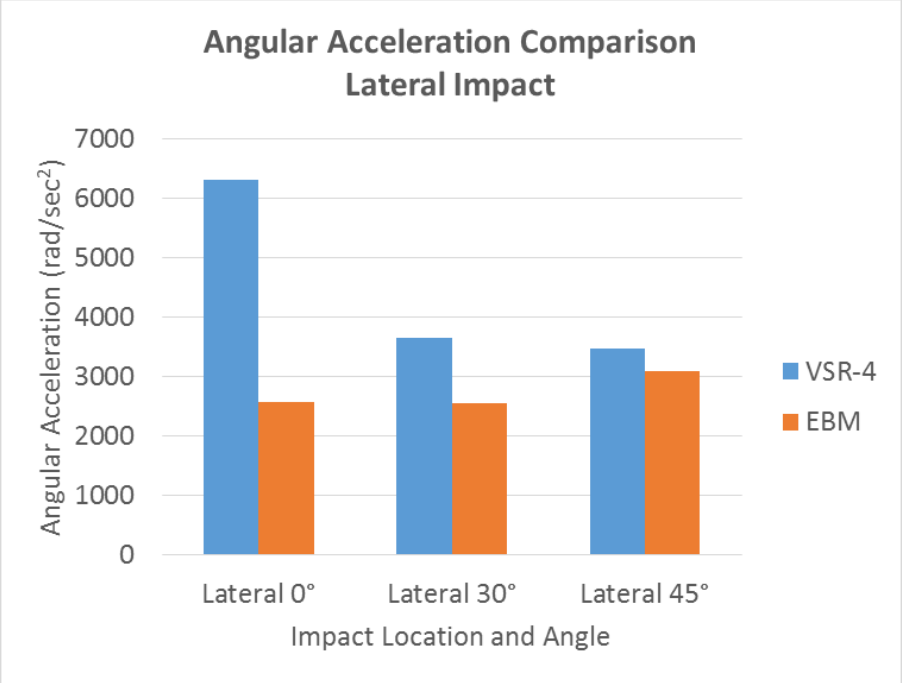

Figure 9-24 VSR4 and EBM Helmet – Lateral Impact - Angular Acceleration Comparison

www.manaraa.com

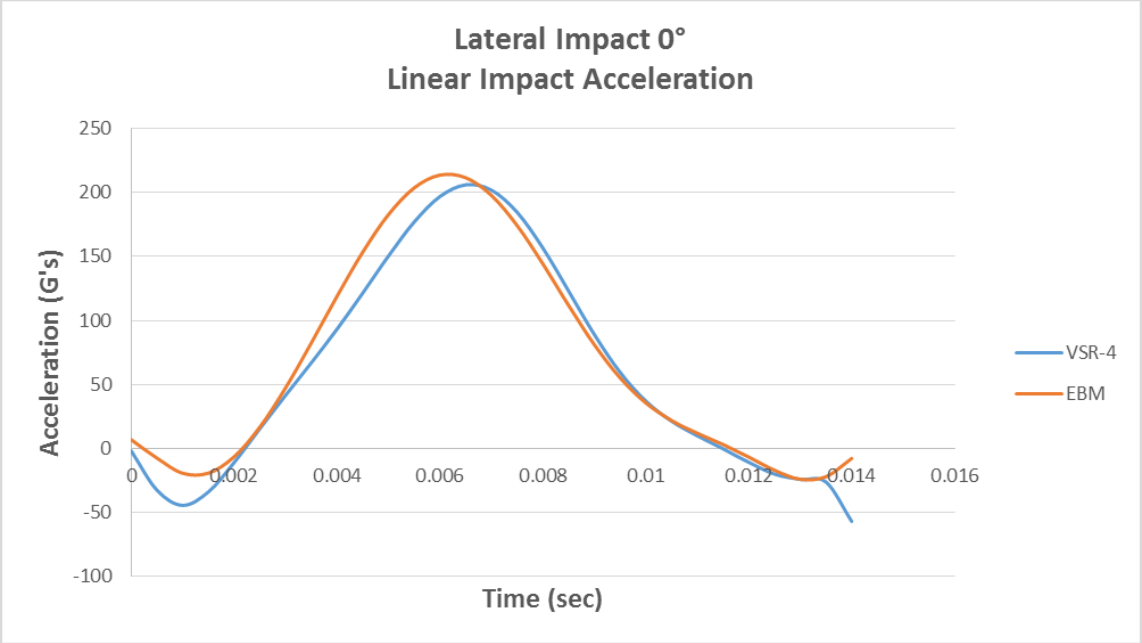

Figure 9-25 VSR4 and EBM Helmet – Lateral Impact - Linear Acceleration

www.manaraa.com

9.3.1 Lateral Impact 0° - von Mises Stresses

The peak stress level, on the posterior region of the brain, for the VSR4 and EBM helmets is between 16.5 kPa to 18.6 kPa for the 0° lateral impact. However, the area of peak stress for the EBM helmet is a very small area compared to the VSR4 helmet. The next stress range of 14.5 kPa to 16.5 kPa is also relatively small for the EBM helmet compared to the VSR4 helmet.

A significant point to mention with the 0° lateral impact as compared to the frontal, posterior, and superior impacts is the overall high stress levels. The peak stresses for a 0° frontal, posterior, or superior impact is in the range of 2.7 kPa to 3.9 kPa, 7.4 kPa to 8.6 kPa, and 3.8 kPa to 5.4 kPa respectively, which is much less than the lateral impact range of 16.5 kPa to 18.6 kPa. This indicates a high level of angular acceleration for a 0° lateral impact angle not observed in the other impacts. Angular acceleration for this impact can be as high as 6,300 rad/sec^2 as compared to less than 1,000 rad/sec^2.

Peak stresses for the lateral impact is primarily located on the lateral and poster regions of the brain. Since the primary angular acceleration is due to rotating about the vertical axis, the higher stresses follow the extreme distance from the impact location.

www.manaraa.com

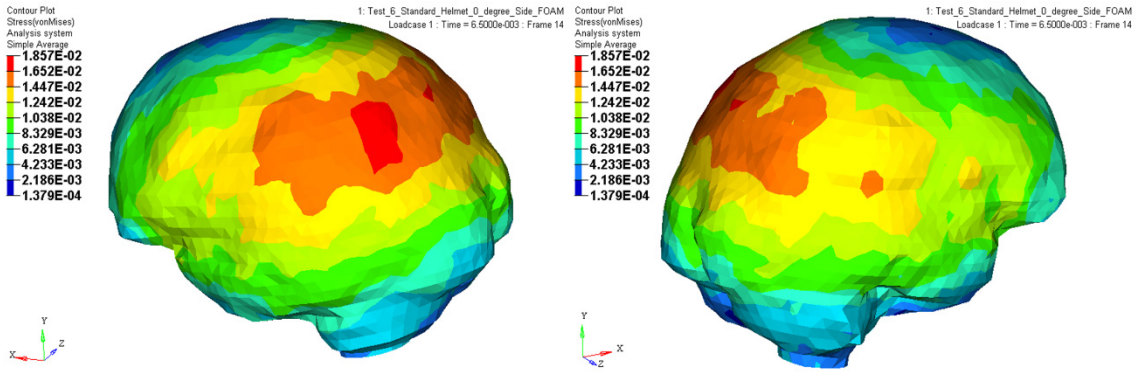

Figure 9-26 VSR4 Helmet - Lateral Impact 0° - von Mises Stress

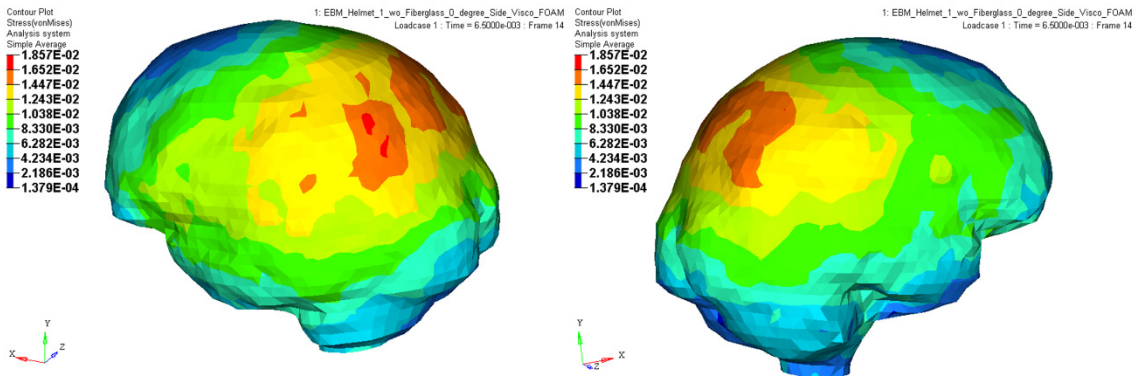

Figure 9-27 EBM Helmet - Lateral Impact 0° - von Mises Stress

www.manaraa.com

9.3.2 Lateral Impact 30° - von Mises Stresses

Once the impact angle is increased to 30°, the area associated with peak stress level on the brain with the VSR4 helmet increase significantly over the EBM helmet. Again, the peak stress levels in both cases remain between 17.6 kPa to 19.6 kPa, however, the area affected is higher with the VSR4 helmet as seen in Figure 9-28 and Figure 9-29.

The next lower level of 14.3 kPa to 17.6 kPa also shows a significant difference between the two helmets. The area of the brain for the VSR4 helmet that has a stress level in this range is much greater as compared to the EBM helmet. Overall, the area of mid-range stress between 10.4 kPa to 14.5 kPa for the EBM helmet is much less compared to the area of the VSR4 helmet.

The percent reduction in angular acceleration for the EBM helmet is approximately 30% over that of the VSR4 helmet. Although this is less than the percent reduction of 60% seem with a 0° side impact, the angular acceleration is still relatively high between 2700 rad/sec^2 to 3700 rad/sec^2.

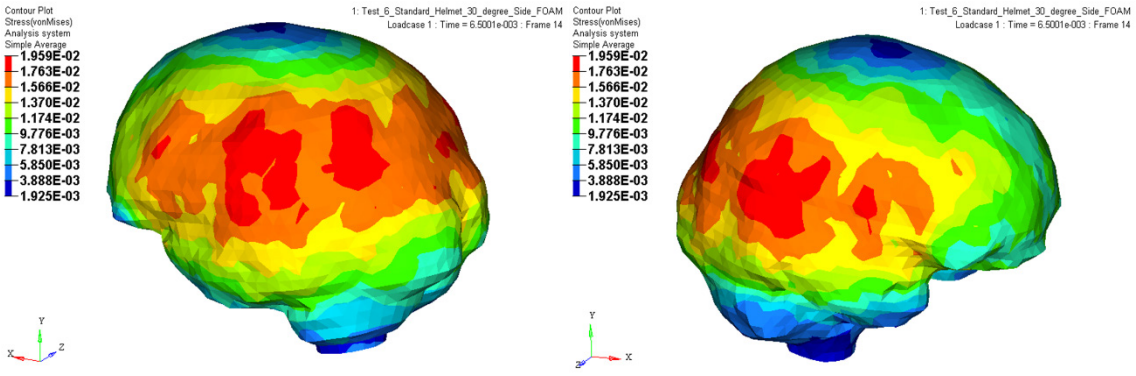

Figure 9-28 VSR4 Helmet - Lateral Impact 30° - von Mises Stress

www.manaraa.com

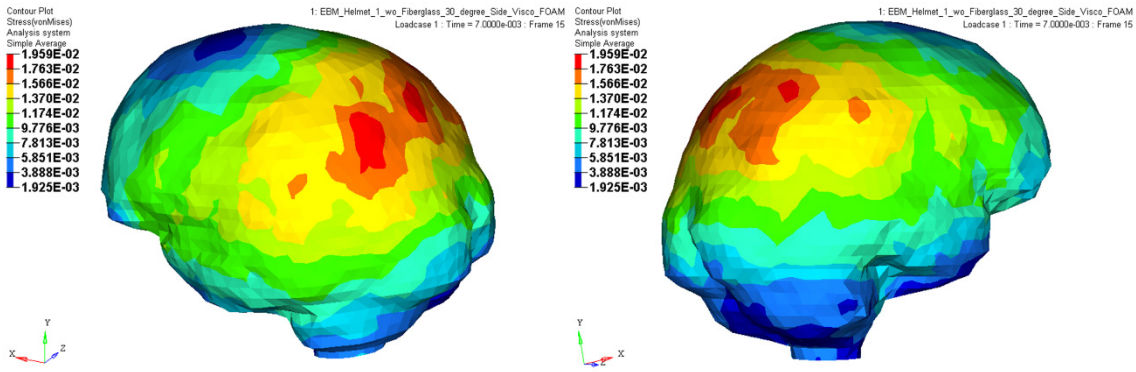

Figure 9-29 EBM Helmet - Lateral Impact 30° - von Mises Stress

www.manaraa.com

9.3.3 Lateral Impact 45° - von Mises Stresses

Although, the amount of angular acceleration reduction for the 45° impact drops to approximately 11% for EBM helmet, the presents of the shear layer provides a stress reducing mechanism for the brain. As seen below, the stress reduction for the EBM helmet is significantly better than the VSR4 helmet. The peak stress for the VSR4 helmet is between 16.2 kPa to 18.0 kPa as compared to a small area of stress between 14.3 kPa to 16.2 kPa for the EBM helmet.

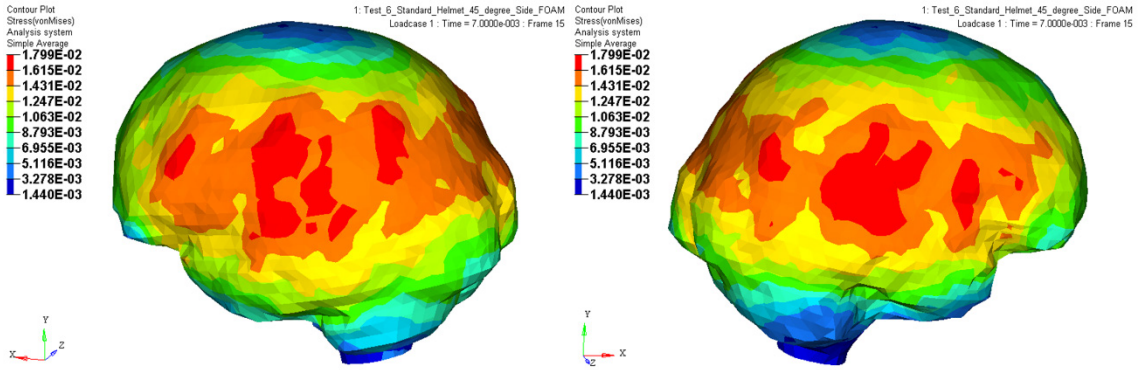

Figure 9-30 VSR4 Helmet - Lateral Impact 45° - von Mises Stress

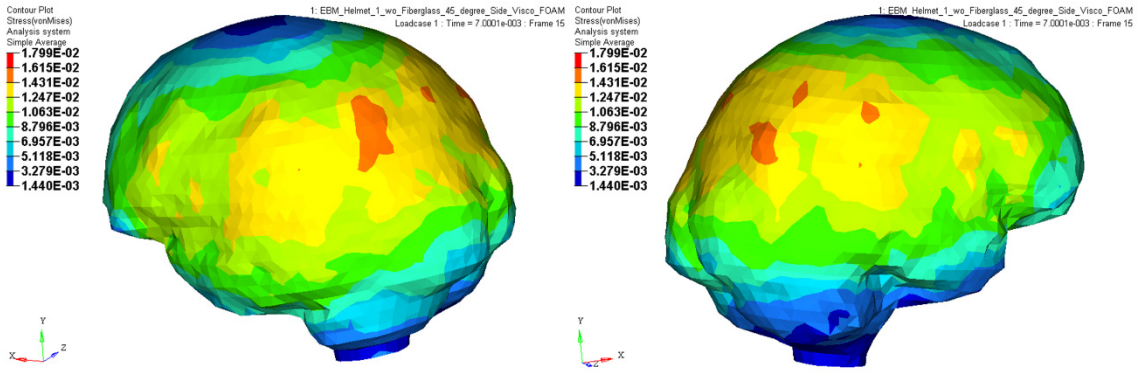

Figure 9-31 EBM Helmet - Lateral Impact 45° - von Mises Stress

www.manaraa.com

For the 45° impact results, a cross-section of the transverse plane and sagittal plane is shown in Figure 9-32 and Figure 9-33. As seen in these stress contours, the highest stress is located around the perimeter surface of the brain, were as, the central portion of the brain is lower. With the peak stress levels being higher with the VSR4 helmet, the central portion of the brain stresses are also higher. The central portion of the brain for the VSR4 helmet are between 3.3 kPa to 5.1 kPa as compared to 1.4 kPa to 3.3 kPa for the EBM helmet. In addition, the overall stress levels observed with the EBM helmet cross-section are significantly lower.

Referring to the sagittal plane cross-section comparison in Figure 9-33, the lower stress level between 1.4 kPa to 3.3 kPa carry over a much larger volume for the EBM helmet compared to the VSR4 helmet. The stress levels in the brain at this range for the VSR4 helmet only covers a small region of the brain stem, whereas, the volume of the brain for the EBM helmet carries through the entire vertical axis.

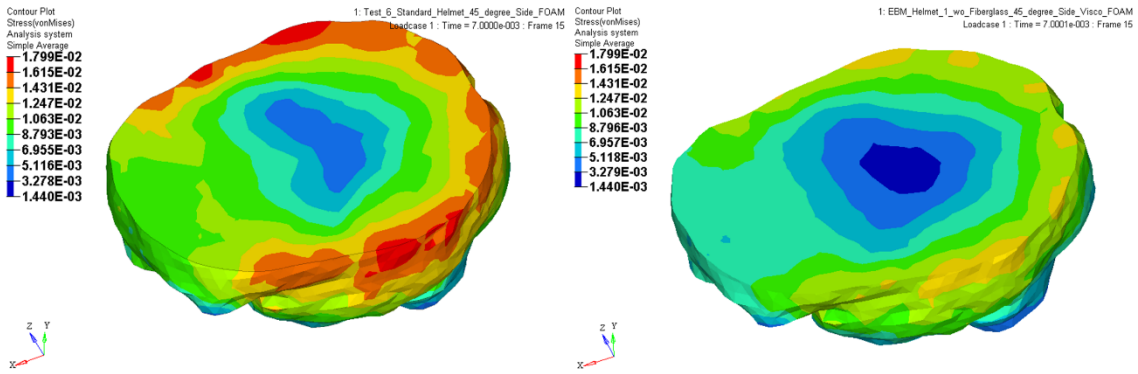

Figure 9-32 VSR4 (left) and EBM (right) Helmet - Lateral Impact 45° - von Mises Stress Traverse Plane Cross-Section

www.manaraa.com

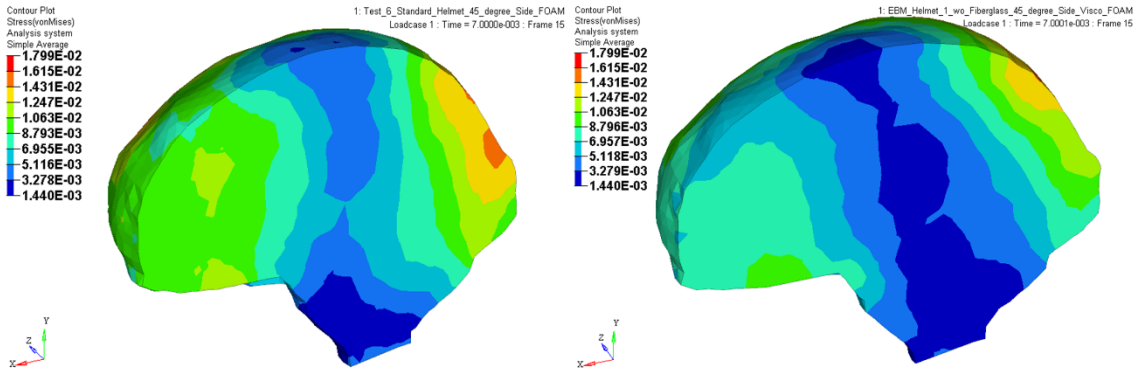

Figure 9-33 VSR4 (left) and EBM (right) Helmet - Lateral Impact 45° - von Mises Stress Sagittal Cross-Section

www.manaraa.com

9.3.4 Lateral Impact 0° - Principal Stresses

Principal stress comparison of the VSR4 and EBM helmets are shown in Figure 9-34 and Figure 9-35. For the principal stresses, the peak stress shown in (red) indicates the region in tension (opposite the site of impact), whereas, the peak stress shown in (blue) is compression (site of impact). With the 0° lateral impact, the peak compressive stress between -0.154 kPa to -0.196 kPa for the EBM helmet is smaller compared to the VSR4 helmet. This indicates the high amount of angular acceleration associated with this type of impact.

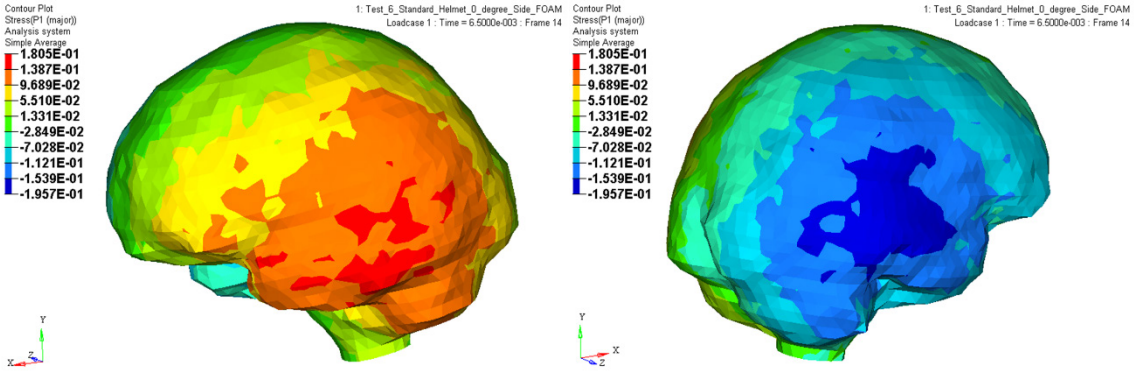

Figure 9-34 VSR4 Helmet - Lateral Impact 0° - Principal Stress

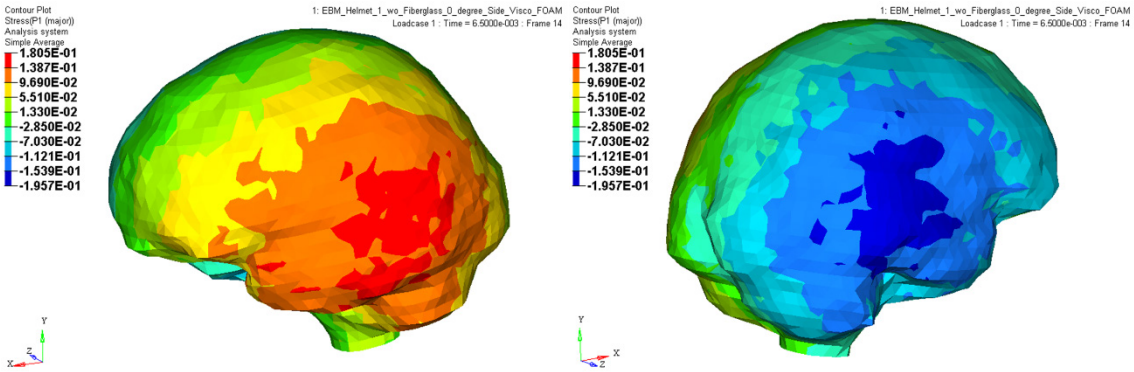

Figure 9-35 EBM Helmet - Lateral Impact 0° - Principal Stress

www.manaraa.com

9.3.5 Lateral Impact 30° - Principal Stresses

The comparison conclusion for the 30° impact follows the same conclusion observed in the 0° side impact where peak principal stress areas for the EBM helmet are less than the VSR4 helmet. Peak principal stresses results are consistent between the two applications.

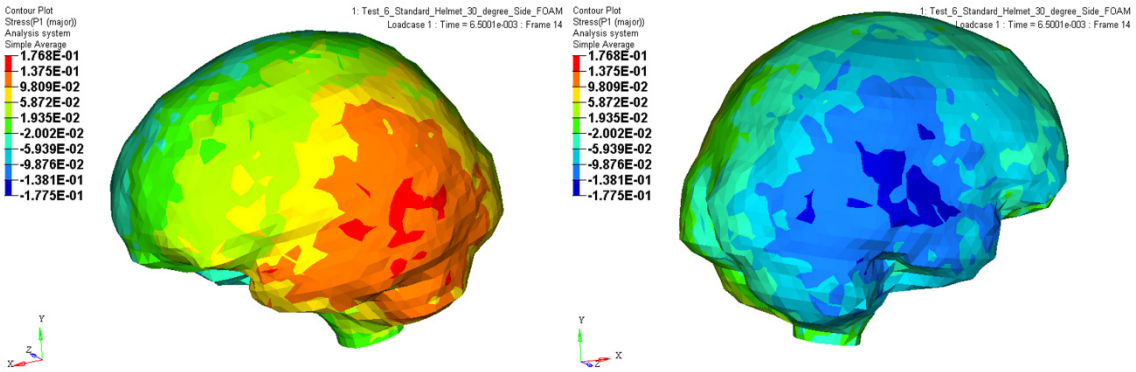

Figure 9-36 VSR4 Helmet - Lateral Impact 30° - Principal Stress

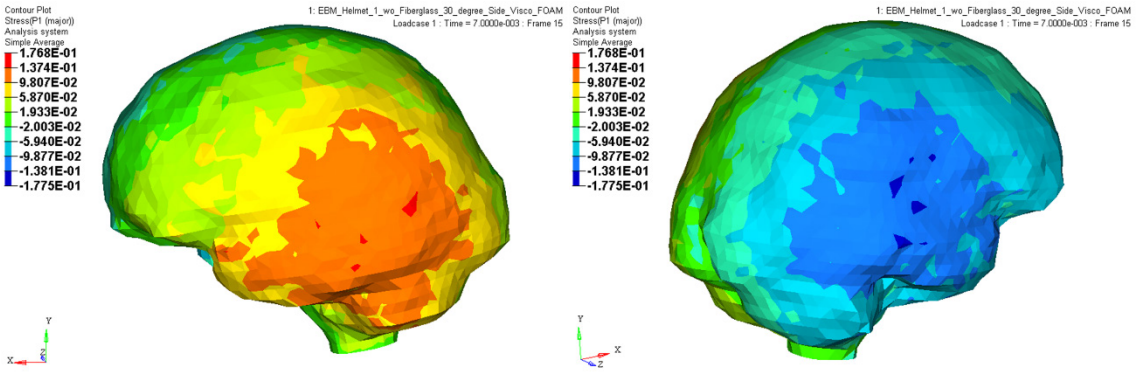

Figure 9-37 EBM Helmet - Lateral Impact 30° - Principal Stress

www.manaraa.com

9.3.6 Lateral Impact 45° - Principal Stresses

Once the angle of impact reaches 45°, the peak principal stresses drop slightly for compression between -0.138 kPa to -0.178 kPa and between 0.138 kPa to 0.177 for tension. Differences between the peak principal stresses for either helmet is insignificant.

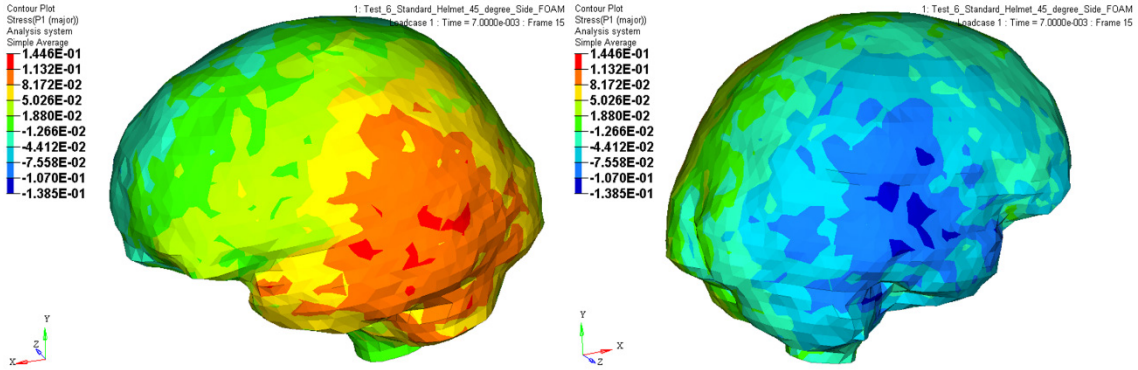

Figure 9-38 VSR4 Helmet - Lateral Impact 45° - Principal Stress

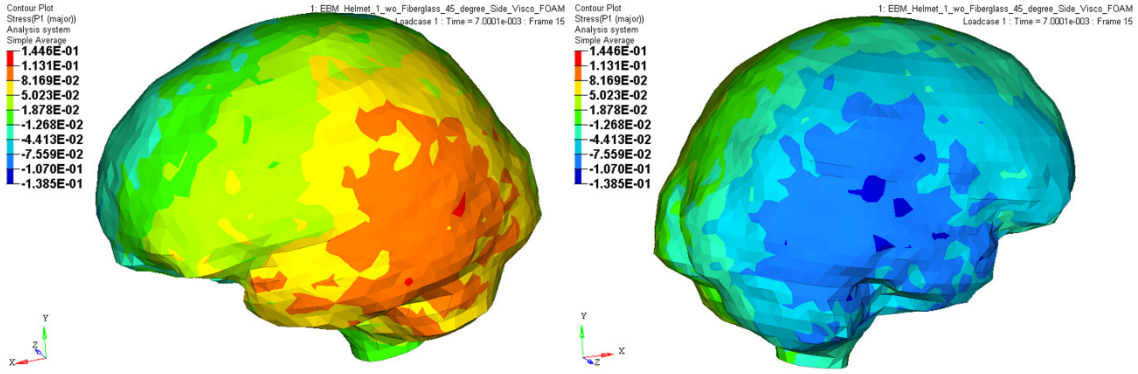

Figure 9-39 EBM Helmet - Lateral Impact 45° - Principal Stress

www.manaraa.com

9.4 Posterior Impact

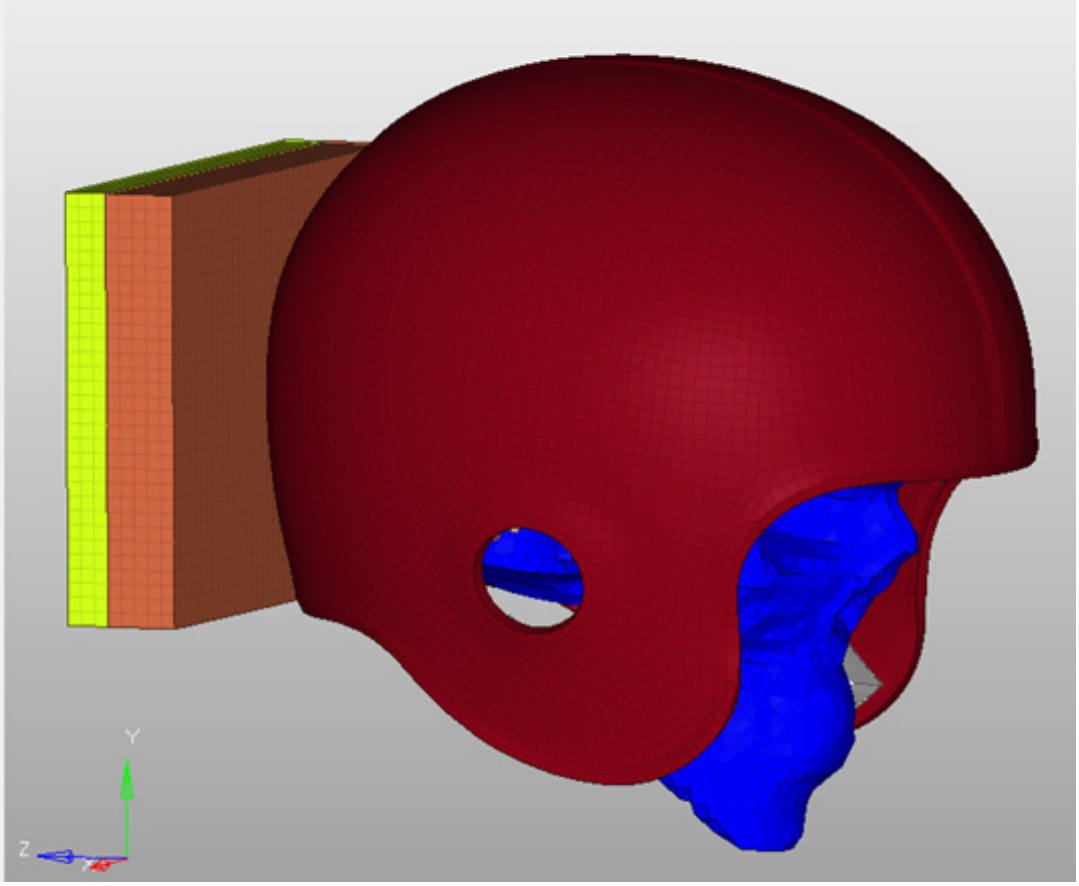

Figure 9-40 Posterior Impact Arrangement

The setup for the posterior impact simulation is shown in Figure 9-40. The head is oriented in line with the global coordinate system and in line with the impacting surface. With the posterior impact, there is no angle of incline associated with the helmet relative to the impactor. This impact configuration coincides with the NOCSAE drop test configuration for posterior impacts. The initial velocity of the head and helmet assembly is 5.47 m/s traveling in the +Z axis, into the impactor plate.

www.manaraa.com

A comparison of the posterior impact results of the EBM and VSR4 helmets are shown in Figure 9-41 through Figure 9-44. The linear impact acceleration for both helmets are very close to each other for the 0° impact simulation, with the VSR4 helmet being slightly higher than the EBM helmet. This difference follows the same logic for the fit between the head and helmet explained in the frontal and side impacts.

With the posterior impact simulations, the relative percent reduction in angular acceleration for the EBM helmet is consistent for 30° and 45°, whereas there is no real reduction at 0°. For the posterior impact at 0°, it can be determined this impact is more in line with the center of mass of the head as compared to the other impact configurations. Although there is still some measurable angular acceleration, the amount is relatively small.

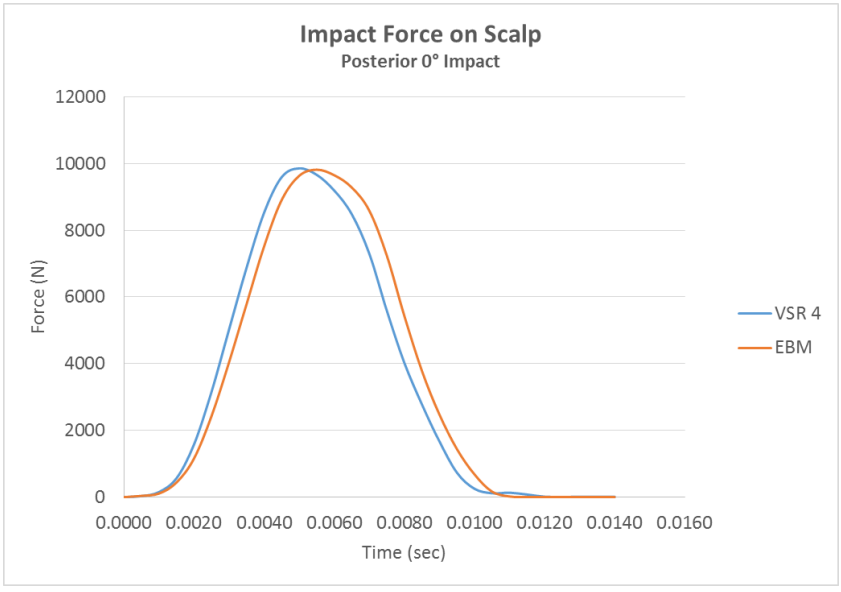

Figure 9-41 VSR4 and EBM Helmet – Posterior Impact – Impact Force on the Scalp at the Site of Impact

www.manaraa.com

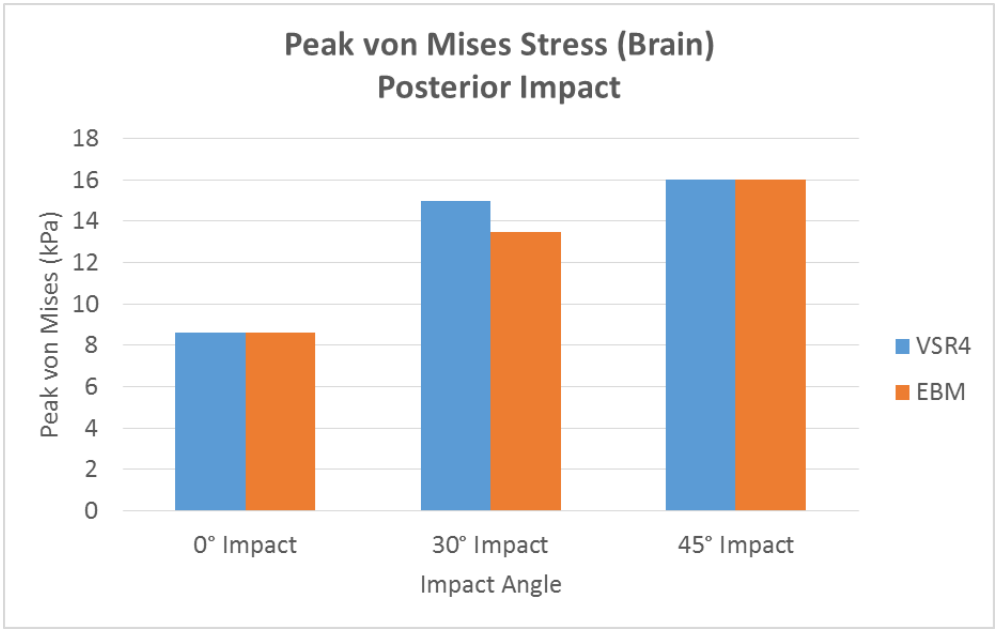

Figure 9-42 VSR4 and EBM Helmet - Posterior Impact – Brain Peak von Mises Stress

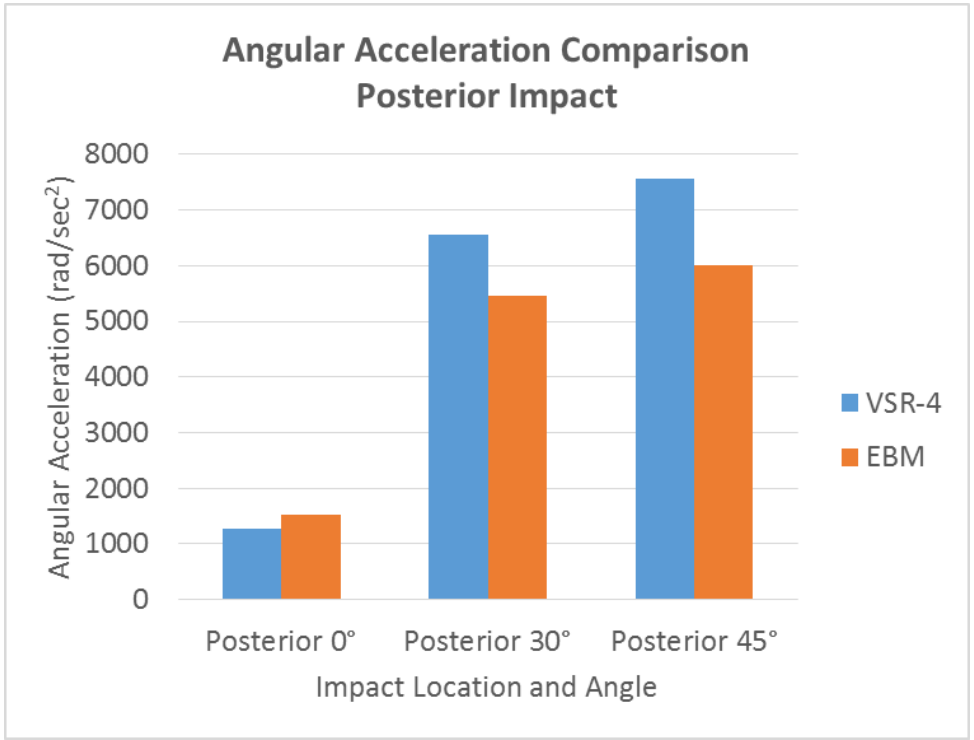

Figure 9-43 VSR4 and EBM Helmet – Posterior Impact - Angular Acceleration Comparison

www.manaraa.com

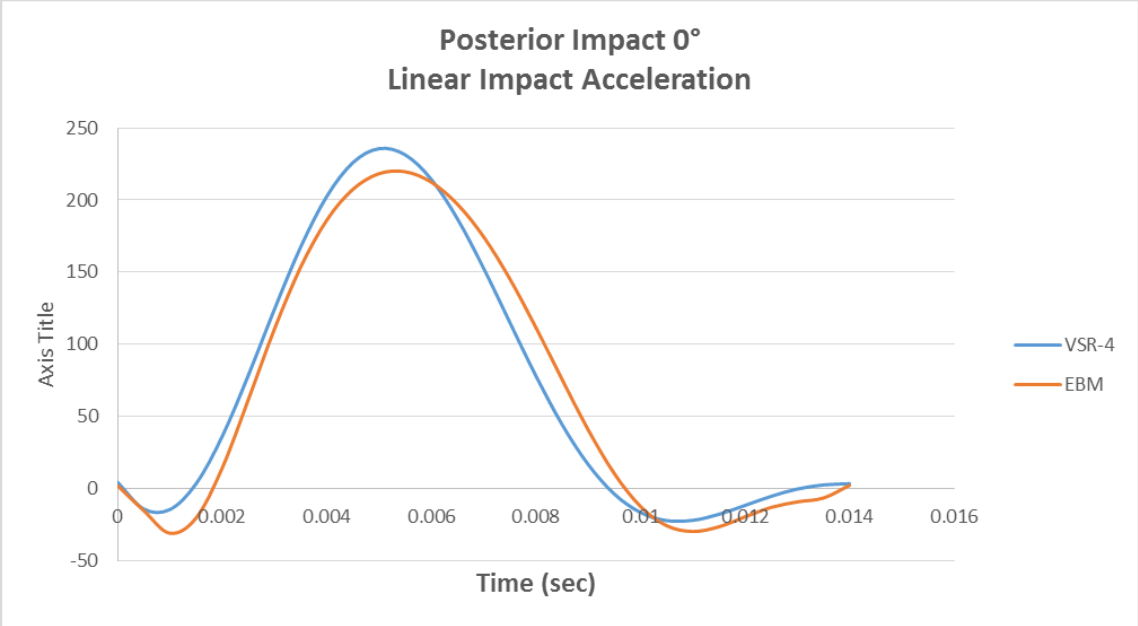

Figure 9-44 VSR4 and EBM Helmet – Posterior Impact - Linear Acceleration

www.manaraa.com

9.4.1 Posterior Impact 0° - von Mises Stresses

The peak stress levels with the 0° posterior impact for the VSR4 and EBM helmets are nearly identical and the differences are insignificant. The peak stress for both helmets is between 7.4 kPa to 8.6 kPa.

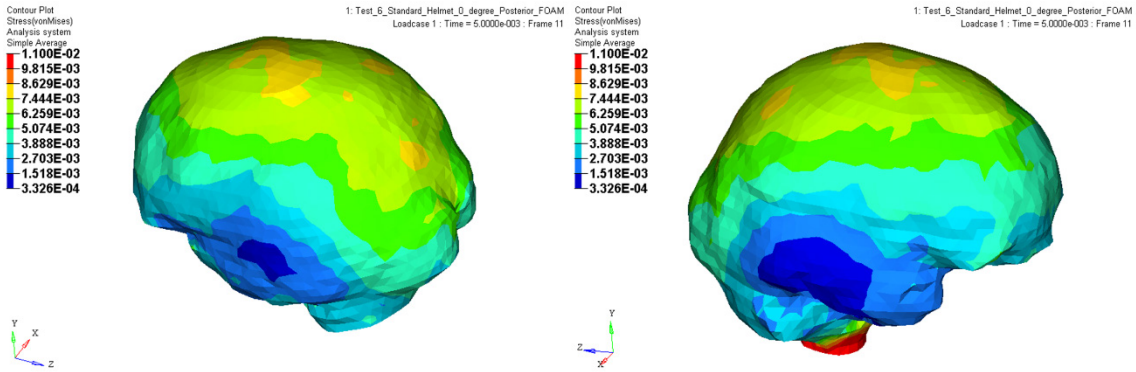

Figure 9-45 VSR4 Helmet - Posterior Impact 0° - von Mises Stress

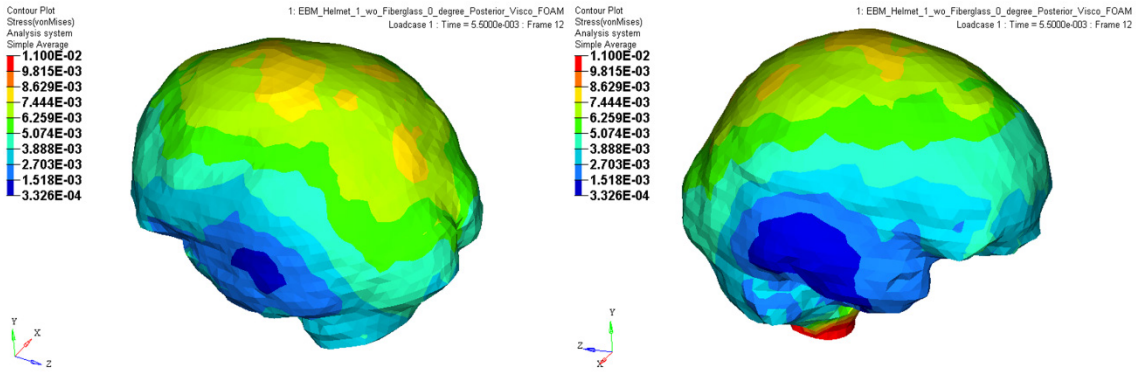

Figure 9-46 EBM Helmet - Posterior Impact 0° - von Mises Stress

www.manaraa.com

9.4.2 Posterior Impact 30° - von Mises Stresses

Once the impact angle is increased to 30°, the area associated with peak stress level on the brain with the VSR4 helmet increases as compared to the EBM helmet. The peak stress levels on the left side of the brain for the VSR4 helmet are between 13.5 kPa to 15.0 kPa, compared to the EBM helmet peak stress between 11.9 kPa to 13.5 kPa. The area of stress between 11.9 kPa to 13.5 kPa for the VSR4 helmet also covers a larger area compared to the EBM helmet.

The area of peak stress on the right side of the brain is also greater for the VSR4 helmet. Stress levels on the right side of the brain for both helmets range between 7.3 kPa and 8.8 kPa, however, the area for the VSR4 helmet is much larger than the area for the EBM helmet.

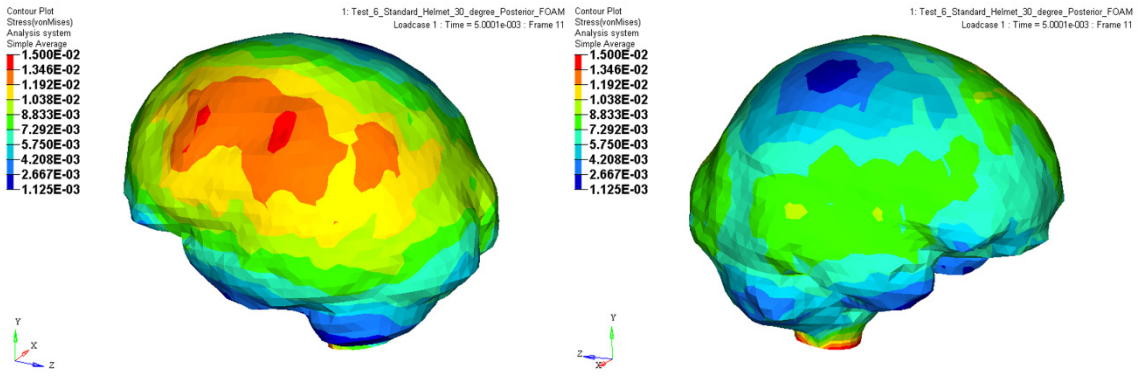

Figure 9-47 VSR4 Helmet - Posterior Impact 30° - von Mises Stress

www.manaraa.com

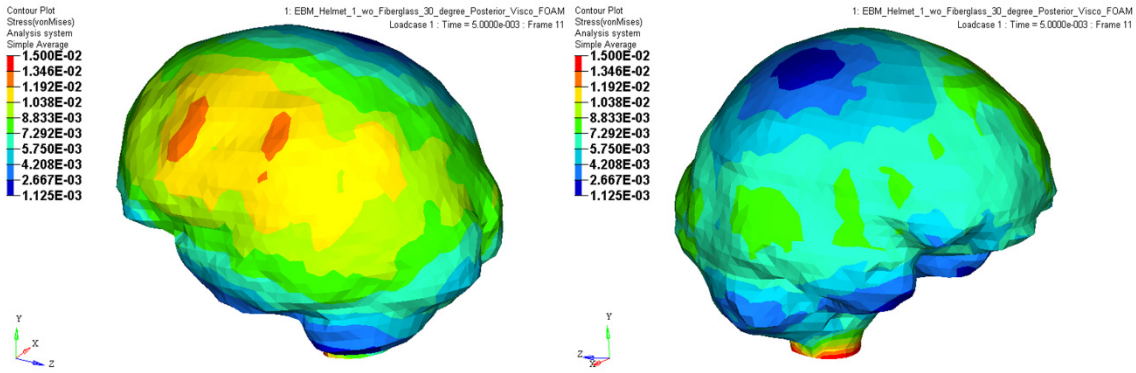

Figure 9-48 EBM Helmet - Posterior Impact 30° - von Mises Stress

www.manaraa.com

9.4.3 Posterior Impact 45° - von Mises Stresses

The peak stress levels with the 0° posterior impact for the VSR4 and EBM helmets are nearly identical and the differences are insignificant. The peak stress for both helmets is between 14.7 kPa to 16.6 kPa.

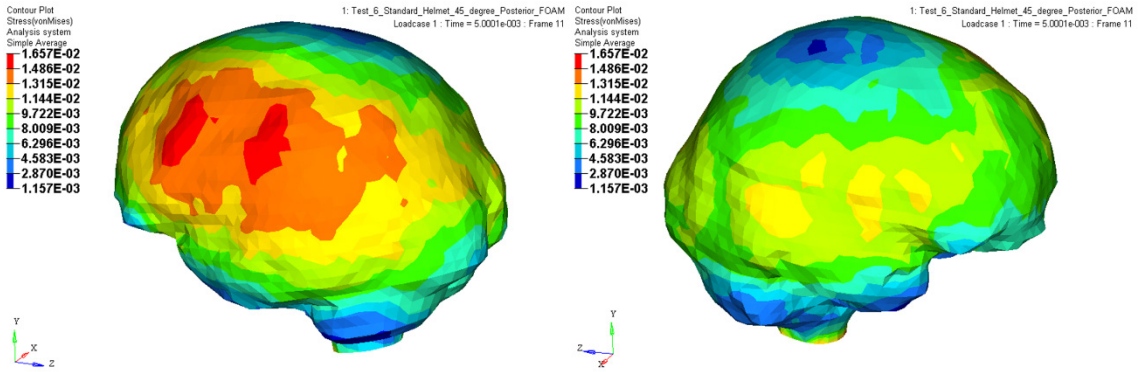

Figure 9-49 VSR4 Helmet - Posterior Impact 45° - von Mises Stress

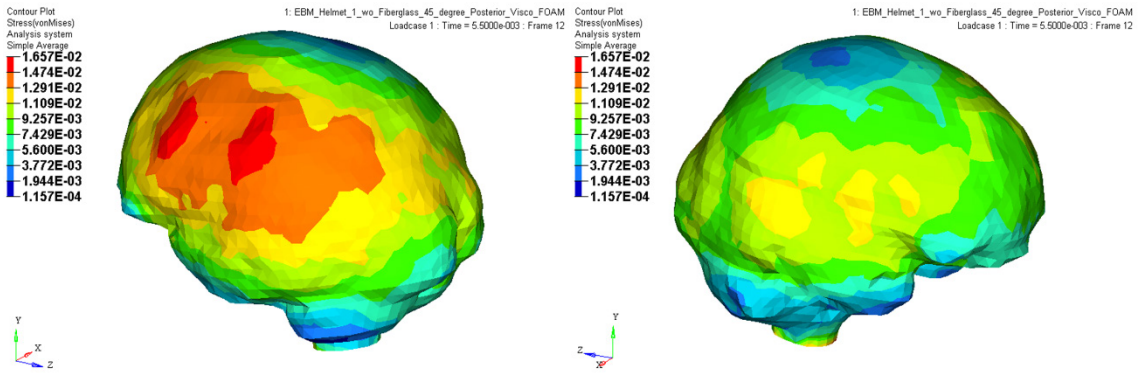

Figure 9-50 EBM Helmet - Posterior Impact 45° - von Mises Stress

www.manaraa.com

For the 45° impact results, a cross-section of the transverse plane and sagittal plane is shown in Figure 9-51 and Figure 9-52. As seen in these stress contours, the highest stress is located around the perimeter surface of the brain, were as, the central portion of the brain is lower. Both helmet simulations show stress levels at the central portion of the brain between 2.9 kPa to 4.6 kPa, however, the EBM helmet shows a slightly larger area at this level.

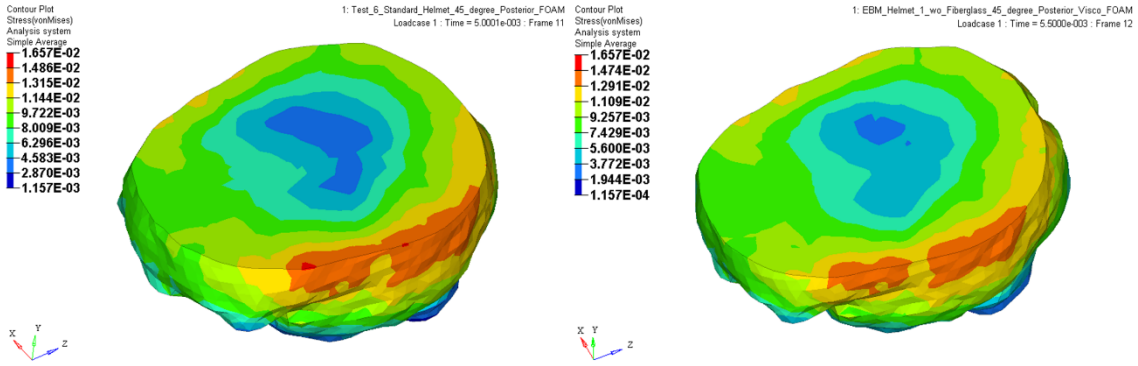

Figure 9-51 VSR4 (left) and EBM (right) Helmet - Posterior Impact 45° - von Mises Stress Traverse Plane Cross-Section

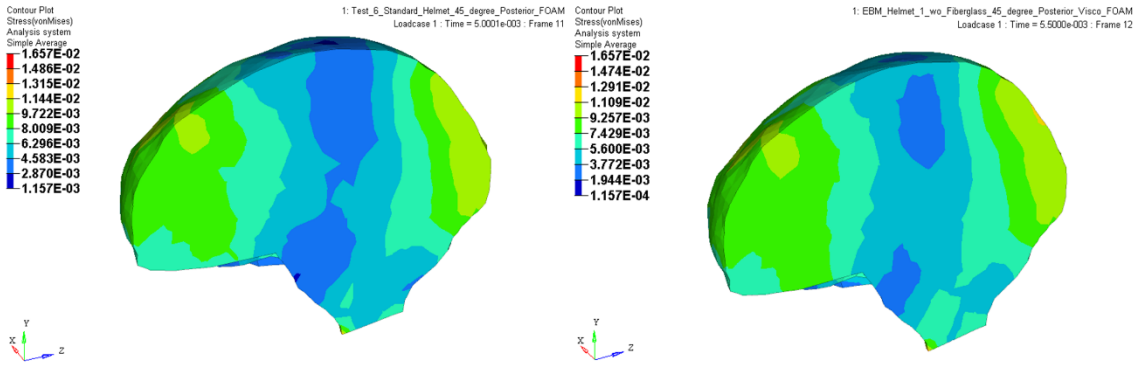

Figure 9-52 VSR4 (left) and EBM (right) Helmet - Posterior Impact 45° - von Mises Stress Sagittal Cross-Section

www.manaraa.com

9.4.4 Posterior Impact 0° - Principal Stresses

Principal stress comparison for the VSR4 and EBM helmets are shown in Figure 9-53 and Figure 9-54. For the principal stresses, the peak stress shown in (red) indicate tensile stress (opposite the site of impact), whereas, the peak stress shown in (blue) is compression (site of impact). Both the VSR4 and EBM helmet yield similar peak compressive stress between -0.167 kPa to -0.214 kPa results, however the area of peak compression for the EBM helmet is smaller as compared to the area of the VSR4 helmet.

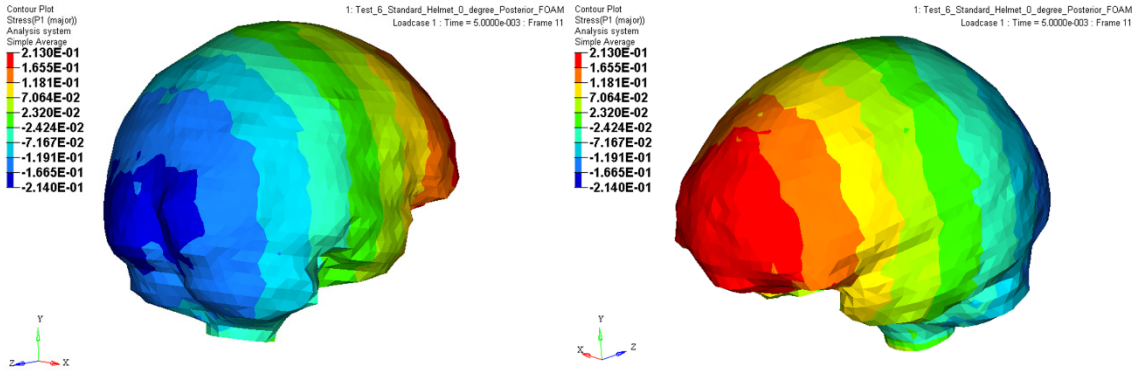

Figure 9-53 VSR4 Helmet - Posterior Impact 0° - Principal Stress

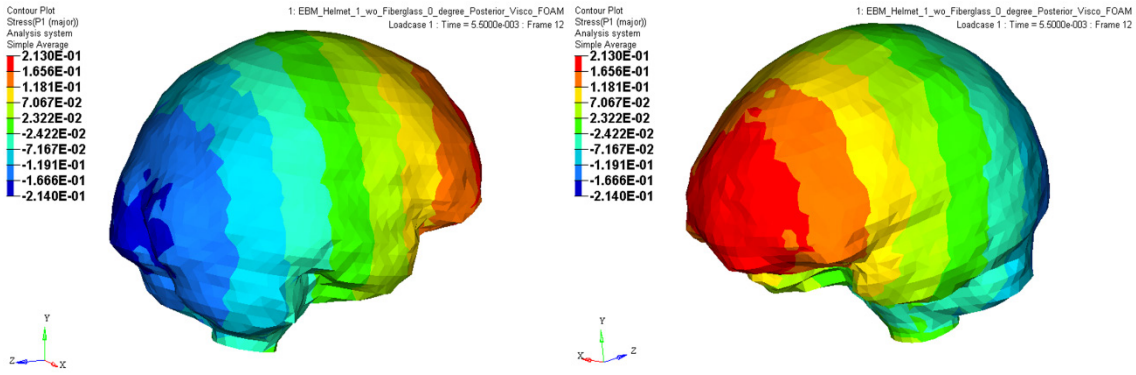

Figure 9-54 EBM Helmet - Posterior Impact 0° - Principal Stress

www.manaraa.com

9.4.5 Posterior Impact 30° - Principal Stresses

Principal stresses for the 30° posterior impact yield similar results for both helmets. Differences between the peak compressive and tensile stresses for either helmet is insignificant.

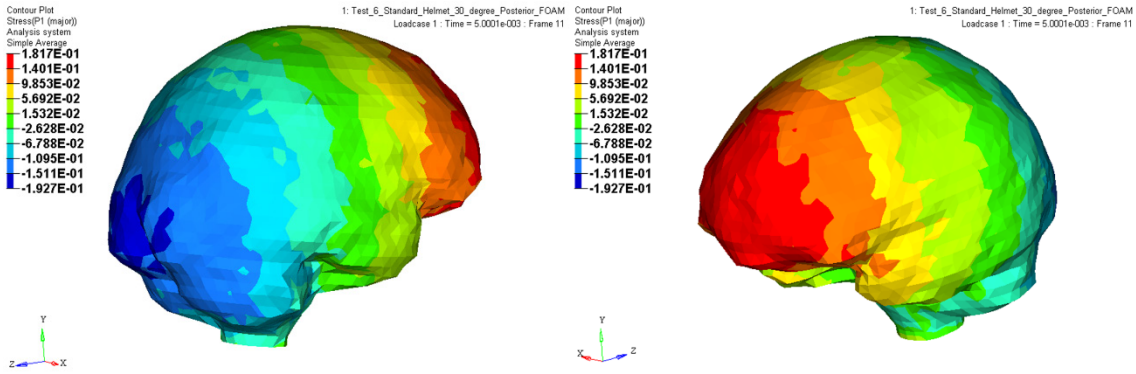

Figure 9-55 VSR4 Helmet - Posterior Impact 30° - Principal Stress

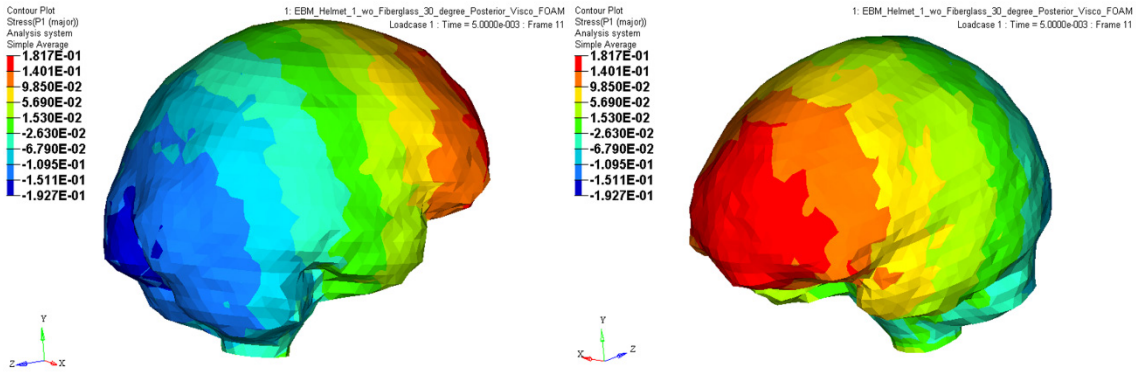

Figure 9-56 EBM Helmet - Posterior Impact 30° - Principal Stress

www.manaraa.com

9.4.6 Posterior Impact 45° - Principal Stresses

Principal stresses for the 45° posterior impact yield similar results for both helmets as seen with the 30° impact angle. Differences between the peak compressive and tensile stresses for either helmet is insignificant.

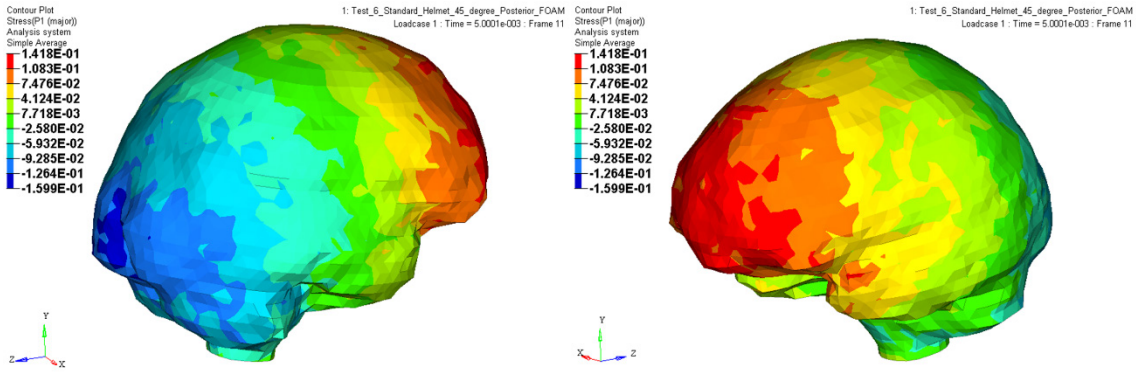

Figure 9-57 VSR4 Helmet - Posterior Impact 45° - Principal Stress

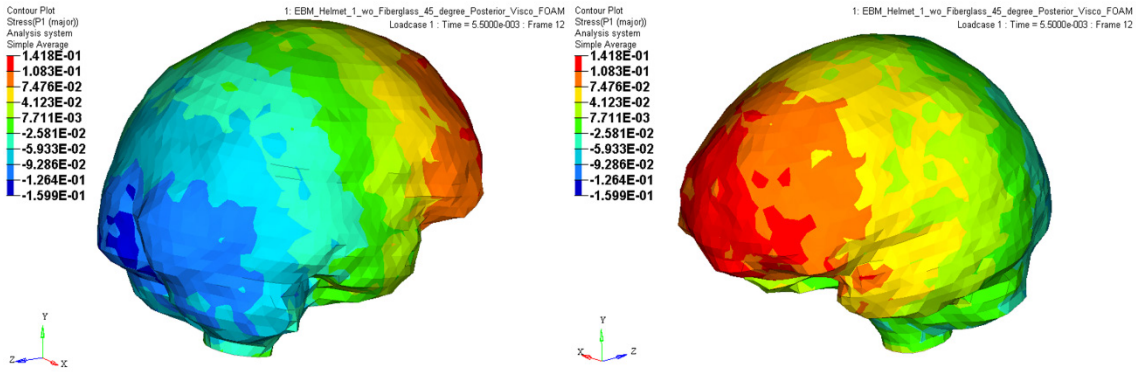

Figure 9-58 EBM Helmet - Posterior Impact 45° - Principal Stress

www.manaraa.com

9.5 Superior Impact

The setup for the posterior impact simulation is shown in Figure 9-59. The head is oriented in line with the global coordinate system and in line with the impacting surface. With the superior impact, there is no angle of incline associated with the helmet relative to the impactor. This impact configuration coincides with the NOCSAE drop test configuration for superior impacts. The initial velocity of the head and helmet assembly is 5.47 m/s traveling in the +Z axis, into the impactor plate.

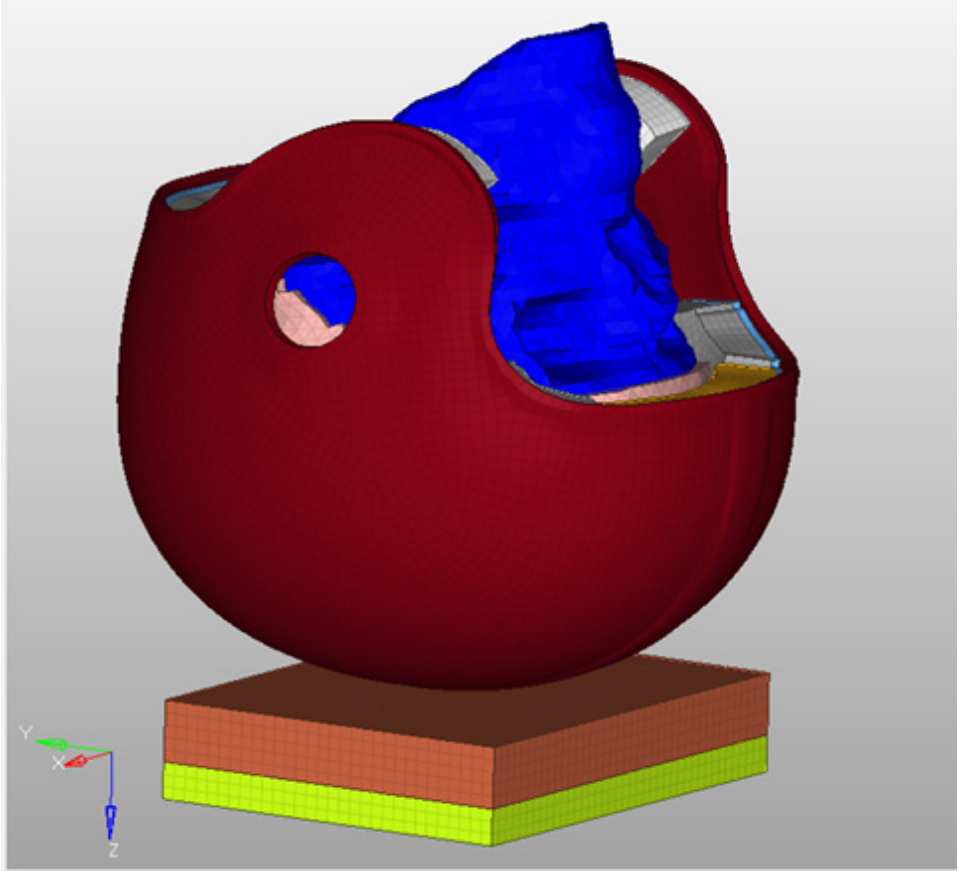

Figure 9-59 Superior Impact Arrangement

www.manaraa.com

A comparison of the superior impact results of the EBM and VSR4 helmets are shown in Figure 9-60 through Figure 9-63. The peak linear acceleration for both helmets are very similar for the 0° impact simulation.

With the superior impact simulations, the angular acceleration for the EBM helmet decreases from 0° to 45°., whereas the VSR4 helmet angular acceleration increases. This increasing angular acceleration associated with the VSR4 helmet indicates the increased rotational motion that is imposed on the helmet during impact simulations. Since the impact vector is further oriented away from the center of mass of the head, the angular acceleration transferred to the head is also increased. The EBM helmet shear layer helps reduce this rotational motion to the brain which is also shown in the stress results for the different impacts.

www.manaraa.com

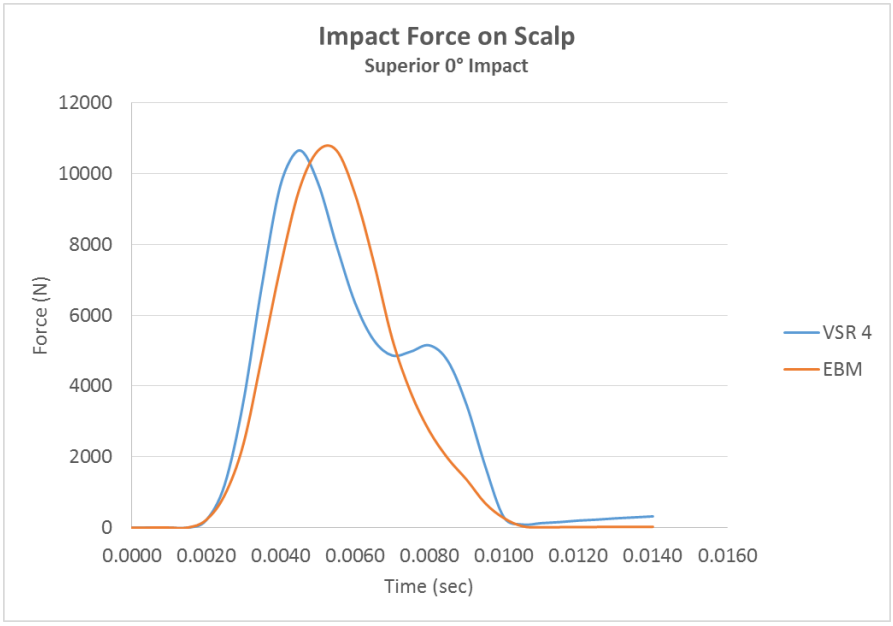

Figure 9-60 VSR4 and EBM Helmet – Superior Impact – Impact Force on the Scalp at the Site of Impact

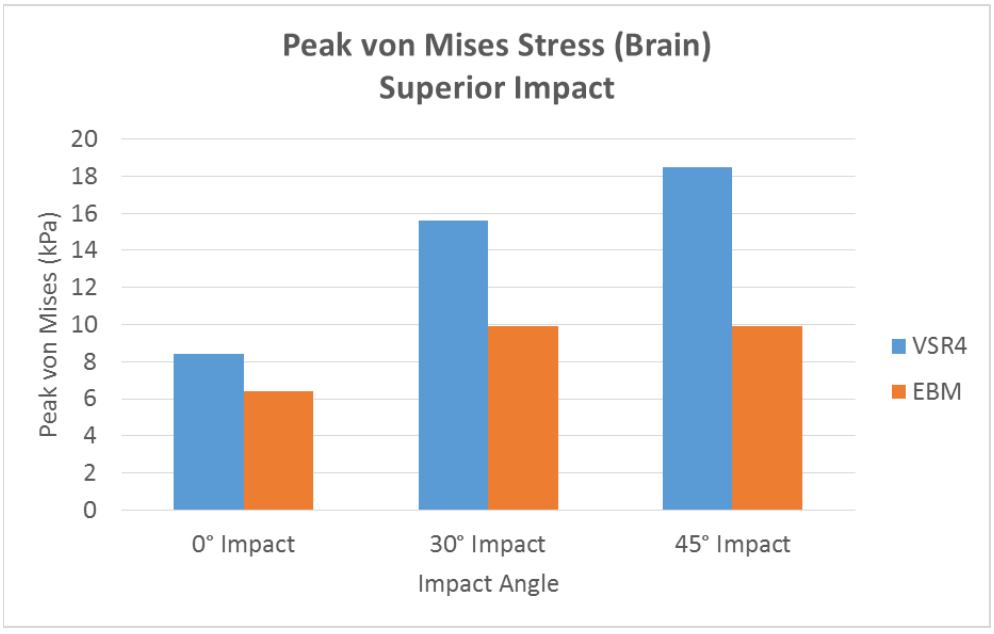

Figure 9-61 VSR4 and EBM Helmet - Superior Impact – Brain Peak von Mises Stress

www.manaraa.com

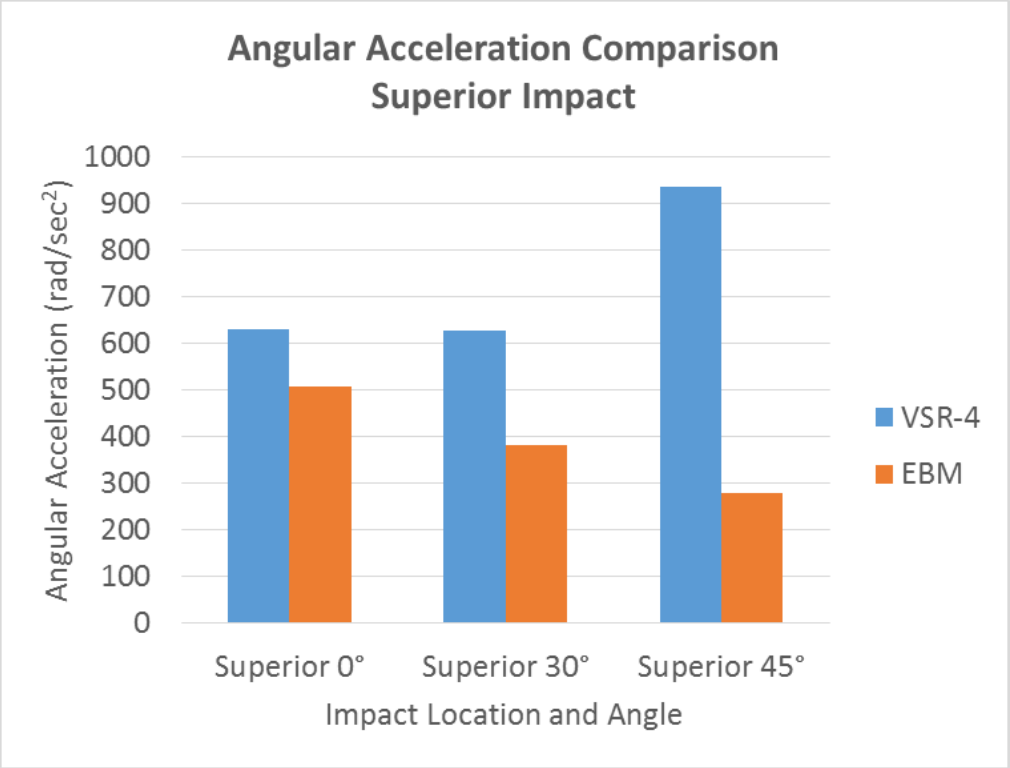

Figure 9-62 VSR4 and EBM Helmet – Superior Impact - Angular Acceleration Comparison

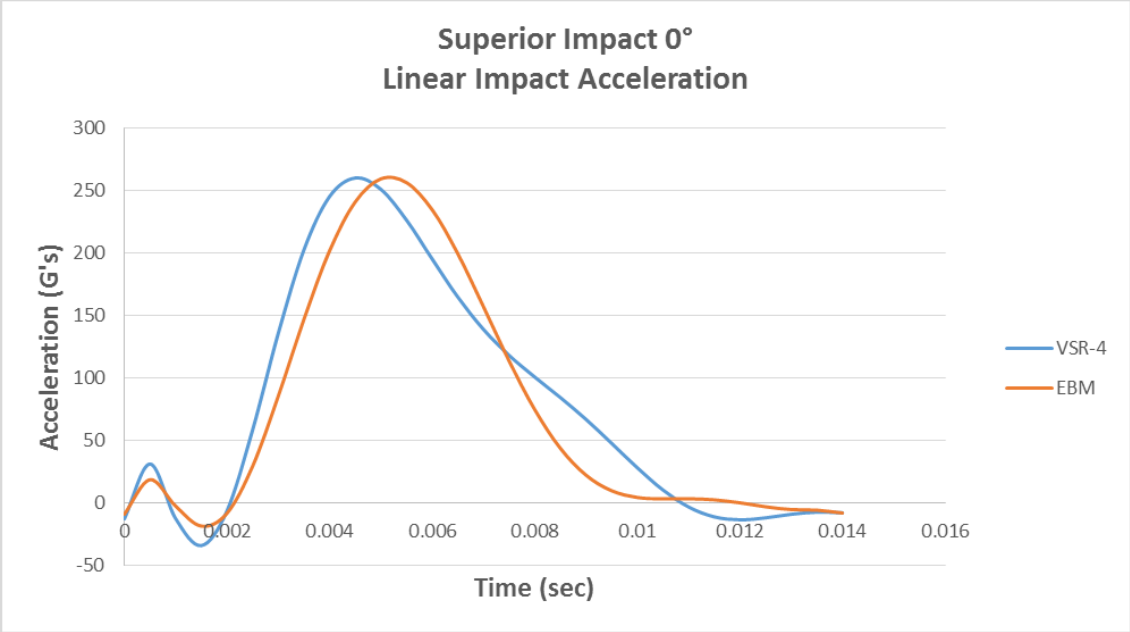

Figure 9-63 VSR4 and EBM Helmet – Superior Impact - Linear Acceleration

www.manaraa.com

9.5.1 Superior Impact 0° - von Mises Stresses

The peak stress level, on the superior region of the brain, is between 6.4 kPa to 8.4 kPa for the VSR4 helmet and between 4.4 kPa to 6.4 kPa for the EBM helmet. The area of stress between 2.4 kPa to 4.4 kPa that outlines the surface of the brain is very similar in both cases. The highest peak stress in both instances, however, is located in the brain stem region, at a value greater than 15.0 kPa.

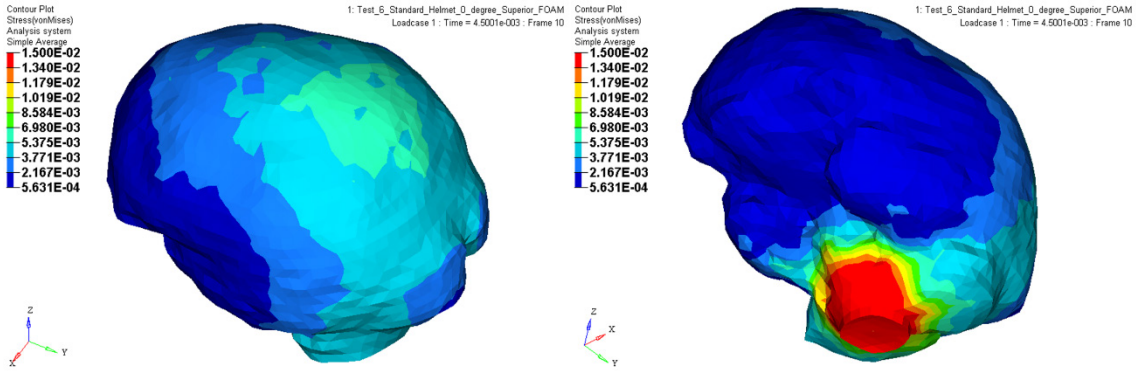

Figure 9-64 VSR4 Helmet - Superior Impact 0° - von Mises Stress

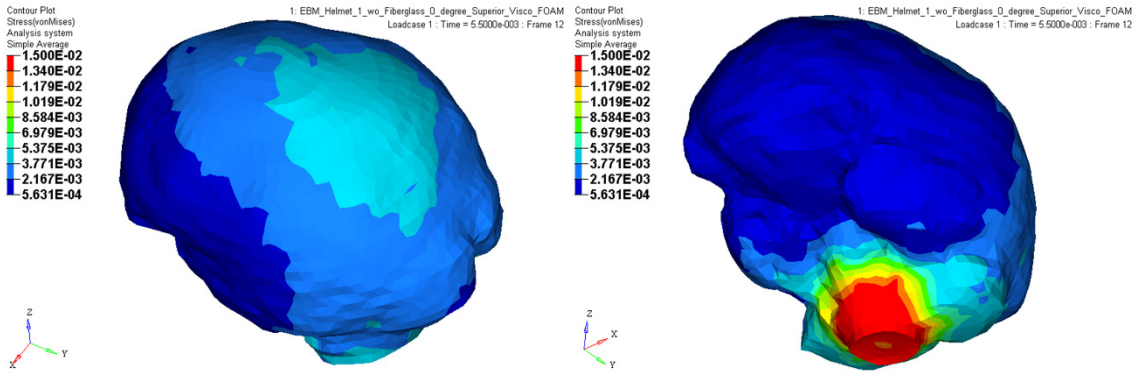

Figure 9-65 EBM Helmet - Superior Impact 0° - von Mises Stress

www.manaraa.com

9.5.2 Superior Impact 30° - von Mises Stresses

At an impact angle of 30°, the peak stress levels with the VSR4 helmet are between 13.7 kPa to 15.6 kPa compared to 8.1 kPa to 9.9 kPa for the EBM helmet. The area of low stress between 0.5 kPa to 2.4 kPa is substantially larger with the EBM helmet as compared to the VSR4 helmet. Although the angular acceleration levels are below 700 rad/sec^2, the EBM helmet provides a 39% reduction, which helps reduce stress.

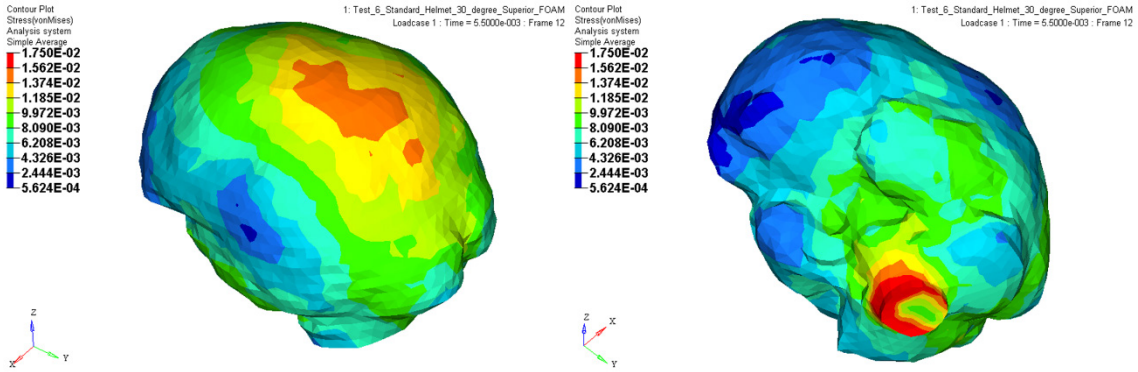

Figure 9-66 VSR4 Helmet - Superior Impact 30° - von Mises Stress

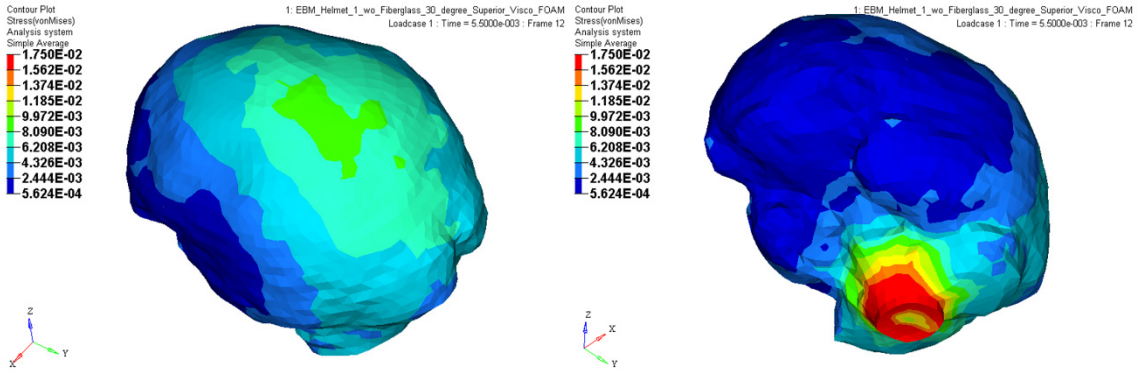

Figure 9-67 EBM Helmet - Superior Impact 30° - von Mises Stress

www.manaraa.com

9.5.3 Superior Impact 45° - von Mises Stresses

At an impact angle of 45°, the peak stress levels are between 16.5 kPa to 18.5 kPa with the VSR4 helmet, as compared to the EBM helmet being between 8.1 kPa to 9.9 kPa. The area of low stress between 0.4 kPa to 2.4 kPa is substantially larger with the EBM helmet as compared to the VSR4 helmet. With the angular acceleration increasing to below 1,000 rad/sec^2, the EBM helmet provides a 70% reduction, which helps to significantly reduce stress.

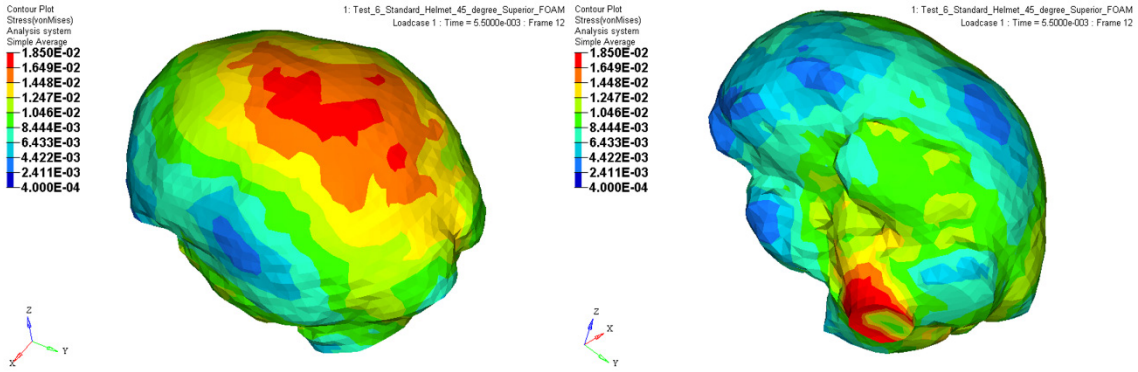

Figure 9-68 VSR4 Helmet - Superior Impact 45° - von Mises Stress

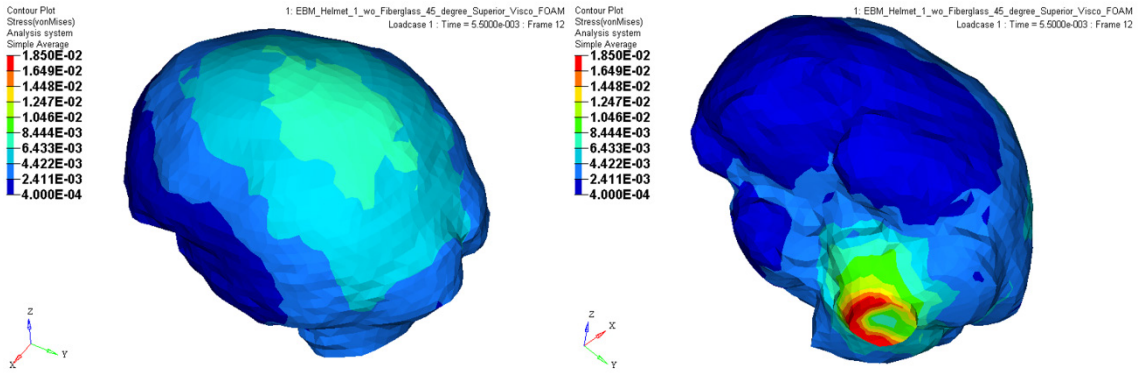

Figure 9-69 EBM Helmet - Superior Impact 45° - von Mises Stress

www.manaraa.com

For the 45° impact results, a cross-section for the transverse plane and sagittal plane is shown. See Figure 9-70 and Figure 9-71. For the EBM helmet results, there is a large region of stress between 0.4 kPa to 2.4 kPa as compared to the VSR4 helmet. The VSR4 helmet has a small region of stress between 4.4 kPa to 6.4 kPa and a region near the frontal lobe between 8.4 kPa to 10.5 kPa, not observed with the EBM helmet.

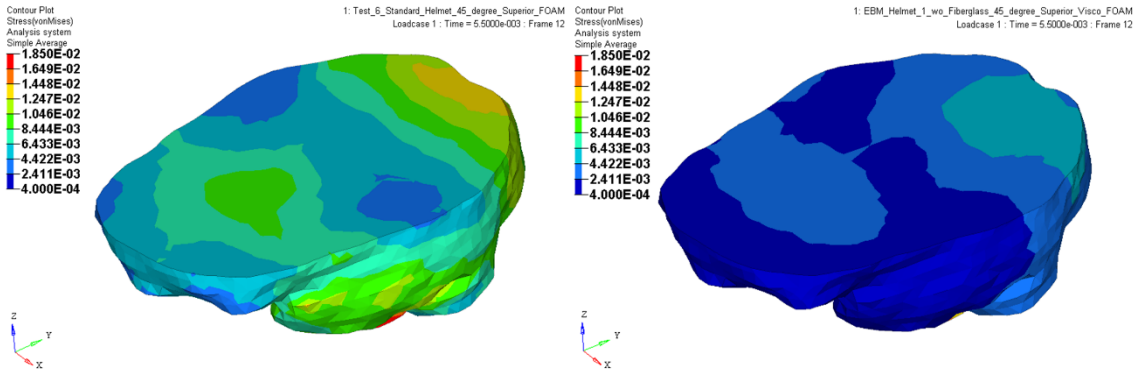

Figure 9-70 VSR4 (left) and EBM (right) Helmet - Superior Impact 45° - von Mises Stress Traverse Plane Cross-Section

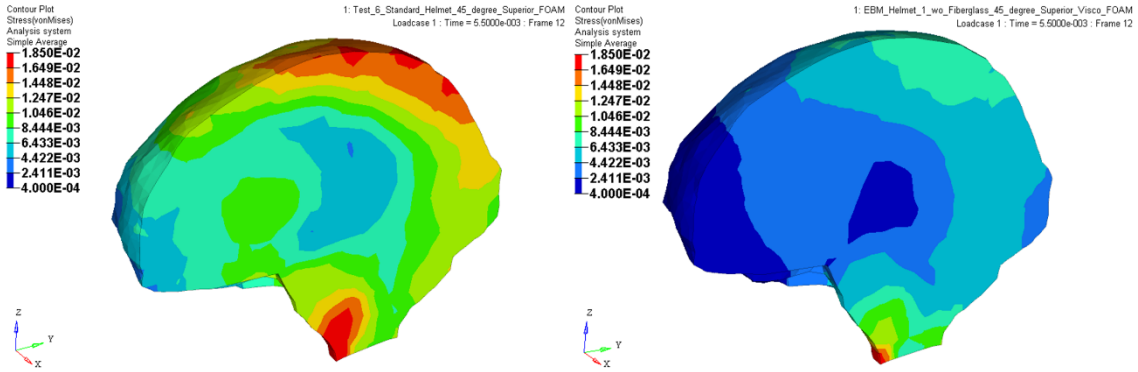

Figure 9-71 VSR4 (left) and EBM (right) Helmet - Superior Impact 45° - von Mises Stress Sagittal Cross-Section

www.manaraa.com

9.5.4 Superior Impact 0° - Principal Stresses

Principal stress comparison of the VSR4 and EBM helmets are shown in Figure 9-72 and Figure 9-73. The peak principal stress, indicating compression, shown in (blue), is at the site of impact. Differences between the peak compressive and tensile stresses for either helmet is insignificant.

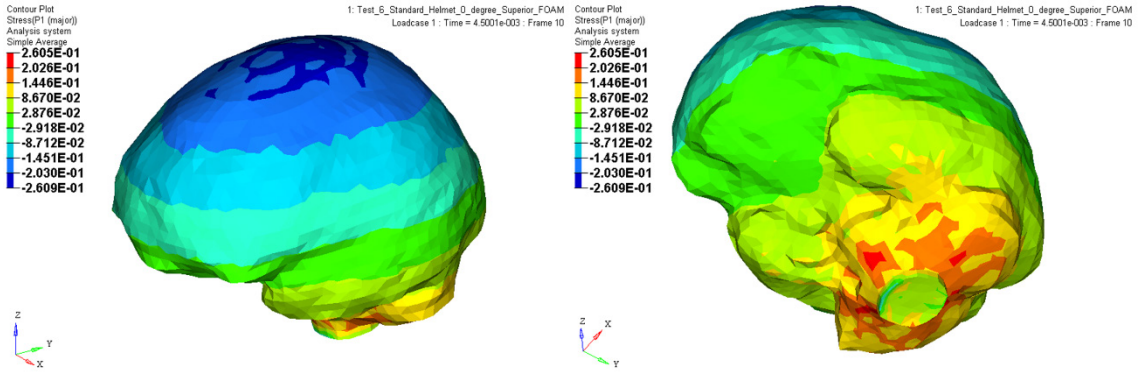

Figure 9-72 VSR4 Helmet - Superior Impact 0° - Principal Stress

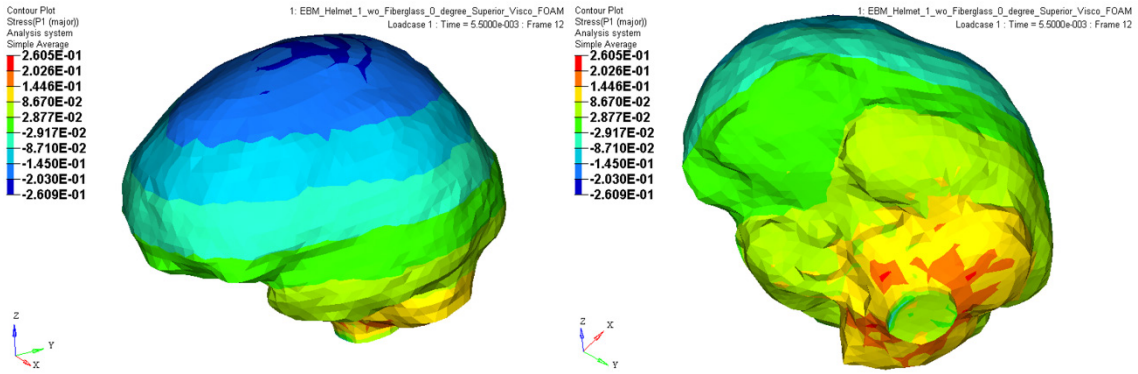

Figure 9-73 EBM Helmet - Superior Impact 0° - Principal Stress

www.manaraa.com

9.5.5 Superior Impact 30° - Principal Stresses

At an impact angle of 30°, the principal stresses for the EBM helmet are substantially different that the VSR4 helmet. The peak compressive stress levels between -0.144 kPa to -0.185 kPa are the same, however the peak area for the EBM is much larger. This is due to the EBM helmet reducing the amount of rotation of the head and making the impact more normal to the center of mass of the head.

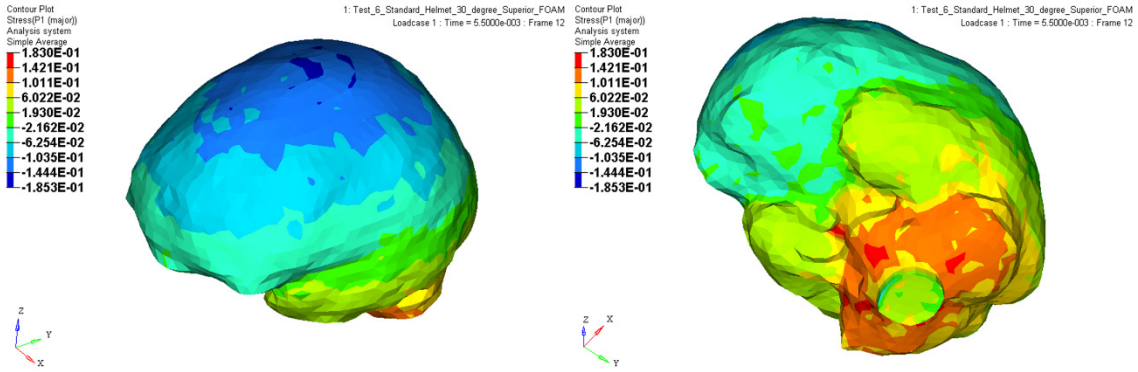

Figure 9-74 VSR4 Helmet - Superior Impact 30° - Principal Stress

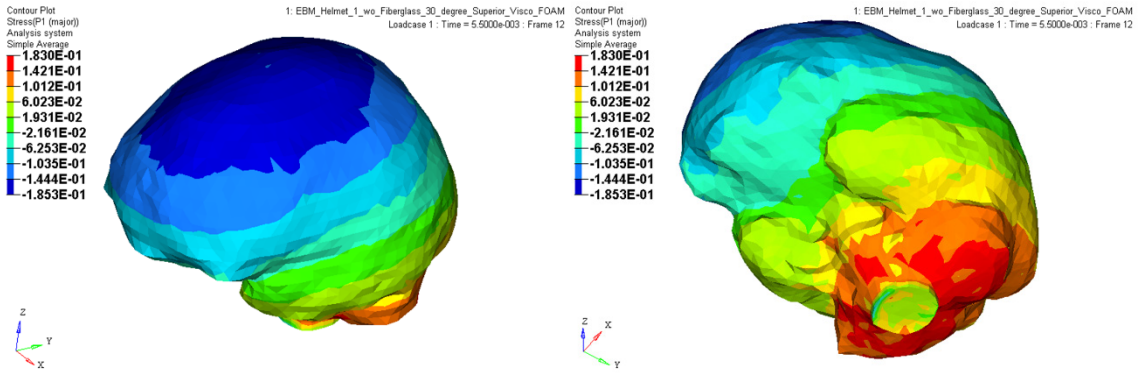

Figure 9-75 EBM Helmet - Superior Impact 30° - Principal Stress

www.manaraa.com

9.5.6 Superior Impact 45° - Principal Stresses

At an impact angle of 45°, the principal stresses for the EBM helmet are still substantially different that the VSR4 helmet, as seen with the 30° impact angle. The peak compressive stress level, which is less than the 30° impact, is between -0.121 kPa to -0.162 kPa are the same, however the peak area for the EBM is much larger. This is due to the EBM helmet reducing the amount of rotation of the head and making the impact more normal to the center of mass of the head.

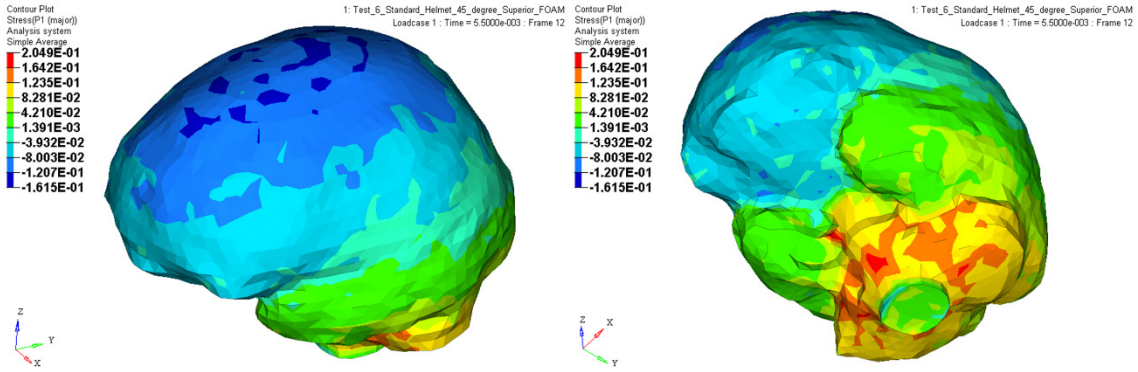

Figure 9-76 VSR4 Helmet - Superior Impact 45° - Principal Stress

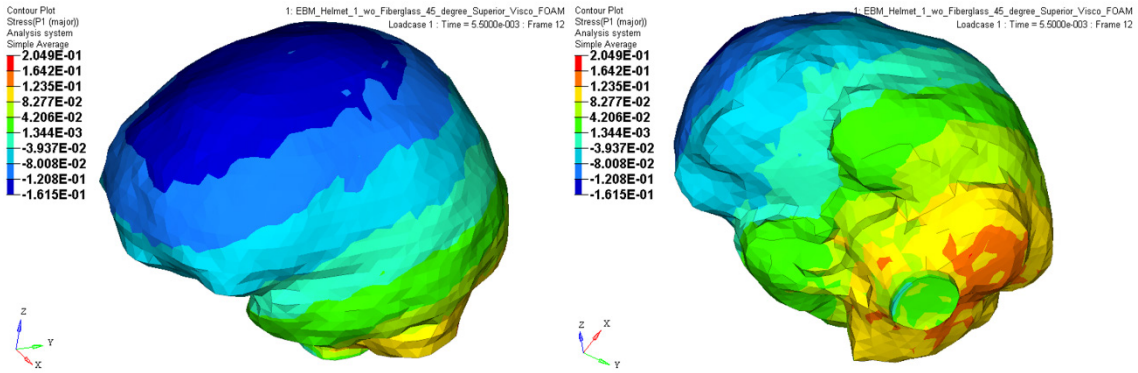

Figure 9-77 EBM Helmet - Superior Impact 45° - Principal Stress

www.manaraa.com

9.6 Summary of Comparison Results

9.6.1 Frontal Impact

One of the key features of the EBM helmet is its ability to reduce the amount of angular acceleration to the brain. From Figure 9-78, it can be observed that as the angle of impact is increased from 0° to 45°, the amount of angular acceleration in the brain also increases. Having the angular acceleration increase once the angle of impact increases is not a surprise. Since the NFL tolerance level for angular acceleration has been proposed to be 5757 rad/sec^2 [27] the EBM helmet provides a mechanism to reduce the amount of angular acceleration to a level that will not cause a Mild Traumatic Brain Injury (MTBI).

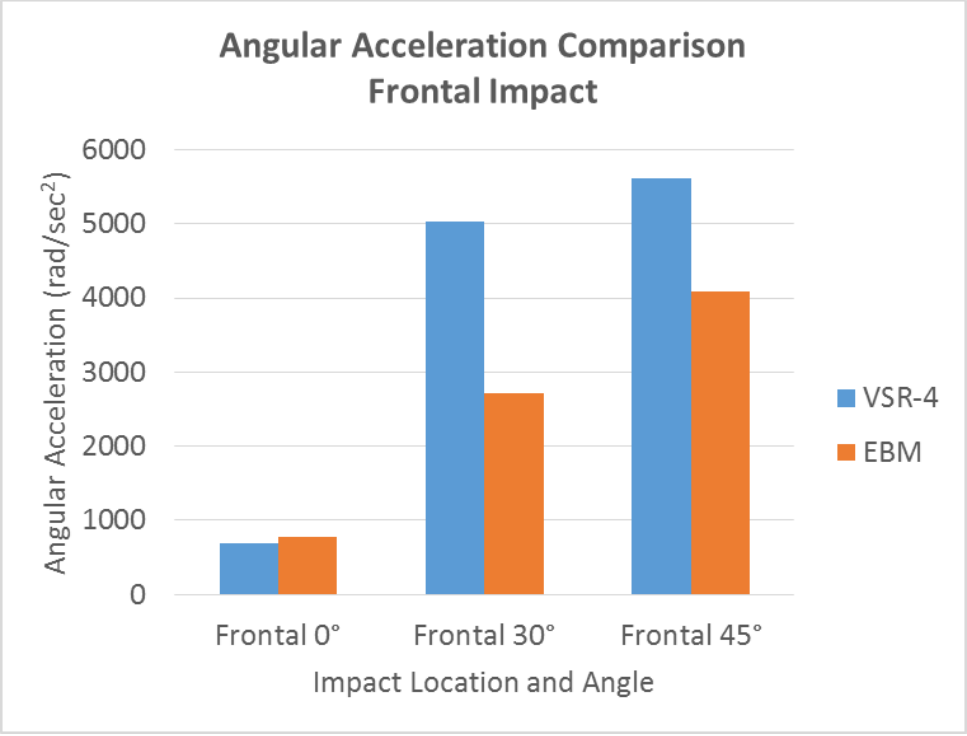

Figure 9-78 VSR4 and EBM Helmet – Frontal Impact - Angular Acceleration Comparison

www.manaraa.com

The results from a 0° for both helmets yield similar results for angular acceleration, whereas, the von Mises stress results for the EBM helmet are slightly higher. Since the EBM has 3mm less padding in the front pad, due to the additional shear layer, this makes sense that the peak stress levels result in a higher resulting value. The stresses are low enough, however, that there is no risk of injury due to angular acceleration.

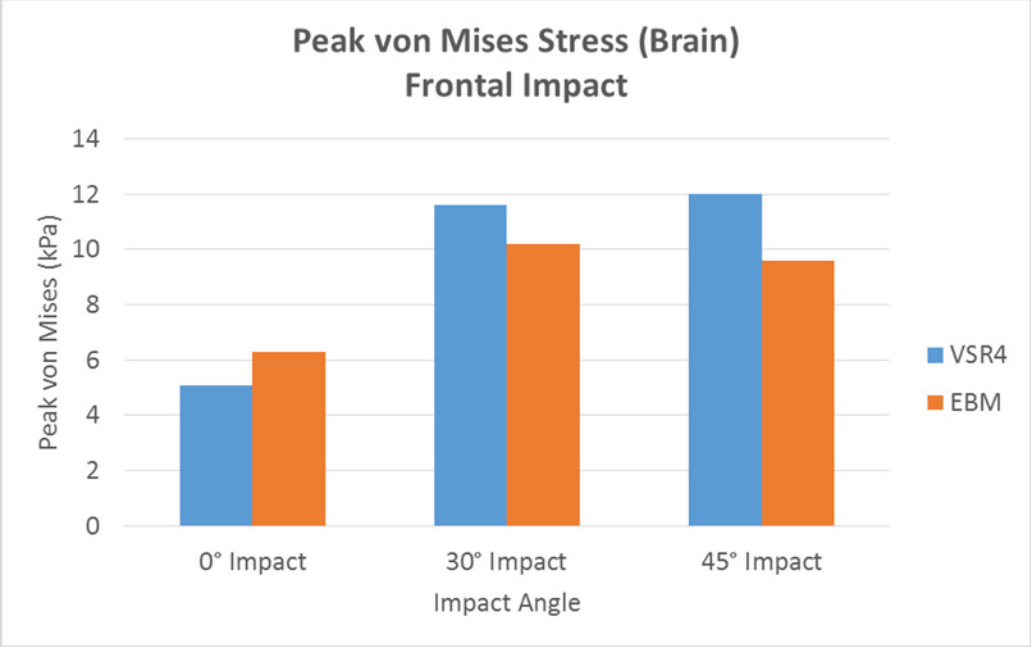

Figure 9-79 VSR4 and EBM Helmet - Frontal Impact – Brain Peak von Mises Stress

Once the angle of impact reaches 30° and 45°, the angular acceleration approaches and then surpasses the tolerance level of 5757 rad/sec^2 published as the injury tolerance due to MTBI caused by angular accelerations [27]. The EBM helmet results show the angular acceleration results are below the threshold, thereby reducing the peak von Mises stresses.

www.manaraa.com

9.6.2 Lateral Impact

The results from the 0° and 15° impact angle simulations yield similar results for peak von Mises stress with both helmets. What is different between the two is the area of peak von Mises stress for each model being larger for the VSR4 helmet as compared to the EBM helmet. The EBM helmet reduces the von Mises stress area significantly. The areas can be observed in Figure 9-26 through Figure 9-31.

Another result observed with the 0° and 15° impact angles is the amount of angular acceleration reduction seen with the EBM helmet. The percent reduction in angular acceleration is 59% for a 0° impact angle and 30% for a 15° impact as seen in Figure 9-81. Once the angle of impact is increased to 45°, the percent reduction is reduced to 11%.

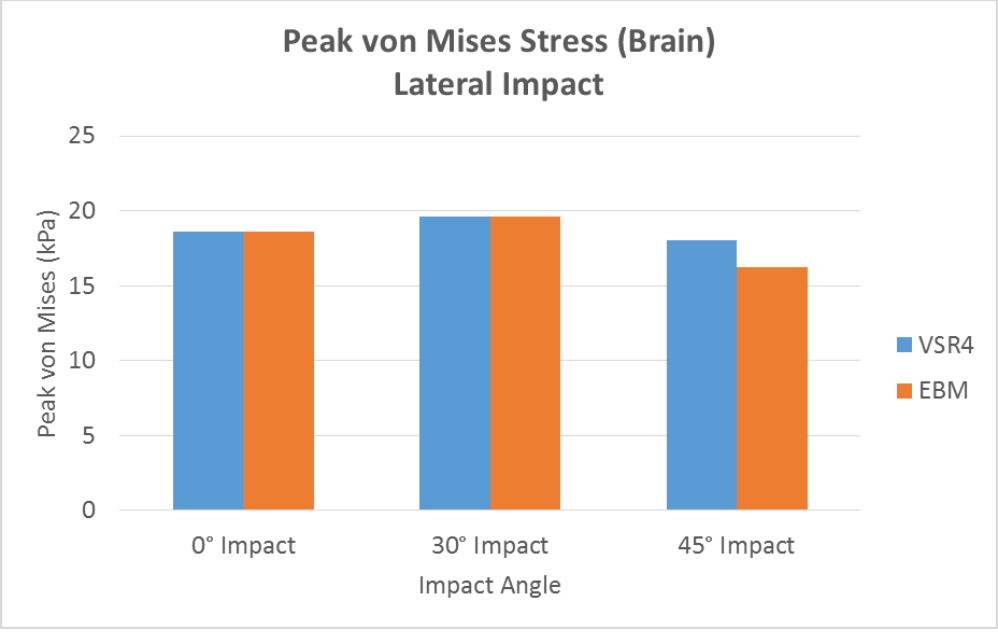

Figure 9-80 VSR4 and EBM Helmet - Lateral Impact – Brain Peak von Mises Stress

www.manaraa.com

In general, the results observed with lateral impacts with football helmets, follows the results observed with the head impact simulations in Chapter 2. The lateral impact, even at an angle of 0°, results in a stress distribution globally around the brain. As was concluded from the head impact simulations in Chapter 2, a so called normal impact force vector is eccentric with respect to the center of mass of the head. This holds true for the simulations with a head and helmet combination as well.

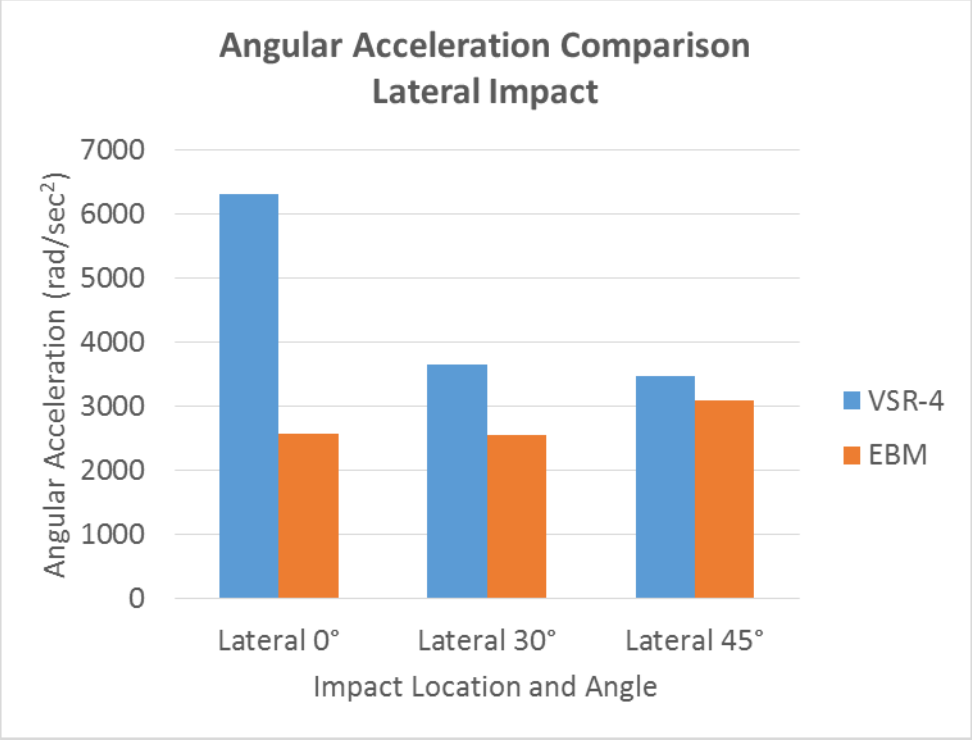

Figure 9-81 VSR4 and EBM Helmet – Lateral Impact - Angular Acceleration Comparison

www.manaraa.com

9.6.3 Posterior Impact

Posterior impacts tend to follow a similar result as the frontal impact where the results for a 0° are similar for both peak von Mises stress and angular acceleration. This type of impact is close to the direction of the center of mass of the head which results in very little angular movement. See Figure 9-82 and Figure 9-83.

With the angle of impact increasing to 30°, the shear layer in the EBM helmet helps to provide a 17% reduction in angular acceleration in the brain. This helps reduce the peak von Mises stress that is present.

Once the angle of impact increases to 45°, the results of the EBM compared to the VSR4 helmet are nearly identical. Although there is a reduction in angular acceleration with the EBM helmet, the differences between the two helmets for von Mises stress peak values and contour plots are insignificant. This can be a result of the amount of padding in the posterior region of the helmet being thinner than all the other areas. The posterior padding in the VSR4 helmet is 20mm and 17mm for the EBM helmet. This reduced thickness for the EBM helmet ma play a role in the overall von Mises stress results, even though providing a 20% reduction in angular acceleration.

www.manaraa.com

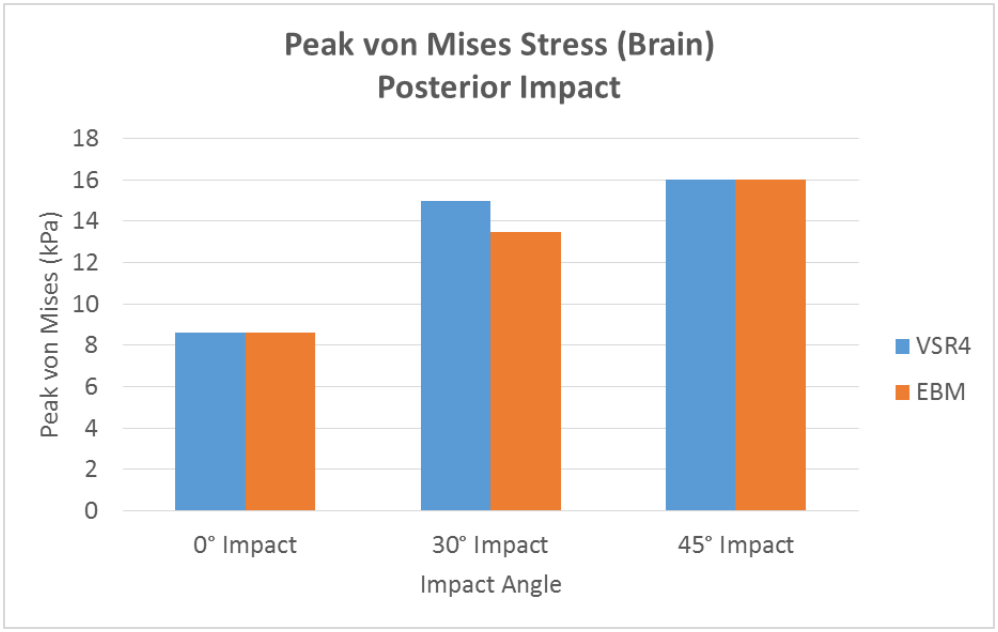

Figure 9-82 VSR4 and EBM Helmet - Posterior Impact – Brain Peak von Mises Stress

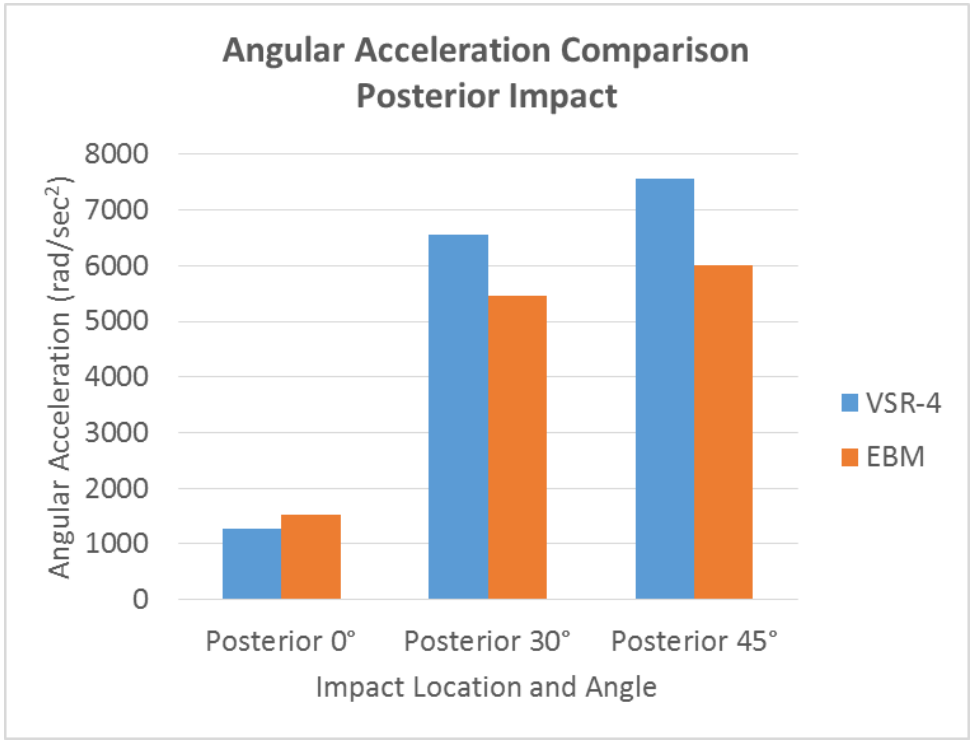

Figure 9-83 VSR4 and EBM Helmet – Posterior Impact - Angular Acceleration Comparison

www.manaraa.com

9.6.4 Superior Impact

Superior impacts results for peak von Mises stress and angular acceleration shown in Figure 9-84 and Figure 9-85 shows that as the angle of impact increases from 0° to 45°, the percent reduction for angular acceleration provides a protecting feature for the human brain against concussion. The percent reduction of angular acceleration increases as the angle of impact increase, causing the peak von Mises stress to be reduced.

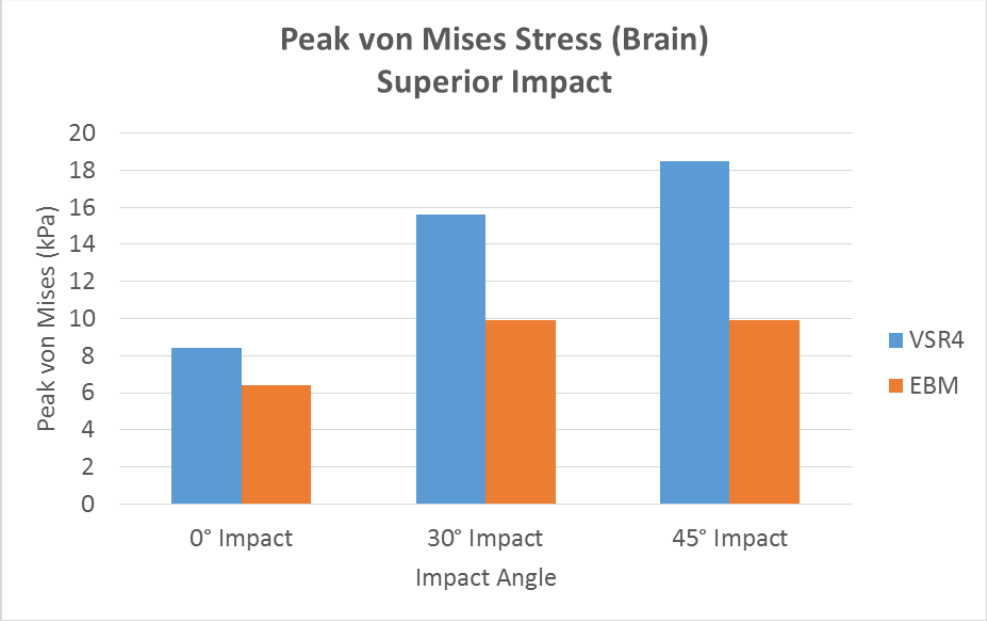

Figure 9-84 VSR4 and EBM Helmet - Superior Impact – Brain Peak von Mises Stress

Although the angular acceleration levels are lower compared to those observed in the other impact simulations, the amount of angular acceleration reduced helps reduce the peak von Mises stress.

www.manaraa.com

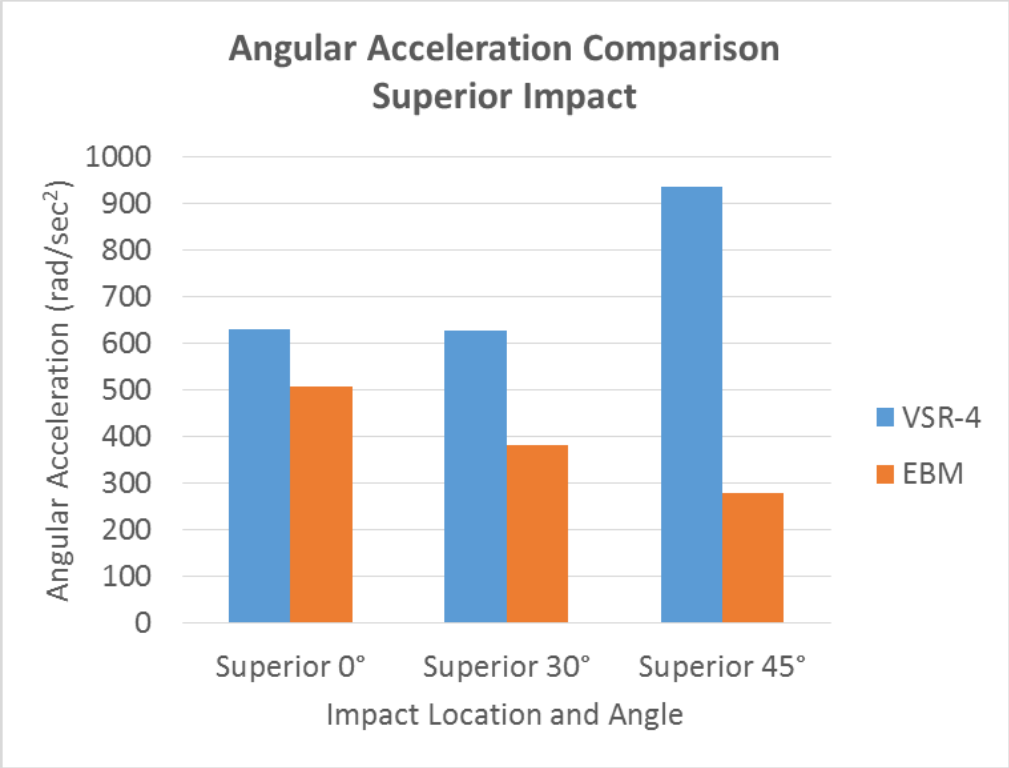

Figure 9-85 VSR4 and EBM Helmet – Superior Impact - Angular Acceleration Comparison

www.manaraa.com

10 Summary

In the course of this study, a 3D finite element of the human head was used to evaluate the efficacy of two football helmets. The commercially available VSR4 helmet by Riddell is used as a comparison to the proposed Enhanced Bio-Morphic (EBM) helmet designed at MTU. As part of this study, the all the components of the football helmet were evaluated to determine their effectiveness once they were combined into a final helmet configuration.

Also part of this study was to look at the development of the human head model. A 50th percentile human male finite element model was developed to further help understand what effect a football helmet has on a player, before a helmet is actually used. The head model developed here has provided an extreme insight into head injuries. It has been a beneficial tool in studying the effect an impact has on the human head.

When looking through the results of the EBM helmet compared to the results of the VSR4 helmet, the overall conclusion is that the helmet works. Not only is the EBM helmet effective in reducing the angular acceleration in the human head, but it is also effective in reducing the peak stress in the brain as a result of these impacts. The additional mass shear layer adds to the EBM helmet and the reduced padding thickness does not have a detrimental effect to the overall performance of the helmet.

www.manaraa.com

It has been shown, that the reduction in angular acceleration the EBM helmet provides is an added benefit when looking at the stress results in the brain. In the majority of impact simulations, the stress results are significantly reduced with the EBM helmet. In some cases where the peak von Mises stress levels are the same between the two helmets, the area contour plots show a much smaller are of peak stress associated with use of the EBM helmet compared to the use of the VSR4 helmet.

www.manaraa.com

11 Recommendations for Future Work

There are a few suggestions to further the study of the EBM helmet presented in this research. The following suggestions can be helpful for future research to further improve the overall study of head impacts, with and without a helmet, and the results obtained in the finite element analysis:

- Given the results of the EBM helmet performance, it's time to build a helmet and start testing the technology.
- Improve the model of the human head. With the advancement in computing, an improved finite element model of the human head should be developed. This could include a more detailed modeling effort of the brain as well. The head model developed at MTU has been used for a number of studies and should continue to be used for future studies.
- Further validation of the human head finite element model. With more research looking into the material properties of biological tissue, further studies can be performed to improve the human head finite element model.
- Develop a model of a youth human head. With more and more youths getting involved in contact sports, the need for evaluating protective headgear is paramount. Sports equipment that's available for youth sports teams does not appear to be as well built as it is for adults. Protection for youth players should have a higher level of priority.

www.manaraa.com

12 References

[1] Centers for Disease Control and Prevention, National Center for Injury Prevention and Control, "Traumatic Brain Injury in the United States: Fact Sheet," 23 March 2017. [Online]. Available: http://www.cdc.gov/traumaticbraininjury/get_the_facts.html. [Accessed 23 March 2017].

[2] Taylor CA, Bell JM, Breiding MJ, Xu L. Traumatic Brain Injury–Related Emergency Department Visits, Hospitalizations, and Deaths — United States, 2007 and 2013. MMWR Surveill Summ 2017;66(No. SS-9):1–16. DOI: http://dx.doi.org/10.15585/mmwr.ss6609a1.

[3] National Library of Medicine "The National Library of Medicine's Visible Human Project,"http://www.nlm.nih.gov/research/visible/visible_human.html.

[4] Altair® HyperWorks® 14.0, A Platform for Innovation®, Copyright© 1986-2017 Altair Engineering Inc.

[5] Nahum, A. M., Smith, R., Ward, C. C., "Intracranial Pressure Dynamics During Head Impact." *Proc. 21st Stapp Car Crash Conf.*, The Society of Automotive Engineers Paper # 770922, 1977.

[6] Kang, H., Willinger, R., Diaw, B. M., Chinn, B., "Validation of a 3D Anatomic Human Head Impact in Motorcycle Accident by Finite Element Modeling." The Society of Automotive Engineers Paper # 973339, 1997.

[7] Raun, J. S., Zhou, C., Khalil, T. B., and King, A. I., *Computer Techniques and Computational Methods in Biomechanics*, Leondes, C., ed., CRC Publishers, pp. 7-1 to 7-40, 2001.

[8] Ward, C., Chan, M., Nahum, A., "Intracranial Pressure – A Brain Injury Criterion." The Society of Automotive Engineers Paper # 801304, pp 3867-3880, 1980.

[9] National Operating Committee on Standards for Athletic Equipment (NOCSAE) Document ND01-06m06, A Standard Drop Test Method and Equipment Used in Evaluating the Performance Characteristics of Protective Headgear.

[10] Sensor Products Inc., "Fujifilm Prescale® Tactile Pressure Indicating Sensor Film," Sensor Products Inc., 2014. [Online]. Available: http://www.sensorprod.com/fuji-prescale.php. [Accessed 25 October 2014].

www.manaraa.com

[11] Abhang, Chandrika, S., “Measuring Head Impact Contact Pressure In Collegiate Football Games to Correlate Head Kinematics to Brain Kinetics Elucidating Brain Injury Dynamics” Michigan Technological University, Houghton, MI, 2014.

[12] O. Anna, K. Clara, P. Andrew, R. Philippe, H. Blaine, M. Shawn, B. Susan, S. Aynsley and C. Michael, "An Examination of Headform Dynamic Response for Concussive and Traumatic Brain Injury," in *1st International Conference on Helmet Performance and Design*, London, UK, 2013.

[13] Sorbothane (2016), “www.sorbothane.com”

[14] Bhushan, Kangana, “A Finite Element Study on the Efficacy of Football Helmet for Direct Versus Oblique Impacts” Michigan Technological University, Houghton, 2006.

[15] Zhang, L., Ramesh, Dwarampudi, Yan, King H., King, Albert I., “Effectiveness of the Football Helmet Assessed by Finite Element Modelling and Impact Testing,” Wayne State University, 2003. Lisbon, Portugal: International Research Council on Biokinetics of Impacts, Bron, France.

[16] American Society of Testing Materials, ASTM F429-01. *Standard Testing Methods for Shock-Attenuation Characteristics of Protective Headgear for Football*.

[17] American Society of Testing Materials, ASTM F717. *Standard Specification for Football Helmets*.

[18] American Society of Testing Materials, ASTM F1446. *Standard Test Methods for Equipment and Procedures Used in Evaluating the Performance Characteristics of Protective Headgear.*

[19] Rowson, S., Brolinson, G., Goforth, M., Dietter, D., Duma, S., 2009, “Linear and Angular Acceleration Measurements in Collegiate Football” ASME J. Biomech. Eng., 131, pp 1-7.

[20] Zhang, L., Yang, K. H., and King, A., 2004, “ A Proposed Injury Threshold for Mild Traumatic Brain Injury,” ASME J. Biomech. Eng., 126(2), pp. 226-236.

[21] King, A., Yang, K. H., Zhang, L., Hardy, W., and Vianno, D. C., 2003, “Is Head Injury Caused by Linear or Angular Acceleration?,” *Proceedings of the International Research Conference on Biomechanics of Impacts (IRCOBI)*, Lisbon, Portugal.

www.manaraa.com

[22] Lovell, Mark R., and Collins, Michael W., 1998, "Neuropsychological assessment of the college football player," J. Head Trauma Rehabil, 13(2), pp. 9-26.

[23] Chu, Chung-Sheng, Lin, Mish-Shyan, Huang, Haw-Ming, Lee, Maw Chaug, 1994, "Finite element analysis of cerebral concussion," J. Biomechanics, Vol. 27, No. 2, pp. 187-194.

[24] Fendrich, Howard, 2010/11, "A concussion-proof helmet? It doesn't and may be an impossible dream," www.cleveland.com

[25] "Virginia Tech helmet research council," Easterbrook, George, ESPN.com, 7/20/2012

[26] "Football Helmets: Do Models Matter?" UW-Madison researchers: On Wisconsin, Winter 2014

[27] "NFL Looks to Helmet Technology to Combat concussion," Nationalgeographics.com/news/2013/13/130202

[28] Pellman, E. J., Vianno, D. C., Tucker, A. M., Casson, I. R., and Waeckerle, J. F., 2003, "Concussion in Professional Football: Reconstruction of Game Impacts and Injuries," Neurosurgery, 53(4), pp. 799-814.

[29] Martin, Luke, A., "A Novel Material Modulus Function for Modeling Viscoelastic Materials," Virginia Polytechnic Institute and State University, 2011.

[30] Labyak, D.M., "Interpretation of Head Injuries Due to Oblique Impact by Finite Element Modeling," 2003, Michigan Technological

[31] Chu, C. S., Lin, M. S., Huang, H. M., Lee, M. C., "Finite Element Analysis of Cerebral Contusion." *J. Biomech*, Vol. 27, pp. 187-194, 1994.

[32] Claessens, M., Sauren, F., Wismans, J., "Modeling of the Human Head Under Impact Conditions: A Parametric Study." The Society of Automotive Engineers Paper # 973338, 1997.

[33] Fan, W.R.S., "Internal Head Injury Assessment." *Proc. 15th Stapp Car Crash Conf.*, The Society of Automotive Engineers Paper # 710870, pp 645-665, 1971.

[34] Gennarelli, T. A., Thibault, L. E., "Biomechanics of Acute Subdural Hematoma." *J. Trauma*, Vol. 22, pp. 680-686, 1982.

www.manaraa.com

[35] Goldsmith, W., "Biomechanics of Head Injury, Biomechanics, Its Foundations and Objectives." Fung, Y. C., Perrome, N., and Ankliker, eds., M., Prentice-Hall, Englewood Cliffs, N.J., pp. 585-608, 1972.

[36] Holbourn, A. H. S., "Mechanics of Head Injuries." *Lancet*, Vol. 2, pp. 438-441, 1943.

[37] Lee, M. –C. and Haut, R. C., "Insensitivity of Tensile Failure Properties of Human Bridging Veins to Strain Rates: Implications in Biomechanics of Subdural Hemotoma." *J. Biomech*., Vol. 22, pp.537-542, 1989.

[38] Miller, R. T., Margulies, S. S., Leoni, M., Nonaka, M., Chen, X., Smith, D. H., Meaney, D. F., "Finite Element Modeling Approaches for Predicting Injury in an Experimental Model of Severe Diffuse Axonal Injury." The Society of Automotive Engineers Paper # 993154, 1999.

[39] Nahum, A. M., Smith, R., "An Experimental Model for Closed Head Impact Injury." The Society of Automotive Engineers Paper # 760825, 1976.

[40] Powell, J. W., Barber-Foss, K. D., "Traumatic Brain Injury in High School Athletes." *JAMA*, Vol. 282, No. 10, pp. 959-963, 1999.

[41] Prange, M.T., Meaney, D.F., Margulies, S.S., "Defining Brain Mechanical Properties: Effects of Region, Direction, and Species." *Proc. 44th Stapp Car Crash Conf.*, 2000-01-SC1, pp. 205-213, 2000.

[42] Prange, M.T., Margulies, S.S., "Regional, Directional, and Age-Dependent Properties of the Brain Undergoing Large Deformation." ASME *J. Biomech Engrg*., Vol. 124, pp. 244-252, 2002.

[43] Raun, J. S., Khalil, T. B., and King, A. I., "Human Head Dynamic Response to Side Impact by Finite Element Modeling." ASME *J. Biomech Engrg*., Vol. 113, pp. 276-283, 1991.

[44] Raun, J. S., Khalil, T. B., and King, A. I., "Dynamic Response of the Human Head to Impact by Three-Dimensional Finite Element Analysis." ASME *J.Biomech Engrg*, Vol. 116, pp. 44-50, 1994.

[45] Shuck, L. Z., and Advani, S. H., "Rheological Response of Human Brain Tissue in Shear." *Journal of Basic Engineering,* pp 905-911, 1972

[46] Stalnaker, R. L, Burke, W.V., Hines, M.H., "Translational Energy Criteria: A Validation Study for Non-Fracture Head Impacts." The Society of Automotive Engineers Paper # 973337, pp 3815-3827, 1997.

www.manaraa.com

[47] Shugar, T.A., "A Finite Element Head Injury Model." Report No. DOT HS 289-3-550-TA, Vol. 1, 1977.

[48] Versace, J., "A Review of the Severity Index." *Proc. 15th Stapp Car Crash Conf.*, The Society of Automotive Engineers Paper # 710881, pp 771-796, 1971.

[49] Zhang, L., Yang, K. H., King, A. I., "Biomechanics of Neurotrauma." *Neurological Research*, Vol. 23, pp. 144-156, 2001.

www.manaraa.com

13 Appendix

David M. Labyak
211 Center Street
Hancock, MI 49930

1 April 1, 2017

Chandrika Abhang
874 E. Loos Street Unit 6
Harford, WI 53027

Dear Chandrika:

I am completing a doctoral dissertation at Michigan Technological University entitled "COMPUTATIONAL STUDIES ON BIOMECHANICS OF CONCUSSION AND ON EFFICACY OF FOOTBALL HELMETS." I would like your permission to reprint in my dissertation excerpts from the following:

Images from your MS Thesis "Measuring Head Impact Contact Pressure In Collegiate Football Games to Correlate Head Kinematics to Brain Kinetics Elucidating Brain Injury Dynamics."

Attached is a copy of Chapter 4 from my dissertation where the images are used and the related information I've referenced from your thesis. Specifically, I would like to use the following images: Figure 3-3, 3-4, 3-5, 3-6, 3-7, 3-8, 3-9, 3-10, 3-11 and Table 3-1.

The requested permission extends to any future revisions and editions of my dissertation, including nonexclusive world rights in all languages, and to the prospective publication of my dissertation.

These rights will in no way restrict republication of the material in any other form by you or by others authorized by you. Your signing of this letter will also confirm that you own the copyright to the above described material.

If these arrangements meet with your approval, please sign this letter where indicated below and return it to me in the enclosed return envelope. Thank you very much.

Sincerely,

[redacted]

David M. Labyak

PERMISSION GRANTED FOR THE USE REQUESTED ABOVE:

[redacted]

Date: April 3rd, 2017

Chandrika Abhang

www.manaraa.com